# RADIO STUDIES OF THE LOWER IONOSPHERE

by

B. C. Lindner, B.Sc. (Hons)

A Thesis
presented for the degree of
DOCTOR OF PHILOSOPHY
at the
UNIVERSITY OF ADELAIDE
(Physics Department)
October 1972

CONTENTS

## SUMMARY

This thesis reports a study of D-region partial reflections, carried out at Buckland Park, South Australia, using a vertical incidence pulsed radar operating at 2 MHz and a large receiving array.

A theoretical basis has been developed for studying the angular spectra of partial reflections using amplitude and phase information from spaced rows of aerials. Observations of the angular spread and the coherence of the angular spectrum as functions of height of reflection have been made and indicate that two distinct height regimes can be distinguished within the D-region. Comparisons have revealed good consistency with other types of evidence.

A study has also been made of D-region electron densities using the Differential Absorption Experiment (DAE) technique. Seasonal variations of the noon electron density profile have been observed and the influence of solar fluxes in the ionization of the D-region below 70 km has been investigated for conditions near maximum solar activity.

Finally statistics of the relative strengths and frequency of heights of occurrence of partial reflections are given for observations extending over a one year period. Stratification of the D-region has often been found but with varying degrees of temporal stability. Some selected records have been interpreted in terms of the apparent temporal variations of the mean electron density between highly preferred reflection heights.

## *PREFACE*

*To the best of the author's knowledge this thesis contains no material previously published or written by another person, except where due reference is made in the text. It contains no material which has been submitted or accepted for the award of any other degree or diploma in any University.*

*(B. C. Lindner)*

*ACKNOWLEDGEMENTS*

*The work described in this thesis was carried out in the Physics Department of the University of Adelaide under the supervision of Dr. B. H. Briggs. The author is grateful to Dr. Briggs for overall guidance in the project and particularly for the influence of his enthusiasm and useful criticism in many inspiring discussions. For his interest and many useful discussions the author would like to thank Dr. R. A. Vincent.*

*The author gratefully acknowledges the assistance of a number of people who contributed to the development, construction and maintenance of the experimental equipment. Mr. J. W. Smith was responsible for the construction of the receiving equipment as well as the maintenance of electronic equipment in general. Dr. Vincent together with Mr. Smith developed the Phase-Path system for monitoring the phase variations of received signals. The scanning gate was developed by Dr. D. G. Felgate.*

*The author was assisted by his wife, Mrs. J. Bowie, and in the latter stages Mrs. N. McCann, in the digitizing of chart records for computer analysis.*

*The assistance of the Weapons Research Establishment, South Australia, in providing pressure data is gratefully acknowledged.*

*Financial support for the project was provided by grants from the Australian Research Grants Committee and the Radio Research Board of Australia. The author was the holder of a University Research Grant postgraduate award.*

# CHAPTER 1

## INTRODUCTION AND SURVEY OF RADIO STUDIES OF THE D-REGION

### 1.1 Early history of D-region work

The knowledge of that weakly ionized region of the earth's atmosphere lying between 50 and 90 km known as the D-region has gradually evolved with the development of various ground based radio techniques, and in later years with the advent of rocket methods. The existence of ionization at D-region heights was implied as early as 1926 (Hollingworth, 1926; Appleton, 1927), although more attention at that time was being paid to the E- and F- regions whose existence had only been confirmed in 1924 and whose properties were the subject of increasing interest. It is not surprising that scant attention was paid to the D-region, as E- and F- region reflections were easy to observe and little was known about them at that time. Some of the earliest evidence for ionization at D-region heights was gathered from observations of the propagation characteristics of LF and VLF transmissions over long propagation paths. Hollingworth (1926) observed interference between signals originating from the same source but propagating along different paths to the point of observation; one wave having travelled along the ground and the other (as he predicted correctly) being a sky-wave reflected from a height of about 75 km. In the years that followed further references to ionization at D-region

heights were made, mainly as a by-product of E- and F- region studies using oblique incidence c.w. techniques (e.g. Appleton, 1930; Appleton and Ratcliffe, 1930; Green, 1932). Further reports of LF/VLF studies similar to those of Hollingworth were also made (Best et al., 1936; Budden et al., 1939) as well as direct observations of the phase and amplitude of the sky wave alone. In these types of observations the apparent heights of reflection were interpreted as indicators of the level of D-region ionization and the diurnal and seasonal variations were investigated, giving broad general information about the D-region.

Another important aspect of early D-region work was the study of vertical incidence absorption of MF and HF waves reflected from the E- and F- layers. In these experiments absorption was attributed to D-region ionization, and the variation of such absorption was studied in relation to solar zenith angle (Farmer and Ratcliffe, 1935; Best and Ratcliffe, 1938), probing frequency (White and Brown, 1936) and also solar sunspot activity (Appleton and Piggott, 1954). Such studies indicated that the D-region, unlike the E- and F- regions, was not a simple Chapman layer and that curious absorption effects occurred in winter. In addition such experiments allowed estimates of collision frequency to be made so that in all many interesting general features of the D-region were deduced as a result of these early absorption studies.

The first vertically incident pulse sounding of the D-region appears to have been made by Sillitoe (1934) in Montreal, Canada, at a

frequency of 3.5 MHz; although there is some doubt as to whether true D-region reflections were observed. His reports attached most significance to a strong echo at 50 km which occurred mainly at night. It is almost certain that this echo would have been a multi-hop E-region echo persisting for longer than the separation of transmitted pulses and therefore appearing at an incorrect apparent range, although brief reference was made to other echoes which could have been true D-region echoes. In the following year Mitra and Syam (1935) reported the existence of echoes at about 55 km and not long after that there was considerable excitement in some quarters when ionized regions as low as 5 km were thought to have been found (Colwell and Friend, 1936; Watson - Watt et al., 1936; Colwell et al., 1936).

It was pointed out by Watson - Watt et al., (1936) that the echoes originating from below about 60 km were significantly different in nature from those above, and shortly after that Mitra (1936) pointed out factors indicating the unlikelyhood of significant ionization existing at these very low heights. An investigation of very low range echoes by Appleton and Piddington (1938) led to the conclusion that such reflections were very rarely observed, and that reflections from aircraft were probably the cause. This latter point was taken up by Watson - Watt and resulted in the development of radar (Watson - Watt, 1945), an achievement especially important at that time in view of the potential military application to the detection of enemy aircraft in the second world war. In recent years short range echoes have been reported and are now known to be land or sea reflections, or of other

non-ionospheric origin (e.g. aircraft), and appreciable ionization is known to exist only above heights of about 50 km.

Although there were few detailed studies of the D-region until about the 1950's there were, since the earliest reports, many references to the existence of D-region reflections (e.g. Rakshit and Bhar, 1936; Syam, 1936; Mitra and Bhar, 1936; Smith and Kirby, 1937; Watson - Watt et al., 1937; Friend and Colwell, 1937, 1939; Piddington, 1939; Yabsley, 1945; Peavey, 1946). A fairly comprehensive survey of these early D-region observations has been compiled by Ellyett (1947). In the early 1950's, following the observation of weak D-region echoes on sensitive ionosonde records by Dieminger (1952), a series of more detailed investigations of the D-region was begun. This marked the beginning of greater interest and progress in the investigation of the D-region.

## 1.2 The formation of ionization in the D-region

The growth of knowledge of ionization production in the lower ionosphere has been aided significantly by the measurement of concentrations of ionizable neutral constituents (e.g. Narcisi and Bailey, 1965; Barth, 1966; Weeks and Smith, 1968) and the flux of ionizing solar radiations penetrating into the upper atmosphere (Friedman, 1960), as well as by laboratory studies of ionization reaction rates.

A remarkable feature of recent work is that relatively minor constituents of the neutral air can play dominating roles in the production and distribution of ionization. For example nitric oxide,

which has a lower ionization potential than the major constituents and is therefore capable of being ionized by radiations which do not affect the other constituents, plays a major role in the production of ionization in the lower ionosphere.

The production and recombination of ionization in the D-region is the result of many complex reactions which vary with differing dynamic conditions. It is not intended to present a detailed discussion of D-region electron production and loss mechanisms here but rather to present the broad general processes thought to be responsible for the formation of the undisturbed D-region, and to briefly mention the processes which are believed to occur during disturbed conditions.

The normal D-region ionization is believed to be produced by three main mechanisms, the relative importance of which varies with height within the D-region. Nicolet (1945), in some of the earliest work in this field, suggested that solar Lyman-α radiation would be able to penetrate to D-region heights and effect the ionization of nitric oxide. Based on further calculations Nicolet and Aikin (1960) proposed a general model for production of the undisturbed D-region of the ionosphere. They suggested that photo-ionization of nitric oxide by solar Lyman-α radiation was most important in the range 70 - 85 km while below 70 km the ionization of all neutral constituents by galactic cosmic rays was postulated. It was proposed that ionization in the region above 85 km was produced by methods similar to those in the E-region and that solar X-rays of wavelengths less than 8 Å ionized all neutral constituents. It is possible that X-rays may

compete with Lyman-α as the ionizing flux below 85 km but this matter has not yet been clarified due to discrepancies between the measurements of nitric oxide concentrations made by several workers (e.g. Barth, 1966; Pearce, 1969). The measurements of Barth would indicate that Lyman-α is the predominant ionizing radiation while those of Pearce would indicate that hard X-rays are a competing mechanism in ionizing metastable oxygen molecules. More recent measurements (Strobel et al., 1970; Meira, 1971) tend to support the measurements of Barth but the possibility of X-rays being important during solar flares cannot be ruled out.

Recent observations indicate that not only X-rays from the sun but also from X-ray stars contribute to the ionizing flux in the D-region. The contribution from this latter source is probably fairly small as X-ray star ionization between 85 and 90 km, has been detected mainly only at night when the solar source is absent (Ananthakrishnan and Ramanathan, 1969; Edwards et al., 1969; Svennesson et al., 1972) although the detection of a distinct daytime effect has been claimed by Ramanamurtry et al., (1970). However it is generally considered that X-ray stars normally only make significant contributions to ionization in the D-region at night.

The calculations of Webber (1962) are a theoretical basis for believing that galactic cosmic rays are a significant ionizing agent in the normal D-region below about 70 km. Tulinov (1967) has suggested that corpuscular radiation may also contribute at mid latitudes.

It is fairly well established that D-region ionization is often present during the night with larger concentration than would be expected on the basis of expected recombination rates. Non-solar origins are therefore necessary. Postulated ionizing sources are nightglow Lyman-α (Ogawa and Tohmatsu, 1966), galactic X-rays (Edwards et al., 1969), galactic cosmic rays (Webber, 1962), corpuscular radiation (Tulinov, 1967) and,to a probably lesser extent, meteor contributions.

The mechanisms of ionization production in disturbed solar conditions are thought to vary with latitude with X-rays becoming dominant at mid and low latitudes and with particle influx, directed into polar regions by the earth's magnetic field, being dominant in high latitude regions.

On the whole in the undisturbed ionosphere the level of ionization is determined by the balance between electron production and loss mechanisms. Generally electron loss is in the form of recombination with positive ions or attachment to neutral molecules to form heavy negative ions. These processes and other D-region processes have been reviewed in detail by Bowhill (1969) and Thomas (1971).

The overall picture is that solar control above about 70 km and cosmic ray control below this are thought to be the dominant factors in the production of ionization in the normal daytime D-region. Finally, Figure 1.1 shows some graphs of ionization production rates given in a review of this topic by Thomas (1971). The graphs correspond to the quiet daytime D-region at solar minimum conditions.

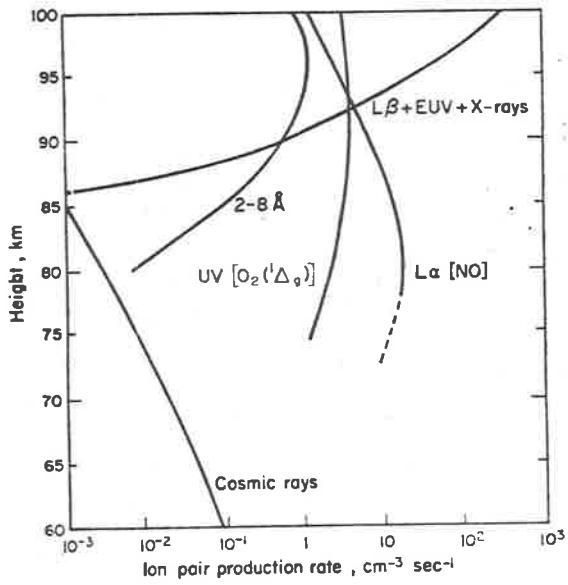


**Figure 1.1** Ionization production rates for the quiet day time D-region at solar minimum conditions (after Thomas, 1971).

## 1.3 Ground based radio studies of the D-region

Probably the greatest contribution to our knowledge of the earth's ionosphere has been made as a result of ground-based radio studies. This is chiefly because such methods are relatively inexpensive and suitable for synoptic studies. The development of the theory of radio-wave propagation in magneto-ionic media (e.g. Appleton, 1935; Booker, 1935; Ratcliffe, 1959; Budden, 1961) has been very important in providing the basis for all forms of radio studies of the ionosphere in general.

From the earliest beginnings of D-region work LF/VLF propagation experiments (Hollingworth, 1926) and absorption measurements (Appleton, 1937) have provided important information about the D-region. While these measurements provide mainly broad information about the D-region they have the advantage that almost continuous monitoring can be carried out. This is especially true for LF/VLF studies where the amplitude and phase of waves from distant radio stations can be studied in relatively simple yet useful experiments (e.g. Bracewell et al., 1951). The variations of phase and amplitude of these waves after reflection from the lower ionosphere at oblique incidence have been interpreted in terms of ionization densities and absorption as well as the variation of apparent height of reflection. Correlations of these features with other parameters have provided information about the D-region such as the X-ray star contribution to ionization (Edwards et al., 1969) and the solar influence on D-region ionization.

As has been already mentioned absorption measurements have provided a great deal of information about properties of the D-region. The idea that the D-region is not normally a Chapman type layer was established from such measurements (Appleton and Piggott, 1954) and the winter anomaly of absorption was also first recognized from such work (e.g. Appleton, 1937). More recent absorption measurements (Schwentek, 1966) have established the regularity of this phenomenon. While LF/VLF propagation studies and absorption studies have contributed a large amount to our knowledge of the D-region they have a feature in common in that only broad general properties of the D-region are usually obtainable. These methods will not be discussed further here but rather those methods which give more detailed information will now be considered.

A useful technique for obtaining D-region electron density profiles is the cross-modulation technique due to Fejer (1955). This experiment employs a two transmitter system where pulse synchronization and transmission geometry are arranged such that alternate pulses vertically reflected from the E-region traverse a narrow height increment in the D-region at the same time that a "disturbing" pulse from an oblique incidence transmitter traverses the same region. The disturbing pulse produces heating in the region of interest and thus modulates the vertically propagating wave. A comparison of the vertically reflected pulses under disturbed and undisturbed conditions allows estimates of electron density, collision frequency and cooling rates to be made.

In the detailed investigation of the D-region another class of ground based radio studies involves the study of the nature of the weak partial reflections which can be obtained from the D-region and the remainder of this section is devoted to a discussion of such studies. Generally high transmitter power and a low noise receiving system are needed owing to the very weak reflected signal strength, reflection coefficients being typically of the order of $10^{-5}$. To effect accurate studies of various reflection properties pulsed transmitter systems are usually used.

The nature and mechanisms of partial reflections from the D-region have been shown to be quite different from E and F-layer reflections. Radiowaves of medium and high frequencies are strongly reflected from the E- and F- ionospheric layers with the heights of reflection varying in a regular and fairly well understood manner with wave frequency and time of day. The weak reflections from below 100 km have been found to behave in an entirely different way. In contrast to E- and F- layer reflections the height of D-region echoes does not vary appreciably with frequency and echo fading rates appear to be somewhat faster, particularly near 90 km (Awe, 1961).

Partial reflections of MF and HF waves from the D-region are known to occur at sharp gradients in refractive index in the propagating medium. These sharp gradients are generally assumed to be due to irregularities in elecrton density although the possibility of the importance of irregularities in collision frequency has been expressed by Piggot and Thrane (1966) and others. The relative importance of

these two possible mechanisms is of importance in the interpretation of various experiments utilizing partial reflections as deductions may be dependent on the reflection model assumed. The spatial extent and distribution of these irregularities which produce partial reflections is an area where little knowledge exists. On the other hand the height distribution of irregularities as deduced from the heights of occurrence of partial reflections has been investigated but at relatively few sites. The existence of preferred heights has been reported by Gregory (1956, 1961) and others and would tend to indicate large scale horizontal stratification of the ionosphere. Reviews of such evidence have been published by Ellyett and Watts (1959) and Titheridge (1962b) with differing conclusions. It is still uncertain to what extent the situation varies with latitude and longitude and further studies are necessary to complete the picture. Although preferred heights of reflection may occur, partial reflections can usually be obtained with varying frequency of occurrence throughout the whole height range of the D-region over the course of a few hours so that detailed height variations of various quantities deduced from partial reflection data can be estimated.

The same irregularities which give rise to partial reflections of MF and HF waves at vertical incidence are believed to cause the phenomenon of VHF "forward scatter" propagation. Here radio waves of frequencies in the range 50 - 100 MHz, leaving a transmitter nearly horizontally, are scattered from the D-region at grazing incidence and can be observed at considerable distances from the source. Practical

use has been made of this mode of propagation which is not subject to interruption during ionospheric storms and may even be enhanced during solar flares (Bailey et al., 1955).

An important technique that utilizes partial reflections for studying motions in the D-region is the spaced receiver drift method (Mitra, 1949). The temporal shifts between fading records recorded at three or more spaced receivers allows the drift velocity of the ionospheric diffracting medium to be studied (e.g. Fraser, 1965, 1968; Rossiter, 1970). A pulsed transmitting system is used to obtain partial reflections from known heights allowing deductions of drift profiles to be made. Yet another technique for observing drifts in this region is that in which the motions of ionized meteor trails are studied by means of radar techniques (e.g. Elford, 1959).

One of the most important developments in the effective use of ground based radio techniques for studying the D-region was the development of a theory of partial reflections of ordinary and extraordinary polarized waves (Gard ner and Pawsey, 1953) and this led the way to an effective method for investigating the average vertical electron density profile, N(h). This method is called the Differential Absorption Experiment (DAE). With some refinements in both theory (Sen and Wyller, 1960) and experimental technique (e.g. Belrose and Burke, 1964) the basic original experiment performed by Gardner and Pawsey is still thought to produce reliable estimates of electron densities. Furthermore, the technique is suitable for synoptic studies.

In recent years other sophisticated ground based radio techniques have been applied to studying the D-region. In this category is the phase path experiment which allows the variations in phase of a given reflected signal to be monitored as a function of time. The coherency of the phase variation so observed is a good indicator of the nature of the reflecting mechanism (Vincent, 1967). Combined with amplitude information detailed studies of the mechanisms of partial reflections are possible and some work of this nature forms part of the experimental work presented in later chapters of this thesis.

## 1.4 Rocket borne radio studies of the lower ionosphere

Another class of radio probing of the lower ionosphere is that in which radio propagation studies are carried out with the aid of rockets. There are some advantages in these methods compared with ground based methods although, as is the case with most rocket work, extensive soundings are prohibitively expensive.

Early reports of rocket techniques in ionospheric studies were made by Berning (1951), Seddon (1953) and Jackson (1954) who employed c.w. techniques to determine information about the earth's magnetic field, electron collision frequency, and electron and ion densities. In the type of experiments these workers described rocket borne transmitters operate at two frequencies, a reference frequency being high enough to be unaffected by the ionosphere while the lower frequency is modulated by ionospheric propagation. A comparison of the two signals received at the ground allows height variations of

refractive index to be calculated using magneto-ionic theory. This method gives only one value of the collision frequency at the height where the extraordinary wave refractive index is zero and in general the method is relatively insensitive to the lower electron densities below about 85 km. Using similar techniques Kane (1959) extended the method to measuring the whole collision frequency profile. The reliability of such measurements depends on the contributions of multi-path propagation effects and rocket induced effects.

Two other radio techniques involving the use of rockets have been described by Seddon (1958). The first involved the measurement of differential absorption of 'O' and 'X' polarized waves in travelling from a rocket borne transmitter to ground receivers. Using a theory similar to that of Gardner and Pawsey (1953) deductions of electron density were made possible. Secondly a Faraday rotation experiment was described in which measurements of the rotation of the plane of polarization of a linearly polarized wave transmitted from the rocket, as monitored on the ground, enabled electron densities to be measured. The change of orientation of the plane of polarization with rocket altitude, z, is given by:

$$\frac{d\psi}{dz} = N(z)\ F(\omega,\ \omega_H,\ \nu(z))$$

so that the electron density N(z) is obtainable after F has been theoretically evaluated. F is a function of exploring frequency $\omega$, gyrofrequency $\omega_H$, and collision frequency $\nu(z)$.

There are, however, some difficulties involved with rocket borne transmission as the power radiated depends on the nature of the propagating medium near the rocket and this changes with height. Aiken et al (1964) have described experiments similar to those above but with ground based transmission and rocket based reception which minimises such errors. Combined with measurements of Lyman-α and X-radiation on the same flight, deductions about the production of ionization were able to be made. An interesting result of these investigations was the postulation of a dust layer at the mesopause (about 83 km). The existence of dust at mesopause heights has also been reported by Witt et al. (1964) but it is not clear whether significant concentrations exist in general. The dust that does exist is possibly injected by meteors.

More recent refinements of radio/rocket techniques have been described by Knoebel and Skaperdas (1966). Faraday rotation measurements in conjunction with differential absorption measurements were used in a technique significantly improved by the transfer of the factors controlling the limiting sensitivity of the experiment to ground based equipment.

A further addition to this technique has been described by Mechtly et al. (1967) who included a Langmuir current probe on their flights. Radio calibration of the probe to give electron densities was carried out at 1 or 2 km intervals which is the typical resolution of radio-measured N(h) profiles. However, the probe current variations were able to be resolved down to 100 metres so that highly detailed N(h) profiles have been produced. These profiles probably represent the

most accurate and detailed description of individual N(h) profiles available for the D-region. In Figure 1.2 two such profiles are reproduced from Mechtly and Smith (1970) and although D-region N(h) profiles are variable they serve to illustrate the nature of D-region electron density profiles.

## 1.5 Motions of the upper atmosphere and interactions with the lower atmosphere

The nature of ionospheric motion is of great importance in deciding the structure of irregularities of ionization and hence the nature of radio wave reflection processes. An understanding of these processes is desirable for the purposes of deducing other properties of the D-region. Most of the knowledge of motions of the ionosphere has been derived from radio studies of drifts of meteor trails and observations of ionospheric drifts using spaced receiver methods as mentioned in Section 1.3. The meteor method of drift measurement is more closely related to neutral air motions; however it is believed that at D-region heights the motion of the neutral air is closely linked to the motion of ionization in view of the relatively high collision frequencies binding them together.

The predominant motion of ionization is known to be in horizontal planes and this motion is thought to be influenced by dynamic coupling and interactions with the lower atmosphere. It is now believed that the atmosphere should be regarded as one entity with varying degrees of coupling between what were previously believed to be dynamically isolated height regimes.

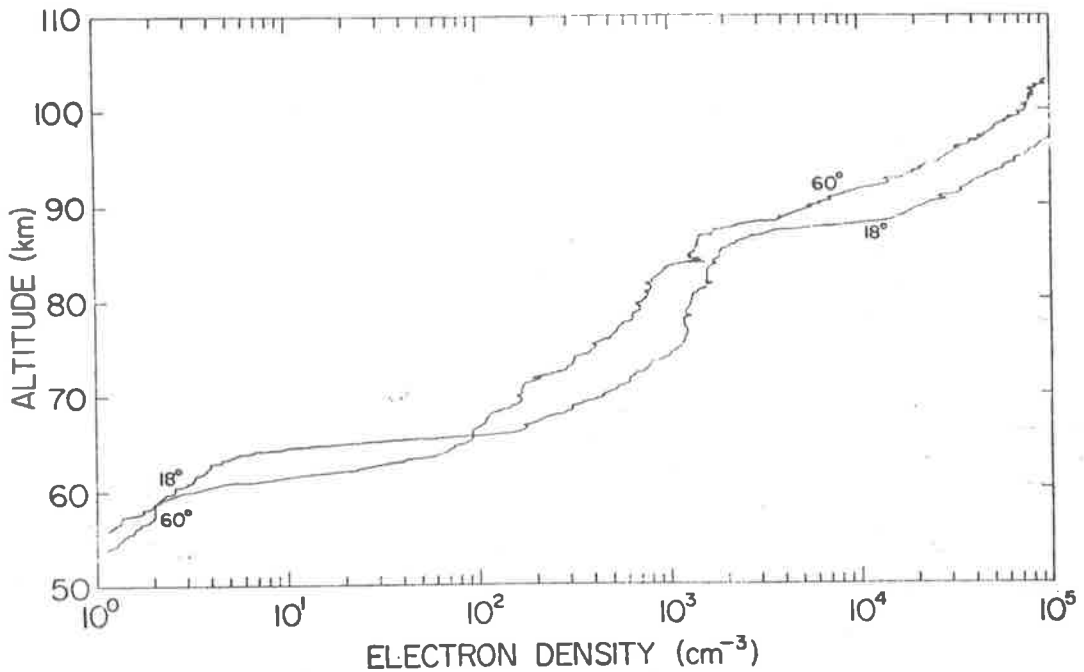


**Figure 1.2** High resolution D-region electron density profiles obtained from rocket probes at Wallops island on 24/7/68 (after Mechtly and Smith, 1970).

The detailed nature of the forces causing ionospheric motions are very complex and are imperfectly understood. The general features are reasonably well established and understood, however, and these include such effects as prevailing and tidal wind motions. Superimposed on these motions are complex and irregular variations in both speed and direction, probably produced by internal gravity waves and turbulence. The prevailing and tidal components are probably generally of little importance in determining small scale irregularities and are a consequence of the earth's rotational motion in the gravitation and radiation fields of the sun. The irregular component of drift motion is probably the dominating factor in the distribution of ionization and formation of small scale ionospheric irregularities, although Roper (1966) has produced evidence showing that large amplitude tidal effects can become non-linear and generate turbulence.

It is believed that a spectrum of upward propagating internal "gravity" waves is largely responsible for irregular motions (Hines, 1960). Tropospheric storm activity is believed to be the principal source of such gravity waves. The periods of these waves lie in the range 5 - 200 minutes and their propagation can generate motions with a broad spectrum of scales, the small scale motions being often identified with turbulence. Theoretical models of these systems give reasonable agreement with experimental observations.

Gregory and Manson (1969) have postulated that another source of energy propagating into the D-region could be planetary and cyclonic waves. These wave motions obey similar equations to gravity waves but

are of much larger temporal and spatial scales. Large scale weather systems and orographic disturbances could be responsible for the generation of such wave motions which theoretically can propagate to D-region heights only in winter (Charney and Drazin, 1961). The possible relationship of such disturbances to electron density changes in the D-region has been discussed by Gregory and Manson (1969). Deland and Friedman (1972) have also inferred the correlation of observed absorption variations with vertically propagating planetary scale waves.

If gravity waves and planetary and cyclonic waves are important operative mechanisms then they exemplify the interaction or coupling between the lower and upper atmosphere, since they are believed to be generated in the troposphere and below and propagate upwards into the mesosphere.

Other evidence of coupling has been produced showing a relation between stratospheric warmings and D-region absorption (Bossolosca and Elena, 1963; Shapley and Beynon, 1965; Manson, 1968; Sinno and Higashimura, 1969). A review of the evidence supporting a connection between winter stratospheric warmings and ionospheric effects has been compiled by Bowhill (1969). A relationship in terms of measured electron densities has also been reported (Rowe et al., 1969). On the other hand a search for such a relationship by Belrose et al. (1966) was unsuccessful.

It seems that in general there is probably a significant interaction between the lower and upper atmosphere in which a complex

interplay of thermal gradients and gravity waves affects mechanical redistribution of D-region ionization and also ionizable neutral constituents producing the observed patchy structure of ionization in the D-region.

Most theories propose that mechanical redistribution of ionization and ionizable neutral constituents are the chief processes in the generation of ionospheric irregularities. Another mechanism that is possibly worthy of consideration is the spatial variability of the flux of ionizing radiations penetrating into the lower D-region. Such a variation could possibly be produced by irregular absorption by irregular distributions of absorbing atmospheric constituents above the lower ionosphere resulting in irregularities in the amounts of ionization produced below. In all probability contributions from several mechanisms play a role and it is uncertain what the relative importance of these is in forming irregularities in the D-region.

## 1.6 The D-region winter anomaly

From the time of the earliest observations of the D-region it was known that ionization production was largely under solar control. However even then a curious departure of D-region properties from the expected was noted in winter and this phenomenon known as the "Winter Anomaly" has puzzled workers until this day. On the basis of solar control electron densities and HF radio wave absorption are expected to be higher in summer than in winter in the D-region. The departure from this expected behaviour was first recognised by Appleton (1937) and Appleton and Piggott (1954) in the form of anomalously high absorption

of MF and HF radio waves in winter. In more recent years Schwentek (1966) has demonstrated a quite regular occurrence of this phenomenon over a period of several years. Figure 1.3 which is reproduced from his work illustrates clearly the winter anomaly phenomenon. The solid curve represents the theoretically expected seasonal variation of absorption and it is seen that the measured summer values (dots) are in general good agreement with the curve. However the circles representing winter measurements show far higher absorption than is expected, with winter absorption often exceeding summer values (e.g. 1960 to 1964).

There appear to be two major characteristics of the occurrences of the winter anomaly:

(1) The greatest anomalous effect is seen in the 80 - 100 km height interval (Lauter and Nitzsche, 1967; Thomas, 1968; Beynon and Rangaswamy, 1969; Gregory and Manson, 1969; Manson and Merry, 1970).

(2) The observable anomaly is confined mainly to mid latitudes. It disappears below about 30° latitude (Lauter and Schaning, 1970) and is probably masked by auroral zone absorption phenomena at high latitudes.

Even while the D-region shows anomalous behaviour a smooth diurnal variation of anomalous values similar to that expected for a solar ionizing flux has been noted by some workers (Lauter and Schaning, 1970; Shrestha, 1971). Nevertheless the day to day variability of the degree of anomalous behaviour has been noticed by several workers

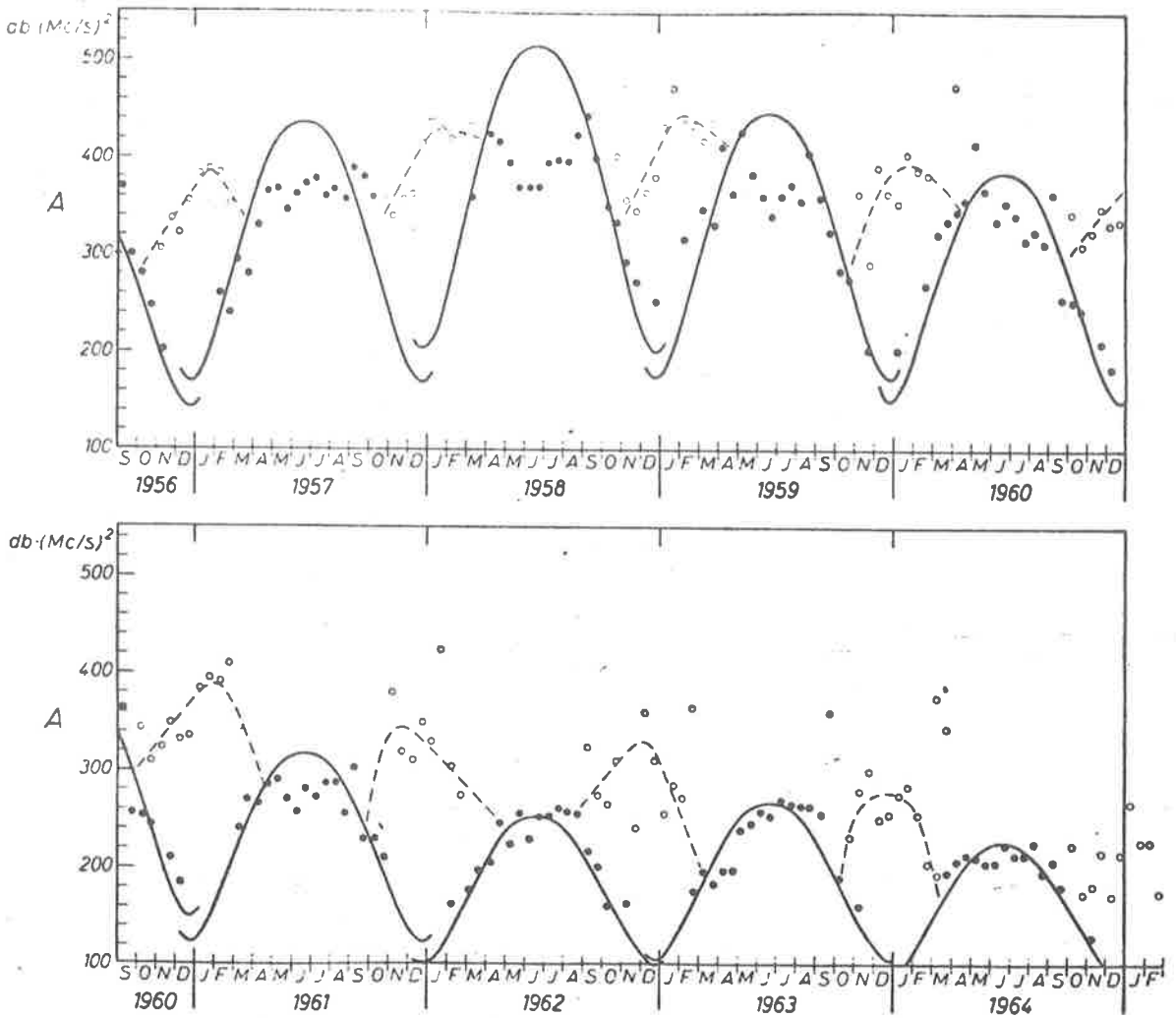


Figure 1.3 Graphs of absorption measurements taken from Schwentek (1966)

(e.g. Schwentek, 1963; Belrose et al., 1966; Gregory and Manson, 1969). Generally the anomaly has been observed from either electron density or absorption measurements with the latter technique being the most widely employed. Taubenheim (1971) has drawn attention to the fact that absorption is dependent on collision frequency as well as electron density and using recently compiled atmospheric parameters (Groves, 1970) has shown a striking feature of the relative collision frequency variability for summer and winter which he suggests might well account for the winter anomaly without the need to invoke increased electron densities. His calculations predict latitude and height variations of the anomaly very similar to those observed; for a sharp cut-off is predicted below 30° latitude with a maximum effect expected between 50° and 60° latitude and in the height range 85 to 100 km. However there is other strong evidence to indicate that electron density enhancements are the prime cause of the anomalous effects. Rowe et al. (1969) have observed anomalously high electron densities at the same time that measured collision frequency profiles showed no unusual trends. In addition, Gregory and Manson (1969) and other workers have observed anomalously high winter electron densities. It is generally thought that these electron density enhancements constitute the winter anomaly rather than collision frequency effects.

The geographic distribution of the winter anomaly on any given occasion is rather uncertain and probably varies. Thomas (1962) suggested a spatial extent of the order of 1000 km while Dieminger et al. (1967) found correlations between occurrences as far apart

as Lindau (Germany) and Ottawa (Canada). Shrestha (1971) has reported the occurrence of very localized anomalous effects in Brisbane (Australia).

While a considerable amount of evidence regarding the occurrence of the winter anomaly exists it is not at all clear what the mechanisms responsible for the winter anomaly are. Studies of the variations of many atmospheric parameters in conjunction with observations of the anomaly have formed the pattern of some investigations in this field. For example, a relationship between stratospheric temperature increases and anomalous absorption has been described by several workers (Bossolasco and Elena, 1963; Shapley and Beynon, 1965; Sinno and Higashimura, 1969) while Shrestha (1971) has noted increased microbarograph activity at ground level during two periods of anomalous absorption. Other observations have indicated that during anomalous conditions ionizable materials are present in anomalous proportions (Vallance-Jones and Gattinger, 1963) and that sunspot activity is also related to the winter anomaly (Schwentek, 1971). The effects of upward propagating large scale waves has been discussed by Gregory and Manson (1969) and various possible transport mechanisms have also been discussed by Christie (1970) and Zimmerman et al. (1970). Christie has shown the feasibility of large scale wave motion transport of ionizable nitric oxide while Zimmerman et al. have demonstrated the possibility of increased turbulence in conjunction with the occurrence of the winter anomaly. In all, many theories and much experimental evidence has been put forward to explain the winter anomaly, and as yet, no clear conception of the detailed mechanisms exists.

## 1.7 Summary

The properties of the D-region ionosphere can be broadly summarised as follows. The D-region is an irregularly ionized medium formed mainly under solar control (by day) except for the lowest regions which are believed to be formed by galactic cosmic ray ionization. The ionization is in a continual state of motion which is influenced by many complex interactions, some of which probably have origins in the lower regions of the atmosphere.

As a result of these complex dynamics the lower ionosphere has a variable and imperfectly understood effect on medium and high frequency radio communications on earth which rely on the ionosphere as a propagating aid. In particular very little is known about D-region reflection processes and the geographic variability of electron density profiles. Ground based radio investigations are being extensively employed to unravel such properties of the D-region and the work described in this thesis is a contribution to these studies.

# CHAPTER 2

# EQUIPMENT AND EXPERIMENTAL PROCEDURES

## 2.1 General

The experimental work which is described in later chapters of this thesis was carried out at the Buckland Park Field Station of the University of Adelaide. The field station is situated on a flat coastal plain 36 km (26 miles) north of Adelaide at 34° 38' South latitude and 138° 37' East longitude.

Due to the weak nature of partial reflections of radio waves from the D-region an installation with low background noise is required in conjunction with sensitive equipment to carry out effective radio studies of the lower ionosphere. The Buckland Park facility with relatively low background noise, a powerful transmitter and large receiving array is eminently suitable for such work.

## 2.2 The transmitting system

### 2.2.1 The transmitter

For the study of weak reflected signals one of the most convenient ways of increasing signal to noise ratio is to increase transmitted power; the signal to noise power ratio for a given reflection being directly proportional to transmitted power. Consequently, in the early stages of the project considerable attention was given to the matter of increasing transmitted power. A former 4 kW transmitter was used to drive a new power amplifier (P.A.) stage capable of 100 kW

peak power transmission. A basic operating frequency of 1.98 MHz was derived from a 990 kHz crystal oscillator and frequency doubler amplifier.

Both the driver and power amplifier stages of the transmitter were pulse modulated. Triggering of the pulses could optionally be locked either to the mains supply frequency or to a phase reference oscillator used in phase path experiments. In the latter stages of the project triggering and synchronization of equipment was derived from an extension of the synchronizing system used in a digitizer/magnetic tape recorder system which was in turn derived from the count down of a 100 kHz crystal oscillator. The pulse modulator provided pulse repetition frequencies of 200, 100, 50, 25, 2 and 1 Hz, with the latter two modes incorporating an automatic polarization change for alternate pulses. Here, pulse pairs, one 'O' and the other 'X' polarized and separated by 60 msec, were provided at 1 or 2 second intervals. These modes were mainly used in the Differential Absorption Experiment (DAE) described in §2.4.2.

In March 1971, a modulator producing a shaped transmitter pulse was brought into use to reduce interference to the adjacent commercial radio band and yet retain the narrow pulsewidth necessary for good range resolution. The shaped pulse envelope produced is closely described by a Gaussian function whereas formerly a rectangular pulse shape was employed.

The range resolution which may be attained using a pulse radar system is inversely proportional to the pulsewidth employed.

However, the extra receiver bandwidth needed to realize superior resolution at narrow pulsewidths introduces extra noise into the receiving system and this factor combined with a consideration for the greater interference problems to other radio users when narrow pulses are employed dictated a lower practical limit to the pulsewidth of about 20 μsec. The pulsewidth was continuously variable from this limit up to 200 μsec but generally a value of 20 - 30 μsec was employed for the work described in this thesis.

The transmitter r.f. pulses were fed from the P.A. stage to the transmitting aerial array via a tuning/impedance-matching network and a phasing cable network using vacuum relays for polarization switching. Figure 2.1 shows the transmitter with the driver stage on the right and the power amplifier stage on the left. The inset shows a photograph of the r.f. pulse taken from a CRO display with a high tension probe connected to the aerial feeder wires. The CRO sweep speed was 10 μsec/cm.

### 2.2.2 The transmitting antennae

The transmitting array consisted of four half-wavelength (71.8 m) folded dipoles, each of 400 ohms impedance, suspended 29.8 metres above the ground and arranged to form the sides of a square. Parallel dipoles were fed in phase with each other and in quadrature with the perpendicular pair to produce the desired circular polarization. Rejection of the unwanted polarization was approximately 30 db and the transmission polar diagram was $25^{\circ}$ wide at the half power

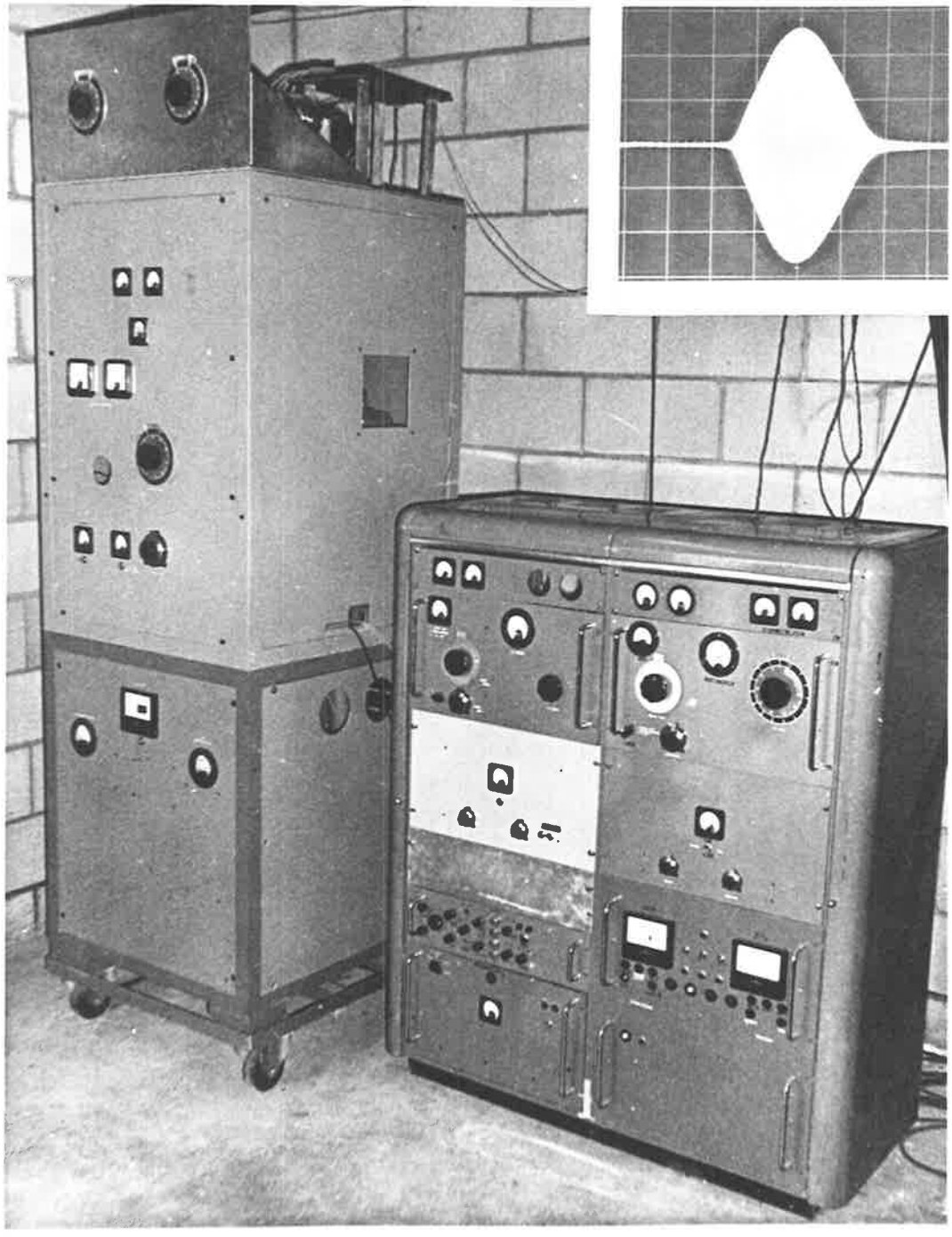

Figure 2.1 The transmitter. Inset shows the shaped r.f. pulse employed.

points. The transmitter and polarization selector were able to be controlled from the central recording laboratory.

## 2.3 The receiving system

### 2.3.1 The receiving antenna array

The Buckland Park antenna array (Briggs, Elford et al., 1969) consists of 89 orthogonally crossed half-wavelength dipoles (178 dipoles in all) and covers an approximately circular area of about 1 km diameter, as shown in Figure 2.2. The wire dipoles are suspended 10.6 metres above ground level and each aerial (which can be used for reception at either 1.98 MHz or 5.995 MHz) is matched with a transformer and series tuned circuits to a 70 ohm coaxial cable which carries received signals underground to the central laboratory. The cable lengths have been accurately cut in order to preserve signal phase at the central laboratory. Here all cables are connected to a 178 pole three position switch which allows switching of the aerials to any one of three outlets. One of these terminates all aerials in two aerial distribution boards corresponding to the N-S and E-W aligned aerials respectively. Output sockets are arranged on a grid of points corresponding to the lattice of Figure 2.2 and this allows versatility in the combinations of aerials which may be selected for various experiments.

### 2.3.2 Tuning the array

With a very large array, attention has to be given to keeping the elements of the array in tune, otherwise, as ground conditions change and aerial reactances change, a very large resultant

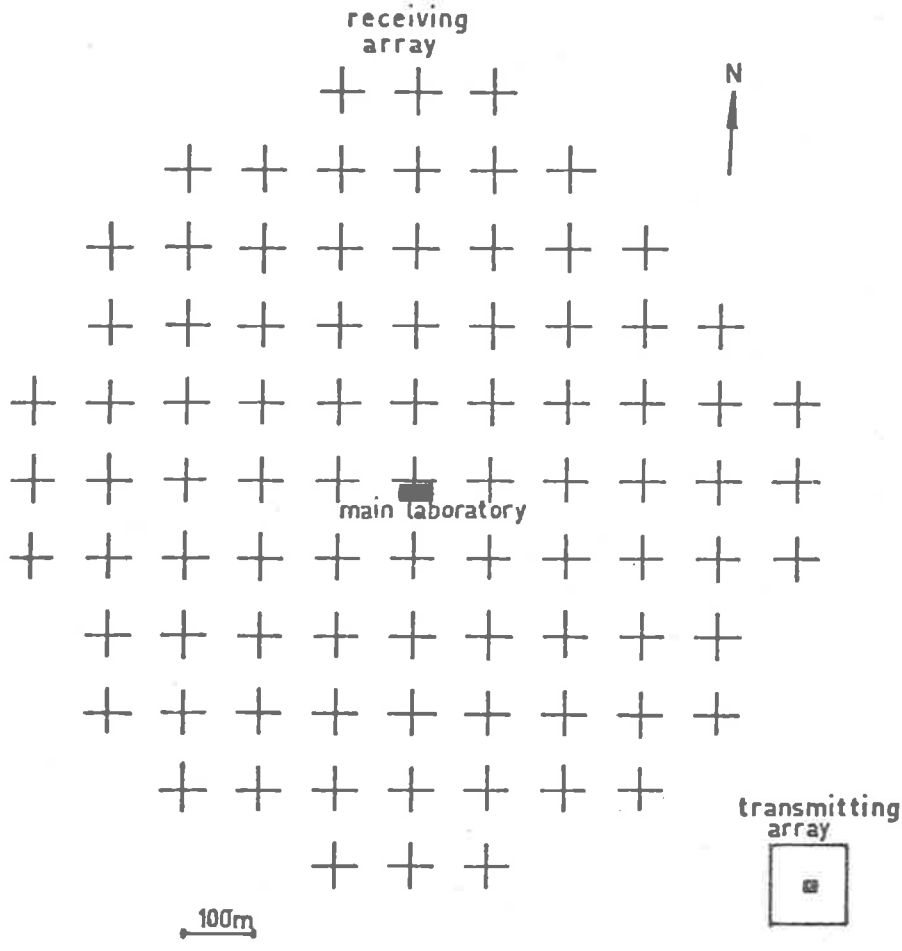


**Figure 2.2** Layout of the Buckland Park aerial array.

reactive component in the output impedance of the whole array ganged in parallel is likely. This is undesirable for matching into the receiving equipment, especially where phase preservation is important. It was found necessary to tune the array several times over the course of the project. A method was adopted whereby the feeder cable from the aerial to the central laboratory was checked for imperfections and the aerial impedance was matched to the cable at 1.98 MHz and at 5.995 MHz. Matching at two frequencies was achieved by using a circuit consisting of a tapped transformer and two separate series tuned circuits connected in parallel.

The tuning procedure was as follows:- the feeder cable (Zo = 70 ohms) was terminated in the central laboratory in a 70 ohm load resistor and disconnected from the aerial. A portable battery operated impedance bridge was used to measure the impedance at the aerial end of the cable. Since the cable lengths are integral multiples of a half wavelength (at 1.98 MHz) the impedance is expected to be 70 ohms unless the feeder cable has been damaged (cut, or water-logged). The aerial circuits were tuned alternately at 1.98 MHz and 5.94 MHz until a unique tuning condition was encountered. The aerial was then reconnected to the feeder cable and the circuit, which is mounted in a box at the top of the aerial pole, was weather-proofed.

The necessity for tuning the aerials was periodically checked by measuring the impedances in the central laboratory at the aerial distribution patchboard.

### 2.3.3 The receivers

To obtain good height resolution in studies of weak partial reflections, short transmitter pulse lengths are required together with high gain and fairly large bandwidth receivers. Four valve receivers each with an overall gain of 120 db and with a bandwidth of 60 kHz were used for the work carried out. The receivers had been previously used for D-region drift studies (Rossiter, 1970) and two were suitable for phase path experiments. Each receiver was capable of being used for either 1.98 MHz or 5.995 MHz reception.

A local oscillator suppression facility was included in the receiver design so that all detected signal outside of a chosen range of interest could be suppressed, thus providing a convenient zero signal reference level.

## 2.4 Experimental techniques and recording equipment

### 2.4.1 The polarization discriminator

The selection of either extraordinary or ordinary polarization in the reception system is desirable so that effects due to impure mode transmission and possible intermode coupling in the ionosphere can be estimated or eliminated. Essentially, the requirement is that the signals from two orthogonal arrays be combined after producing a phase lag of 90° in the signal of either array - depending on which polarization is required.

Several methods of achieving this, including the use of electronic phase shifters, were investigated but were rejected on one or more of the following counts:-

(1) Accurate and stable phase shifts are difficult to obtain.

(2) Extra "transistor noise" is introduced into the system.

(3) Frequent calibrations and adjustments are required.

(4) Isolation of the two orthogonal receiving arrays is difficult.

Subsequently, a coaxial cable Hybrid-ring system was devised which suffered none of these disadvantages and this was the discriminator finally used. The circuit of the discriminator is shown in Figure 2.3. The matching conditions and operation of the system require some further explanation.

Consider the two receiving arrays as signal generators of e.m.f. $E_1$ and $E_2$ and having output impedances $Z_1$ and $Z_2$ respectively. Then if two receiver input impedances are represented by $R_a$ and $R_b$ respectively it is clear that combination of e.m.f.'s $E_1$ and $E_2$ will occur with the required phase lags such that signals of opposite circular polarizations will be produced at B and D respectively.

A simple qualitative argument shows that the signal generators (or arrays) are perfectly isolated from each other, as are the receivers, and that exact matching is theoretically possible. The signal from $E_1$ can traverse two paths to get to A, viz CBA, and CDA. The paths have a $180^\circ$ phase difference and so "cancellation" of $E_1$ at A occurs, i.e. $E_1$ is isolated from $E_2$. (Similarly, point B is isolated from point D.) Thus we may consider, for matching purposes,

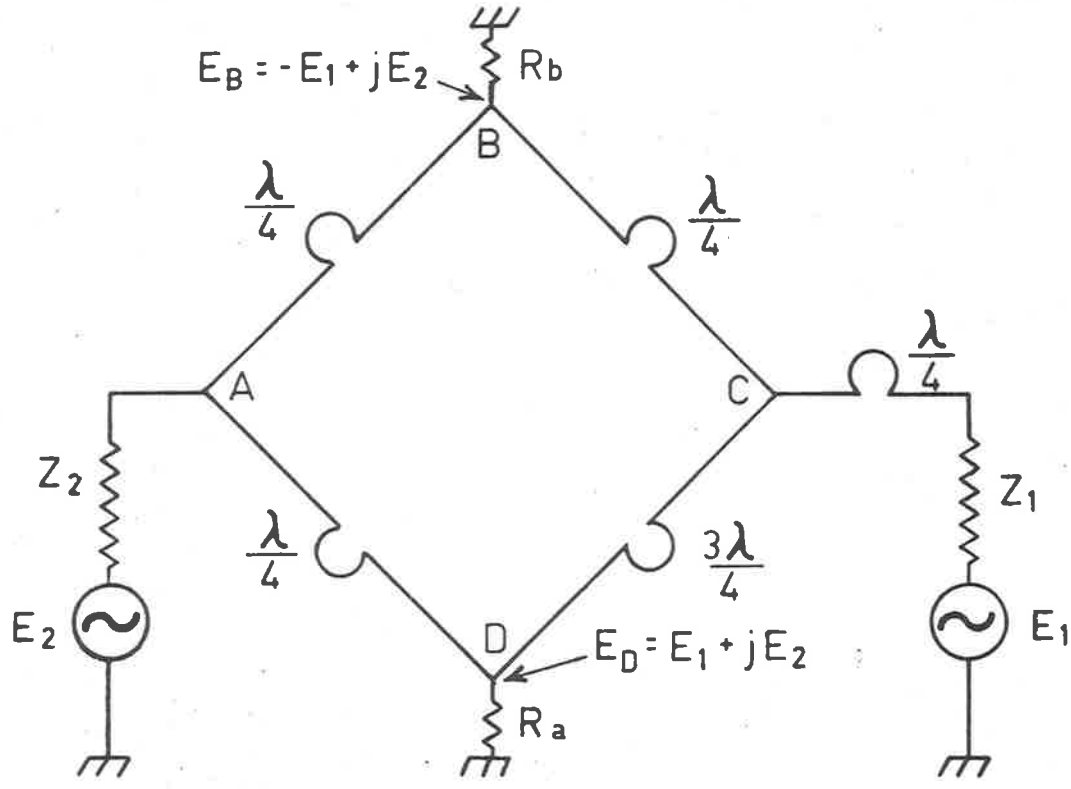


**Figure 2.3** The hybrid ring polarization discriminator.

that looking from the $E_1$ side of the hybrid ring there is a short circuit to ground at A. Simplifying the circuit further we can say that this is equivalent to an infinite impedance at B and D in parallel with $R_b$, $R_a$ respectively. Assuming for simplicity that we can arrange for $Z_1 = Z_2 = R_a = R_b = R$ (say) then it can be easily shown that $Zo = \sqrt{2}R$ where Zo is the characteristic impedance of the cable used in the ring (viz. A B C D). A quarter wavelength cable of characteristic impedance = R ohms is required to connect $E_1$ to C. A convenient choice of values is R = 50 ohms and $Zo = 50 \times \sqrt{2} = 70$ ohms and these were the values used. The discriminator used had a measured rejection of the unwanted mode of greater than 60 db.

2.4.2 The photographically recorded Differential Absorption Experiment

Two methods were used for measuring the differential absorption of extraordinary and ordinary polarized waves in the D-region.

The first and principal method used was essentially very similar to a method used by other workers (e.g. Belrose and Burke, 1964; Thrane, 1966) and employed a photographic recording system. Transmission was modulated in pairs of pulses (separated by 60 msec) at a repetition rate of 1 pair/sec. Each pair of pulses consisted of one extraordinary and one ordinary polarized pulse. The two orthogonal receiving arrays were each connected to the polarization discriminator and the discriminated signal appropriate to the transmitted polarization was fed to a receiver. The detected output of the receiver was displayed as an A-Scan, the sense of deflection being inverted between

'O' and 'X' polarized pulses. The display sweep was in the vertical direction and a 35 mm camera with continuous film feed of 1"/sec in a horizontal direction was used to record the pair of A-Scans that were displayed at 1 second intervals. The camera was able to accommodate 400 ft. reels of film so that 80 minutes of continuous recording was possible without reloading film. A block diagram of the complete system is shown in Figure 2.4.

Range calibration was provided in the form of high intensity dots on the CRO trace. High accuracy range markers were derived from the count down of a 3 MHz crystal oscillator. Range marker separations of 1, 2, 5, 10, 20, 50, 100 km were selectable in various combinations, each set of range markers having a characteristic width. A configuration using 2 km range markers with a broader mark at every 10 km was generally used. Zero range was set at the centre of the transmitted pulse in all experiments.

After processing, the film records were reduced to punched card data using a film reader/digitizer coupled to an IBM 026 card punching machine. The cards were then processed using the University's CDC 6400 computer. The film reader had a four digit read out with a measurement resolution of .004" on a screen image of 36X magnification this being more than adequate for digitizing the A-Scans which had trace-widths of approximately .05" on the image screen.

While this method of measuring differential absorption is reasonably accurate it suffers in particular from one practical drawback. The accurate reduction of film records to punched cards is a

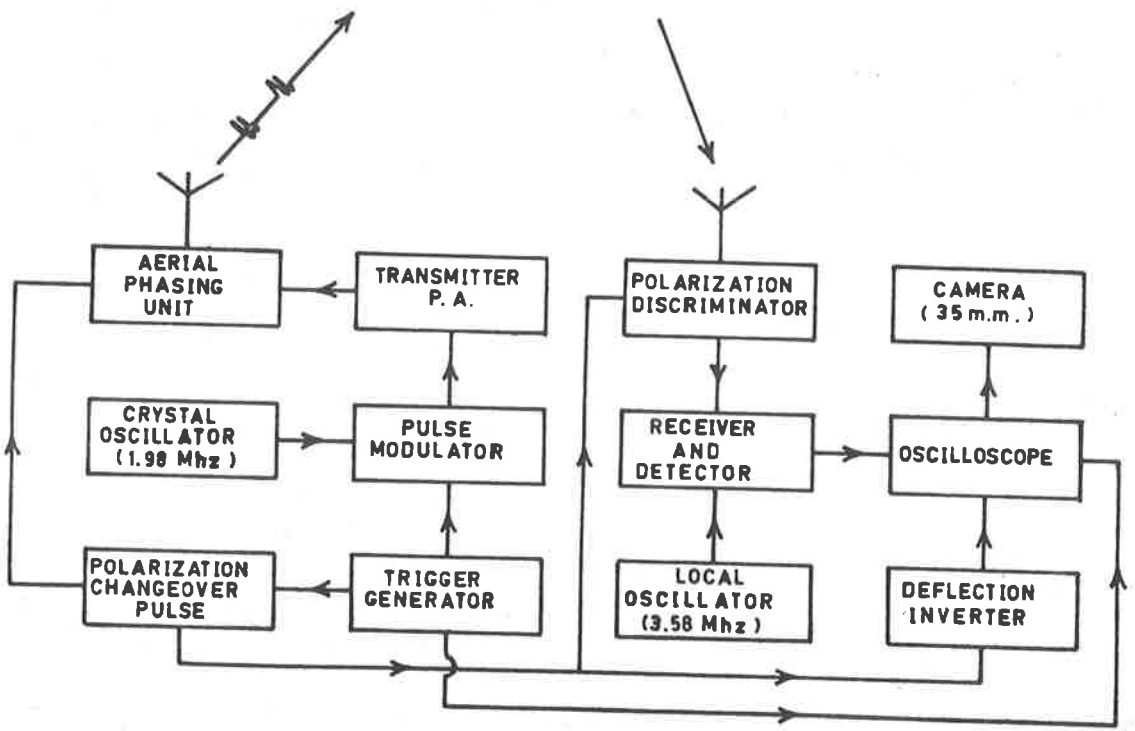


Figure 2.4 Block diagram of the system for photographic recording of DAE data.

slow process, so that extended recording periods were not possible. A large amount of time was spent in digitizing the film records taken, as from ½ to 1 hour was required to digitize each minute of film record.

2.4.3 The magnetic tape DAE system

A second method for measuring differential absorption became operational in October, 1971. The transmitter was operated at a p.r.f. of 50 Hz with a change in polarization every 10 seconds. The detected output signal from the receiver was sampled by a range-scanning gate, digitized and fed in to a magnetic tape recorder. A block diagram of this system is shown in Figure 2.5. The whole system was synchronised to a 100 kHz crystal oscillator which formed part of the digitizer unit.

The range scanning gate had selectable gate widths of 2, 5 or 10 km, the gate being shifted one height increment by each transmitter trigger. The range scanned was able to be selected from several alternatives. Starting heights of 40, 50, 60, 80, 100, 120 km and cycle lengths of 5, 10, 20 and 40 steps could be combined to provide a versatile system suitable for various different experiments.

The sampled signal was digitized into one of 64 levels and written on to tape. Every ten seconds an end of record pulse was written on to the tape and this also triggered the transmitter and receiver polarization selectors.

A 2400' reel of tape was sufficient for 3 hours of recording. Each tape was computer processed in order to condense data and transfer it to a high density tape. The high density form

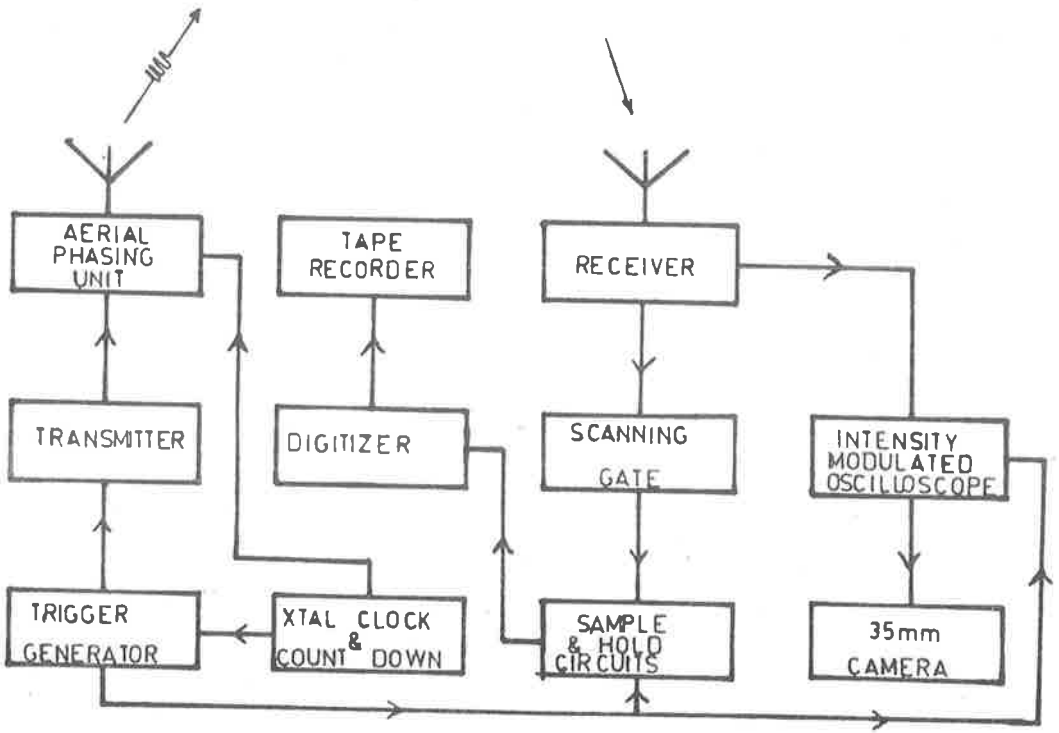


Figure 2.5 Block diagram of the magnetic tape system for recording differential absorption data.

contained all of the original information but was condensed to one fortieth of the tape space. The magnetic tape system is inherently more suitable for extended recording than is the photographic system, as there is a significant labour reduction in producing results. Also, the recording medium is reusable after analysis of the data.

2.4.4 The Phase-Path equipment

Methods for measuring the variations in phase path of a reflected radio wave have been described by several authors (e.g. Findlay, 1951; McNicol and Thomas, 1960). Essentially the same method of obtaining phase path variations has been used in this work but with the modifications described by Vincent (1967), and the method has been utilized for measuring the angular spread of received reflected waves.

The measurement of phase path variations involves comparing the phase variations of a reflected radio pulse with a c.w. phase reference oscillator of slightly differing frequency which bears a constant phase relationship to the transmitted wave. The comparison is effected by beating the reflected signal, of frequency $f_t$ say, with the phase reference oscillation, of frequency $f_r$ say, to obtain a beat frequency $f_b = f_t - f_r$. The beat oscillation will be detected after the transmitted pulse with a delay corresponding to the travel time of the radio pulse to the virtual reflection height and back.

It can be shown (e.g. Vincent, 1967) that the beat signal may be represented by an expression

$$E(t) = A(t)\ \mathrm{Cos}\ \left(2\pi\ \left(f_b t - \frac{Pf_t}{c}\right)\right) \qquad 2.1$$

where $A(t)$ is the peak beat amplitude at any instant $t$ and is determined by the reflection coefficient of a radio pulse reflector at a distance corresponding to a pulse travel time $t$, $P$ is the corresponding phase path in wavelengths and $f_t$ and $f_b$ are as previously defined.

From equation 2.1 $E(t)$ has maxima at times $t_n$ given by

$$t_n = \frac{Pf_t}{c.f_b} \quad . \qquad 2.2$$

In the system used, a beat frequency of 85 kHz was used giving about 3 "fringes" for an echo using a transmitter pulsewidth of 25 μsec. As $P$ varies equation 2.2 shows that a time shift in the occurrence of beat maxima also occurs, for a change $\Delta P$ causes a shift in $t_n$ given by

$$\Delta t_n = \frac{\Delta P f_t}{c f_b} \ ,$$

or rearranging,

$$\Delta P = \frac{c f_b\ \Delta t_n}{f_t} \quad . \qquad 2.3$$

Thus phase path changes are directly proportional to time shifts in the occurrence of beat signal "fringes" and can be monitored by monitoring the temporal variations of the beat fringes.

The above is a simplified description of the system actually used. A block diagram of the system is shown in Figure 2.6. It will be seen that $f_t$ corresponds to 1.60 MHz, $f_r$ corresponds to 1.685 MHz and thus $f_b$ = 85 kHz.

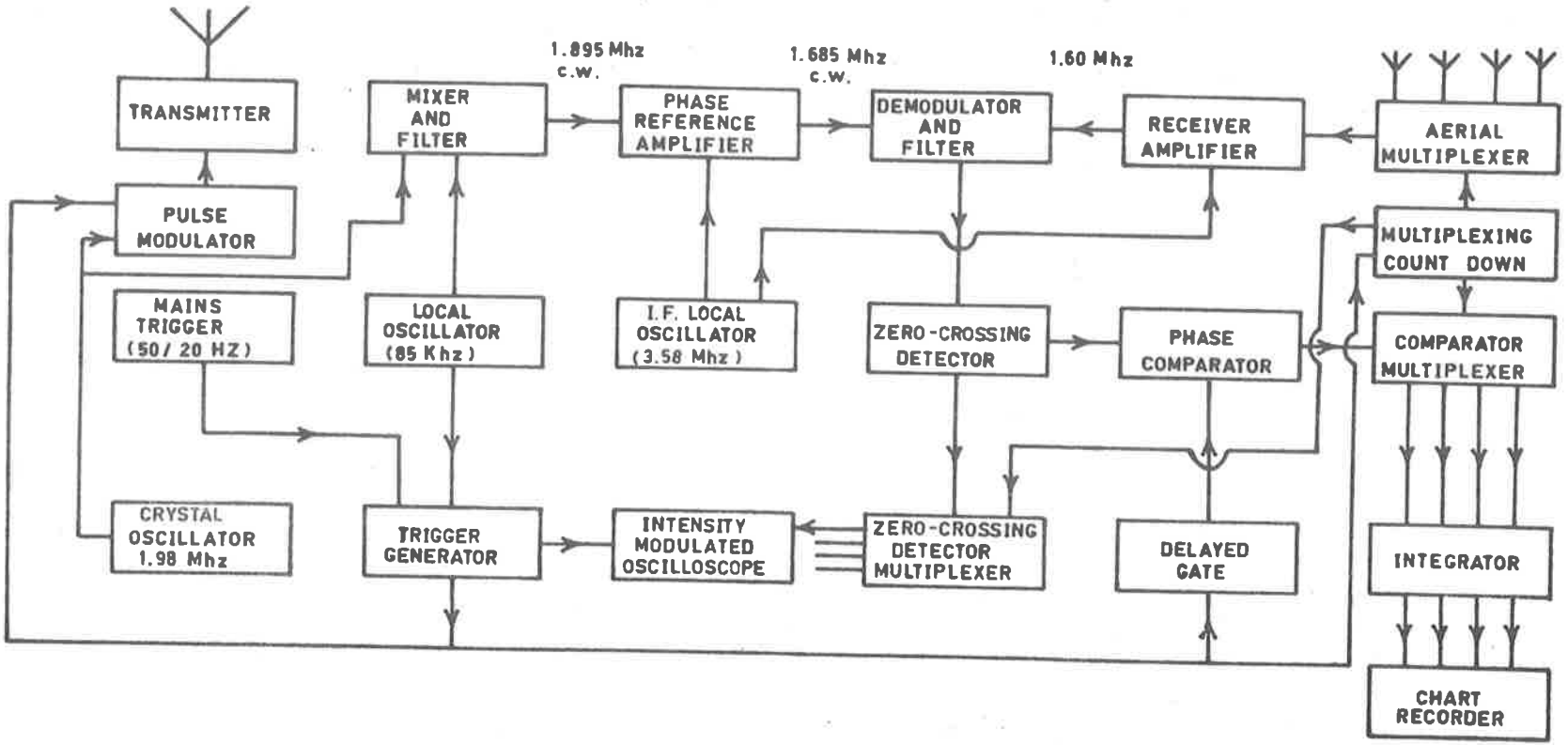


**Figure 2.6** Block diagram of the phase path system.

At the same time that the differential absorption system was modified to allow magnetic tape recording of data the phase path system was modified to enable tape recording of phase path records. This entailed changing the local oscillator (which, together with the 1.98 MHz oscillator, generated the phase reference oscillator) to 100 kHz. This frequency was conveniently derived from the reference oscillator of the digitizer/tape recorder unit. In this case the above equations have $f_t$ = 1.60 MHz, $f_r$ = 1.70 MHz, and thus $f_b$ = 100 kHz.

Two methods of recording phase path changes were possible. The first method allowed phase variations over a given range of interest to be simultaneously recorded. The beat signal described above was amplified and clipped before being used to intensity modulate a vertical oscilloscope trace which also formed a range axis. Range markers could be mixed with the bright up signal to give calibrated range dots on the oscilloscope trace. A 35 mm film moving at right angles to the trace provided the time base on the photographic records so produced. A second method involved the monitoring of only one echo at a time. A range gate was centred on an echo of interest and the variation in delay of a beat signal fringe (zero) relative to the leading edge of the gate was converted to a d.c. voltage - the voltage being proportional to the delay. As successive fringes moved through the reference level a discontinuity in voltage occurred corresponding to a phase jump, of either 0 to $2\pi$ (phase path decreasing) or $2\pi$ to 0 (phase path increasing). The voltage was then recorded on

chart or used to obtain a measure of the angular spread as described below.

2.4.5 The system for studying the angular spread of downcoming waves

The phase path equipment already described was able to produce a time varying dc voltage proportional to the variation of phase of a received gated echo. Using a multiplexer and smoothing system the method was able to be extended to monitoring the phase variations of a given echo at several different aerials.

The system for measuring the angular spread of downcoming reflected radiation was based on a 2-dimensional theory given in Chapter 3, where phase differences of signals between spaced reception points are required. Consequently, parallel connected rows of aerials, which produce an approximately 2-dimensional 'fan beam' response pattern, were used in the experiment. Figure 2.7 shows the cross sections of the computed response in the vertical planes (a) parallel to and (b) at right angles to the length of a row of aerials. A computer produced density plot of the same response is shown in Figure 2.8. Here dark regions indicate high response while light regions less response. The intensity levels cannot be taken as indicating accurate relative response but are chosen to best display the geometry of the side lobes. The use of a narrow response beam as depicted in Figures 2.7 and 2.8 also carried the advantage of reducing "sky noise" contribution to the received signal and this became an important consideration for the observation of the very weak partial reflections.

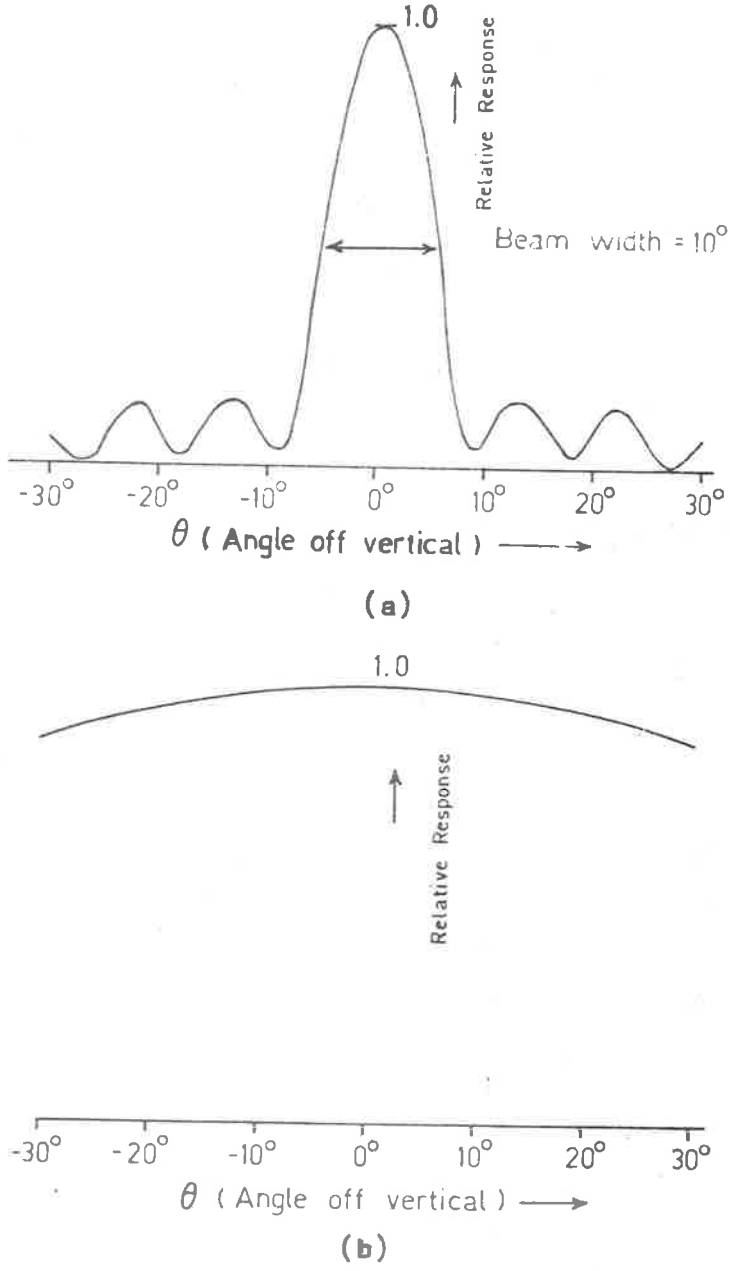


Figure 2.7 Cross sections of the response of a row of 11 dipoles:

(a) in the vertical plane parallel to the length of the row.

(b) in the vertical plane perpendicular to the length of the row.

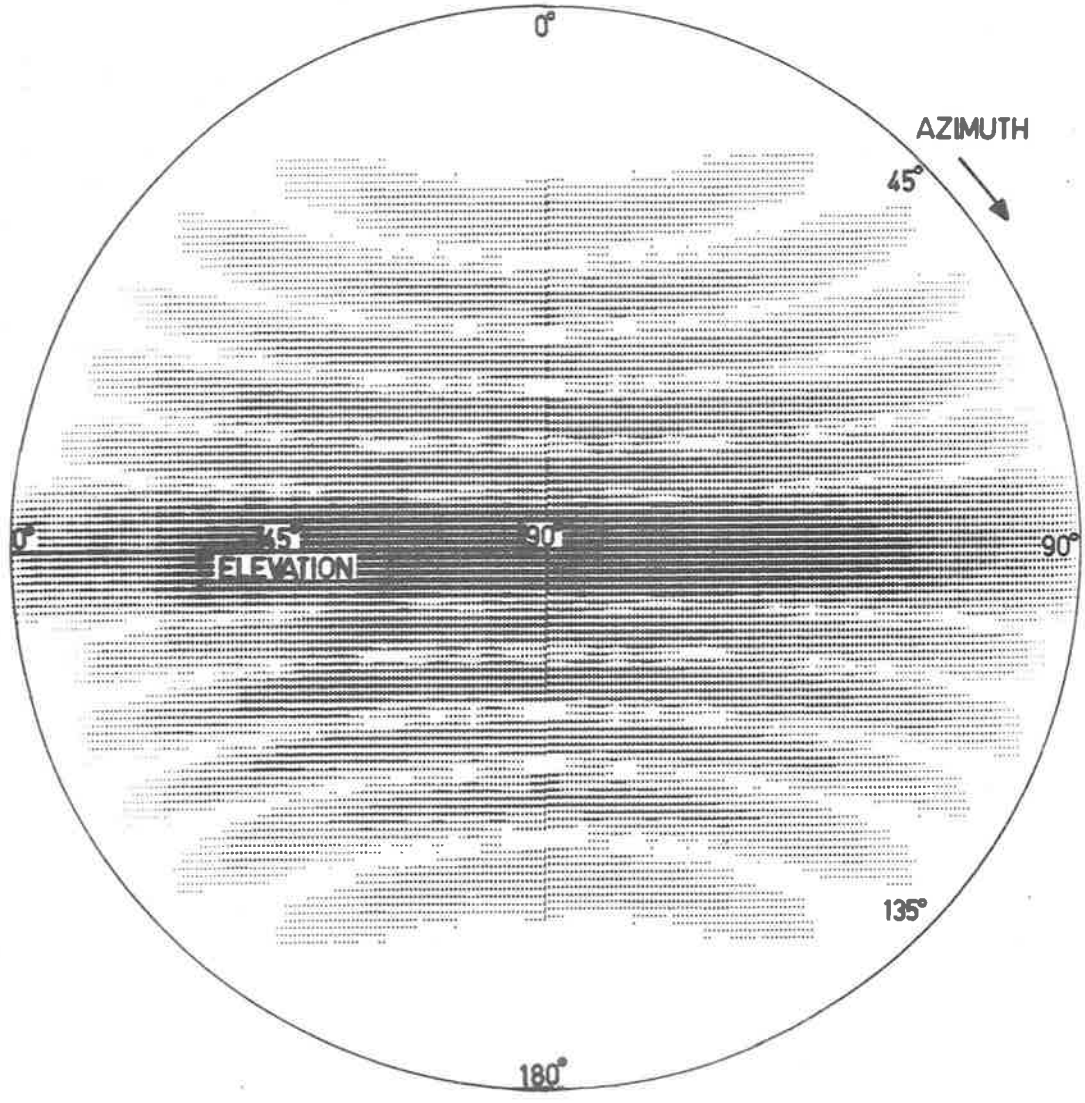


Figure 2.8 A computer produced density plot of the response of a row of receiving aerials connected in parallel.

The theory for determining the angular spread of reflected waves required the phase differences between rows of aerials, and simple difference amplifiers of calibrated gain and high linearity were used to generate proportional time varying dc voltages from the individual voltages corresponding to the phases at separate rows of aerials. Recording of phase differences was favoured over the recording of individual phases to reduce chart reading time and to enable accurate phase differences to be generated when signal phases changed rapidly. The record also directly displayed the qualitative nature of the angular spread which was proportional to the phase difference between two rows of aerials.

In practice three parallel rows of aerials were used in an experimental arrangement depicted in Figure 2.9. The phase differences between the outside rows and the centre row were formed, with one of these quantities being recorded and the difference between them being recorded as well. This latter difference of phase differences quantity was recorded in order to enable qualitative assessments of the agreement of the two estimates obtainable for the angular spread. The individual quantitative assessments could still be performed quite easily as the phase difference not recorded could simply be regained by subtraction of the two records, allowing the second determination of the angular spread to be made.

### 2.4.6 The system for studying scattering processes

The availability of amplitude and phase properties of ionospheric echoes allows deductions of the scattering processes giving

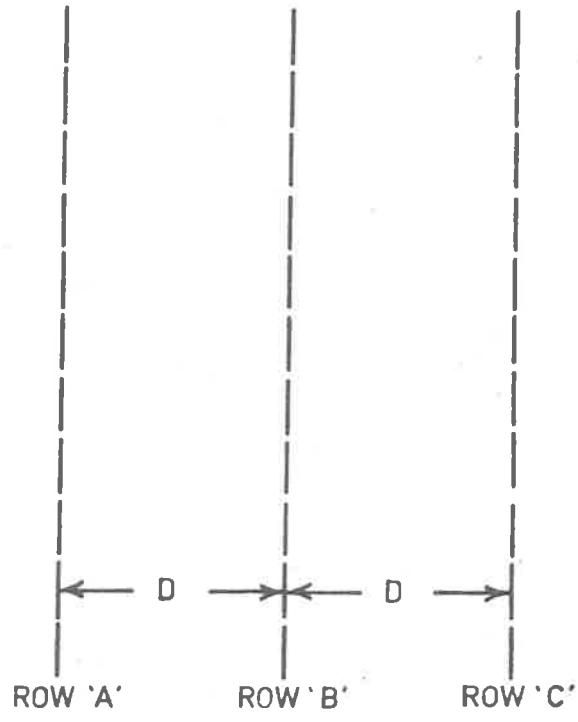


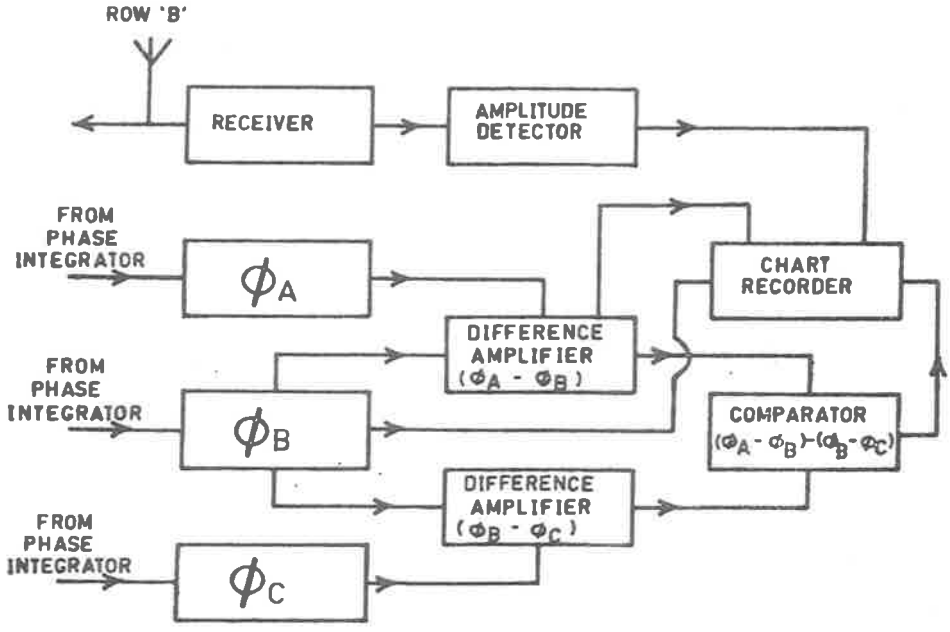


Figure 2.9 Block diagram of the system used for measuring the angular spread of downcoming waves.

rise to these echoes to be made. An experimental system was employed which was based on the theory of Chapter 3 where it is described how such deductions can be made. Again a 2-dimensional theory was employed which required the amplitudes and phases of signals at spaced rows of aerials to be determined.

With the development of the range scanning gate and associated sample and hold circuitry it became practicable to obtain amplitude and phase information for up to four rows of aerials using a signal multiplexer. Four rows of aerials in a system depicted by Figure 2.10 were used to investigate the scattering models in two planes at right angles. This enabled tests for asymmetry of the scattering geometry to be carried out.

Chart recordings of amplitudes, phases and phase differences were made on an eight channel Sanborn hot wire recorder. The recordings were subsequently digitized and converted to punched cards for computer processing.

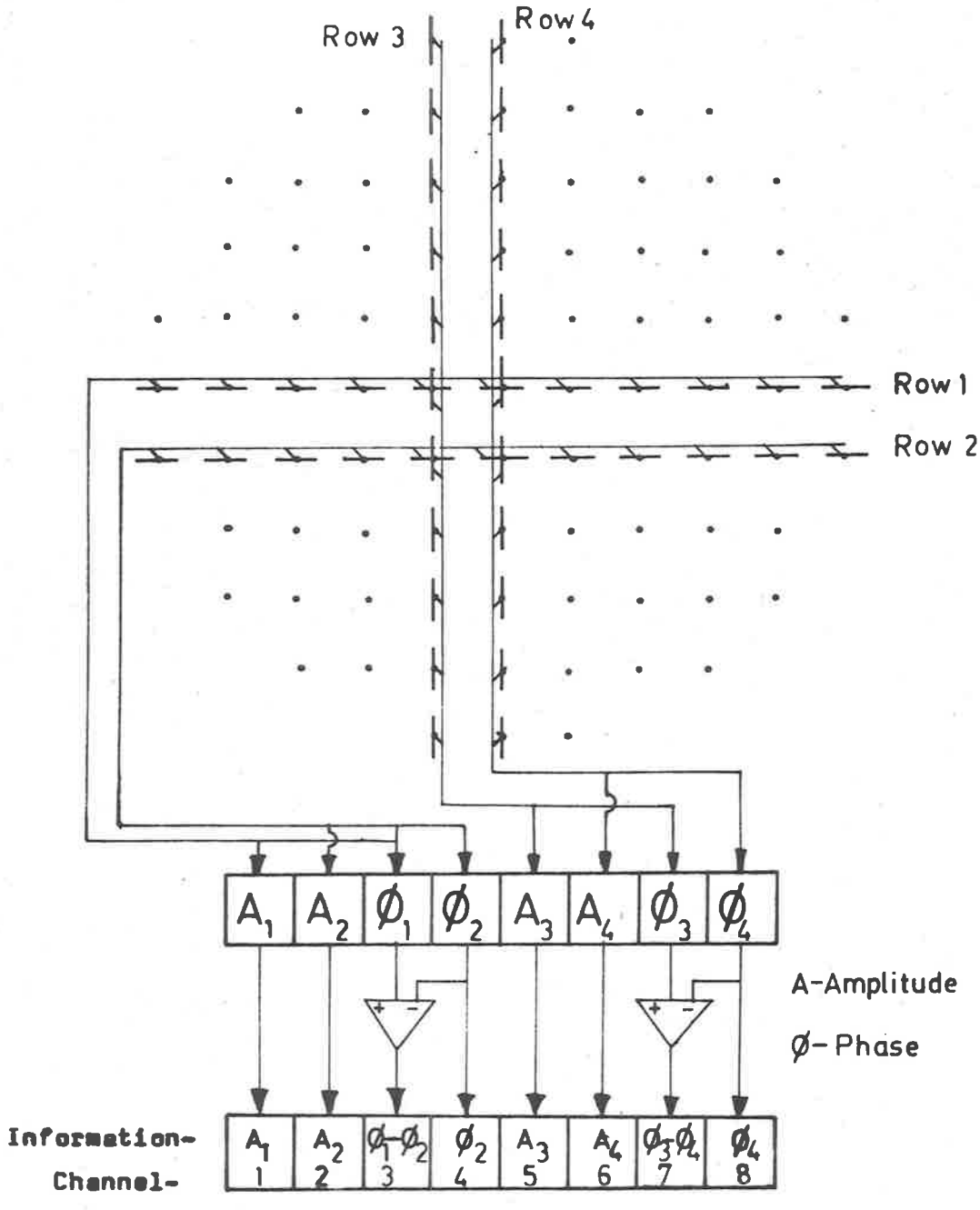


Figure 2.10 The aerial system used and information recorded on the 8 channel chart recorder, for the study of scattering models.

# CHAPTER 3

# THEORETICAL CONSIDERATIONS OF THE NATURE OF IONOSPHERIC REFLECTIONS

## 3.1 Introduction

The reliability of deductions of properties of the ionosphere using ground based radio techniques is often dependent on a knowledge of the diffractive reflection processes which give rise to the reflections observed in such experiments. This is largely due to the fact that computed reflection and absorption coefficients are dependent on the reflection process assumed.

In this chapter theoretical considerations which might form the basis for the investigation of ionospheric reflection models are described and it is shown that, subject to some assumptions, measured statistical properties of the ground diffraction pattern formed by ionospherically reflected waves may be used to derive parameters descriptive of the angular spectrum of reflected waves. The parameters which may be deduced include:-

(1) The angular spread of downcoming reflected waves,

(2) The scale of the ionospheric irregularities producing the spectrum of reflected radiation,

(3) The coherence ratio (or "signal to noise" ratio) of the reflected spectrum of waves. There are commonly two definitions of the coherence ratio depending on whether the amplitude or the

power of returned signals is considered. The coherence ratio is defined as the ratio of received power (or amplitude) due to a coeherent or specular component to the power (or amplitude) due to an incoherent or "noise" component. In the present work both forms of definition have been used to maintain consistency with the conventions adopted in related published material, but it should be clear from the context which definition applies in any particular case.

Firstly some discussion of the information derivable from amplitude information alone is presented followed by a discussion of reflection models. Initially a simple model of reflection is described in terms of phase information. Following that an approach based on that of Bramley (1951) is described, where the statistics expected for assumed reflection models are compared with experimentally measured statistics to give a model of best fit. In this approach both amplitude and phase statistics of the ground diffraction pattern, as deduced from signals received on a pair of spaced aerials, are taken into consideration. Bramley's equations are, however, subject to a restriction of high correlation between the signals received on the spaced sampling aerials. Since practical situations have often arisen where fairly low correlation occurs the equations have been generalised to remove the restriction of high correlation. The theory allows an estimation to be made of the angular spread of reflected waves as well as the relative contribution of coherent and non coherent components to the received signal, provided that the coherence ratio is large compared with unity. Section 3.4 outlines some aspects of generalised

correlation theory which describes the relation between the angular power spectrum of reflected waves and the scale of the scattering ionospheric irregularities. Finally a discussion and summary of the various techniques is given.

## 3.2 Deductions from amplitude distributions

Amplitude information is commonly the most easily obtained quantity in experimental systems for observing ionospheric reflections. A simple assessment of the coherence ratio for a given signal might be made from such observations. If Figure 3.1a depicts a hypothetical record of the variation with time of the amplitude of a given echo, where the coherence or signal to noise ratio is large, then a displaced Gaussian distribution of amplitude such as that shown by the solid curve in Figure 3.1b might be reasonably expected. A reasonable estimate of the amplitude coherence ratio would then be $A_m/A_n$, where $A_m$ is the mean amplitude and $A_n$ is the standard deviation from the mean. However when even a completely incoherent signal is received this ratio would not be zero as can be seen from the Rayleigh distribution expected in this case and shown by the dashed curve in Figure 3.1b, so that in such a situation the estimate of coherence ratio becomes inaccurate. This method is therefore suitable only for large values of coherence ratio and another technique needs to be used for determining small values of coherence ratio.

One such technique is based on the theory of Rice (1945). Although Rice's work applied to electric circuits, the theory is completely analogous for an ionospheric reflection model which assumes

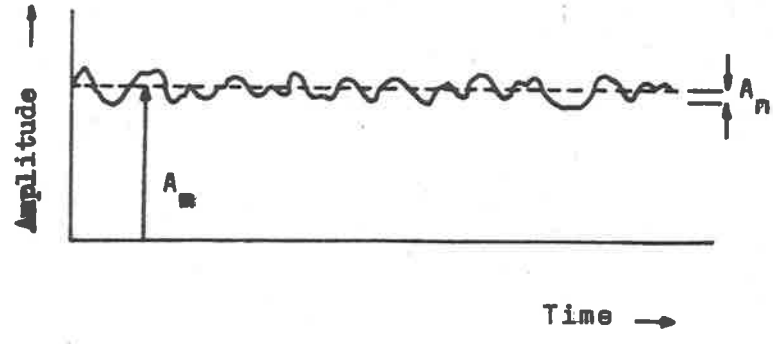


(a)

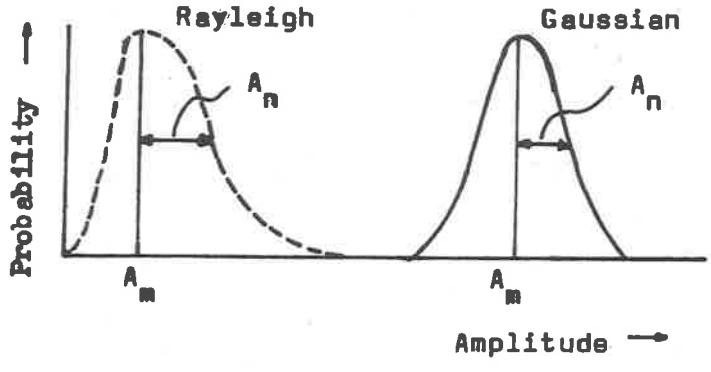


(b)

Figure 3.1 (a) A hypothetical record of the variation of amplitude with time for a signal having a high coherence ratio.

(b) The amplitude distributions expected for zero (dashed curve) and large (solid curve) coherence ratios.

that a steady signal of constant amplitude and phase is received in the presence of a spectrum of randomly phased contributions. A family of amplitude distributions with the coherence (or signal to noise) ratio as a parameter can then be calculated directly from Rice's (1945) theory. Fitting an observed amplitude distribution to one of this family of curves theoretically allows the coherence ratio to be determined. For zero coherence ratio an asymmetric Rayleigh distribution, as depicted by the dashed curve of Figure 3.1b, is expected while for increasing coherence ratios a transition to the symmetric displaced Gaussian distribution is obtained.

## 3.3 Reflection models

Many installations for studying ionospheric reflections employ sophisticated techniques for studying the phase as well as the amplitude of reflected signals and this extra information can provide further information about the nature of reflected signals. The remainder of this chapter is devoted to a discussion of amplitude and phase statistics as expected for different assumed reflection models.

### 3.3.1 A specular reflection wandering about in direction of arrival

A simple model worthy of consideration is one where a single specular signal is returned from an off-vertical angle varying in time about some mean direction, say vertical. If we consider a two dimensional case where the ray is confined to a vertical plane containing the line joining the centres of two receiving aerials, the phase difference $\phi$ between such aerials at any instant will be

$$\phi = \frac{2\pi d \, \mathrm{Sin}\theta}{\lambda} \quad ,$$

where $\theta$ is the angle the ray is making with the vertical at that instant, d is the aerial spacing and $\lambda$ is the probing wavelength. If $\theta$ is small enough (so that $\mathrm{Sin}\theta \simeq \theta$) rearrangement of the above equation gives the absolute deviation of the ray from vertical as

$$|\theta| = \frac{\lambda \, |\phi|}{2\pi d} \quad ,$$

so that the mean absolute deviation from vertical is

$$\overline{|\theta|} = \frac{\lambda \, \overline{|\phi|}}{2\pi d} \quad . \qquad 3.1$$

Equation 3.1 shows that a record of the phase difference between a spaced pair of receiving aerials allows an estimate of $\overline{|\theta|}$ to be made if such a reflection model is appropriate. The determination of an appropriate model from experimental measurements is discussed in the following sections.

3.3.2 A continuous distribution of randomly phased rays

A pair of receiving aerials is assumed to be under the influence of a continuous distribution of randomly phased reflected waves which is confined to the vertical plane containing the line joining the centres of the spaced aerials. The amplitude and phase statistics expected for such a distribution, as derived by Bramley (1951), will now be outlined and extensions of Bramley's theory to cover general correlation conditions will be described.

3.3.2a Amplitude statistics

Let $W(\theta)d\theta$ be the power contribution from an angular sector $\theta \pm \frac{1}{2}d\theta$ where $\theta$ is the angle from vertical. The total power arriving due to all rays in the contributing plane is then

$$W_o = \int_{-\pi/2}^{+\pi/2} W(\theta)d\theta \ . \qquad 3.2$$

Following Bramley (1951) a convenient correlation function R is now defined, for a pair of aerials separated by a distance d and receiving signals of wavelength $\lambda$, by the relation

$$R^2 = \frac{\alpha^2 + \beta^2}{W_o^2} \ , \qquad 3.3a$$

where

$$\alpha = \int_{-\pi/2}^{+\pi/2} W(\theta) \cos\left(\frac{2\pi d \ \mathrm{Sin}\theta}{\lambda}\right) d\theta \qquad 3.3b$$

and

$$\beta = \int_{-\pi/2}^{+\pi/2} W(\theta) \sin\left(\frac{2\pi d \ \mathrm{Sin}\theta}{\lambda}\right) d\theta \ . \qquad 3.3c$$

If we now assume $W(\theta)$ has the Gaussian form

$$W(\theta) = \frac{W_o}{(2\pi)^{\frac{1}{2}}\theta_o} \times \exp\left(\theta^2/2\theta_o^2\right) \qquad 3.4$$

then equations 3.3a, b, c can be used to evaluate R in terms of the parameter $\theta_o$, which is the rms width of the distribution of equation 3.4. The evaluation is rather complicated unless $W(\theta)$ is assumed to be appreciable only for fairly small values of $\theta$, and then it can be shown (Bramley, 1951) that

$$R = \exp - \left\{2\left(\frac{\pi d}{\lambda}\ \theta_o\right)^2\right\} \ . \qquad 3.5$$

Now Rice (1945) has shown that if $A_1$ and $A_2$ are the amplitudes received at the two aerials, then the joint probability distribution of $A_1$ and $A_2$ is given by

$$p(A_1,A_2) = \frac{A_1\,A_2}{W_o^2(1-R^2)}\, I_o\left\{\frac{RA_1\,A_2}{W_o^2(1-R^2)}\right\} \times \exp - \left\{\frac{A_1^2 + A_2^2}{2W_o(1-R^2)}\right\}, \qquad 3.6$$

where $I_o$ is the hyperbolic Bessel function of zero order and the other symbols have already been explained. Since the quantities $\overline{A_1\,A_2}$ and $\overline{A_1} = \overline{A_2}$ can be evaluated from equation 3.6 in terms of R, then the amplitude correlation coefficient $\rho_A$, where

$$\rho_A = \frac{\overline{(A_1 - \overline{A_1})\,(A_2 - \overline{A_2})}}{\{\overline{(A_1 - \overline{A_1})^2(A_2 - \overline{A_2})^2}\}^{\frac{1}{2}}},$$

can also be evaluated in terms of R, and hence related to $\theta_o$ through equation 3.5. It can then be shown (Bramley, 1951) that

$$\rho_A = \frac{4\{E(R) - \tfrac{1}{2}(1-R^2)K(R)\} - \pi}{4 - \pi}, \qquad 3.7$$

where K(R) and E(R) are complete elliptic integrals of the first and second kind respectively. It is difficult to obtain values of $\theta_o$ using equations 3.7 and 3.5 unless the assumption that R = 1 is made, whereupon the elliptic integrals simplify considerably and Bramley has shown that the following result is obtained:

$$(4 - \pi)(1 - \rho_A) = 1 - R^2$$

$$= 4\left(\frac{\pi d}{\lambda}\,\theta_o\right)^2. \qquad 3.8$$

Making $\theta_o$ the subject of this equation gives

$$\theta_o = \frac{(4 - \pi)^{\frac{1}{2}} \lambda \ (1 - \rho_A)^{\frac{1}{2}}}{2\pi d} \ , \qquad 3.9$$

which then allows an estimate of $\theta_o$ to be made from a measurement of $\rho_A$, the correlation coefficient between amplitudes received on two aerials separated by a distance d, with the restriction that $R \simeq 1$. An alternative approach which allows $\theta_o$ to be evaluated for general values of R is one where the correlation coefficient, $\rho_{A^2}$, between squared amplitudes is measured, where the correlation coefficient is defined in the same manner as for $\rho_A$. Equation 3.6 allows an evaluation of the quantities

$$\overline{A_1^2 \ A_2^2} = 4W_o^2(1 + R^2)$$

and

$$\overline{A_1^4} = \overline{A_2^4} = 8W_o^2 \ .$$

The correlation coefficient $\rho_{A^2}$ can then be found to be

$$\rho_{A^2} = R^2 \ . \qquad 3.10$$

Using this equation in conjunction with equation 3.5 we now obtain

$$\theta_o = \frac{\lambda}{2\pi d} \{- \log_e \ (\rho_{A^2})\}^{\frac{1}{2}} \ , \qquad 3.11$$

which is an estimate of the angular spread of reflected signal without restrictions on the degree of correlation, R, between the aerials.

Bramley has shown that another estimate of $\theta_o$ from amplitude difference measurements is also possible. The joint probability distribution of equation 3.6 allows the distribution of $x = A_1 - A_2$ , the difference in amplitudes at the two aerials, to be estimated from

$$p(x) = \int_o^\infty p(A_1, A_1 - x)dA_1 \ . \qquad 3.12$$

For values of R near to unity, this distribution is normal (Bramley, 1951) and is given by

$$p(x) = \frac{1}{\{2\pi W_o(1 - R^2)\}^{\frac{1}{2}}} \exp - \{x^2/(2W_o(1 - R^2))\} \ . \qquad 3.13$$

Then calculating

$$\overline{|x|} = 2\int_o^\infty x\, p(x)dx$$

$$= \frac{2}{\pi}\overline{A}\,(1 - R^2)^{\frac{1}{2}}$$

and putting $\overline{|x|}/\overline{A} = \rho_D$ (the difference correlation coefficient) gives

$$\rho_D = \frac{2}{\pi}(1 - R^2)^{\frac{1}{2}} \ . \qquad 3.14$$

This equation can be used in conjuntion with equation 3.5 to obtain

$$\theta_o = \frac{\lambda\rho_D}{4d} \ , \qquad 3.15$$

which gives another estimate of the angular spread under the model assumed, and in terms of the measurable quantity $\rho_D$. However, again this estimate is subject to the restriction that R be close to unity as the distribution of equation 3.13 was based on this assumption. The form of this distribution for general values of R has been shown by Fürth and MacDonald (1947) to be

$$p(x) = \left(\frac{1 - z^2}{8\,\overline{A}^2}\right)^{\frac{1}{2}} \times \exp - \left\{\frac{\pi x^2}{4\,\overline{A}^2(1 - z^2)}\right\}$$

$$\times \int_o^\infty \frac{(1 + \xi)\exp\{\pi x^2\xi/8\overline{A}^2(1 - z^2)\}}{\xi^{\frac{1}{2}}\{(1 + \xi)^2 - z^2\}^{3/2}}\, d\xi \qquad 3.16$$

where $z = \exp - \{(1 - R^2)/2\}$ .

It can be shown that the definition

$$\overline{|x|} = 2 \int_o^\infty x\, p(x)dx$$

leads to the relation

$$\rho_D = \frac{\overline{|x|}}{\overline{A}} \simeq (2 - \sqrt{2})\{1 - \exp\,(R^2 - 1)\}^{\frac{1}{2}} \,. \qquad 3.17$$

Using equations 3.5 and 3.17 the following expression for $\theta_o$ has been derived:-

$$\theta_o = \frac{\lambda}{2\pi d}\left[-\log_e\{\log_e\,(1 - \rho_D{}^2/(6 - 4\sqrt{2})) + 1\}\right]^{\frac{1}{2}} \,. \qquad 3.18$$

This expression is valid for general values of R.

3.3.2b Phase statistics

Rice (1945) has calculated the form of the joint probability distribution $p(A_1, A_2, \psi_1, \psi_2)$ where $A_1$, $A_2$, $\psi_1$ and $\psi_2$ are the amplitudes and phases of the signals received at two spaced aerials. Integrating this probability over all values of $A_1$ and $A_2$ from 0 to $\infty$ the joint distribution of phases $p(\psi_1, \psi_2)$ has been determined by MacDonald (1949) as

$$p(\psi_1, \psi_2) = \frac{1 - R^2}{4\pi^2}\left\{\frac{1}{1 - g^2} + \frac{g}{(1 - g^2)^{3/2}}\,(\pi/2 + \text{arc sin}(g))\right\} \,, \qquad 3.19$$

where $g = R \cos\,(\psi_1 - \psi_2)$ .

Bramley (1951) has calculated the probability distribution of phase differences from this distribution and this is given by

$$p(\phi) = \frac{1 - R^2}{2\pi}\left\{\frac{1}{1 - R^2\cos^2\phi} + \frac{R\cos\phi}{(1 - R^2\cos^2\phi)^{3/2}}\left[\pi/2 + \text{arc sin}\,(R\cos\phi)\right]\right\}$$

3.20

where $\phi = \psi_1 - \psi_2$ .

The mean absolute phase difference $\overline{|\phi|}$ is thus able to be calculated and the following simple result has been obtained by Bramley:-

$$\overline{|\phi|} = 2 \int_o^\pi \phi \, p(\phi) d\phi$$

$$= \text{arc cos}(R) \, . \qquad 3.21$$

For R close to unity $\overline{|\phi|}$ can thus be expanded in terms of $\Delta = (1 - R)$ as

$$\overline{|\phi|} = \sqrt{2\Delta} \, (1 + \Delta/12 + 3\Delta^2/160 + \ldots.)$$

so that

$$1 - R \simeq \tfrac{1}{2} \, \overline{|\phi|}^2 \, .$$

From equation 3.5 one obtains

$$\theta_o = \frac{\lambda \, \overline{|\phi|}}{2\pi d} \, , \qquad 3.22$$

which gives an estimate of the angular spread in terms of the mean absolute phase difference between the aerials when R is close to unity. To generalise this expression for $\theta_o$ to all values of R we can use the general result of equation 3.21 with equation 3.5 to obtain

$$\theta_o = \frac{\lambda}{\sqrt{2}\,\pi d} \{- \log_e (\cos \overline{|\phi|}) \}^{\frac{1}{2}} \, . \qquad 3.23$$

This equation is not subject to the restriction that R should be close to unity.

At this point it is interesting to compare equations 3.2 and 3.22. It is clear that the same relation between $\overline{|\phi|}$ and a measure of the angular spread of downcoming waves holds even for two models of opposite extremes; one model assuming a single specular reflection

varying in direction of arrival and the other assuming a fan of randomly phased rays. It might be intuitively suggested that the same relation holds for models which represent a combination of these two models or even that the relation is a completely general one covering all situations. Some experimental evidence tending to support the latter hypothesis is discussed in the next chapter.

3.3.3 A continuous distribution of randomly phased rays in the presence of a steady signal

The foregoing analysis applies to a continuous distribution of waves with random phases, as might be expected after diffractive reflection from a rough surface. The term "rough" is used in comparing the scale of irregularities in the diffracting surface with the wavelength of the propagating radio waves. This section considers the case where such a distribution of rays exists simultaneously with a coherently reflected signal of fixed amplitude and direction. Such a situation might arise when a stable strong reflector has weak fine scale irregularities imposed upon it, or when a reflecting surface has weak irregularities below it.

3.3.3a Amplitude statistics

Again using the approach of Bramley (1951) we consider m coplanar rays with random phases incident on a spaced pair of aerials. The voltages induced on the aerials will be

$$v_1 = \sum_{r=1}^{m} a_r \cos(\omega t + \psi_r + \chi_r) \qquad 3.24a$$

and

$$v_2 = \sum_{r=1}^{m} a_r \cos(\omega t + \psi_r - \chi_r) , \qquad 3.24b$$

where $\chi_r = \frac{\pi d}{\lambda} \sin \Omega_r$ and $\Omega_r$ = off vertical angle of arrival of the $r^{th}$ ray. Following the approach of Rice (1945) equations 3.24a,b can be rewritten

$$v_1 = B_{1c} \cos \omega t - B_{1s} \sin \omega t \qquad 3.25a$$

$$v_2 = B_{2c} \cos \omega t - B_{2s} \sin \omega t \qquad 3.25b$$

where

$$B_{1c} = \Sigma a_r \cos (\psi_r + \chi_r)$$

$$B_{2c} = \Sigma a_r \cos (\psi_r - \chi_r)$$

$$B_{1s} = \Sigma a_r \sin (\psi_r + \chi_r)$$

$$B_{2s} = \Sigma a_r \sin (\psi_r - \chi_r)$$

and these summations extend over the m rays. We also note in passing that $\overline{B_{1c}B_{2c}} = \overline{B_{1s}B_{2s}} = \alpha$ and $\overline{-B_{1c}B_{2s}} = \overline{-B_{2c}B_{1s}} = \beta$, if the summations are converted to integrals, where $\alpha$ and $\beta$ have been defined in section 3.3.2. If now a steady signal in the presence of this "noise" is considered the expressions of 3.25 become

$$v_1 = S \cos (\omega t + \chi_o) + B_{1c} \cos \omega t - B_{1s} \sin \omega t \qquad 3.26a$$

$$v_2 = S \cos (\omega t - \chi_o) + B_{2c} \cos \omega t - B_{2s} \sin \omega t \qquad 3.26b$$

where $S \cos (\omega t + \chi_o)$ and $S \cos (\omega t - \chi_o)$ are the voltages produced in the respective aerials by a steady signal of amplitude S and arriving from an off vertical direction $\Omega_o$ so that

$$\chi_o = \frac{\pi d \sin \Omega_o}{\lambda}$$

is half the phase difference of the signal between the spaced aerials.

Equations 3.26 then give

$$A_1^2 = S^2 + 2S(B_{1c} \cos \chi_o + B_{1s} \sin \chi_o) + B_{1c}^2 + B_{1s}^2 \qquad 3.27a$$

$$A_2^2 = S^2 + 2S(B_{2c} \cos \chi_o - B_{2s} \sin \chi_o) + B_{2c}^2 + B_{2s}^2 \ , \qquad 3.27b$$

whence

$$\overline{A_1^2} = \overline{A_2^2} = S^2 + 2W_o \ , \qquad 3.28$$

where $W_o$ has been defined by equation 3.2. The amplitude correlation statistics may now be evaluated. The evaluation is difficult unless the coherence ratio ($b = S/\sqrt{2W_o}$) is large compared to unity, and then equation 3.27 gives

$$A_1 \simeq S + B_{1c} \cos \chi_o + B_{1s} \sin \chi_o + \frac{1}{2S} (B_{1c} \sin \chi_o - B_{1s} \cos \chi_o)^2 \qquad 3.29a$$

$$A_2 \simeq S + B_{2c} \cos \chi_o - B_{2s} \sin \chi_o + \frac{1}{2S} (B_{2c} \sin \chi_o + B_{2s} \cos \chi_o)^2 \ . \qquad 3.29b$$

The quantities $A_1$, $\overline{A_1}\,\overline{A_2}$ and $\overline{A_1 A_2}$ may now be evaluated in order to calculate the amplitude correlation coefficient $\rho_A$. The result (Bramley, 1951) is

$$\rho_A = \frac{1}{W_o} \int_o^{2\pi} W(\Omega) \cos \left\{\frac{2\pi d}{\lambda} (\cos \Omega - \cos \Omega_o)\right\} d\Omega \ . \qquad 3.30$$

If the distribution W is assumed to have the Gaussian form of equation 3.4 then equations 3.30 and 3.2 show that

$$\rho_A = R \ . \qquad 3.31$$

Assuming a correlation of approximately unity in equation 3.5 yields the result

$$\theta_o = \frac{\lambda}{\pi d} \left(\frac{1 - \rho_A}{2}\right)^{\frac{1}{2}} \ . \qquad 3.32$$

This equation gives the angular spread in terms of the measured amplitude correlation coefficient, between a pair of spaced receiving aerials, when a system of randomly phased contributions with one steady component is present. The restriction that R be close to unity is easily removed by deducing the analytic expression for $\theta_o$ from equations 3.31 and 3.5. The result is

$$\theta_o = \frac{\lambda}{\sqrt{2}\,\pi d} \{- \log_e (\rho_A)\}^{\frac{1}{2}} . \qquad 3.33$$

An estimation of the coherence ratio b can be made from a measurement of the amplitude difference correlation coefficient. Bramley (1951) has shown that the distribution of $x = A_1 - A_2$ is given by

$$p(x) = \frac{1}{2(\pi W_o)^{\frac{1}{2}}(1 - R)^{\frac{1}{2}}} \cdot \exp - x^2/4\, W_o(1 - R) \qquad 3.34$$

and that

$$\overline{|x|} = 2\left\{\frac{W_o(1 - R)}{\pi}\right\}^{\frac{1}{2}}$$

$$\simeq \frac{\overline{A}}{b} \left\{\frac{2(1 - R)}{\pi}\right\}^{\frac{1}{2}} . \qquad 3.35$$

Putting $\overline{|x|}/\overline{A} = \rho_D$ and using equations 3.35 and 3.31 the coherence ratio is

$$b = \frac{1}{\rho_D} \left\{\frac{2(1 - \rho_A)}{\pi}\right\}^{\frac{1}{2}} . \qquad 3.36$$

This expression is valid for general values of correlation so that further generalisation is unnecessary.

3.3.3b Phase statistics

Bramley (1951) has shown that for the case where there is a strong coherent signal in the presence of randomly phased incoherent components ("noise") the resultant phase at either aerial is normally distributed. Furthermore he has shown that the correlation coefficient between phases, $\rho_\psi$, is equal to the amplitude correlation coefficient and both are equal to R. Since $\rho_\psi = R$ we may use equation 3.5 to obtain $\theta_o$ as

$$\theta_o = \frac{\lambda}{\sqrt{2}\,\pi d} \{- \log_e (\rho_\psi)\}^{\frac{1}{2}} . \qquad 3.37$$

This provides another estimate of $\theta_o$ from a measurement of $\rho_\psi$. The distribution of $\phi = (\psi_1 - \psi_2 - 2\chi_o)$ has been deduced by Bramley as

$$p(\phi) = \frac{b}{\{2\pi(1 - R)\}^{\frac{1}{2}}} \cdot \exp - \left\{\frac{b^2\phi^2}{2(1 - R)}\right\} .$$

Hence the mean absolute phase difference $\overline{|\phi|}$ is found to be

$$\overline{|\phi|} = \frac{1}{b} \left\{\frac{2(1 - R)}{\pi}\right\}^{\frac{1}{2}} . \qquad 3.38$$

Rearranging this expression and using equation 3.31 the expression for b becomes

$$b = \frac{1}{\overline{|\phi|}} \left\{\frac{2(1 - \rho_A)}{\pi}\right\}^{\frac{1}{2}} . \qquad 3.39$$

This gives a second estimate of the coherence ratio and is valid for general values of the correlation function R.

## 3.4 Generalised auto-correlation techniques

While the preceding analysis provides a basis for the investigation of the scattering model it does not include the relationship of the scale size of ionospheric scattering irregularities to the observed scattering parameters. A more complete and elegant description of the total picture and in particular of the relationship of the scattering parameters to the physical properties of the diffractively reflecting "screen" is provided by generalised correlation theory. In the following sections this approach as applied to considerations of the ionosphere is outlined. A more detailed description may be found in Ratcliffe (1956) on which most of the following work is based.

### 3.4.1 Generalised auto-correlation functions

Up until now all of the correlation analysis described has separated the amplitude and phase statistics. A more generalised approach is that in which the diffraction pattern is described in terms of a complex wave field, containing both phase and amplitude information.

Consider a two dimensional fan of downcoming radiation producing a one dimensional variation of complex wave field $E(x)$ on the ground. The function $E(x)$ might suitably be represented by

$$E(x) = a(x) \exp (i\phi(x)) \qquad 3.40$$

Two "generalised" (or 'complex') auto-correlation functions, the widths of which are a measure of the scale size of irregularities in $E(x)$, may now be defined as follows:-

$$r_E(\xi) = \frac{[E(x)E^*(x+\xi)]_{av}}{[E(x)E^*(x)]_{av}} \qquad 3.41$$

and

$$\rho_E(\xi) = \frac{[E(x)E^*(x+\xi)]_{av} - |[E(x)]_{av}|^2}{[E(x)E^*(x)]_{av} - |[E(x)]_{av}|^2} . \qquad 3.42$$

An experimental determination of these functions from amplitude and phase information might well reveal the nature of these functions to be as depicted in Figure 3.2. The effect of a coherent component in the presence of randomly scattered power with a coherence ratio B is evident. Here B is the power coherence ratio and in terms of the formerly used symbol b is, $B = b^2$. The function $r_E(\xi)$ tends to a lower limit B/B + 1 as $\xi$ increases expressing the fact that, due to the steady coherent component, some correlation exists between signals at spaced points even for very large separations. On the other hand $\rho_E(\xi)$, which by the definition of equation 3.42 has the mean field (due to the steady component) removed, tends to zero as $\xi$ increases, expressing the fact that little correlation between widely spaced points is expected for the randomly scattered component. As might be reasonably expected, for a given separation $\xi$, the value of $r_E(\xi)$ will be greater than $\rho_E(\xi)$ since the former function includes the effect of the specular or steady component in its evaluation. Ratcliffe (1956) has shown that $r_E(\xi)$ and $\rho_E(\xi)$ are in fact related by the expression

$$r_E(\xi) = \frac{B + \rho_E(\xi)}{B + 1} . \qquad 3.43$$

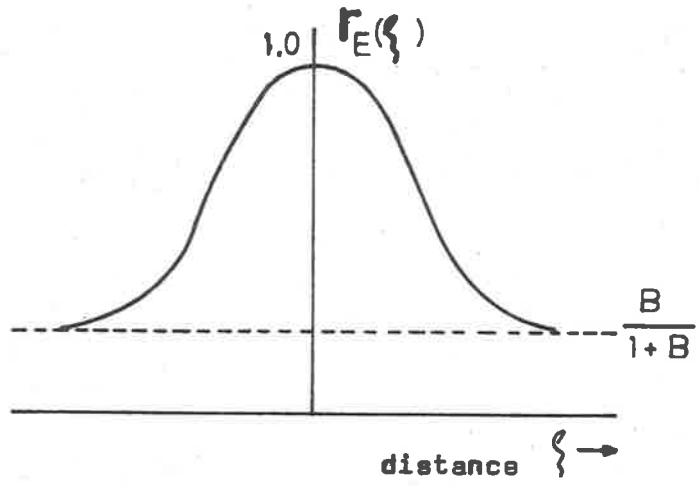


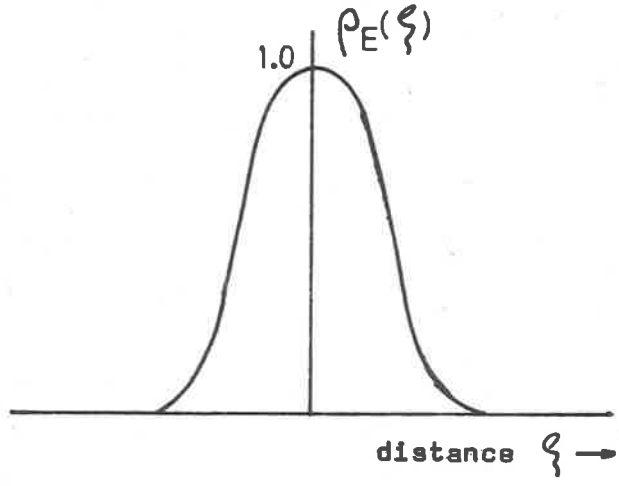


**Figure 3.2** Two forms of generalized spatial auto-correlation function of a complex wave field E.

It is worth mentioning, in passing, the relation of the functions $\rho_E(\xi)$ and $r_E(\xi)$ to the function R described in the analysis of previous sections. It can be shown that in general

$$R^2 = |\rho|^2$$

if $\rho$ is complex. If scattering is symmetrical about some mean direction $\rho$ will be real and the following relation holds

$$R = \rho.$$

The relation between R and $r_E(\xi)$ now simply follows from equation 3.43.

3.4.2 The angular power spectrum

The Wiener-Khintchine theorem conveniently describes the angular power spectrum as the Fourier transform of the generalised auto-correlation function of the complex wave field immediately after diffraction by the ionospheric "screen". Booker, Ratcliffe and Shinn (1950) have shown that the generalised auto-correlation function, however, is the same in all planes parallel to the diffracting screen independent of their distance from the screen so that a measurement of the generalised auto-correlation function is equally well made on the ground rather than near to the ionospheric screen. The Fourier transform relations between the correlation functions $r(\xi)$ and $\rho(\xi)$ and their respective angular power spectra are discussed in the following section and are summarized by Figure 3.3.

### 3.4.3 The angular spread of downcoming waves and the scale size of diffracting irregularities

If $\Delta N(x)$ is a function representing the difference from the mean of the electron density in the scattering screen then the generalised auto-correlation function $\rho_{\Delta N}(\xi)$ contains information about the scale size of irregularities in the ionization $N(x)$. It is of interest to determine what the relation is between this function and the functio $\rho_E(\xi)$ which may be measured on the ground. The answer to this lies in two parts depending on the nature of the scattering screen. Ratcliffe (1956) has shown that in general the complex amplitudes $f(x)$ of a wave on emerging from a scattering screen may be represented by

$$f(x) = \exp \{i\Delta\phi(x)\} , \qquad 3.44$$

where

$$\Delta\phi(x) = C \exp (i\psi)\cdot\Delta N(x) . \qquad 3.45$$

Here $\Delta\phi(x)$ is the complex phase and C and $\psi$ are constants characteristic of the medium, where

$$\tan \psi = - \nu/\omega . \qquad 3.46$$

Using such a representation, and assuming $\Delta N(x)$ is a random function normally distributed with standard deviation $N_m$, Bramley (1955) has shown that the auto-correlation function of $f(x)$ is given by

$$r_f(\xi) = \exp \{- \phi_m^2 (1 - \rho_{\Delta N}(\xi))\} , \qquad 3.47$$

where $\phi_m$ is the standard deviation of $|\Delta\phi(x)|$ and may be expressed as

$$\phi_m = (A_o^2 + \phi_o^2)^{\frac{1}{2}} ,$$

where $A_o$ is the standard deviation of the amplitude in nepers and $\phi_o$ the standard deviation of the phase in radians which has been impressed

on the incident wave by the diffracting screen. Two important cases for equation 3.47 now arise.

(1) $\phi_m^2 \ll 1$ . In this case the scattering is called weak in that the returned spectrum of waves contains a large undeviated (specular) component as well as diffuse components. Then equation 3.47 becomes

$$r_f(\xi) = 1 - \phi_m^2 \{1 - \rho_{\Delta N}(\xi)\} . \qquad 3.48$$

Comparison with equation 3.43 shows that

$$b = 1/\phi_m^2 \quad \text{and} \quad \rho_E(\xi) = \rho_{\Delta N}(\xi) . \qquad 3.49$$

If $\rho_E(\xi)$ is of the form

$$\rho_E(\xi) = \exp - (\xi^2/\ell^2) \qquad 3.50$$

then where $\xi = \ell$ this function falls to 1/e and $\ell$ is a measure of the scale of the ground diffraction pattern and hence also of the ionospheric ionization irregularities (see equation 3.49). In fact due to the transmitter being effectively a point source the ground pattern scale will be twice the true ionospheric scale (Ratcliffe, 1956).

(2) $\phi_m^2 \gg 1$ . In this case the scattering is termed strong as large changes are imposed on the incident radio waves by the scattering medium. Bramley (1955) has shown that then, if

$$\rho_{\Delta N}(\xi) = \exp (- \xi^2/\xi_o^2 ) , \qquad 3.51$$

equation 3.47 becomes

$$r_f(\xi) = \exp\{-\phi_m^2\xi^2/\xi_o^2\} \quad , \qquad 3.52$$

which shows that the wave field has a scale $1/\phi_m$ times that of the electron density. In this case the scale of irregularities observed on the ground can be much smaller than the scale of ionospheric irregularities. Unfortunately it is not simple to differentiate in practice between the two types of scatter processes from ground observations and even if the second type is established it becomes difficult to estimate $\phi_m$. Hence determinations of the scale of ionospheric irregularities become uncertain.

If $\rho(\xi)$ has the form described by equation 3.50 then the angular power spectrum corresponding to it is given by

$$|P_\rho(S)|^2 = \exp\{-\pi^2\ell^2S^2\} \quad ,$$

where $S = \sin\theta$. The power is seen to drop to $1/e$ when $S = 1/\ell\pi$. This provides a convenient measure of the angular spread of received radiation and we see that this angular spread depends on the fineness of the structure in the diffracting screen. If $\rho(\xi)$ is given by equation 3.50 then equation 3.43 shows that $r(\xi)$ is defined as

$$r(\xi) = \frac{1}{B+1}\exp\{-\xi^2/\ell^2\} + \frac{B}{B+1} \quad . \qquad 3.53$$

It is seen that this function reduces to $\rho(\xi)$ when $B = 0$. The power spectra $|P_r(S)|^2$ and $|P_\rho(S)|^2$ corresponding to $r(\xi)$ and $\rho(\xi)$ respectively are shown in Figure 3.3 and it seen that one differs from the other only by the addition of a delta function of amplitude B at the origin. This feature corresponds to a specular component in the angular power spectrum.

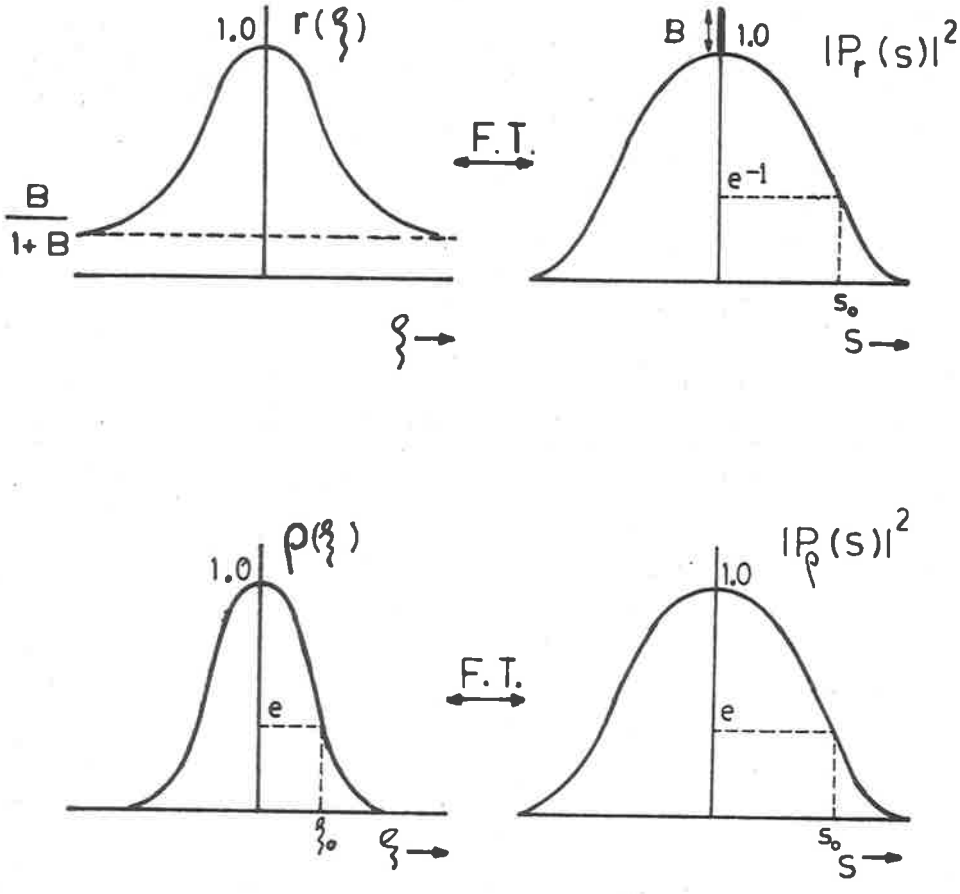


**Figure 3.3** The Fourier Transform relation between the generalized auto-correlation functions and their associated angular power spectra.

### 3.4.4 The determination of the coherence ratio

The relationship between $\rho(\xi)$ and $r(\xi)$ as described by equation 3.43 allows an estimate of B to be made. Making B the subject of the formula the result

$$B = \frac{\rho(\xi) - r(\xi)}{r(\xi) - 1} \qquad 3.54$$

is obtained, showing that an estimate of $\rho(\xi)$ and $r(\xi)$ for a given separation $\xi$ allows an estimate of B to be made.

Another method of calculating B can be deduced from the analysis of Whale and Gardiner (1966) who have shown that the probability P that the phase difference between a pair of separated points on the ground lies between $-\pi/2$ and $+\pi/2$ is given by

$$P = 1 - \frac{1 - \rho(\xi)}{2} \exp\{-B\} . \qquad 3.55$$

Rearranging to make B the subject of the formula gives

$$B = -\log_e \{2(1 - P)/(1 - \rho(\xi))\} . \qquad 3.56$$

It is to be noted that P as well as $\rho$ will depend on the separation of the observing points.

## 3.5 Discussion

In the preceding sections some theories have been described where amplitude and phase information are required. A number of workers in this field of enquiry have been able to obtain only amplitude information and a common method of investigation has been based on the work of Rice (1945), as has been described in section 3.2. It has been noted by various workers (e.g. Whale and Gardiner, 1966) that the probability

distribution must be measured very accurately to give good estimates of the coherence ratio. As this requires the analysis of long records the requirement that the records represent a statistically stationary situation then poses uncertainties.

Another assumption which is common to the Rice theory as well as the other theories described in this chapter for measuring the coherence ratio is that only one signal, or coherent component, of constant amplitude and direction of arrival is present. In practice this might well be rather an idealised model and departures from these requirements which might occur are not allowed for in any of the theories presented here. Furthermore, the theories discussed in this chapter implicitly assume that variations of the wave field observed on the ground are due to diffractive interference effects between the components of the angular spectrum. Instances of departure from these conditions possibly could occur, due, for example, to fading of signals introduced by spatial variations of reflection coefficient, or due to variable absorption below the height of reflection, so that in these cases an "equivalent" model may be derived which is possibly not truly descriptive of the screen itself. In view of such uncertainties the theory described in section 3.3, which has as its criterion for acceptance of a model the need for consistency between several independent estimates of a given parameter, or the generalised theory of section 3.4 is probably more reliable to apply to the investigation of coherence ratios than the Rice (1945) method above.

While the presence of variable absorption below the height of reflection might influence the amplitude pattern on the ground by other than interference effects the phase of a given signal might also be "spuriously" affected. For a completely random scattering process, the phase of the wave field observed at any point on the ground is expected to be evenly distributed over the range 0 - $2\pi$. However, the reverse implication, that is if the phase is evenly distributed over 0 - $2\pi$ then a randomly phased spectrum of waves is present is not true as can be demonstrated by a simple example. If we have a plane specularly reflecting ionosphere whose height above a point of observation on the ground is varying then any signal which is reflected from it to the point of observation will have phase variations impressed on it which are not due to interference effects. Less ideal ionospheric reflecting layers which may be drifting in range will also produce such effects, causing estimates from phase information to be misleading unless treated with caution. Nevertheless, phase difference quantities will not be affected by such means so that resulting estimates of angular spread are expected to be unaffected by such an effect. Since the theory described in section 3.3 allows estimates of angular spread and coherence ratio to be made from amplitude and phase information, the criterion of consistency of the accepted model clearly minimises the possibility of such spurious effects going unnoticed.

## 3.6 Summary

A theoretical basis has been described for the investigation of ionospheric irregularities and their scattering properties. The

statistics for an assumed randomly phased angular spectrum of waves have been given and some of Bramley's (1951) results have been generalised to remove the restriction of high correlation between signals received on spaced aerials. The generalised equations 3.11, 3.18 and 3.23 provide the basis for calculating the angular spread $\theta_o$ of such a system of waves from a measurement, at spaced aerials, of the squared amplitudes correlation coefficient $\rho_A^2$, the amplitude difference correlation coefficient $\rho_D$, and the mean absolute phase difference $\overline{|\phi|}$, respectively. Similarly, statistics are given for a similar distribution of waves but accompanied by a steady signal of constant amplitude and direction of arrival . The equations for a determination of the coherence ratio and the angular spread in terms of measured values of $\rho_A$, $\rho_D$ and $\overline{|\phi|}$ are equations 3.33, 3.36, 3.37 and 3.39. It has also been shown that equally well a knowledge of the generalised auto-correlation function of the complex wave field on the ground would allow deductions to be made about the angular power spectrum and the scale size of ionospheric irregularities.

It has been pointed out that due to other than interference effect true specular reflections may be masked by "spurious" effects such as variable absorption and changing reflection range so that a certain degree of degeneration of any coherent system of reflected waves towards apparent randomness might be expected. It is also pointed out that phase difference quantities probably lead to the most reliable indication of the angular spread of a system of downcoming waves.

Finally, it is appreciated that due to the possibility of "spurious" effects an accepted model might not describe the true ionospheric "screen" precisely.

# CHAPTER 4

# OBSERVATIONS OF THE NATURE OF PARTIAL REFLECTIONS

## 4.1 Introduction

The theories discussed in the last chapter have formed a basis for an experimental investigation of the nature of D-region partial reflections, and in this chapter the results obtained and the interpretations they have been given are presented. Experimental observations were made over the period February 1971 to March 1972. In section 4.2 observations of the angular spread of downcoming partially reflected waves from measurements of phase differences between spaced rows of aerials are presented. The angular spread, as pointed out in chapter 5, is a parameter important in determining the reliability of electron density profiles deduced from the Differential Absorption Experiment (DAE), in view of the errors associated with off vertical reflections. In section 4.3 the more detailed nature of the scattering processes is considered. Firstly, some observations using a simple approach are presented, followed by results of quantitative studies of scattering models. Other results relevant to these studies are described in section 4.4. Finally, the results presented in this chapter are discussed and compared with other available evidence.

## 4.2 Observations of angular spread using phase differences

In chapter 3 it was pointed out that the mean absolute phase difference between a spaced pair of aerials is probably the most

reliable indicator of the angular spread of the spectrum of waves falling on those aerials. The angular spread $\theta_o$ was shown to bear the same relation to the mean absolute phase difference for both a wandering specular signal and a continuous spread of randomly phased signals, provided that the aerials were spaced closely enough, and this relation was

$$\theta_o = \frac{\lambda \overline{|\phi|}}{2\pi d} ,$$

where $\overline{|\phi|}$ is the mean absolute phase difference and d is the separation of the two rows of aerials. It was considered that this relation would suffice to describe all situations which could be regarded as variations or combinations of the two extreme models mentioned above. Some experimental evidence for the generality of the above expression is discussed in §4.3.4.

The major proportion of observations of the angular spread of downcoming partially reflected waves was made using phase difference information from spaced rows of aerials as described in §2.4.5. Measurements using this system were taken from mid February 1971 to the end of November 1971. In most months, records were taken on one or two days near the middle of the month. The majority of the records were taken near local noon but some observations were made near sunrise and sunset and a few observations were made at night. This section is devoted to a discussion of these results.

### 4.2.1 Examples of records

The experimental arrangement for the measurement of angular spread has been described in chapter 2 and a schematic of the system was shown in Figure 2.9. Briefly recapitulating; three parallel rows of aerials were used to study the signals arriving in a vertical plane at right angles to the length of the rows. The phase differences between the centre row and each outer row were separately obtained. One of these quantities was recorded as well as the difference between the two phase difference quantities. Figure 4.1 shows some typical records for partial reflections from various heights. An inspection of these reveals several generally observed characteristics. It is immediately apparent that the mean absolute phase difference, which is a direct indicator of the angular spread of the received spectrum of waves, increases with increasing height. The records also show a generally observed increase of fading speed with increasing height. Some quantitative assessments of these observations will now be discussed.

### 4.2.2 Results

The monthly results obtained for the angular spread are summarized by the plots of Figure 4.2. The results for the first three months of data are plotted on the one graph since less results were taken in the initial stages. The successive graphs each contain all of the results obtained for each of the following months and virtually a full seasonal cycle is covered. The solid curves depict the mean angular spread as a function of height.

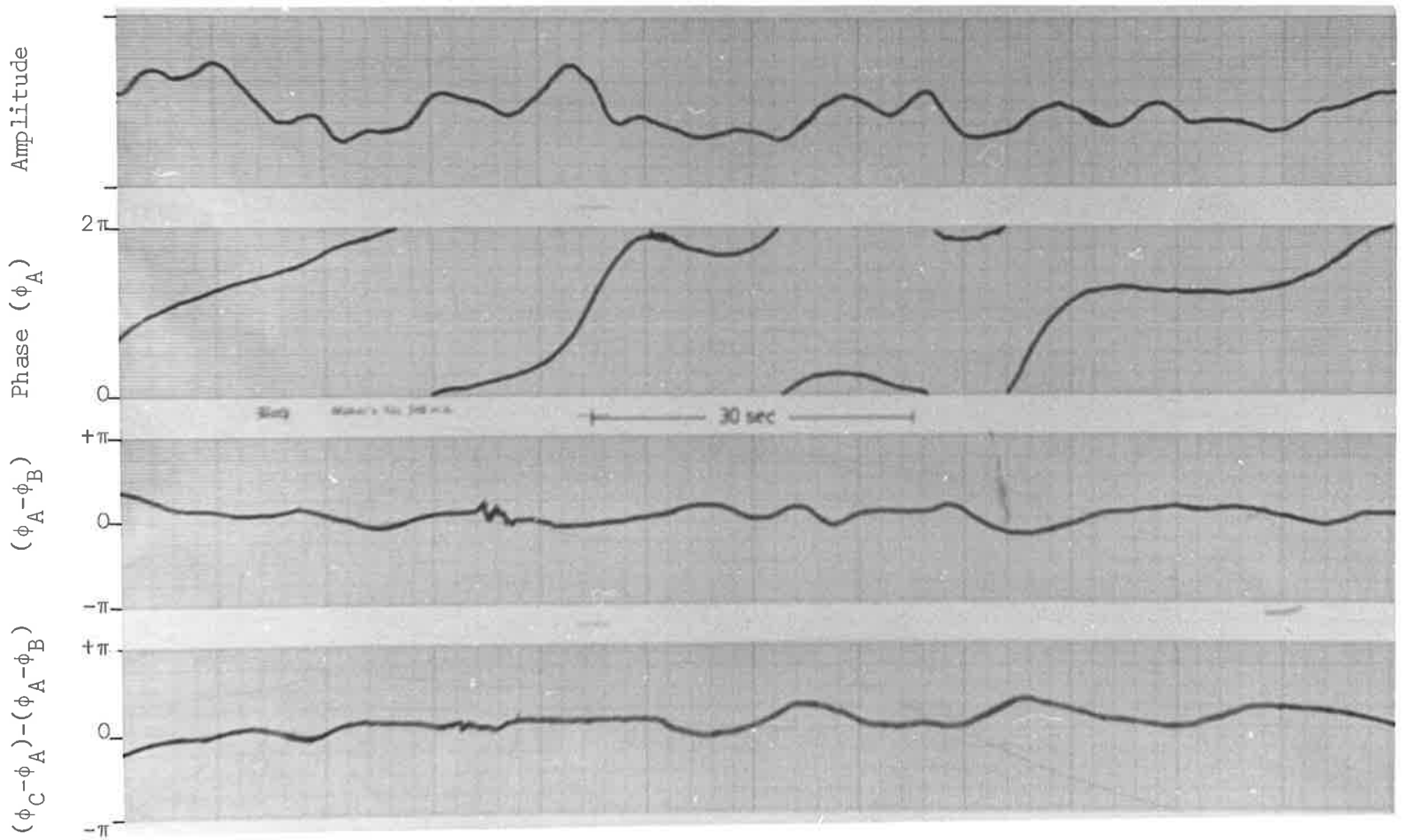


Figure 4.1a. Segment of 70km. chart record taken on 17/9/71 at 1115hrs for the determination of angular spread.

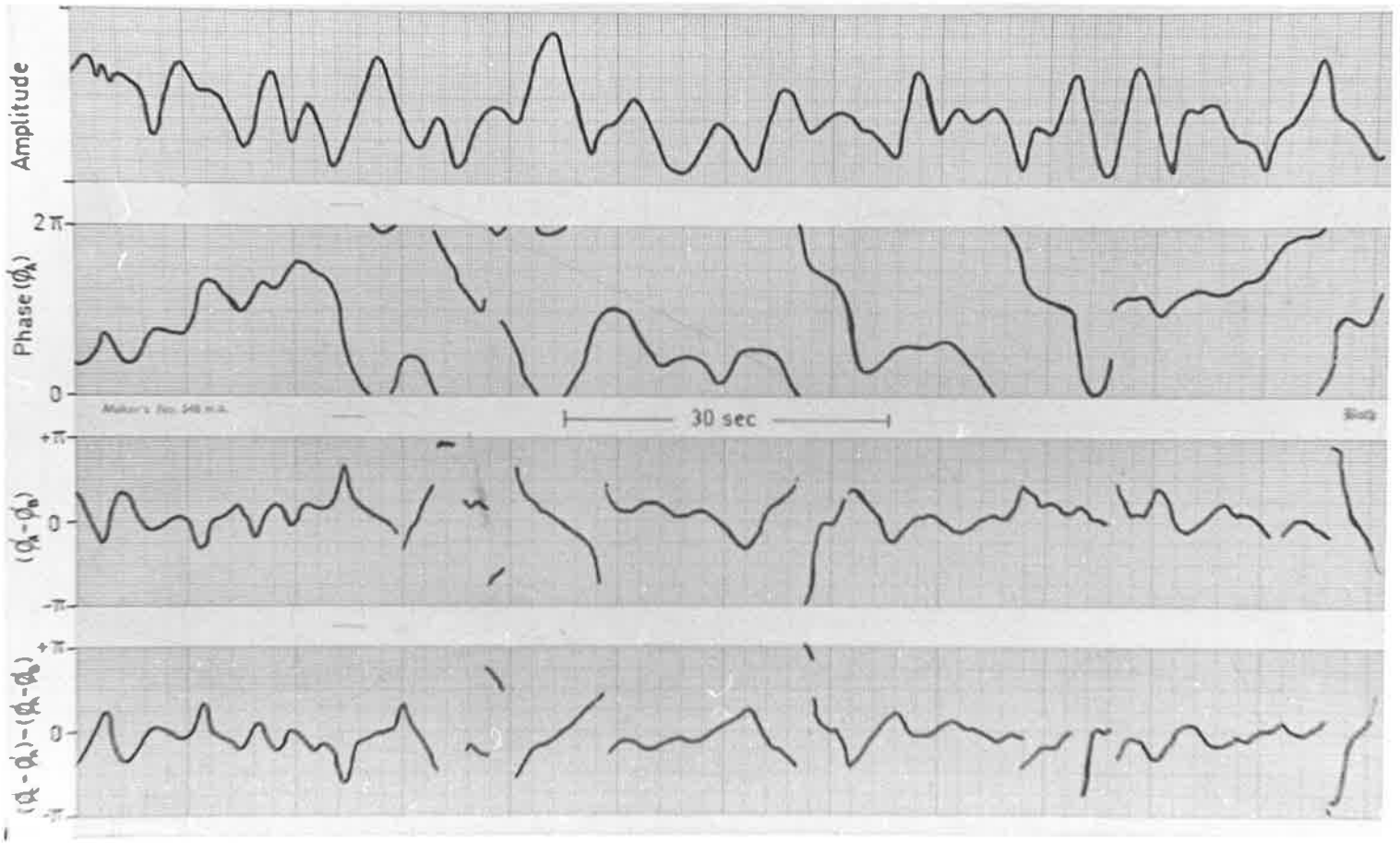


Figure 4.1b Segment of 85 km chart record taken on 17/9/71 at 1120hrs for the determination of angular spread.

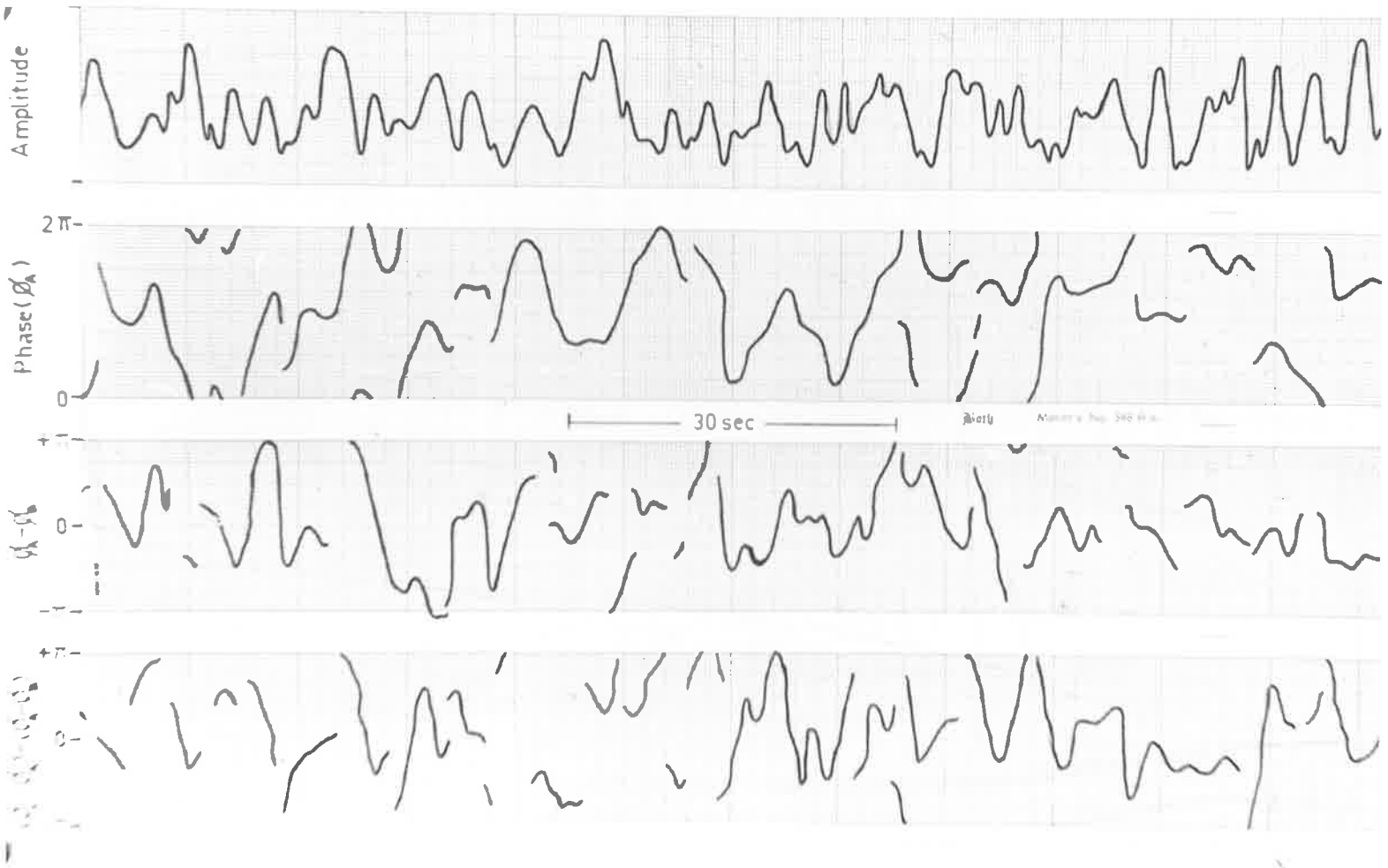


Figure 4.1c. Segment of 92km chart record taken on 17/9/71 at 1130hrs for the determination of angular spread.

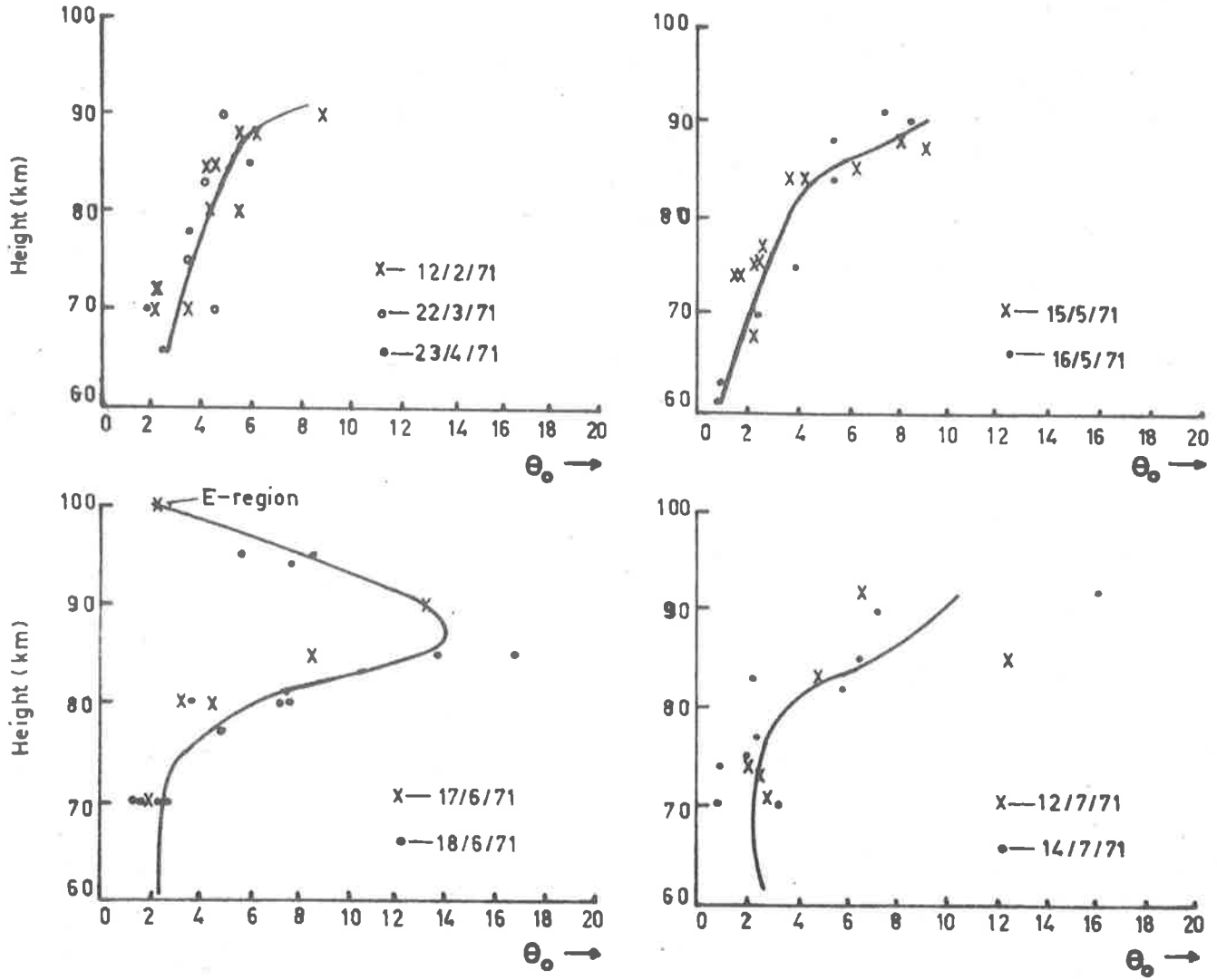


Figure 4.2 Scatter plots of the measured angular spread of partial reflections ...../

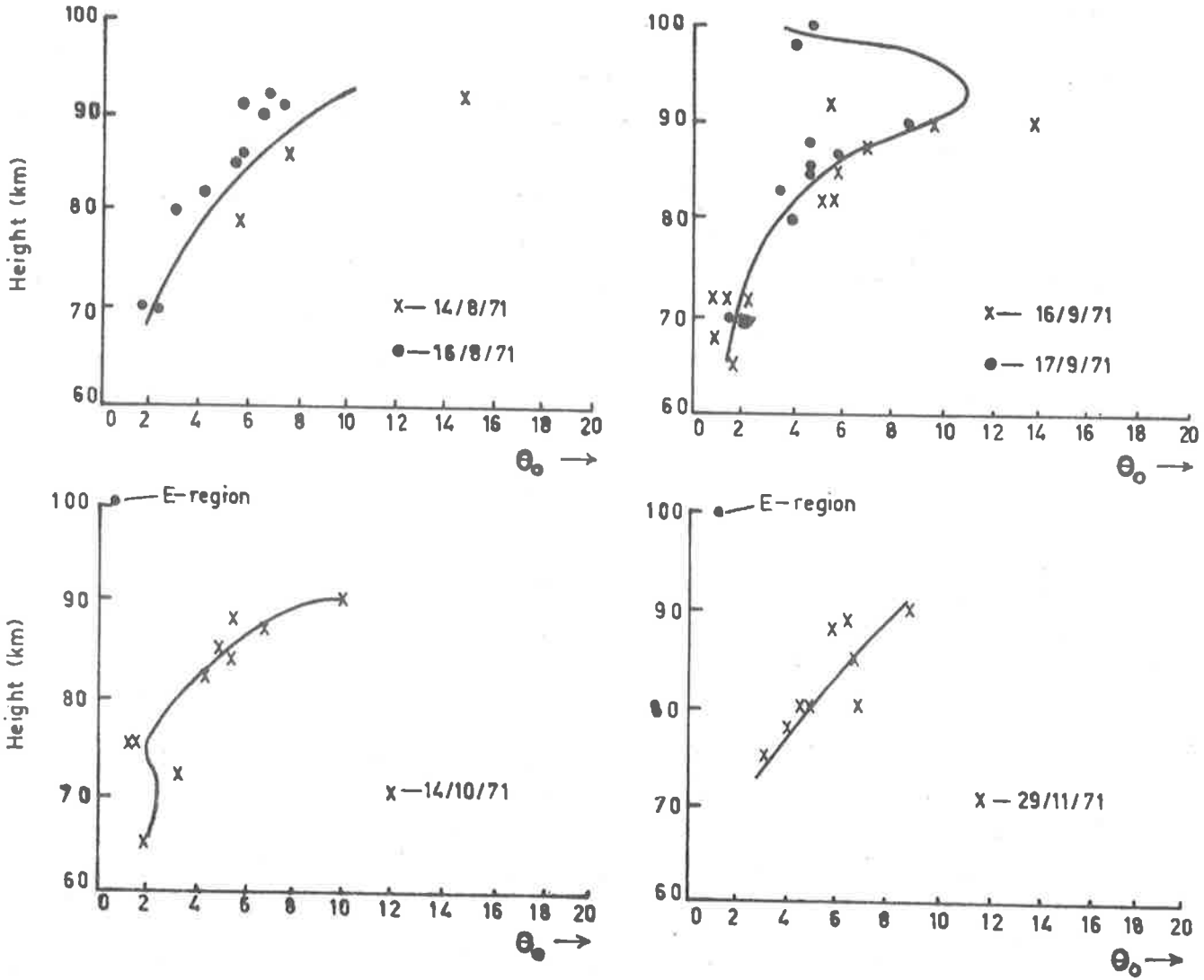


**Figure 4.2** Scatter plots of the angular spread of partial reflections.

A significant feature of all of the graphs is the fairly steady increase of angular spread with increasing height up to about 90 km, with a sharp increase being evident in several profiles at about 85 km. The few results taken above 90 km show that a decrease of angular spread is evident. A few E-region total reflection results are distinguished on some of the graphs and indicate that the angular spread of E-region reflections is generally less than for any of the D-region partial reflections.

4.2.3 Seasonal and daily variations

The solid curves of Figure 4.2 have all been included on the one graph in Figure 4.3a. The graphs indicate a marked increase in spread during June in the height range 75 to 90 km but other than that the curves show hardly any more variation throughout a season than is expected in day-to-day variations in any one month, as indicated by the scatter of points in the plots of Figure 4.2. If a distinction between the curves for all months is made, however, no systematic seasonal trends are found below 85 km but above this there is evidence of a small systematic increase of angular spread until winter, when a sudden increase occurs in June, followed by a decrease towards summer. Finally, Figure 4.3b shows the mean profile of angular spread averaged over all months.

The scatter of points in the plots of Figure 4.2 show that there is a clear seasonal trend in the variability of the measured angular spread of partially reflected waves observed on different occasions. In June there is a marked increase in the scatter of

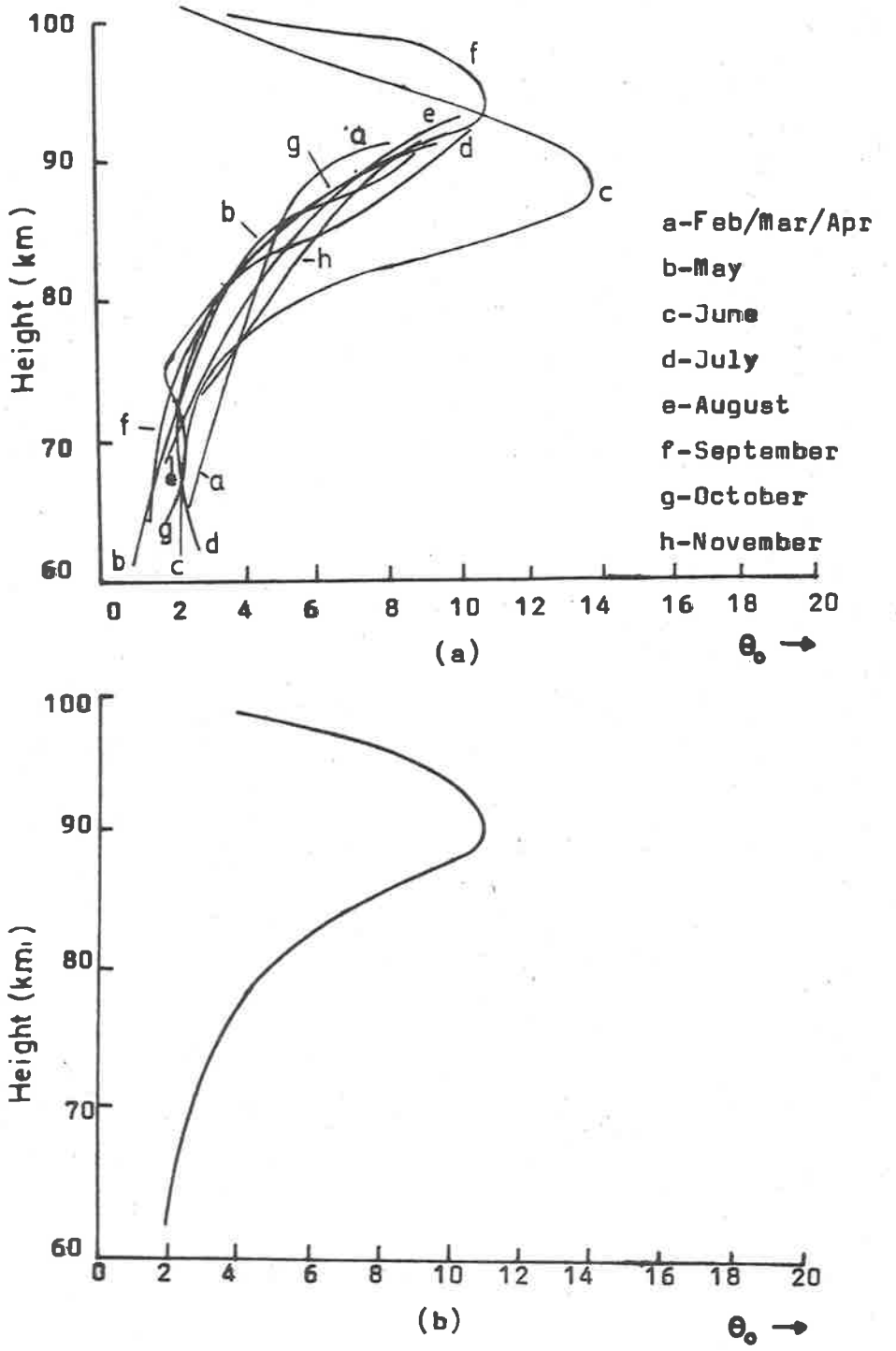


Figure 4.3 (a) Monthly profiles of angular spread taken from Figure 4.2.

(b) The mean profile of angular spread over the months February to November 1971.

values obtained at any given height, particularly above 75 km. This variability still exists but to a lesser degree in the July results and after that the results become much more consistent in the 80 to 90 km height region.

## 4.3 Investigations of D-region partial reflection models

### 4.3.1 Phasor diagrams

Before going on to discuss the main quantitative results it is worthwhile considering a simple approach to studying the qualitative nature of D-region reflections. The wave field at one point on the ground and at one instant of time may be represented in the usual way by a phasor drawn from an arbitrary origin. The path of the end point of this phasor as time advances provides a simple and direct visual representation of the nature of the fluctuations of the complex wave field. For example a reflection consisting of a strong specular component in the presence of weak randomly phased components would be expected to have a fairly stable amplitude and phase and the phasor diagram in such a situation would then take the form of a "ball of wool" set at some distance from the origin as depicted in Figure 4.4a. In such circumstances a reasonable estimate of the signal to noise amplitude ratio might be made from the ratio of the distances $E_s$ and $E_n$ provided $E_s \geqslant E_n$, where $E_s$ is the distance of the origin from the centre of the "ball of wool" and $E_n$ is its radial half-width. In the case where a received signal is comprised of a completely randomly phased spectrum of contributions, the phase of the resultant signal is expected to be evenly distributed over the range $0 - 2\pi$ and a "ball of wool" centred on the origin as in Figure 4.4b might be expected.

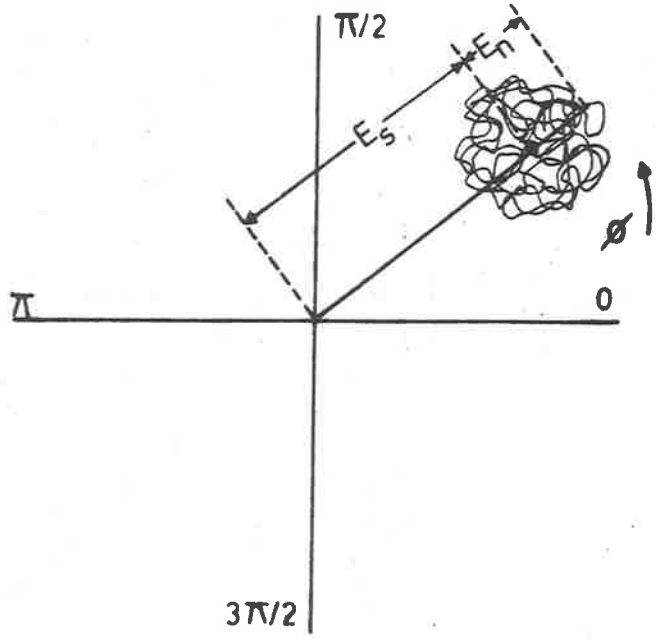


(a)

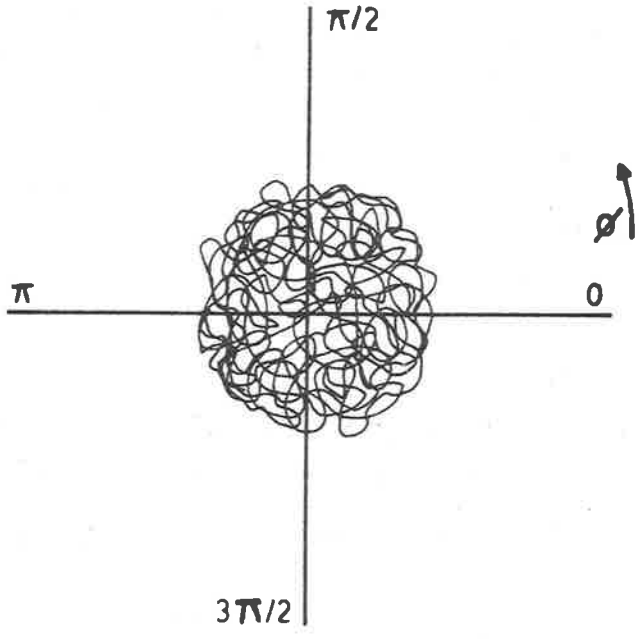


(b)

Figure 4.4 Hypothetical phasor diagrams for:
(a) a steady signal in the presence of "noise",
(b) a completely randomly phased or "noise" signal.

The practical plotting of phasor diagrams has been accomplished with the aid of a computer plotter. Many plots have been made from measurements of the amplitude and phase of the signals reflected from the D- and E-regions but only a few typical plots will be discussed here. In Figure 4.5 some phasor diagrams and segments of the amplitude and phase records to which they correspond are given. All plots have approximately the same number of points, so that effective comparisons of the randomness of the patterns can be made. An inspection of Figure 4.5 shows some interesting features:-

(1) The 103 km (E-region) plot shows characteristics typical of a strong specular signal in the presence of weak randomly phased "noise" contributions.

(2) The 95 km plot shows a typical instance where no coherent contribution to the resultant signal is apparent and a "ball of wool" centred close to the origin is obtained.

(3) While the phase is almost uniformly distributed over the range 0 - $2\pi$ for the 75 km record, it is plain that a completely randomly phased signal is not received. The example serves well to emphasize a point which was discussed in the last chapter. In the particular case shown here, it is apparent that two strong phase coherent contributions are beating together and are dominating the resultant received signal. The distinction between the 75 km and 95 km phase records illustrates the apparent difference in the mechanisms which are producing the almost uniform distributions of phase in the two cases.

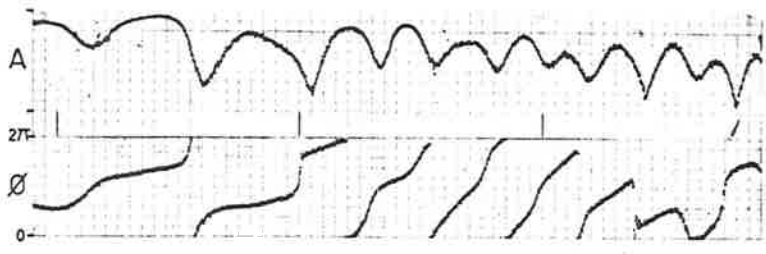


30/11/71 75Km.

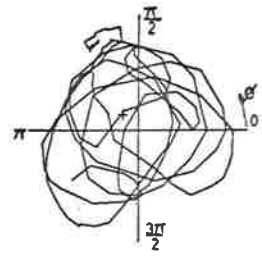


75 Km Phasor plot

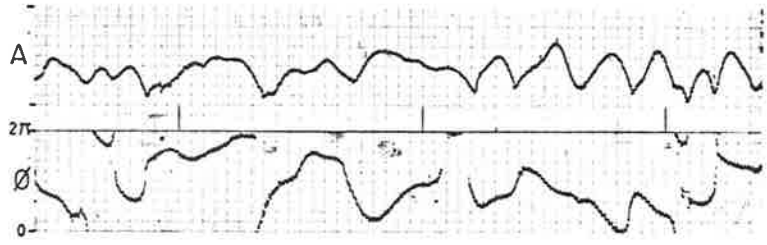


30/11/71 85Km.

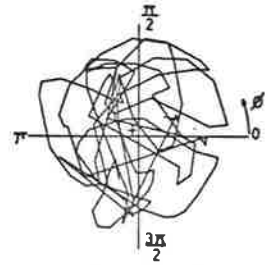


85 Km Phasor plot

10 SEC

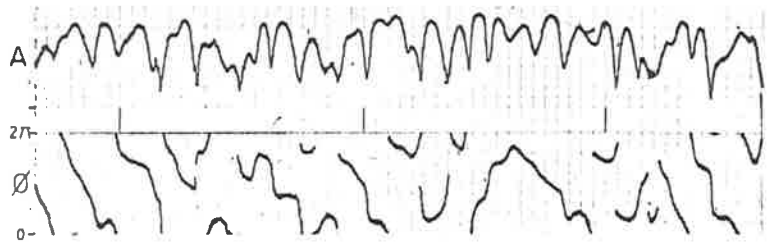


30/11/71 95Km.

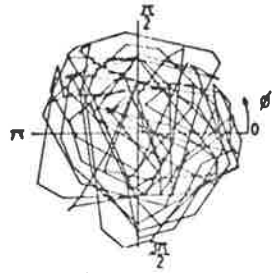


95 Km Phasor plot

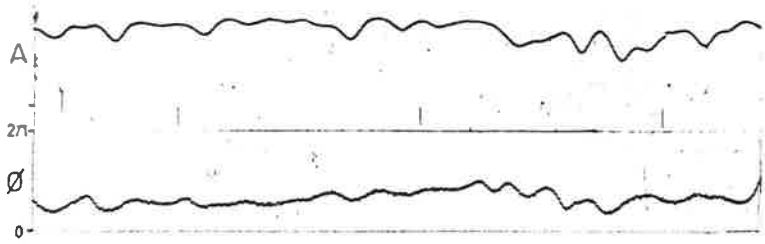


27/3/72 · 103Km. (E-region)

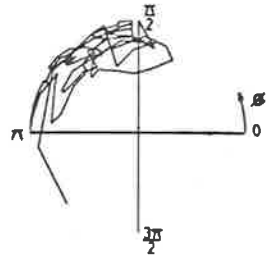


103Km Phasor plot

Segments of amplitude and phase records with corresponding phasor representation.

Figure 4.5

(4) A comparison of the results for the different heights shows what has been found to be a typical feature of most records; an increase of apparent randomness of the signal with increasing height. This is neglecting the E-region where a completely different total reflection process occurs. The same feature is evident in the phase records and in the phasor diagrams from the more dense and tangled plots obtained at greater heights. The amplitude records tend also to support this observation when it is seen that the fading speed increases with increasing height. This latter aspect is discussed further in §4.4.2.

While the results depicted in Figure 4.5 are chosen to be fairly typical of the nature of D-region partial reflections it is to be noted that variations from these conditions do occur. For example, Figure 4.6 illustrates a comparison of the nature of the received signal from 75 km on 15/5/71 and 16/5/71. On the first day the 75 km echo persisted throughout the day with apparently high coherence as shown by the diagram of Figure 4.6a. During the following day the echo was still present for long periods of time but with generally lower coherence which frequently lapsed into the fairly incoherent state shown in Figure 4.6b.

It has bee found convenient in these phasor diagram studies to distinguish between two height regimes within the D-region on the basis of the nature of the reflections observed, and the boundary between these regions is best placed at approximately 85 km. Below this height reflections have been observed to display generally fairly coherent

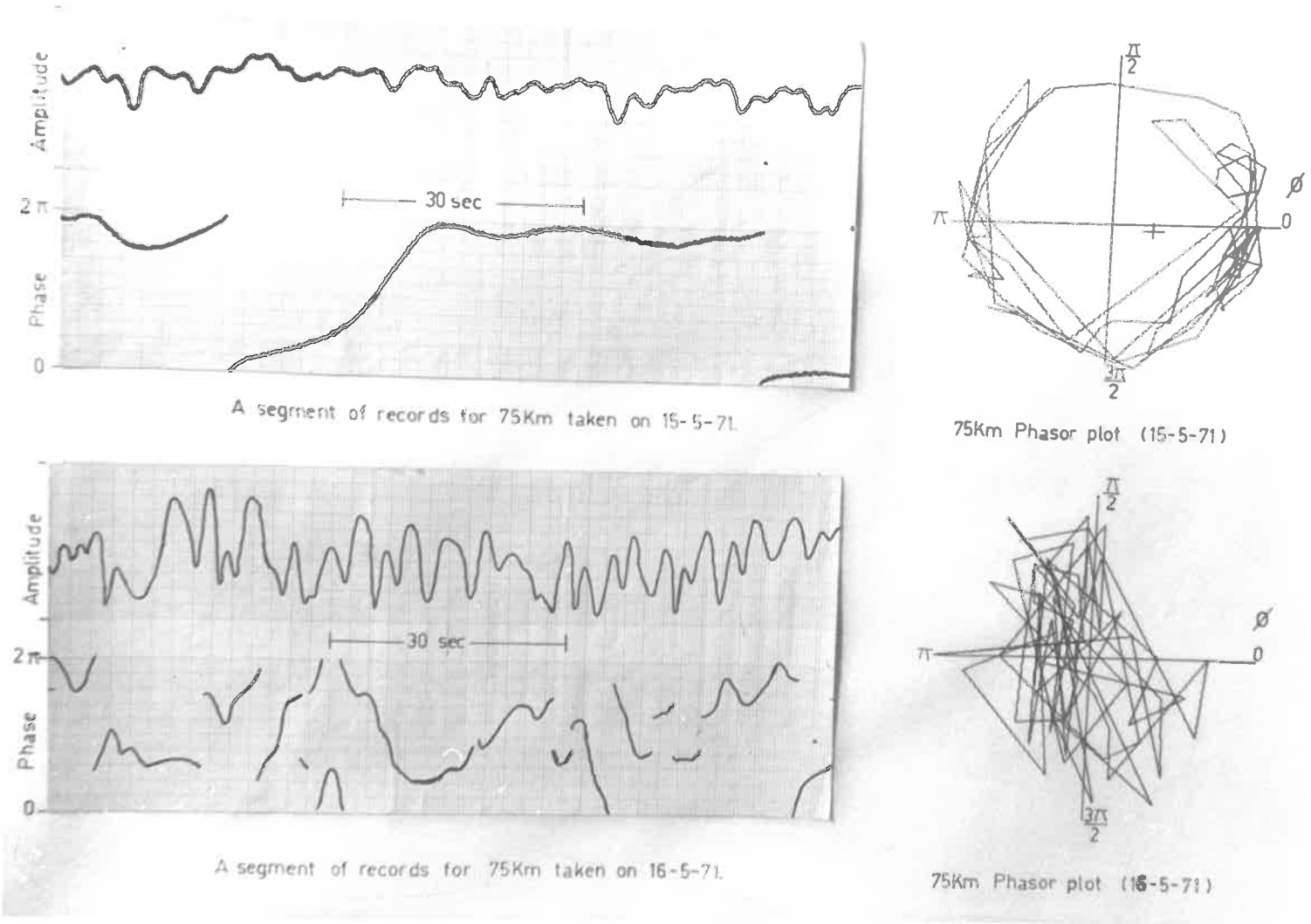


Figure 4.6 Comparison of two different scattering processes observed for 75km one day apart.

characteristics but with occasional occurrences of random like signals. Above 85 km the reflected signals have consistently displayed a comparatively random behaviour with very few exceptions.

4.3.2 The equations for studying reflection models

From the end of November 1971 experiments directed towards the determination of the applicability of two alternative scattering models were carried out. The theories described in the last chapter in §3.2 provided a means for examining the suitability of either of the two models considered. The first model assumed a two dimensional spectrum of randomly phased component signals while the second model assumed that in addition to this random component a strong coherent signal of fixed amplitude and direction of arrival was present. For convenient reference the equations relating measurable statistical properties of the received signals to the angular spread and coherence ratio of the angular spectrum of downcoming waves are all tabulated in Table 4.1.

The various symbols used are defined as follows:-

$\theta_o$ - spread of the angular spectrum of waves.

b - coherence ratio (for amplitudes).

$\lambda$ - probing radio wavelength.

d - separation of the pair of receiving aerials.

$\rho_A$ - correlation coefficient between the amplitudes at these two aerials.

$\rho_A^2$ - correlation coefficient between amplitudes squared at the two aerials.

TABLE 4.1

(a) Model 1 (randomly phased components only)

| Equation | High Correlation | Equation | General Correlation |
|---|---|---|---|
| 4.1 | $\theta_o = \frac{(4-\pi)^{\frac{1}{2}}\lambda(1-\rho_A)^{\frac{1}{2}}}{2\pi d}$ | 4.2 | $\theta_o = \frac{\lambda(-\log_e(\rho_{A^2}))^{\frac{1}{2}}}{2\pi d}$ |
| 4.3 | $\theta_o = \frac{\lambda\rho_D}{4d}$ | 4.4 | $\theta_o = \frac{\lambda}{2\pi d}[-\log_e\{\log_e(1-\rho_D^2/(6-4\sqrt{2}))+1\}]^{\frac{1}{2}}$ |
| 4.5 | $\theta_o = \frac{\lambda\overline{\lvert\phi\rvert}}{2\pi d}$ | 4.6 | $\theta_o = \frac{\lambda}{\pi d}\left\{\frac{-\log_e(\text{Cos}\ \lvert\phi\rvert)}{2}\right\}^{\frac{1}{2}}$ |
| (b) Model 2 (randomly phased components plus one specular component) | | | |
| 4.7 | $\theta_o = \frac{\lambda}{\pi d}\left(\frac{1-\rho_A}{2}\right)^{\frac{1}{2}}$ | 4.8 | $\theta_o = \frac{\lambda}{\sqrt{2}\,\pi d}\{-\log_e(\rho_A)\}^{\frac{1}{2}}$ |
| 4.9 | $b = \frac{1}{\rho_D}\left\{\frac{2(1-\rho_A)}{\pi}\right\}^{\frac{1}{2}}$ | | - b also given by equation 4.9 |
| 4.10 | $b = \frac{1}{\overline{\lvert\phi\rvert}}\left\{\frac{2(1-\rho_A)}{\pi}\right\}^{\frac{1}{2}}$ | | - b also given by equation 4.10 |

$\rho_D$ - amplitude difference correlation coefficient between the two aerials.

$\overline{|\phi|}$ - the mean absolute phase difference between signals received at the pair of spaced aerials.

The criterion for acceptance of either model has been that consistency of either the three estimates for $\theta_o$ in model 1 or of the two estimates of b in model 2 is evident from measurements of $\rho_A$, $\rho_A^2$, $\rho_D$ and $\overline{|\phi|}$ calculated from the recorded data.

4.3.3 Examples of records

The experimental arrangement has been described in chapter 2 but it will be briefly recapitulated here. Generally, four separate rows of receiving aerials were used. One pair was aligned at right angles to the other pair as depicted in Figure 2.10. The amplitude for each row, the phase difference between parallel rows and the phase for one row of each parallel pair were all recorded on an eight channel chart recorder. Phase information could be resolved to $\pm 3.5^{\circ}$. The use of orthogonal rows of aerials enabled a check for asymmetry of the angular spectrum of returned waves. Figure 4.7 is a reproduction of a segment of chart record used for investigating the nature of the received partially reflected signal. Many records of a similar kind were obtained and these were digitized and the data punched onto cards for subsequent computer analysis.

4.3.4 A comparison of parameters calculated from the equations of Table 4.1

For the purposes of comparison, some typical results are tabulated in Table 4.2 where the parameters $\theta_o$ and b have been

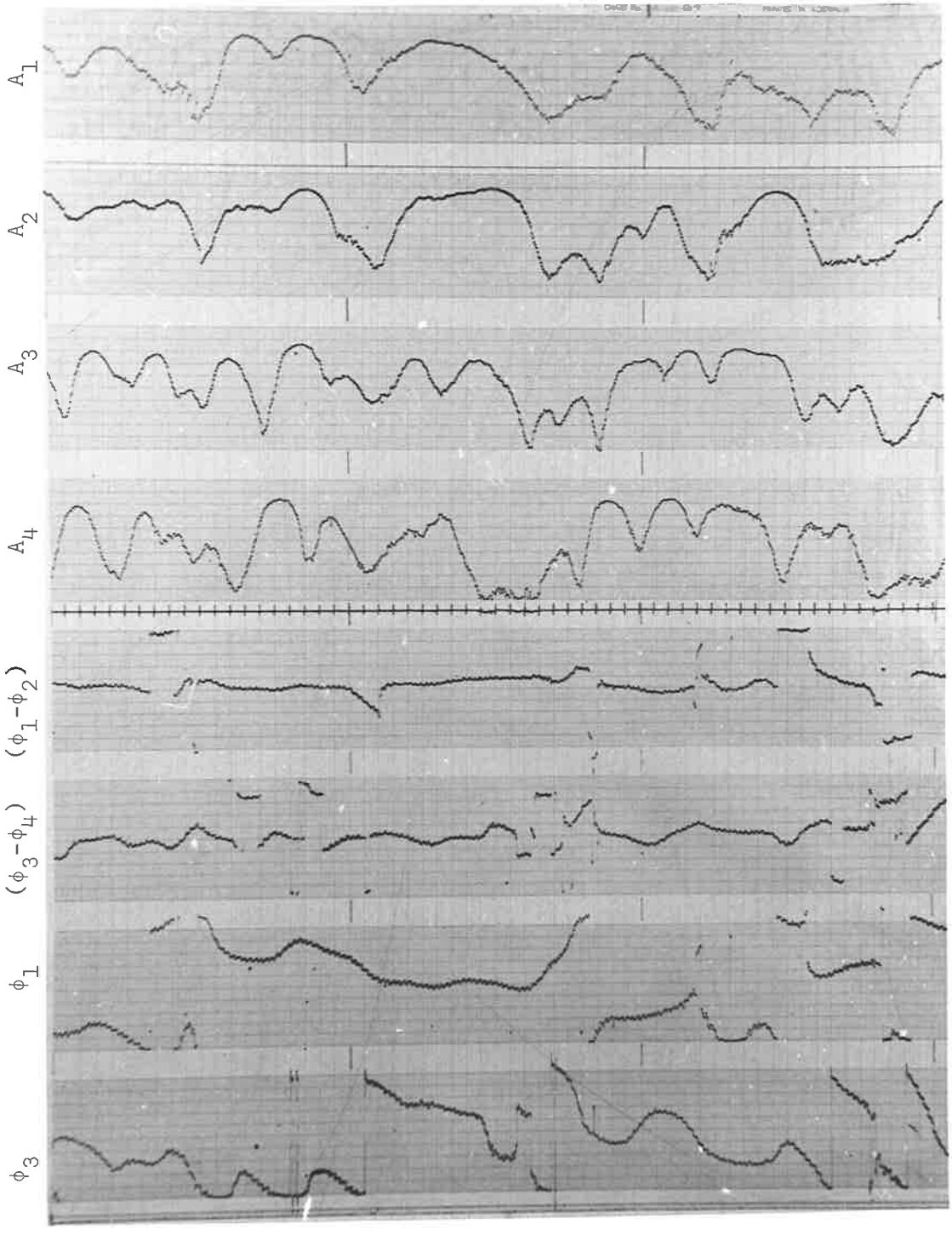


Figure 4.7 A segment of chart record for 90km showing the quantities recorded for studying scattering models.

| Hrs. (LT) 13/12/71 | Obs. plane | Ht. (km) | $\rho_A$ | $\rho_{A^2}$ | $\rho_D$ | $\overline{\lvert\phi\rvert}$ | High Correlation | | | | | | General Correlation | | | | | |
|---|---|---|---|---|---|---|---|---|---|---|---|---|---|---|---|---|---|---|
| | | | | | | | Model 1 | | | Model 2 | | | Model 1 | | | Model 2 | | |
| | | | | | | | $\theta_o$ | $\theta_o$ | $\theta_o$ | b | b | $\theta_o$ | $\theta_o$ | $\theta_o$ | $\theta_o$ | b | b | $\theta_o$ |
| | | | | | | | 4.1 Equn. → | 4.3 | 4.5 | 4.7 | 4.9 | 4.10 | 4.2 | 4.4 | 4.6 | 4.8 | 4.9 | 4.10 |
| 1206 | E-W | 88 | .74 | .81 | .22 | .40 | 7.2 | 5.1 | 6.0 | 1.0 | 1.9 | 11.0 | 6.9 | 6.0 | 6.1 | 1.0 | 1.9 | 11.8 |
| 1206 | N-S | 88 | .76 | .74 | .26 | .44 | 6.8 | 6.3 | 6.6 | .9 | 1.5 | 10.4 | 8.2 | 7.7 | 6.7 | .9 | 1.5 | 11.1 |
| 1210 | E-W | 95 | .44 | .45 | .34 | 1.0 | 10.4 | 8.0 | 15.0 | .6 | 1.8 | 15.9 | 13.5 | 10.7 | 16.7 | .6 | 1.8 | 19.3 |
| 1210 | N-S | 95 | .33 | .30 | .40 | .98 | 11.4 | 9.5 | 14.8 | .7 | 1.6 | 17.4 | 16.6 | 15.0 | 16.3 | .7 | 1.6 | 22.4 |
| 1215 | E-W | 90 | .59 | .60 | .25 | .62 | 9.0 | 5.9 | 9.4 | .8 | 2.0 | 13.7 | 10.9 | 7.2 | 9.7 | .8 | 2.0 | 15.5 |
| 1215 | N-S | 90 | .40 | .42 | .34 | .62 | 10.8 | 8.2 | 9.4 | 1.0 | 1.8 | 16.5 | 14.1 | 11.2 | 9.7 | 1.0 | 1.8 | 20.4 |
| 1420 | E-W | 88 | .80 | .82 | .20 | .39 | 6.3 | 4.8 | 5.8 | .9 | 1.8 | 9.6 | 6.8 | 5.5 | 5.9 | .9 | 1.8 | 10.1 |
| 1420 | N-S | 88 | .72 | .63 | .24 | .37 | 7.4 | 5.7 | 5.6 | 1.1 | 1.8 | 11.3 | 10.2 | 6.8 | 5.7 | 1.1 | 1.8 | 12.2 |

TABLE 4.2. A comparison of results computed firstly using a theory assuming high correlation and secondly using an extension of this theory to cover general correlation conditions. Model 1 assumes a randomly phased spectrum of waves while model 2 assumes an additional specular component. References to the equations from which the various parameters are calculated are given at the top of each column. $\overline{\lvert\phi\rvert}$ is given in radians, while $\theta_o$ is in degrees.

calculated using firstly Bramley's (1951) theory assuming high correlation between spaced observing aerials and secondly using the generalisation of these equations as derived in the last chapter to cover all correlation conditions.

Where the degree of correlation, as represented by $\rho_A$ or $\rho_A^2$ is high, it can be seen from Table 4.2 that there is little difference between the two sets of calculated parameters. However, when the correlation becomes small, as is often the case for signals returning from above 80 km, the results show that usually the angular spread $\theta_o$ is significantly underestimated unless the generalised equations are used in calculating $\theta_o$. A notable exception is where $\theta_o$ is calculated from $\overline{|\phi|}$ and this is considered to lend justification to the assumption that the relation $\theta_o = \lambda \overline{|\phi|}/2\pi d$, as used in section 4.2, is of quite general validity. Throughout the investigations the generalised equations of Table 4.1 have been used. Table 4.3 shows a set of results obtained in such a manner. Omissions occur in the table where either certain information was not recorded due to technical difficulties or the parameter was undefined according to the working equations.

4.3.5 The applicability of the scattering models

For the sake of convenience, as in Table 4.1, the model assuming a randomly phased spectrum of waves with no specular component will be referred to as model 1 while the model which assumes an additional specular component will be referred to as model 2. Several different features are evident in the results of Table 4.3, but generally a result falls into one of the following categories:

TABLE 4.3

| Date | Local time | Observing plane | Ht (km) | from equns. → | Model 1 | | | Model 2 | | |
|---|---|---|---|---|---|---|---|---|---|---|
| | | | | | $\theta_o$ | $\theta_o$ | $\theta_o$ | b | b | $\theta_o$ |
| | | | | | 4.2 | 4.4 | 4.6 | 4.10 | 4.9 | 4.8 |
| 30-11-71 | 1600 | E-W | 80 | | 3.4 | 3.1 | 3.3 | .8 | 1.5 | 4.8 |
| | 1615 | E-W | 73 | | 2.0 | 3.1 | 3.6 | .6 | 1.2 | 3.6 |
| | 1619 | E-W | 85 | | 11.9 | 7.2 | 9.9 | .7 | 1.9 | 15.8 |
| | 1625 | E-W | 95 | | 5.8 | 3.6 | - | .3 | 2.3 | 8.8 |
| 1-12-71 | 1155 | E-W | 72 | | 2.2 | 1.7 | 2.4 | .8 | 2.0 | 3.5 |
| | 1155 | N-S | 72 | | 1.8 | 3.4 | 2.7 | .6 | .8 | 2.7 |
| | 1205 | E-W | 82 | | 8.9 | 5.2 | 7.0 | .8 | 2.2 | 13.2 |
| | 1205 | N-S | 82 | | 10.8 | - | 5.8 | 1.0 | 1.1 | 13.9 |
| | 1345 | E-W | 90 | | 7.3 | 5.0 | 5.0 | 1.0 | 2.0 | 10.9 |
| | 1345 | N-S | 90 | | 8.1 | - | 6.5 | .9 | 1.0 | 12.7 |
| | 1450 | E-W | 75 | | 1.6 | 1.8 | 2.1 | .7 | 1.6 | 2.9 |
| | 1450 | N-S | 75 | | 2.3 | 1.8 | 1.7 | 1.0 | 1.7 | 3.1 |
| | 1500 | E-W | 80 | | 7.2 | 3.3 | 3.0 | 1.5 | 2.6 | 9.9 |
| | 1500 | N-S | 80 | | 3.2 | - | 2.1 | 1.4 | .6 | 5.4 |
| | 1510 | E-W | 83 | | 11.3 | 5.6 | 13.1 | .5 | 2.2 | 14.9 |
| | 1510 | N-S | 83 | | 9.1 | - | 5.6 | 1.0 | 1.2 | 13.8 |
| 13-12-71 | 1200 | E-W | 100(E) | | 5.4 | 4.4 | 4.6 | .8 | 1.7 | 7.6 |
| | 1200 | N-S | 100(E) | | 4.4 | 3.8 | 4.8 | .7 | 1.7 | 6.6 |
| | 1206 | E-W | 88 | | 6.9 | 6.0 | 6.1 | 1.0 | 1.9 | 11.8 |
| | 1206 | N-S | 88 | | 8.2 | 7.7 | 6.7 | .9 | 1.5 | 11.1 |
| | 1210 | E-W | 95 | | 13.5 | 10.7 | 16.7 | .6 | 1.8 | 19.3 |
| | 1210 | N-S | 95 | | 16.6 | 15.0 | 16.3 | .7 | 1.6 | 22.4 |
| | 1215 | E-W | 90 | | 10.9 | 7.2 | 9.7 | .8 | 2.0 | 15.5 |
| | 1215 | N-S | 90 | | 14.1 | 11.2 | 9.7 | 1.0 | 1.8 | 20.4 |
| | 1420 | E-W | 88 | | 6.8 | 5.5 | 5.9 | .9 | 1.8 | 10.1 |
| | 1420 | N-S | 88 | | 10.2 | 6.8 | 5.7 | 1.1 | 1.8 | 12.2 |

TABLE 4.3 (CONT'D)

| Date | Local time | Observing plane | Ht (km) | from equns. → | Model 1 | | | Model 2 | | |
|---|---|---|---|---|---|---|---|---|---|---|
| | | | | | $\theta_o$ | $\theta_o$ | $\theta_o$ | b | b | $\theta_o$ |
| | | | | | 4.2 | 4.4 | 4.6 | 4.10 | 4.9 | 4.8 |
| 13-12-71 | 1428 | E-W | 95 | | 6.7 | 5.6 | 4.2 | 1.1 | 1.7 | 9.7 |
| | 1428 | N-S | 95 | | 3.4 | 4.2 | 4.5 | .6 | 1.3 | 5.2 |
| | 1435 | E-W | 88 | | 7.5 | 6.0 | 6.0 | .8 | 1.8 | 10.6 |
| | 1435 | N-S | 88 | | 8.6 | - | 7.3 | .8 | 1.5 | 13.2 |
| 15-12-71 | 1430 | E-W | 82 | | 6.3 | 4.7 | 7.0 | .7 | 2.0 | 9.8 |
| | 1430 | N-S | 82 | | 9.7 | - | 9.0 | .7 | 1.4 | 13.7 |
| | 1435 | E-W | 90 | | 9.0 | 7.5 | 9.5 | .6 | 1.7 | 12.6 |
| | 1435 | N-S | 90 | | 9.3 | 9.1 | 12.9 | .5 | 1.7 | 14.4 |
| | 1430 | E-W | 88 | | 8.2 | 7.7 | 9.1 | .8 | 1.7 | 13.0 |
| | 1430 | N-S | 88 | | 9.2 | 9.5 | - | - | 1.6 | 14.6 |
| | 1447 | E-W | 100(E) | | 5.9 | 4.4 | 5.1 | .9 | 1.9 | 8.8 |
| | 1447 | N-S | 100(E) | | 4.6 | 4.9 | 7.3 | .5 | 1.5 | 7.0 |
| | 1540 | E-W | 90 | | 7.0 | 5.7 | 11.3 | .5 | 1.7 | 9.2 |
| | 1540 | N-S | 90 | | 6.9 | - | 10.5 | .5 | 1.2 | 9.7 |
| | 1542 | E-W | 96 | | 10.3 | 9.4 | 10.5 | .6 | 1.7 | 14.5 |
| | 1545 | E-W | 104(E) | | 3.3 | 2.3 | 2.2 | 1.2 | 2.0 | 4.8 |
| | 1545 | N-S | 104(E) | | 2.3 | 2.5 | 2.8 | .8 | 1.6 | 4.1 |
| | 1550 | E-W | 90 | | 4.9 | 3.7 | 5.5 | .7 | 1.8 | 7.1 |
| | 1550 | N-S | 90 | | 7.0 | 8.7 | 7.8 | .6 | 1.4 | 9.8 |
| | 1555 | E-W | 95 | | 9.6 | - | 9.1 | .7 | 1.5 | 13.3 |
| | 1555 | N-S | 95 | | 11.2 | - | 10.8 | .6 | 1.5 | 15.7 |
| | 1600 | E-W | 75 | | 4.3 | 4.3 | 2.1 | 1.5 | 1.5 | 6.1 |
| | 1600 | N-S | 75 | | 2.1 | 4.5 | 2.9 | .8 | 1.0 | 4.2 |
| | 1610 | E-W | 85 | | 6.1 | 6.8 | 4.9 | .9 | 1.5 | 9.1 |
| | 1610 | N-S | 85 | | 9.7 | 13.2 | 4.9 | 1.2 | 1.6 | 13.6 |

TABLE 4.3 (CONT'D)

| Date | Local time | Observing plane | Ht (km) | from equns. → | Model 1 | | | Model 2 | | |
|---|---|---|---|---|---|---|---|---|---|---|
| | | | | | $\theta_o$ | $\theta_o$ | $\theta_o$ | b | b | $\theta_o$ |
| | | | | | 4.2 | 4.4 | 4.6 | 4.10 | 4.9 | 4.8 |
| 16-3-72 | 1015 | E-W | 85 | | 7.8 | 4.9 | 7.4 | .9 | 2.3 | 11.8 |
| | 1015 | N-S | 85 | | 8.8 | 5.5 | 8.3 | .8 | 2.2 | 12.9 |
| | 1020 | E-W | 75 | | 4.8 | 2.7 | 2.7 | 1.3 | 2.2 | 6.2 |
| | 1020 | N-S | 75 | | 4.4 | 3.8 | 3.2 | 1.2 | 1.7 | 6.7 |
| | 1025 | E-W | 95 | | 11.2 | 5.1 | 17.2 | .5 | 2.7 | 15.6 |
| | 1025 | N-S | 95 | | 18.9 | 18.8 | 23.2 | .6 | 1.6 | 26.6 |
| 27-3-72 | 1155 | E-W | 93 | | 9.2 | 4.8 | 10.4 | .6 | 2.3 | 14.1 |
| | 1155 | N-S | 93 | | 9.3 | 6.1 | 9.7 | .6 | 1.9 | 13.3 |
| | 1210 | E-W | 83 | | 3.2 | 3.0 | 4.1 | .7 | 1.7 | 5.3 |
| | 1210 | N-S | 83 | | 2.7 | 2.3 | 2.3 | .9 | 1.7 | 4.0 |
| | 1215 | E-W | 78 | | 3.4 | 2.9 | 3.2 | .8 | 1.6 | 4.8 |
| | 1215 | N-S | 78 | | 2.9 | 2.8 | 2.5 | 1.0 | 1.6 | 4.4 |
| | 1220 | E-W | 90 | | 6.9 | 5.2 | 7.4 | .7 | 1.9 | 10.1 |
| | 1220 | N-S | 90 | | 7.1 | 6.0 | 8.0 | .6 | 1.7 | 9.9 |
| | 1225 | E-W | 83 | | 2.3 | 2.1 | 2.7 | .8 | 1.7 | 3.7 |
| | 1225 | N-S | 83 | | 2.7 | 2.5 | 2.6 | .9 | 1.7 | 4.4 |
| | 1345 | E-W | 78 | | 4.5 | 5.0 | 2.6 | 1.2 | 1.3 | 6.1 |
| | 1345 | N-S | 78 | | 4.9 | 3.4 | 2.5 | 1.5 | 2.0 | 7.1 |
| | 1350 | E-W | 72 | | 2.2 | 1.3 | 2.0 | 1.0 | 2.6 | 3.6 |
| | 1350 | N-S | 72 | | 3.0 | 2.0 | 1.2 | 2.4 | 2.5 | 5.3 |
| | 1355 | E-W | 70 | | 4.5 | 2.4 | 3.0 | 1.1 | 2.5 | 6.3 |
| | 1355 | N-S | 70 | | 2.6 | 1.4 | 1.9 | 1.2 | 2.9 | 4.2 |
| | 1400 | E-W | 88 | | 9.0 | 10.4 | 10.9 | .6 | 1.5 | 12.3 |
| | 1400 | N-S | 88 | | 5.8 | 5.9 | 5.2 | .8 | 1.5 | 8.2 |
| | 1405 | E-W | 95 | | 8.0 | 5.2 | - | .4 | 2.1 | 12.3 |
| | 1405 | N-S | 95 | | 5.6 | 3.0 | 15.3 | .4 | 2.5 | 8.3 |
| | 1415 | E-W | 80 | | 8.2 | 9.5 | 6.7 | .8 | 1.5 | 11.5 |
| | 1415 | N-S | 80 | | 4.1 | 4.4 | 4.0 | .8 | 1.4 | 6.0 |

TABLE 4.3 (CONT'D)

| Date | Local time | Observing plane | Ht (km) | from equns. → | Model 1 | | | Model 2 | | |
|---|---|---|---|---|---|---|---|---|---|---|
| | | | | | $\theta_o$ | $\theta_o$ | $\theta_o$ | b | b | $\theta_o$ |
| | | | | | 4.2 | 4.4 | 4.6 | 4.10 | 4.9 | 4.8 |
| 27-3-72 | 1420 | E-W | 72 | | 2.0 | 1.9 | 2.5 | .5 | 1.2 | 2.2 |
| | 1420 | N-S | 72 | | 2.5 | 3.0 | 1.9 | 1.1 | 1.3 | 3.8 |
| | 1425 | E-W | 103(E) | | 1.2 | .3 | 1.1 | .9 | 4.8 | 1.7 |
| | 1425 | N-S | 103(E) | | 2.3 | .3 | .5 | 3.2 | 7.2 | 2.6 |
| | 1430 | E-W | 95 | | 15.0 | 10.2 | 17.6 | .5 | 1.8 | 21.3 |
| | 1430 | N-S | 95 | | 13.1 | 8.9 | 9.8 | .7 | 1.8 | 18.2 |
| | 1440 | E-W | 90 | | 7.0 | 6.0 | 9.2 | .5 | 1.6 | 9.2 |
| | 1440 | N-S | 90 | | 9.5 | - | 11.1 | .6 | 1.3 | 14.6 |
| | 1445 | E-W | 85 | | 8.7 | - | 8.5 | .7 | 1.3 | 11.6 |
| | 1445 | N-S | 85 | | 8.3 | - | 6.9 | .8 | 1.4 | 11.5 |
| | 1450 | E-W | 103(E) | | 1.0 | .3 | .1 | 9.7 | 4.3 | 1.4 |
| | 1450 | N-S | 103(E) | | 1.0 | .3 | .4 | 2.1 | 4.5 | 1.4 |
| | 1455 | E-W | 78 | | 4.6 | 4.6 | 4.4 | .8 | 1.6 | 7.0 |
| | 1455 | N-S | 78 | | 3.6 | 3.6 | 2.7 | 1.0 | 1.4 | 5.0 |
| | 1535 | E-W | 78 | | 2.0 | 2.4 | 3.7 | .5 | 1.5 | 3.6 |
| | 1535 | N-S | 78 | | 3.3 | 3.2 | 8.3 | .4 | 1.7 | 5.5 |
| | 1540 | E-W | 90 | | - | 9.3 | 9.6 | .8 | 2.0 | - |
| | 1540 | N-S | 90 | | 9.8 | 6.2 | 8.6 | .7 | 1.9 | 13.1 |
| | 1545 | E-W | 95 | | 10.5 | 8.0 | 11.3 | .6 | 1.8 | 14.6 |
| | 1545 | N-S | 95 | | 11.5 | 7.4 | 17.4 | .5 | 1.9 | 17.6 |
| | 1550 | E-W | 88 | | 8.1 | 4.6 | 9.2 | .6 | 2.2 | 11.3 |
| | 1550 | N-S | 88 | | 9.0 | 5.5 | 10.7 | .6 | 2.1 | 13.0 |

(1) Model 1 is appropriate.

(2) Model 2 is appropriate.

(3) Neither model is appropriate.

(4) Asymmetry for the orthogonal observing planes is evident.

Some of the results fall somewhere in between these broad classifications. For example in Table 4.3 the results for the 73 km echo at 1615 hrs on 30/11/71 fit neither model well, although possibly model 1 might be favoured. On the other hand, since model 2 assumes that b is large compared with unity, it is possible that a weak specular component is present and that consistency for the second model breaks down because b is not large. The results for 80 and 85 km on the same date are considered to be in good agreement with model 1.

As with the phasor diagram results of §4.3.1 it has been found convenient to distinguish between two regions within the D-region in the present investigation and the boundary between these is again best placed at about 85 km. Table 4.4 summarizes the classification of all results obtained making this distinction. The few E-region results obtained have not been included for the region above 85 km. Although fewer observations were made for the lowest D-region, due to smaller reflected signal levels (being accented in summer), it is thought this factor is not significant enough to invalidate any of the conclusions drawn.

| Appropriate Model | < 85 km | ⩾ 85 km |
|---|---|---|
| Model 1 | 50% | 81% |
| Model 2 | 26% | 2% |
| Neither model | 24% | 17% |

TABLE 4.4. Comparison of scattering models for two height regimes within the D-region.

An inspection of Table 4.4 reveals that there is a clear distinction between the two height regimes distinguished in the D-region. Below 85 km 50% of the time random scatter has been observed while above 85 km this figure has risen to 81%. The very small occurrence of the specular component model above 85 km is a very striking result shown in Table 4.4, this model being established in only 2% of observations. This model was fairly well established on 26% of occasions below 85 km showing a considerable difference between the two regions. A significant occurrence of records where neither model was appropriate is evident from Table 4.4, with about the same percentage occurrence for both height regions. Some further discussion of these features is appropriate at this stage.

4.3.6 The breakdown of the assumed models

The significant occurrence (about 20%), for all heights in the D-region, of records where neither model is appropriate leads to speculation as to an appropriate explanation. In chapter 3 various factors which might affect the statistics of the reflected wave field were mentioned. The conclusion that has been drawn is that there

might well be a tendency for the 'true' scattering model to be masked by variable absorption and reflection coefficient effects with a resultant degeneration towards apparent randomness of the observed signal. From such reasoning it is suggested that in Table 4.4 the figures for agreement with model 1 might be regarded as an upper limit while those for model 2 as a lower limit. One point which is quite significant is that all of those records which are not in agreement with model 1 have had some coherent or specular contribution but in many cases this has not complied with the stringent assumptions of model 2 and the precise definition of the coherence ratio. If we were to consider that all records which are not in agreement with model 1 are classified as having some specular component (not necessarily a statistically stationary situation) then we would find (see Table 4.4) that 19% of records above 85 km and 50% of those below 85 km exhibit some form of coherent contribution. It seems fairly well established then that a significantly greater occurrence of specular or coherent contributions occurs in the lower height regions of the D-region. The possibility that "masking" effects, due to variable absorption and reflection characteristics, are more pronounced above 85 km is recognized and it is felt that although such an effect is possible, it probably would not account for the difference observed for the two height regions distinguished in this work. This subject could present an interesting line of theoretical enquiry, although no such attempt has been made in the present study.

### 4.3.7 The inflexibility of model 2 and the concept of coherence ratio

In view of the results summarized by Table 4.4 the assumption, for model 2, that only a single specular component of fixed amplitude and direction of arrival is present often proves to be a restrictive one. A consideration of the physical situation, in which we have an ionosphere probably in continual motion with drift velocities of the order of 50 m/sec, demonstrates that such a result is perhaps not surprising. By definition the specular component is a plane wave of fixed amplitude and direction of arrival. However, any wave reflected from the ionosphere will almost certainly vary in direction to some extent, so that the allowable limits of direction change within a specified time interval must be defined before a wave can be classed as specular or not. These limits will depend on the accuracy with which phase measurements can be made. With the equipment used, a resolution of $\pm 3.5^{\circ}$ was achieved and at a row spacing of about 200 metres and a wavelength of about 150 metres the allowable variation in direction of arrival of a "specular" component before it is considered to be changing in direction of arrival is less than $1^{\circ}$. Such a limit places stringent requirements on the stability of the ionosphere over a recording period (typically about 5 minutes) and such requirements, on the evidence of Table 4.4, are often not met.

The strict definition of coherence ratio would prescribe a low value for a completely "coherent specular" reflection wandering in direction of arrival. In this sense the formal coherence ratio is at variance with what one would normally intuitively associate with the

concept of coherence. It is well known that more than about five simultaneous specular components with independently varying phases are indistinguishable from a random spectrum of waves (Goldstein, 1958) and in this case the prescribed coherence ratio is a useful quantity, especially since the observed "coherence" properties of reflections are often sufficient for many purposes where a detailed morphology of the reflection processes themselves are not required.

In summarizing the foregoing discussion it is concluded that those results in Table 4.4 which do not fit either of the assumed models may represent one or more of the following situations:-

(1) Up to three or four separate specular components are present (if there were more, the results would fit the random model reasonably well).

(2) The specular component(s) wander about in direction of arrival.

(3) The specular component(s) have time varying amplitudes.

(4) The specular component(s) may not account for a large fraction of the power returned, contrary to the assumption in model 2 that $b \gg 1$.

On inspection of Table 4.3 it is felt that evidence for the existence of one or more wandering specular components is provided by the fact that b, as estimated from the mean absolute phase difference (equation 4.10) is usually lower than b calculated from amplitude statistics (equation 4.9). A wandering specular component

could be expected to leave the amplitude statistics virtually unaffected whereas the mean absolute phase difference would be increased, producing a discrepancy with b calculated from the amplitude results in the same sense evident in the results given in Table 4.3.

4.3.8 Asymmetric records

In the present context "asymmetry" may arise in two distinct forms:-

(1) A difference in the appropriate classification of models for the orthogonal observing planes occurs.

(2) Consistent models fit both planes but a significant difference in the angular spread or coherence ratio is obtained for the two planes.

An example of a record classified in category (1) is that for 72 km taken at 1350 hrs on 27/3/72. In the N-S plane model 2 fits well, whereas in the E-W plane model 1 is probably a closer fit. A physical situation which would give rise to such a circumstance is one where a specular component arriving from an off vertical angle lies closely in the N-S observing plane. Varying degrees of asymmetry might be expected depending on the geometrical aspect of the specular reflection with respect to the two orthogonal observing planes. On the one extreme, one plane may agree with model 1 and the other with model 2 or, alternatively, both may agree with model 2 but have differing calculated coherence ratios, purely due to the geometrical projection of an off vertical component onto both planes. An example of the latter possibility is afforded by the results of Table 4.3 for

75 km at 1600 hrs on 15/12/71. This case overlaps with the second category of asymmetry listed above.

Two good examples of results in the second category, where the angular spread was asymmetric, are shown for 88 km at 1400 hrs and for 80 km at 1415 hrs, both on 27/3/72. In these cases model 1 fitted both planes but the angular spread, in both cases, differed by a factor of about two between the orthogonal planes, with the larger spread in the E-W plane. A similar case occurs at 90 km at 1550 hrs on 15/12/71 as seen in Table 4.3 and this asymmetry is seen to be consistent with the examples of records shown in Figure 4.7 from which these results were derived. It is apparent that in such situations the mechanism for producing such an asymmetry effect will be different from that required to explain the type of asymmetry of the first category. Where reflecting irregularities are elongated in one direction such a situation might arise. It was surmised that possibly a factor contributing to such an anisotropy might be a peculiarity in the drift velocity. Since the experimental method employed inherently requires the amplitude records for spaced rows of aerials in orthogonal planes, the necessary velocity information is able to be derived from the records obtained. The flexibility of the experimental arrangement becomes evident, for drift velocity determinations, simultaneous with scattering model investigations, are able to be made. A compilation of the drift velocities showed that at 88 km at 1400 hrs the velocity was 34.8 m/sec in a direction 50° East of North while at 80 km at 1415 hrs the velocity was 44.5 m/sec in a direction 131° East of North. At 1550 hrs the velocity at 88 km was 30.1 m/sec in a direction 72° East

of North and on this occasion no asymmetry of angular spread in the two planes was evident. Unfortunately a corresponding check for the 80 km echo could not be made but it is felt that the drift velocities show no peculiarities which might account for the asymmetry effects observed in the angular spread. In fact in this case the direction of drift was closely symmetrical with respect to the two observing planes. The occurrence of asymmetry in the records has been fairly small.

## 4.4 Other results

### 4.4.1 Some night time measurements of angular spread

No extensive night time results were obtained although a few results worthy of presentation will now be described. Figure 4.8a shows a plot of the angular spreads measured during the 24 hr period from 12 noon on 16/8/71 to 12 noon on 17/8/71. It can be seen that after about 1800 hrs no echoes were monitored below 85 km. Echoes at 85 and 90 km were able to be monitored throughout the night and showed a definite minimum in the angular spread during the interval 2000 to 24000 hrs. The lower echoes are seen to appear again in the morning at about 0730 hrs. All night time measurements have been included in a scatter plot in Figure 4.8b and it can be seen that, although there is a large scatter of values, at night the angular spread is often significantly smaller than the average daytime values of Figure 4.6b. In fact some values obtained were lower than any values ever obtained for the corresponding height during the daytime. It is suggested that the dynamics and scattering mechanisms in the night time D-region are significantly different from the day time ones, and that coherent

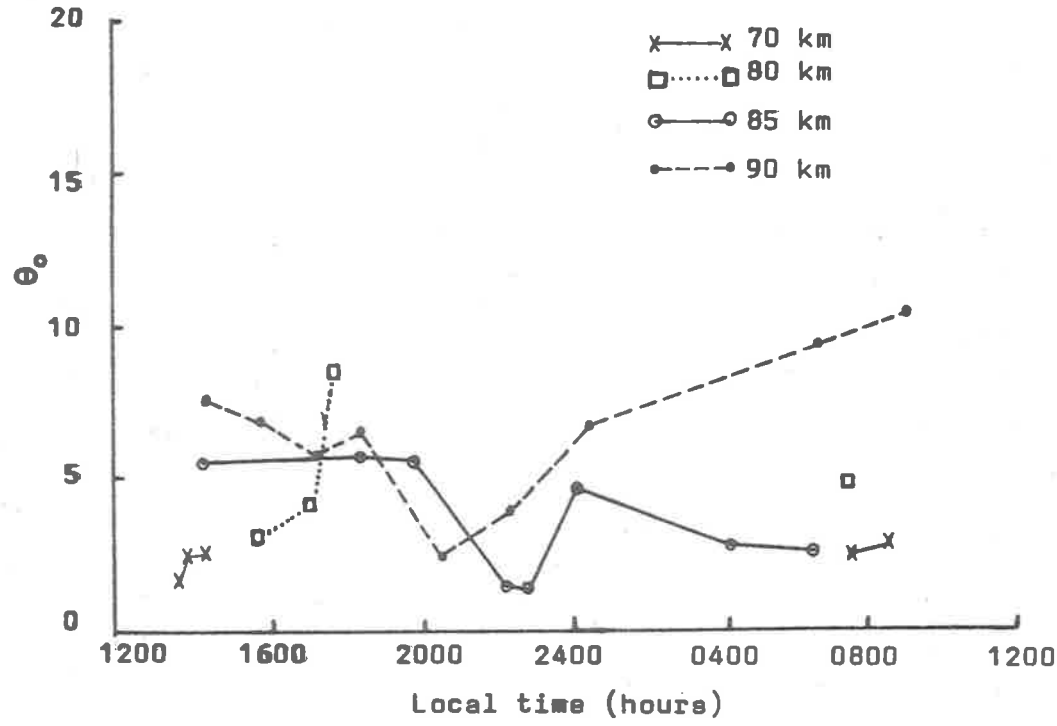


Figure 4.8a Observations of angular spread during a 24 hour period from noon 16/8/71 to noon 17/8/71.

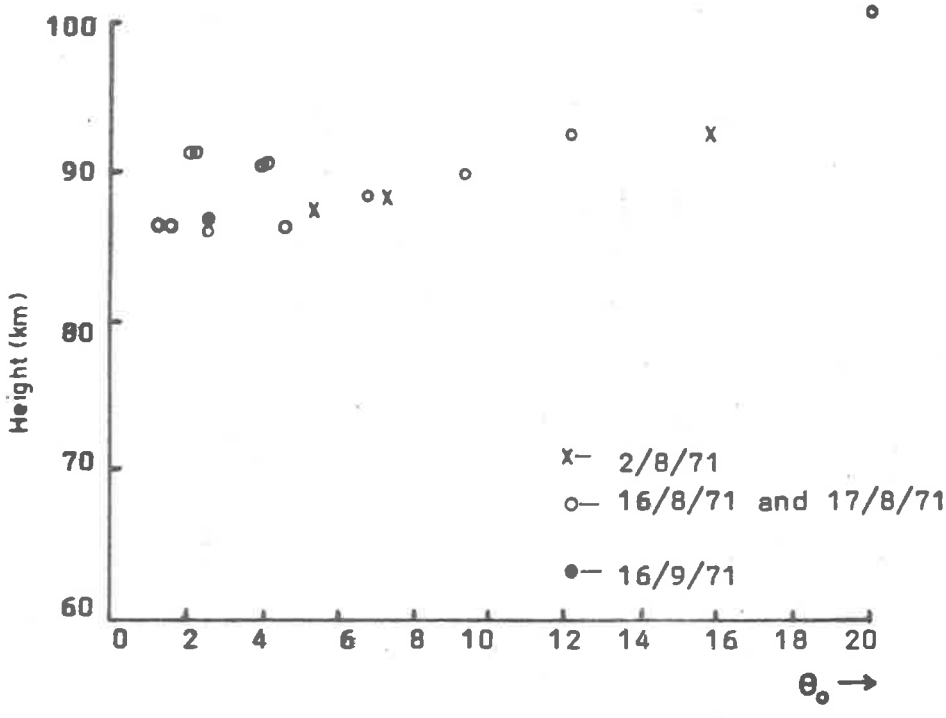


Figure 4.8b Night time observations of angular spread.

contributions from above 85 km are obtained occasionally at night but rarely during the day.

4.4.2 Amplitude fading periods

During 1971 many amplitude records for partial reflections were taken, most of these being recorded at the same time as the phase difference information for measuring the angular spread. From these records a survey of the amplitude fading characteristics has been carried out and the results are summarised in Figure 4.9. Reflections have been classified into the height intervals shown in the figure where points representing monthly mean values have been joined by solid lines. It can be seen that below 75 km the fading was of considerably longer period in February than for the following months up to June. The most rapid fading occurred in May and June. From August to December there was a slow increase in the mean fading period towards the summer months. An increase in the mean fading period by more than a factor of two is evident for the July results for all heights below 80 km. Above 80 km little seasonal variation in the mean fading speeds can be detected. Figure 4.10 is a scatter plot of all amplitude fading periods measured for the various heights in the D-region. The solid curve depicts the mean height profile of the amplitude fading period. It can be seen that below about 80 km substantially slower fading occurs than for the region above 80 km where the fading period is usually about three seconds. The wide range of periods below 80 km are considered to be consistent with the scattering model results and indicate that the scattering mechanism varies somewhat.

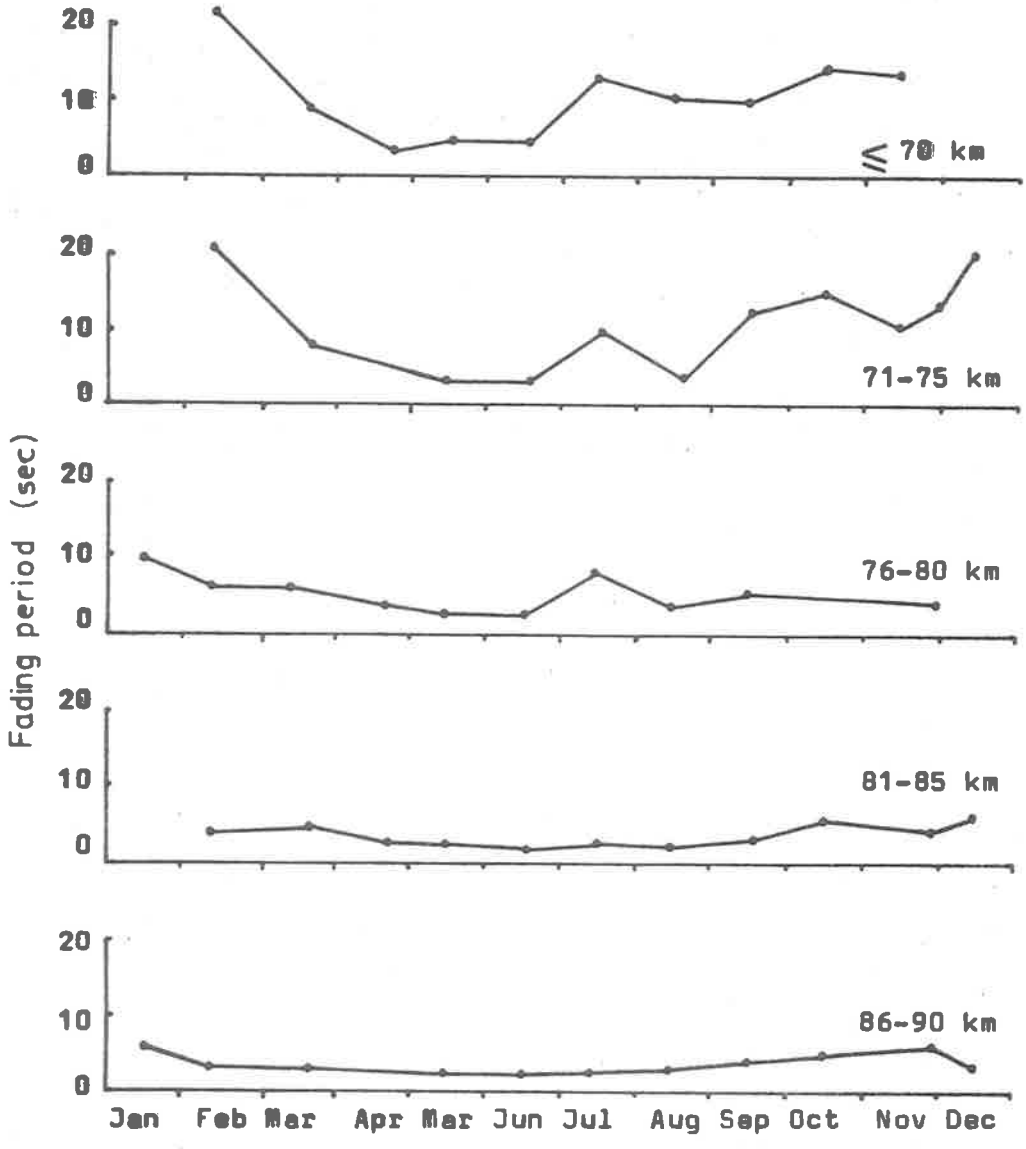


**Figure 4.9** Seasonal variations of amplitude fading periods for D-region partial reflections.

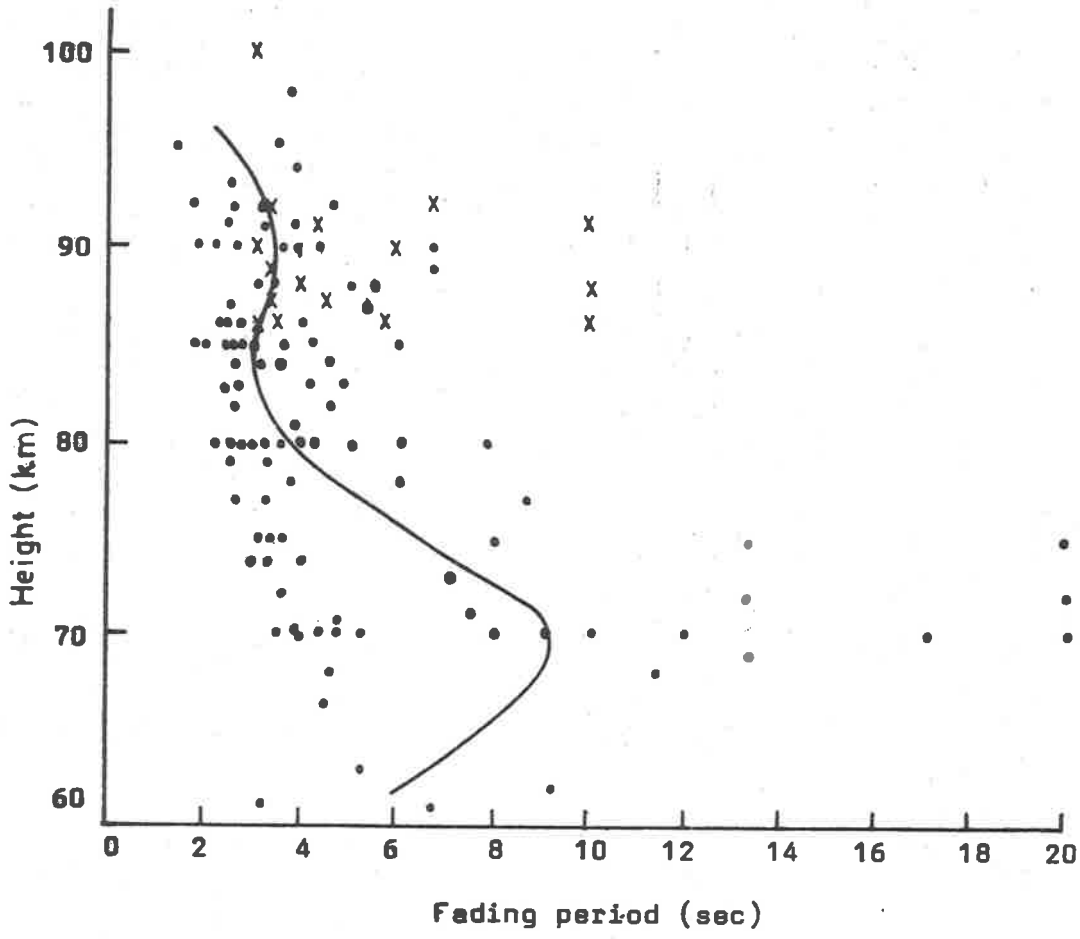


Figure 4.10 Scatter plot of all measurements of day time fading periods (marked •) and some night time measurements (marked x).

The few night time results available have been plotted as crosses and indicate that on many of the occasions the fading period is much longer than is ever observed during the day at the same heights. These occasions corresponded to the occasions where night time values of angular spread were much lower than normal day time values at the same heights (see Figure 4.8b). No night time reflections were observed below about 85 km.

### 4.4.3 The effects of the transmitted pulsewidth on the measurements of angular spread

In most of the investigations carried out a transmitted pulse of about 30 μsec duration was employed. It can be appreciated from geometric considerations as depicted in Figure 4.11a, that the transmitter pulsewidth can impose an artificial upper limit on the observable angular spread of waves reflected from a given height. It is of interest to assess whether such artificial limits may have been imposed on the angular spreads measured.

Due to the narrow but finite pulsewidth $\tau$ necessary to achieve good height resolution, reflections returning from $c\tau/4$ either side of a given range H can be construed as arriving from an apparent height H. If we consider an infinitely thin horizontal layer situated at a height H which is reflecting, then the maximum angle $\theta_m$, say, at which it can still contribute to the range H is given by

$$\cos \theta_m = \frac{H}{H + c\tau/4} \quad , \qquad 4.11$$

where c = velocity of the radio wave. Using $\tau$ = 30 μsec, equation 4.11 describes the limiting angle $\theta_m$ as a function of height. This curve is

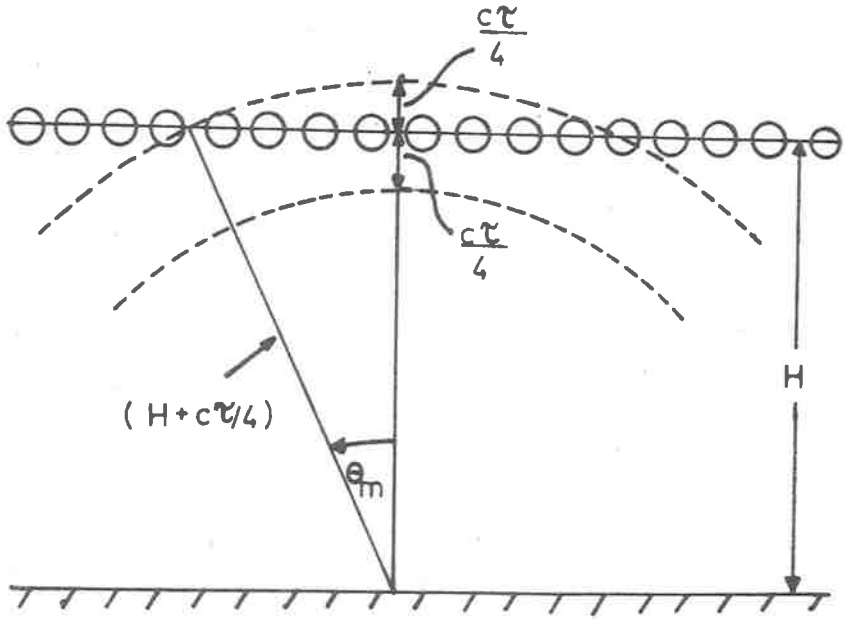


Figure 4.11a The geometry of the scattering volume centred on range H using a pulsewidth of $\tau$ μsec.

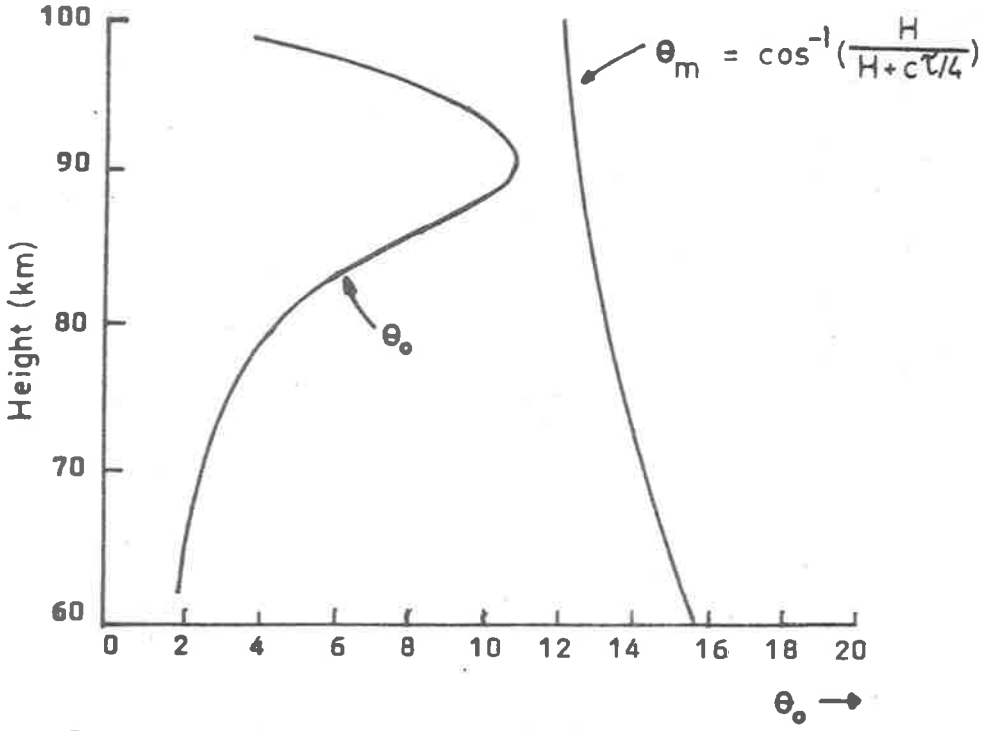


Figure 4.11b Comparison of the mean angular spread profile with the upper limit $\theta_m$ imposed on measurements by a finite pulsewidth $\tau$.

plotted on the same graph together with the average profile of angular spread given in Figure 4.3b and the result is shown in Figure 4.11b. It is seen that the measured angular spreads are generally well below the artificial upper limit although near 90 km individual readings might occasionally have been limited by the pulsewidth. On 15/12/71 the results presented in Table 4.3 were obtained using a pulsewidth of 30 μsec up until 1540 hrs, after which the pulsewidth was doubled. It can be seen that no appreciable increase in angular spread was detected for any given height. It is felt that in general the pulsewidth was not so narrow as to limit the measured angular spread in the manner described above.

## 4.5 Discussion and comparison of results with other evidence

The experimental evidence presented in this chapter suggests that the D-region may be divided into two fairly distinct height regimes with a boundary at about 85 km. The angular spread of reflected waves shows a sharp increase above this height as shown in Figure 4.3b. This division into two height regimes is also consistent with the observations of the scattering models as summarized by Table 4.4 where it is seen that a randomly phased angular spectrum of waves is generally obtained from above 85 km, while below this height significant occurrences of coherent reflections are observed. It is apparent that scale sizes of ionospheric irregularities decrease with increasing height giving increasing angular spreads with increasing height. Another result which is consistent with the notion of two distinct height regimes within the D-region is the observed height variation

of amplitude fading periods described in §4.4.2 and it is seen that distinctly slower fading, consistent with more stable conditions, occurs in the lower D-region. It is interesting to compare these results with the observations of the angular spread $\theta_o$ reported in section 4.2. If the drift velocity is assumed to be constant to the first order, the fading speed will be inversely proportional to the scale of the pattern, which is, in turn, inversely proportional to $\theta_o$. Thus rapid fading should correspond to large values of $\theta_o$. The observed seasonal and diurnal changes and height variation of fading period are reasonably consistent with this interpretation.

There is generally a paucity of experimental evidence regarding the nature of D-region scattering so that only a few comparisons of the present results with observations of other workers are possible. An isolated measurement of the spread of the angular spectrum of waves partially reflected from the D-region has been made by Golley and Rossiter (1970) from amplitude observations used for drifts analysis, and they reported a calculated cone semi-angle of $15^{\circ}$ at about 90 km. The results presented in Figure 4.2 show that angular spreads of about this magnitude were observed near 90 km during the course of the present investigations. In Figure 4.12 the winter (1971) profile of angular spread measured at Adelaide is compared with a winter (1970) profile obtained by Vincent (1972) at Ottawa. The latter worker used a beam switching experiment in which the relative signal powers received with a 4 dipole and a 40 dipole array were used to deduce the angular spread of downcoming waves.

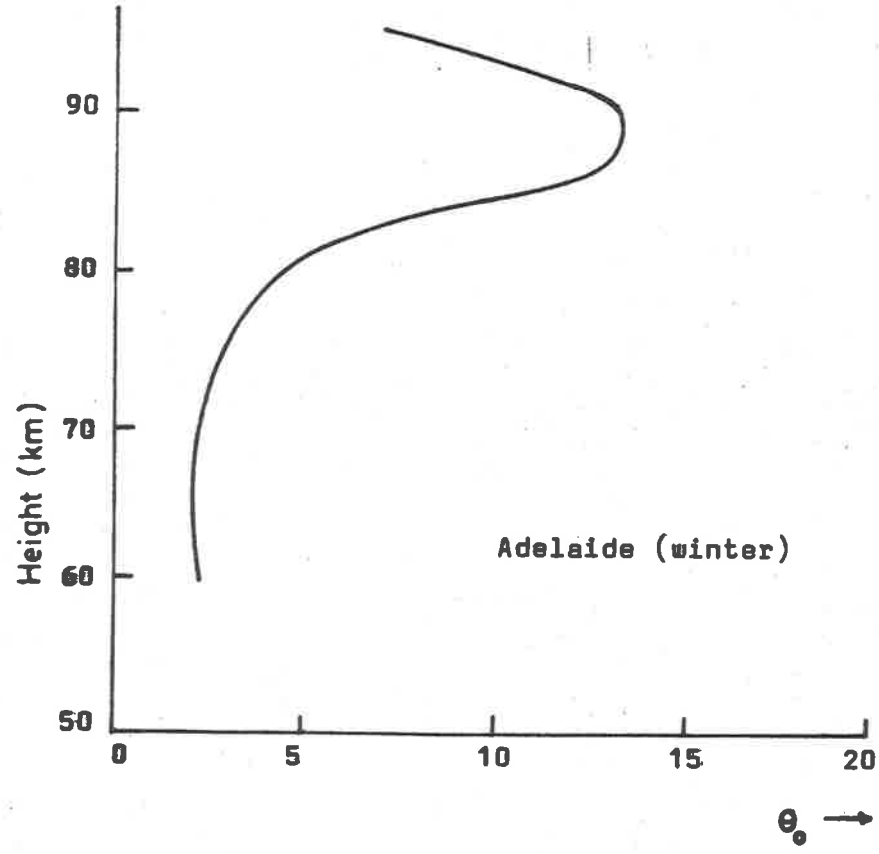


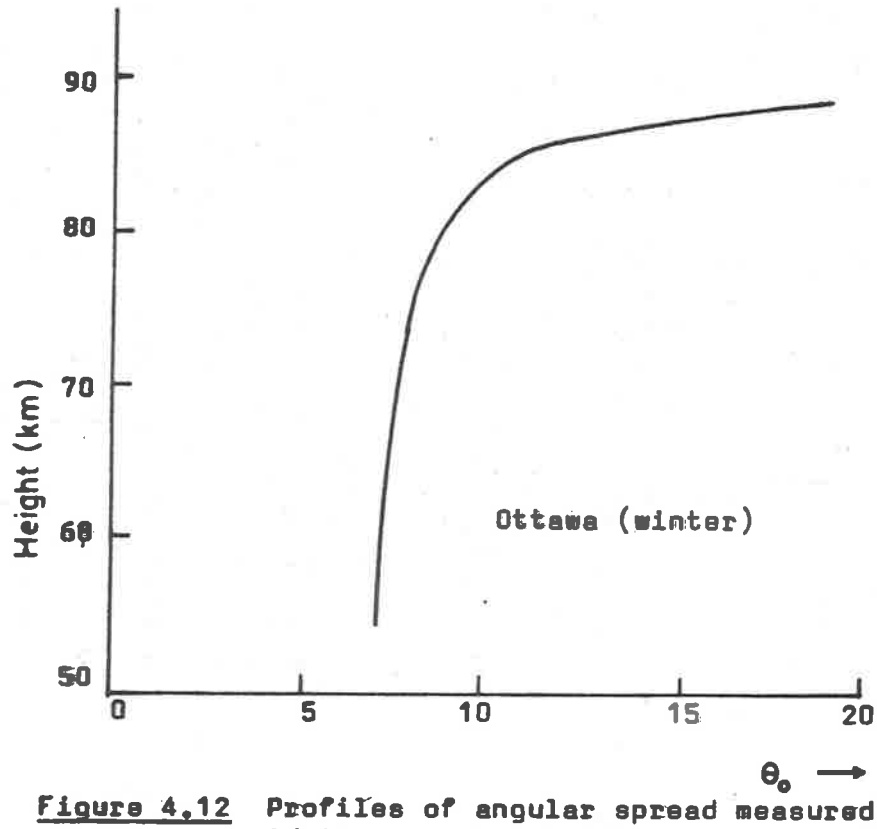


Figure 4.12 Profiles of angular spread measured at Adelaide and at Ottawa.

Although a quantitative comparison of the profiles is difficult, unless a transformation between the two dimensional approach used here and the three dimensional approach used by Vincent is made, strong similarities in the profiles are seen. A slowly increasing angular spread with increasing height up to about 85 km and then a sharp increase at about 85 km is evident in both profiles. No data above 90 km is available for Ottawa and the Adelaide results show a peak in spread at about 90 km. Another conclusion which was drawn by Vincent (1972) from a study of amplitude statistics was that many echoes resulted from scatter from several irregularities usually greater than four in number, although significant occurrences of specular contributions were noted. Although Vincent has not directly distinguished between two height regimes in his work, the overall agreement of the present results in Table 4.3 is quite good.

The present results show consistency with the work of Vincent (1967), and Fraser and Vincent (1970), the latter work being based on observations of the coherence and scale size of phase variations of the ground diffraction pattern formed by partial reflections. The coherence index derived by these workers showed that generally much higher coherence was observed for the 70 - 79 km region than for the 80 - 89 km region. The smallest pattern size, highest fading rates and the lowest coherence were all observed in winter and support the present results which indicate that the greatest angular spread and variability as well as highest fading rates occur in winter. The notion that the D-region is most disturbed in winter has also been subscribed to by

many workers including Gregory and Manson (1969) who showed that anomalous behaviour and greatest variability of D-region electron densities occurred in winter. They postulated that these findings could be associated with the upward propagation of large scale wave motions which theoretically can propagate to D-region heights only in winter (Charney and Drazin, 1961). Nordberg and Smith (1963) and Nordberg at al. (1965) from rocket grenade studies of D-region temperatures at Wallop's Island ($38^{o}$N) have arrived at similar conclusions regarding the seasonal stability of the D-region. Their mean temperature profiles show that the mesosphere is warmer in winter than in summer. Summer profiles show smooth height variations of temperature with good consistency from day to day. The winter profiles however often exhibit multiple peaks or inversions which appear to be unstable in that they lack day to day consistency. The results are therefore consistent with a less stable winter D-region.

Another aspect of D-region studies is concerned with the vertical thickness of D-region scattering regions. Gregory and Vincent (1970) showed that in the 80 - 90 km height interval substantially thicker regions appeared to contribute to a given reflection than for reflections received from below this region. This finding is consistent with a physical situation where there are a greater number of independent components contributing to reflections from above 80 km resulting in less coherent echoes from that region, and in this respect the present results may therefore be considered to be consistent with those of Gregory and Vincent.

Austin and Manson (1969) have reported that observations of D-region reflection characteristics are best explained by the presence of several scatterers filling only a minor portion of the available scattering volume. It is suggested that the results of the present investigation which fit neither of the models investigated may well be explained by a model similar to that of Austin and Manson (1969), where several "coherent" components may be present. It is uncertain whether the results which were found to be consistent with a spectrum of randomly phased components are due to a continuous volume scatter process or due to several independent coherent components greater than about five in number producing an equivalent effect.

In contrast to the good agreement which has been found between the present results and the results of other workers, as has been just discussed, some results of von Biel (1971) appear to be in disagreement with the present results and those of other workers. The conclusions of von Biel, derived from studies of amplitude distributions using the theory of Rice (1945), are in direct contrast to the results encountered in the present investigation in that they show predominantly a randomly phased Rayleigh type scatter for the lower D-region with a significant increase in the occurrence of reflections having a specular component at heights of 85 and 90 km. The opposite effect has been found in the present results. The present studies and those of von Biel were carried out at different times of the year at somewhat different latitudes, but it is considered unlikely that such considerations can account for the difference in results obtained. The results of von Biel

show an inconsistency with the characteristics of D-region partial reflections as observed at the same site by other workers (e.g. Fraser and Vincent, 1970; Gregory and Vincent, 1970) and consequently they must be regarded as suspect.

## 4.6 Conclusions

In this chapter results have been presented which are consistent with the notion of decreasing coherence of partial reflections with increasing height in the D-region. A rapid transition in this sense appears to occur at about 85 km, this being inferred from the evidence of three observed characteristics of the received echoes. Firstly, a sharp increase of angular spread occurs at 85 km (see Figure 4.3b); secondly, the scattering from above 85 km shows far less coherence than for the lower D-region (see Table 4.4); and finally, slower fading is observed below 85 km than for the higher regions, indicating greater stability and coherence of the partial reflections from the lower D-region.

Finally, it is to be noted that these observations quantitatively verify similar conclusions which were drawn from qualitative assessments of chart records and the associated phasor diagram representations of the complex wave field observed on the ground, examples of which were shown in Figure 4.5. On the whole, the results presented in this chapter show good agreement with the small amount of other available evidence relevant to the nature of D-region partial reflections.

# CHAPTER 5

# THEORETICAL ASPECTS OF THE DIFFERENTIAL ABSORPTION EXPERIMENT FOR STUDYING D-REGION ELECTRON DENSITIES

## 5.1 Introduction

In chapter 1, in the survey of ground based radio methods for studying the ionosphere, two ground based radio techniques for studying D-region electron densities were briefly described. One of these, the Differential Absorption Experiment (DAE) was employed as part of the project described in this thesis for investigating the D-region, and in this chapter the preliminary theoretical aspects which need consideration before such an experiment can be interpreted are discussed. The theoretical framework for determining electron densities along with the underlying assumptions, properties and deficiencies of the theory are discussed.

## 5.2 The reflection model

Two important processes affecting received partial reflection amplitudes must be considered in determining electron densities from partial reflection measurements; these are absorption and reflection processes. Some controversy has arisen in recent years (Flood, 1969; Holt, 1969; Belrose, 1970) as to the theoretical description of such processes that should be applied to the interpretation of experimental investigations. The original theory of Gardner and Pawsey (1953) assumed that partial reflections arise from Fresnel reflection at

sharp discontinuities in refractive index of large horizontal extent. In later years Flood (1968, 1969) has given a rigorous theory for the situation where a given reflection is composed of a continuum of contributions from a scattering volume geometrically determined by the transmitted pulsewidth and antenna beamwidth. This theory took into account differential absorption of the 'O' and 'X' mode waves in the scattering volume itself to arrive at a sophisticated iterative process for determining electron densities.

Belrose and Burke (1964) have shown that, using the Booker scattering model to describe contributions from a scattering volume (but neglecting differential absorption within that volume), the same ratio of 'X' and 'O' reflection coefficients $R_x/R_o$ is obtained as for the strict Fresnel model employed by Gardner and Pawsey. While the results of chapter 4 would indicate that on occasions a volume scattering model could be appropriate, it is now generally agreed that in most situations there is little difference between electron densities deduced from the various rival theories (Holt, 1969; Flood, 1969; Belrose, 1970). Some results given in chapter 8, which may be interpreted as being consistent with this finding, show that well defined preferred heights of reflection often exist in the D-region, suggesting that reflecting regions tend to be of limited vertical extent and possibly occupy a space smaller than the allowable scattering volume, in which case the volume scattering theory would be expected to reduce to the simpler Fresnel theory. The simpler Fresnel theory of reflection has been adopted for the DAE work described in this thesis and only this theory will be described here.

Various workers have considered that the presence of off-vertical reflections in the DAE has produced significant uncertainties in calculated electron density profiles as a result of uncertainties in the true heights from which signals are being reflected. With the large aerial array used in the present study, the signals received were confined to within about $5^{\circ}$ of vertical. The measurements of angular spread reported in the last chapter, show that reflections from heights greater than about 75 km can come from larger angles than this, so that the use of the large receiving array has helped to minimize the effects of off-vertical reflections in such cases. Simple geometric arguments show that both the transmitted pulsewidth and the angles of arrival of reflected waves determine the range of heights which can contribute to an apparent reflection height. In the present system, with a reception polar diagram of beamwidth $\pm 5^{\circ}$ and a 20 μsec pulsewidth, the error in equating the apparent height to the true height of reflection is less than 2 km for heights below 90 km.

## 5.3 The working equations assuming Fresnel reflection

In general, the amplitude A of a signal reflected from a height h in the ionosphere will depend on the reflection and absorption coefficients as follows:

$$A \propto R \exp\left(-2\int_{o}^{h} K dh\right), \qquad 5.1$$

where R and K are the reflection and absorption coefficients respectively; both being functions of height. The factor of two in the absorption integral allows for equal absorption on the upward and

downward propagation paths. If we now appreciate that R and K and hence A may differ in magnitude for oppositely polarized waves 'O' and 'X', then subscripting these quantities accordingly it follows from equation 5.1 that

$$\frac{A_x}{A_o} = \frac{R_x}{R_o} \exp - 2 \int_o^h (K_x - K_o)\, dh. \qquad 5.2$$

The possibility of determining electron densities emanates from the proportionality of the differential absorption $(K_x - K_o)$ to local electron density. Taking natural logarithms of both sides of equation 5.2 as applied to some height $h_1$, say, yields

$$\log_e A_1 = \log_e R_1 - 2 \int_o^{h_1} (K_x - K_o)\, dh\ , \qquad 5.3$$

where we have written $A_1 = A_x/A_o$ at height $h_1$ etc. Similarly, for a height $h_2$ we get

$$\log_e A_2 = \log_e R_2 - 2 \int_o^{h_2} (K_x - K_o)\, dh\ . \qquad 5.4$$

Now if $h_1$ and $h_2$ are heights close enough so that the differential absorption factors between these two heights can be considered as being approximately constant for the purposes of integration, equations 5.3 and 5.4 show that

$$\log_e (A_1/A_2) = \log_e (R_1/R_2) - (K_x - K_o)(h_2 - h_1)\ . \qquad 5.5$$

Since $K_x$ and $K_o$ are proportional to the electron density between the heights $h_1$ and $h_2$, we may substitute $K_x - K_o = (k_x - k_o)\, N$ into equation 5.5 (where N is the mean density in the height interval) and solve for N to get:-

$$N = \frac{\log_e \left(\frac{A_1 R_2}{A_2 R_1}\right)}{2(k_x - k_o)(h_2 - h_1)} \quad . \qquad 5.6$$

Using this equation to derive electron density profiles involves

(1) experimental determinations of the variation with height of reflection of the amplitude ratio $A_x/A_o$ as measured on the ground.

(2) Theoretical determinations of the expected height variation of electron collision frequency, the ratio of reflection coefficients $R_x/R_o$ and also the differential absorption factor $(k_x - k_o)$.

The factors involved in (2) will be considered in the following section

## 5.4 Electron collision frequency profiles

In the calculation of the variations of $R_x/R_o$ and $(k_x - k_o)$ with height, an assumption of the height variation of electron collision frequency is required. Phelps and Pack (1959), from laboratory measurements, have shown that the collision frequency of mono-energetic electrons in air is proportional to the electron energy. From this and the gas law ($pV = nRT$) it follows that for electrons of energy kT the collision frequency is proportional to atmospheric pressure. For the purposes of the theoretical calculations described in the following work the pressure profiles of Rofe (1966), measured at Woomera, Sth. Australia, have been adopted and collision frequencies have been evaluated using the relation given by Gregory and Manson (1969), viz:

$$\nu = 6.4 \times 10^4 P \ \text{sec}^{-1} \ ,$$

where $\nu$ is the collision frequency in terms of the atmospheric pressure P in dynes/cm$^2$. The seasonal variation in pressure, which amounts to approximately 10%, has been allowed for in all subsequent calculations by compiling monthly collision frequency profiles. It is considered that the adoption of Rofe's pressure profiles, which differ from U.S. Standard Atmosphere values by up to 35% near 85 km, would significantly contribute to the reliability of deduced electron densities.

## 5.5 Calculations of the variations of $R_x/R_o$ and $(k_x - k_o)$ with height

Apart from the question of the applicability of either a volume scattering or a Fresnel reflection model, some uncertainty as to the actual causes of the sharp gradients in refractive index at the levels of partial reflection require some assumption to be made in order to calculate $R_x/R_o$ profiles. It is generally thought that these abrupt changes in refractive index can arise from either of, or a combination of, two possible situations:-

(1) Abrupt changes of electron density.

(2) Abrupt changes of the collision frequency of electrons with neutral molecules.

While the former process has been widely assumed to be the dominant one, several workers have pointed out that changes of collision frequency could be important and there have been several theoretical investigations of this problem (e.g. Piggott and Thrane, 1966a; Manson, 1966; Belrose et al., 1967; Belrose, 1970).

Assuming Fresnel reflection takes place at a sharp boundary which has refractive indices $n_1$ and $n_2$ on either side of the boundary, then the reflection coefficient will be

$$R = \frac{n_2 - n_1}{n_2 + n_1} ,$$

and if $n_1 \simeq n_2 \simeq 1$ this relation becomes

$$R \simeq \frac{\Delta n}{2n} . \qquad 5.7$$

The ratio of reflection coefficients for 'O' and 'X' waves then becomes

$$\frac{R_x}{R_o} = \frac{\Delta n_x \cdot 2n_o}{2n_x \cdot \Delta n_o} \simeq \frac{\Delta n_x}{\Delta n_o} . \qquad 5.8$$

Sen and Wyller (1960) have shown that the complex refractive index in a magneto-ionic medium is given by:

$$n^2 = \left(\mu - \frac{ick}{\omega}\right)^2 = \frac{A + B \sin^2\phi \pm (B^2 \sin^4\phi - C^2 \cos^2\phi)^{\frac{1}{2}}}{D + E \sin^2\phi} \qquad 5.9$$

where $\phi$ is the angle the direction of propagation makes with the earth's magnetic field and A,B,C,D and E are constants which depend on the radio wave frequency $\omega$, the electron gyro-frequency $\omega_H$ and the collision frequency. The $\pm$ signs apply to 'O' and 'X' polarizations.

The relative significance of the two possible causes of abrupt changes in refractive index listed earlier in this section is most conveniently described in terms of the parameter

$$\alpha = \frac{\Delta\nu/\nu}{\Delta N/N} , \qquad 5.10$$

where $\Delta\nu/\nu$ and $\Delta N/N$ are the fractional changes in collision frequency and electron density respectively. For $\alpha = 0$ we have the customary

assumption that only changes in electron density are important while for $\alpha = \infty$ changes of collision frequency are dominant. Piggott and Thrane (1966a) have shown that the ratio of reflection coefficients can now be expressed in terms of $\alpha$ as

$$\left|\frac{R_x}{R_o}\right| = \left|\left(\frac{n_o}{n_x}\right)^2\right| \cdot \left|\frac{N\frac{\partial}{\partial N}(n_x^2) + \alpha\nu_m \frac{\partial}{\partial \nu_m}(n_x^2)}{N\frac{\partial}{\partial N}(n_o^2) + \alpha\nu_m \frac{\partial}{\partial \nu_m}(n_o^2)}\right| . \qquad 5.11$$

This expression has been used to determine monthly profiles of $R_x/R_o$ using $\alpha$ as a parameter and using equation 5.9 for $n_{x,o}$. Examples of these profiles, appropriate to the Buckland Park system, are shown in Figure 5.1. It is evident that considerable error in the determination of electron densities might result if an inappropriate reflection process is assumed, for the $R_x/R_o$ profiles vary significantly with $\alpha$. In fact it is the slope of the logarithm of the $R_x/R_o$ curve which is used in equation 5.6 to determine N. This equation can be rearranged to give

$$N = \frac{\log_e (A_1/A_2)}{2(k_x - k_o)(h_2 - h_1)} + \frac{\log_e (R_2/R_1)}{2(k_x - k_o)(h_2 - h_1)} . \qquad 5.12$$

The second term in this equation is the only one affected by the choice of $\alpha$. This term has been computed for various values of $\alpha$ and the result compared with the value when the customary assumption that $\alpha = 0$ is made. Curves of these absolute differences are shown in Figure 5.2. The results are consistent with the calculations of other workers (e.g. Piggott and Thrane, 1966a; Manson, 1966; Belrose et al., 1967; Belrose, 1970) and show that considerable errors in the deduced profiles can result especially below about 70 km

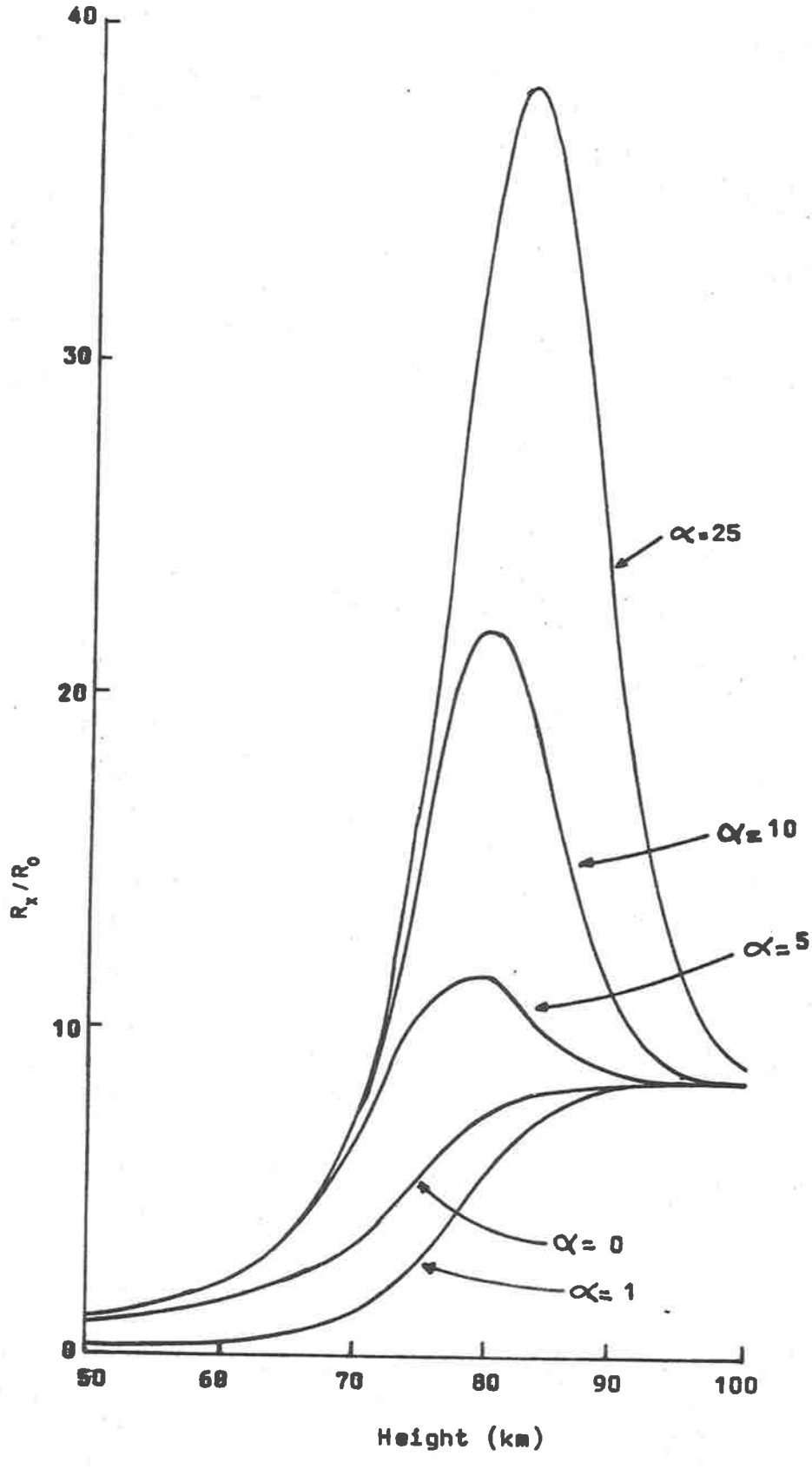


Figure 5.1 Computed Rx/Ro profiles for January as a function of assumed reflection mechanism.

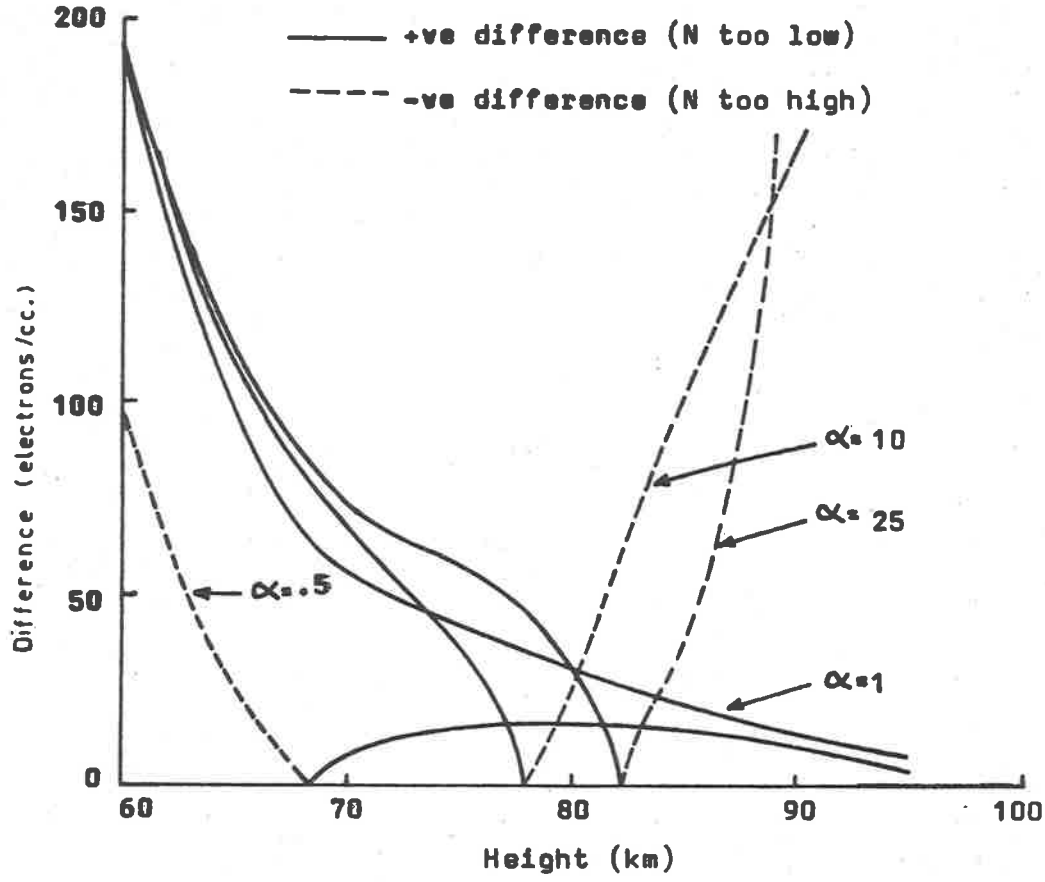


Figure 5.2 The difference between the electron density obtained if $\alpha = 0$ is assumed and the true electron density if another value of $\alpha$ is relevant.

if incorrect values of $\alpha$ are assumed in the data reduction. If $\alpha$ were unity the graphs show that electron densities would be underestimated over the whole height range if a value of $\alpha = 0$ were assumed in the reduction processes. If $\alpha$ was much greater than unity, electron densities would tend to be overestimated above about 80 km, as a result of the change in sign of the slope of the $R_x/R_o$ curves of Figure 5.1 at about this height. Since only absolute errors in N are shown in Figure 5.2, a comparison of the relative errors throughout the height range is not directly obtainable unless N(h) is known. However, since electron densities are expected to be much larger above about 80 km, the relative errors are expected to be smaller and this result is consistent with the findings of Manson (1966) and Thrane et al. (1968). The graphs of Figure 5.2 show that even small collision frequency perturbations will give large errors in calculated N(h) profiles below about 70 km if $\alpha = 0$ is assumed. Due to the existing lack of information regarding the mechanisms of partial reflections, the customary assumption that $\alpha = 0$ has been used in the present study.

Equation 5.9 describes the variation of the refractive index with height once the parameters relevant to the observing location are inserted and gives the dependence of $(k_x - k_o)$ on the collision frequency from the imaginary part of the refractive index. This dependence is shown in Figure 5.3. The establishment of a collision frequency profile thus allows the $(k_x - k_o)$ profile to be determined. Monthly collision frequency profiles as previously described have been used to obtain monthly $(k_x - k_o)$ profiles suitable for use in the reduction of experimental data.

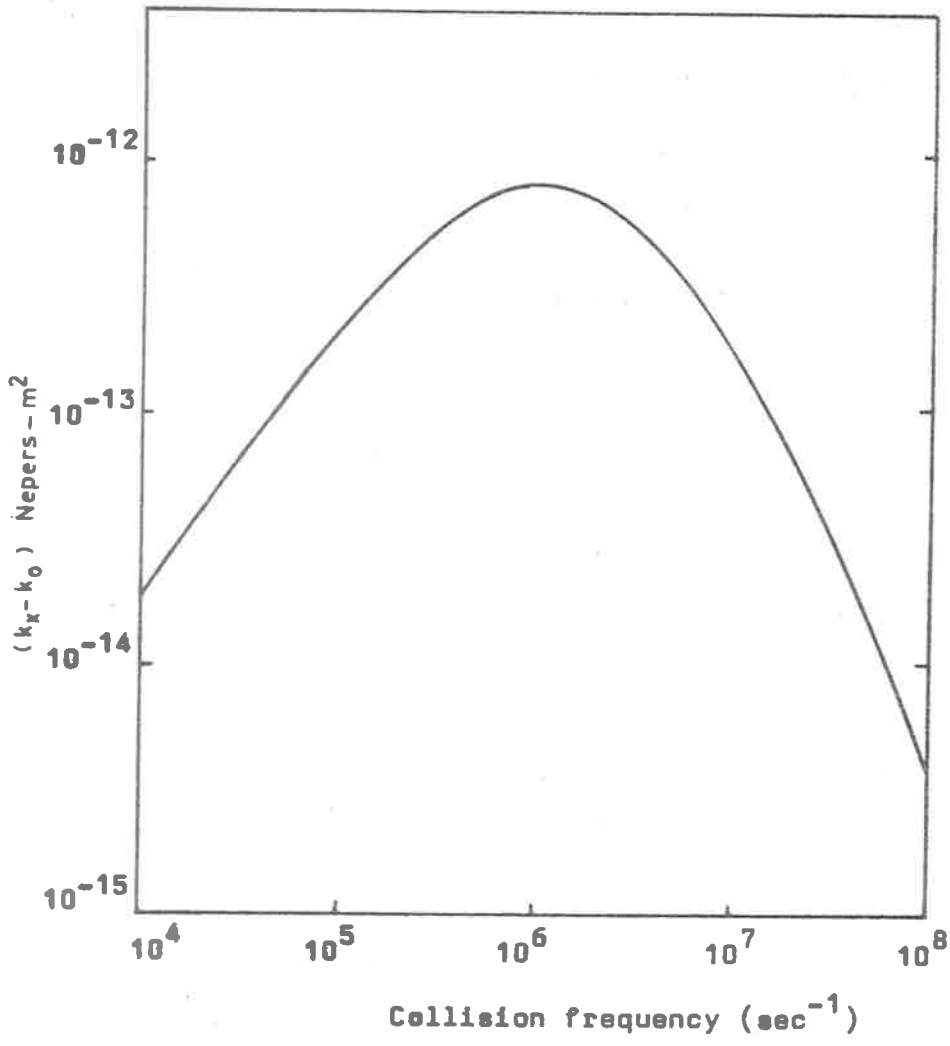


Figure 5.3 The dependence of the differential absorption factor on collision frequency, for 1.98MHz radio waves at vertical incidence for a magnetic dip of $67^o$.

## 5.6 The effect of the variation of the earth's magnetic field with height

It is well known that the earth's magnetic field varies with height above the earth and although the variation is only of the order of 3% in the range 50 - 100 km, the height variation of magnetic field based on the International Geophysical Reference Field was adopted in calculations of $R_x/R_o$ and $(k_x - k_o)$. It was confirmed, as expected, that insignificant differences of only a few percent were obtained when compared with calculations assuming a constant magnetic field.

## 5.7 Properties of the working equations

### 5.7.1 The measurement of collision frequencies at low heights

It was pointed out in section 5.4 that a collision frequency profile must be assumed to enable calculations of $R_x/R_o$ and $(k_x - k_o)$ to be made. It can be shown from the equations given in previous sections that some check on the assumed collision frequency can in theory be carried out for low D-region heights. From equation 5.2 it can be seen that when differential absorption is low (i.e. where electron densities are smallest as in the low D-region)

$$\frac{A_x}{A_o} \approx \frac{R_x}{R_o} \quad . \qquad 5.13$$

Since $R_x/R_o$ is related to the collision frequency, measurements of $A_x/A_o$ at low heights, in theory, enable the collision frequency to be estimated.

Several practical considerations make these evaluations less straightforward than appears at first sight. It was pointed out

in the previous section that the relation between $R_x/R_o$ and the collision frequency depends, in turn, on the nature of the reflection mechanism assumed so that uncertainties arise in the determination of the collision frequency using the relation of equation 5.13. This point has been discussed in detail by Piggott and Thrane (1966a). The possibility of a determination of collision frequency also depends on the occurrence of echoes from heights sufficiently low to ensure that differential absorption is negligible. The results of many workers indicate that, particularly during summer, few reflections are observed from low enough heights to enable accurate assessments of collision frequencies. The above factors combined with the presence of a strcng reflection of non-ionospheric origin at a range of about 55 km severely restricted the possibility of measurements of collision frequency in the present studies.

5.7.2 The $A_x/A_o$ "turnover" height

If, as is customary, irregularities in electron density are assumed to be responsible for D-region partial reflections then the $R_x/R_o$ profiles of Figure 5.1 show that 'X' polarized waves are generally expected to be reflected more strongly than 'O' polarized waves with this effect increasing with height. In the absence of differential absorption the $A_x/A_o$ profile measured on the ground would be expected to closely follow the $R_x/R_o$ profile and increase with increasing height throughout the D-region. However, in practice, the higher absorption of 'X' waves in the D-region opposes this increase and eventually, with increasing height, the integrated differential

absorption factor of equation 5.2 becomes dominant and $A_x/A_o$ values rapidly fall. The height at which the resultant peak in $A_x/A_o$ occurs is commonly called the $A_x/A_o$ "turnover" height. The integrated differential absorption factor of equation 5.2 depends on the integrated electron density so that this turnover height is a good general indicator of the level of ionization in the lower D-region. Variations of $(k_x - k_o)$ due to collision frequency variations can also contribute to the determination of the turnover height, but this effect is expected to be fairly small with only a small seasonal variation.

## 5.8 Estimation of electron densities below the $A_x/A_o$ turnover height

In the practical estimation of electron densities in the Differential Absorption Experiment many workers have noticed the extreme sensitivity of the electron density to the slope of the $A_x/A_o$ profile below the turnover height, resulting in greater uncertainties, or even in cases the impossibility, of the normal method at these heights (e.g. Belrose, 1970). Below the turnover height, differential absorption is very small and thus the slope of the experimentally obtained $A_x/A_o$ curve must be very accurately known to obtain accurate electron densities. Often the occurrence and the strength of the echoes from these low heights is insufficient to guarantee such accuracy. To overcome some of these difficulties Belrose and Burke (1964) have, with some theoretical justification, proposed an alternative method for estimating electron densities below the turnover height. They have shown that estimates can be made on the assumption that the measured mean '0' amplitude is proportional to local electron density

at the height of reflection. This method has also been occasionally employed in the present work to give an indication of the electron density below the turnover height, and these portions of the N(h) profiles have accordingly been distinguished in the results to be presented.

## 5.9 Summary

In this chapter the widely used theory of the Differential Absorption Experiment has been briefly outlined. It has been shown that a measurement of the amplitude ratio $A_x/A_o$ as a function of height of partial reflection in the D-region can be used to determine D-region electron density profiles if a reflection mechanism and an electron collision frequency profile are assumed. The uncertainties associated with the assumption of a reflection mechanism have been described and it was found that uncertainties in calculated electron densities are likely to be greatest below about 70 km. It was shown that, in principle, a measurement of $A_x/A_o$ for heights below which differential absorption is negligible allows a determination of collision frequency to be made. Finally it was pointed out that the DAE method for determining electron densities can become unreliable for heights below the $A_x/A_o$ turnover height. For such cases a commonly used alternative method was described where electron densities are assumed to be proportional to the 'O' ray echo amplitude.

# CHAPTER 6

# RESULTS OBTAINED FROM PHOTOGRAPHIC RECORDS OF DIFFERENTIAL ABSORPTION

## 6.1 Introduction

Although studies of electron densities in the lower ionosphere using the DAE have been carried out for many years most observations have been made at relatively few sites so that there is a poor geographic distribution of observing stations. This state of affairs has been especially evident in the southern hemisphere, where the need for more observing sites to give better world wide coverage has been expressed by workers reviewing observations of D-region electron densities (e.g. Belrose, 1970). This lack of observing stations is probably largely due to the difficult experimental conditions encountered in studying D-region partial reflections; for powerful transmitters and large receiving arrays are necessary to carry out effective studies.

To date, two stations have provided the bulk of D-region electron density information in the southern hemisphere. Gregory and Manson (1969) have reported electron densities from DAE observations made over a period of five years (1963-1967) at Birdling's Flat, New Zealand ($44^{o}$S). These workers have established seasonal electron density variations and have found that

(1) mean electron densities between 79 and 88 km are larger in winter and spring than in summer in contrast to the seasonal variation below these heights where direct solar control has been found.

(2) There is a suggestion of a peak in electron density below 70 km.

(3) Electron densities tend to be more variable in winter than in summer. This effect, together with the winter increase in mean electron density were considered to be related to the dynamics of the atmosphere.

Another group of workers at Armidale, Australia ($30^{\circ}$S), employing a pulse wave-interaction experiment have also provided useful information regarding D-region electron densities (Smith et al., 1965), although these workers have concentrated mainly on night time and sunrise/sunset conditions, of which little knowledge exists. Two daytime electron density profiles which these workers have published showed a peak in electron density just below 75 km and they concluded that this peak appeared to be predominantly under solar control. Recently, Bourne et al., (1972), working at the same site, have commenced studies of D-region electron densities employing the Differential Absorption Experiment and a Differential Phase Experiment in conjunction with the wave interaction system.

The system used in the present studies consisted of a powerful transmitter, a large receiving array, for confining off-vertical reflections to within about $\pm 5^{\circ}$ of vertical, and polarized

transmission and reception with an overall measured discrimination of about 60 db. Such specifications are considered to be good for a DAE system, allowing reliable estimates of D-region electron densities to be made. The results which are presented in this chapter were obtained from a series of differential absorption experiments conducted on several days near the middle of each month at Buckland Park over the period January to December 1971. Over this period, the Zürich sunspot number ranged from 20 to 110 with a mean of about 66. No solar flare effects are believed to be present in the mean electron density profiles presented in this chapter. Unfortunately, the sheer weight of labour of reduction processes precluded the possibility of analysing all of the many records taken.

## 6.2 The photographic records

All results presented in this chapter were deduced from 35 mm film records of A-scans displayed on a cathode ray oscilloscope. The experimental method has been described in §2.4.2 and involves recording a graphic trace (A-scan) of received echo amplitude as a function of height for 'O' and 'X' polarized waves. The sense of deflection of the trace is reversed for opposite polarizations, allowing a clear comparison of the height variation of received signal strength for the two polarization modes. Examples of frames taken from such records are shown in Figure 6.1 and illustrate the recording technique. Accurate range markers are shown as bright up dots on the traces at 2 km intervals with brighter dots every 10 km. A sequence of such frames was used to compile a height profile of the ratio of received signal

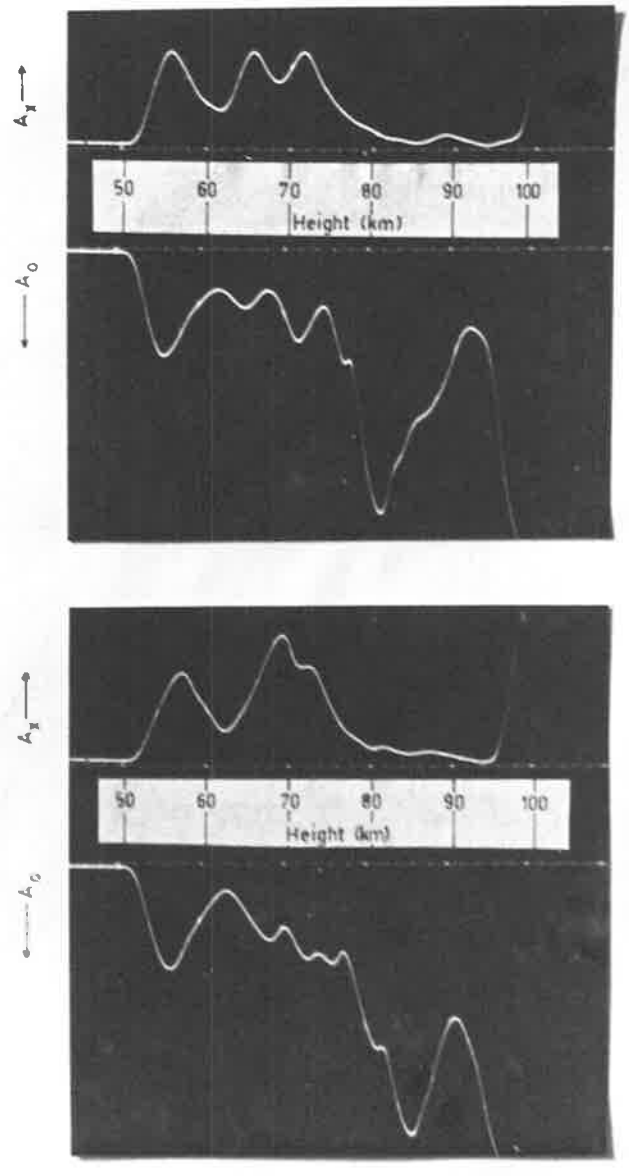


Figure 6.1 Examples of photographically recorded DAE data.

amplitudes $A_x/A_o$. The two frames shown in Figure 6.1 were recorded on the same occasion but about one minute apart, and typically indicate that reflections can occur from a series of different heights in the D-region over the course of a recording period, allowing a fairly detailed and well resolved $A_x/A_o$ curve to be calculated as a function of height of reflection. In these examples, the echoes at 56 km are known to be predominantly of non-ionospheric origin.

## 6.3 The $A_x/A_o$ curves

### 6.3.1 Evaluation of the curves

$A_x/A_o$ curves were generally compiled from 5 to 15 minutes of recorded data with the majority being estimated from more than ten minutes data. The commonly used "peak-scaling" method was used to reduce records into digitized form on computer cards. The amplitude was scaled only at heights where a fairly clear peak in 'O' and 'X' amplitude occurred. This technique contrasts with the "envelope-scaling" method where the recorded traces are digitized at fixed intervals, regardless of the echo structure. A comparison of the two techniques (Belrose, 1970) shows that little basic difference in the resulting profiles of electron density ensue for these two methods of compiling the $A_x/A_o$ curve, although this result is not likely to be as clear at southern latitudes where, in contrast to the northern hemisphere, preferred heights of reflection are often observed (Gregory, 1959, 1961). Where stratification of the D-region occurs, the envelope scaling method is liable to lead to greater uncertainties than the peak scaling method. The peak scaling method was adopted in

the present work to optimize height resolution and to avoid the more tedious envelope scaling procedures that would be necessary in a manual reduction of film records.

It is a well known feature of the DAE that during a recording period, some scatter in the instantaneous values of the quantities $A_x$, $A_o$ and $A_x/A_o$ occurs for a given height of reflection. Nevertheless, a mean height variation can be measured with fair precision, depending on the amount of data averaged. This dependence of accuracy on the averaging interval generally limits the temporal resolution of electron density profile variations to those variations greater than a few minutes. In the computer reduction of data the amplitude information was grouped into 1 km height increments and an $A_x/A_o$ curve was compiled at corresponding intervals. As a consequence of the use of a finite transmitter pulsewidth, it is evident that a certain contribution of signal from neighbouring intervals could influence any given height interval. Several simple smoothing procedures were investigated and five separate procedures for formulating a smoothed $A_x/A_o(h)$ curve from the raw data were investigated.

(1) The curve was formed from the average of the instantaneous ratios:-

$$\text{viz.} \quad A_1(h) = \overline{(A_x/A_o)} \ .$$

(2) The average $A_x$ and $A_o$ profiles were individually calculated and the ratio of these was formed:-

$$A_2(h) = \overline{(A_x)}/\overline{(A_o)} \ .$$

(3) The curve of (1) was smoothed using a 3-point weighted filter:-

$$A_3(h) = w_1A_1(h - 1) + w_2A_1(h) + w_3A_1(h + 1)$$

where $w_1 + w_2 + w_3 = 1$ for normalisation. The three point filter allowed for an adjustment due to the height increments either side of the height under consideration.

(4) The curve of (2) was smoothed using a 3-point weighted filter in the same manner as in (3):-

$$A_4(h) = w_1A_2(h - 1) + w_2A_2(h) + w_3A_2(h + 1) .$$

(5) The average $A_x$ and $A_o$ profiles were individually smoothed using a 3-point weighted filter and the ratio of these smoothed profiles was calculated:-

$$A_5(h) = \frac{w_1A_x(h - 1) + w_2A_x(h) + w_3A_x(h + 1)}{w_1A_o(h - 1) + w_2A_o(h) + w_3A_o(h + 1)} .$$

N(h) profiles calculated using these five methods of obtaining an $A_x/A_o$ curve show little basic difference from each other except that the "filtered" profiles tend to lack those features which are smaller than the uncertainties associated with the calculated profile. The N(h) profiles have generally been compiled using $A_x/A_o$ curves calculated by method (5) for the following reason. It is contended that smoothing of the individual $A_x$ and $A_o$ curves is more consistent with the physical situation where a contribution of signal from adjacent heights directly affects the individual amplitudes rather than the more indirect effect on $A_x/A_o$. This distinction

between the smoothing processes in practical applications has been found to be fairly small. In Figure 6.2a a comparison of two ways of calculating the $A_x/A_o$ curve are shown. Here curves calculated using methods (1) and (5) above are shown and represent the two extremes of the smoothing procedures. The resultant smoothing effect on the electron density profile by using method (5) is shown in Figure 6.2b. The general shape of the $A_x/A_o$ curves shown in Figure 6.2a is quite characteristic of the $A_x/A_o$ curves generally obtained in that they follow the $R_x/R_o$ profile (see §5.7.2) up to a turnover height (about 66 km in this case) where the higher absorption of the 'X' mode wave begins to dominate and $A_x/A_o$ values begin to fall rapidly with increasing height.

### 6.3.2 The seasonal variation of the noon $A_x/A_o$ turnover height

It was stated in §1.2 that in the formation of D-region ionization, the calculations of Webber (1962) are a basis for believing that galactic cosmic rays are the principle source of ionization in the low D-region (see Figure 1.1). It was also pointed out that uncertainties in the concentration of nitric oxide make it difficult to assess the contribution of solar produced ionization below about 75 km. The ionization production rate due to cosmic rays is expected to fall by a factor of two between minimum and maximum solar activity (Webber, 1962) while solar ionizing fluxes increase with solar activity. It would appear then that at solar maximum the role of solar ionization might be important in the lower D-region. The most obvious way to investigate this situation using the DAE would appear to be to

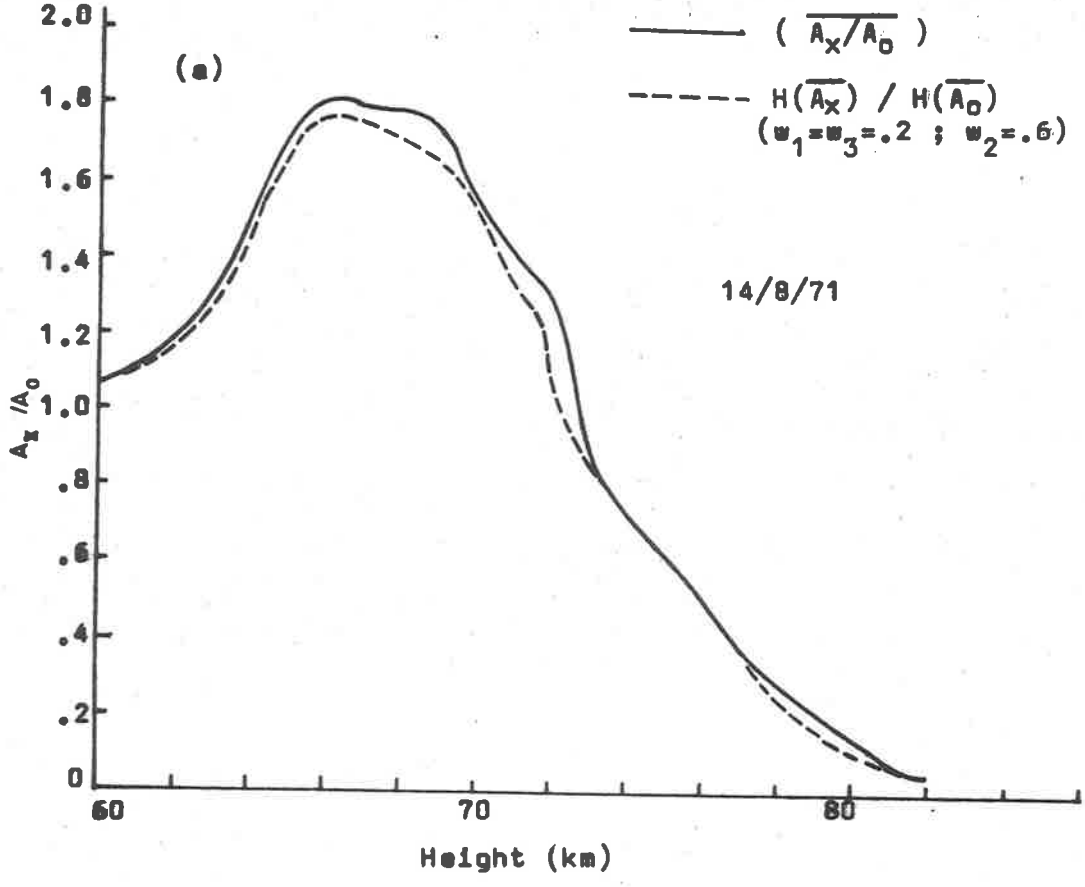


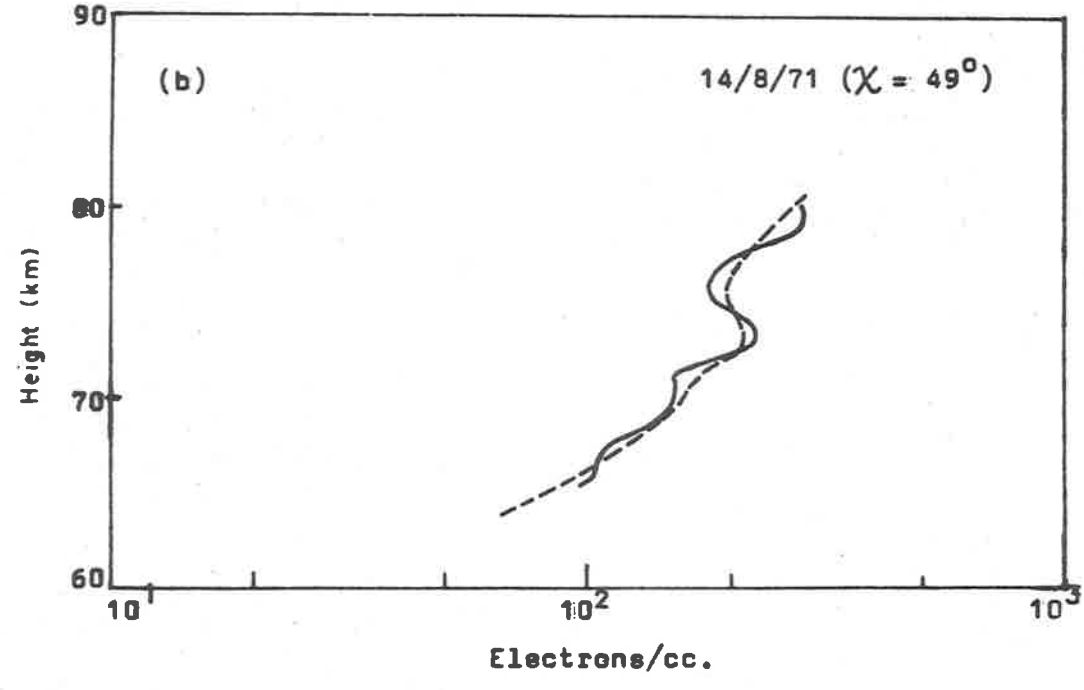


**Figure 6.2** (a) A comparison of smoothed and unsmoothed $A_x/A_o$ curves.

(b) Corresponding electron density profiles.

study the seasonal or diurnal variations of the electron densities below about 70 km. However, the evaluations of electron densities below the height at which $A_x/A_o$ becomes a maximum (and this generally means below about 70 km in practice) often becomes rather unreliable and it is preferable to obtain an approximate profile using the assumption of Belrose and Burke (1964) that the electron density is proportional to the average 'O' mode amplitude. In view of the approximate nature of the lower portions of the N(h) profiles so obtained and the uncertainties of the normal method, it was felt that some uncertainty in any evidence of solar produced ionization would be present, and an alternative approach was therefore examined. This involved determining the seasonal variation of the $A_x/A_o$ turnover height at noon.

In §5.7.2 the factors affecting the height at which this maximum occurs were discussed. The seasonal variation of collision frequency which affects $R_x/R_o$ and $(k_x - k_o)$ values is expected to have some effect as well as the electron densities in the lower D-region. In Table 6.1 some theoretical $R_x/R_o$ and $(k_x - k_o)$ values for summer and winter are given for the lower D-region.

TABLE 6.1

| Height (km) | $R_x/R_o$ Winter | $R_x/R_o$ Summer | $(k_x - k_o)$, Nepers.m$^2$ Winter | $(k_x - k_o)$, Nepers.m$^2$ Summer |
|---|---|---|---|---|
| 50 | 1.187 | 1.169 | 1.486E-14 | 1.239E-14 |
| 55 | 1.367 | 1.329 | 4.821E-14 | 3.998E-14 |
| 60 | 1.692 | 1.705 | 1.326E-13 | 1.107E-13 |
| 65 | 2.345 | 2.368 | 3.226E-13 | 2.819E-13 |
| 70 | 3.462 | 3.532 | 6.002E-13 | 5.501E-13 |

It is seen that in winter the increased differential absorption factor (see Table 6.1) would work to lower the $A_x/A_o$ turnover height compared with summer values, this being in the opposite sense to that expected from ionization under solar coltrol; for increased summer electron densities would be expected to lower the turnover height in summer. Since there is a difference in the winter and summer $R_x/R_o$ profiles, it is not completely clear what effect the seasonal variations of collision frequency will have on the turnover height. Using a wide range of the various approximate N(h) profiles that were obtained for below 70 km for all seasons, it was found that the maximum change in expected $A_x/A_o$ turnover height for any given N(h) profile as a result of separately assuming the seasonal range of $R_x/R_o$ and $(k_x - k_o)$ profiles was about 1 km. It was concluded that in most practical situations a seasonal variation in collision frequency could contribute up to a 1 km change in turnover height, with almost invariably the height being changed in the opposite sense to that expected from solar influenced changes in electron density. Figure 6.3

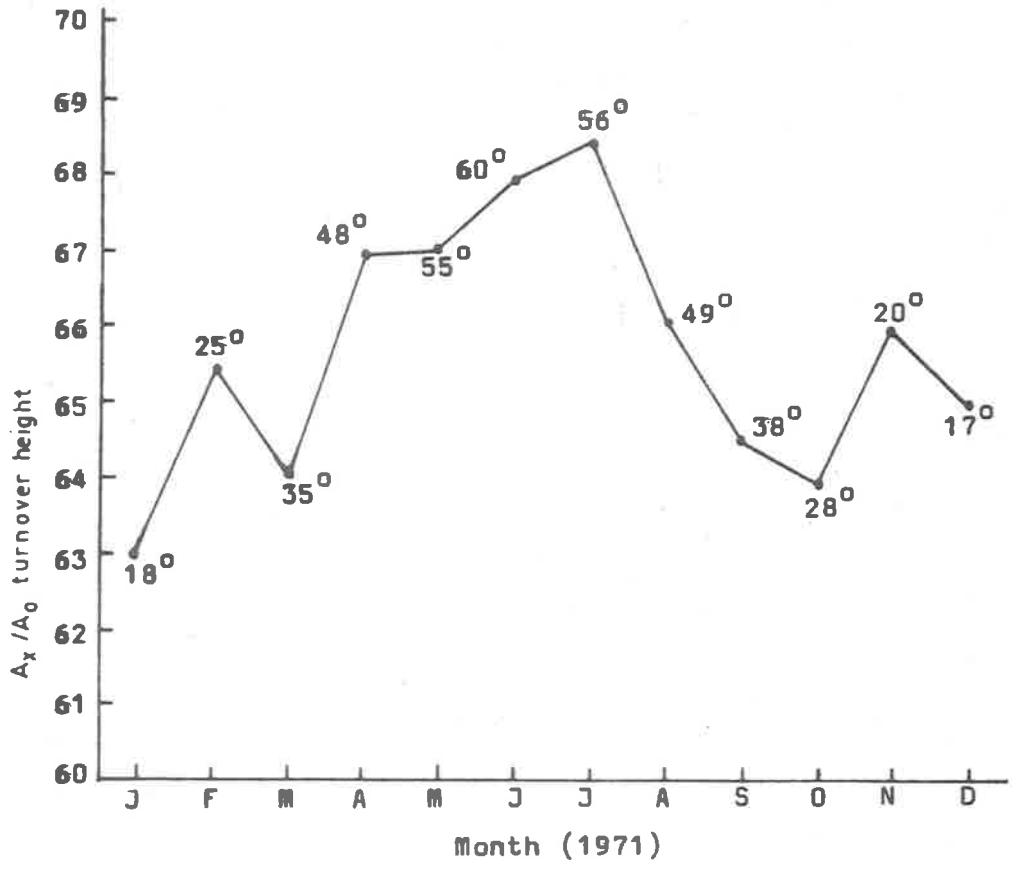


Figure 6.3 Seasonal variation of the moon $A_x/A_o$ "turnover" height.

shows the experimentally measured seasonal variation of mean noon turnover height. The mean solar zenith angle at which the turnover height was estimated (approximately local noon) is given beside each plotted point. The seasonal variation from winter to summer is seen to be in excess of the uncertainty which could be due to seasonal collision frequency variations. This seasonal variation in turnover height as depicted in Figure 6.3 is interpreted as demonstrating a distinct solar influence in the production of ionization in the lower D-region at solar maximum conditions.

## 6.4 The electron density profiles

### 6.4.1 Calculation of electron density profiles

In §5.3, equation 5.6 was derived for calculating electron densities from differential absorption measurements. In practice, a routine application of this equation using a measured $A_x/A_o$ height profile and a chosen steplength, say 2 km, might yield reasonable N(h) profiles on the average. However, some consideration of other related matters, such as the possibility of preferred heights of reflection during an experimental recording period, is required before optimum reliability of a calculated N(h) profile is realized. The computer program which was used to process the punched card data obtained from digitizing the photographic DAE records also compiled statistics of the heights of occurence of scaled echoes in addition to calculating the $A_x/A_o$ and N(h) profiles on a fixed steplength basis. Statistics of the heights of occurrence will be discussed more specifically in chapter 8 but they require some consideration at this stage to

appreciate the way in which special situations were recognized and treated. Figure 6.4 shows two examples of such statistics, plotted out in the computer analysis for data from two successive days. The histograms show the relative frequency of occurrence of echoes from throughout the height range, while the solid curves represent the mean $A_o$ amplitude as a function of height. Both results were compiled from 15 minutes of recorded data and the graphs have been normalized for the convenience of computer plotting in the format shown. Some interesting features are seen in Figure 6.4:-

(1) The results for 16/6/71 show a marked degree of stratification, or preferred heights of reflection, compared to the 15/6/71 results although the latter also show some evidence of preferred heights.

(2) Peaks in received 'O' mode amplitude show a strong tendency to occur at strongly preferred reflection heights as shown in Figure 6.4b.

Although both of these observations are interesting in themselves, we shall concern ourselves at present with the inferences of the first observation in relation to the determination of N(h) profiles, and a more detailed consideration of features of statistics such as those shown in Figure 6.4 will be described in chapter 8. The $A_x/A_o$ curves corresponding to the results shown in Figure 6.4 are shown in Figure 6.5. The preferred reflection heights are marked by arrows on the height axis for the 16/6/71 results shown in Figure 6.5b. It might be questioned whether, and to what extent, due to a finite

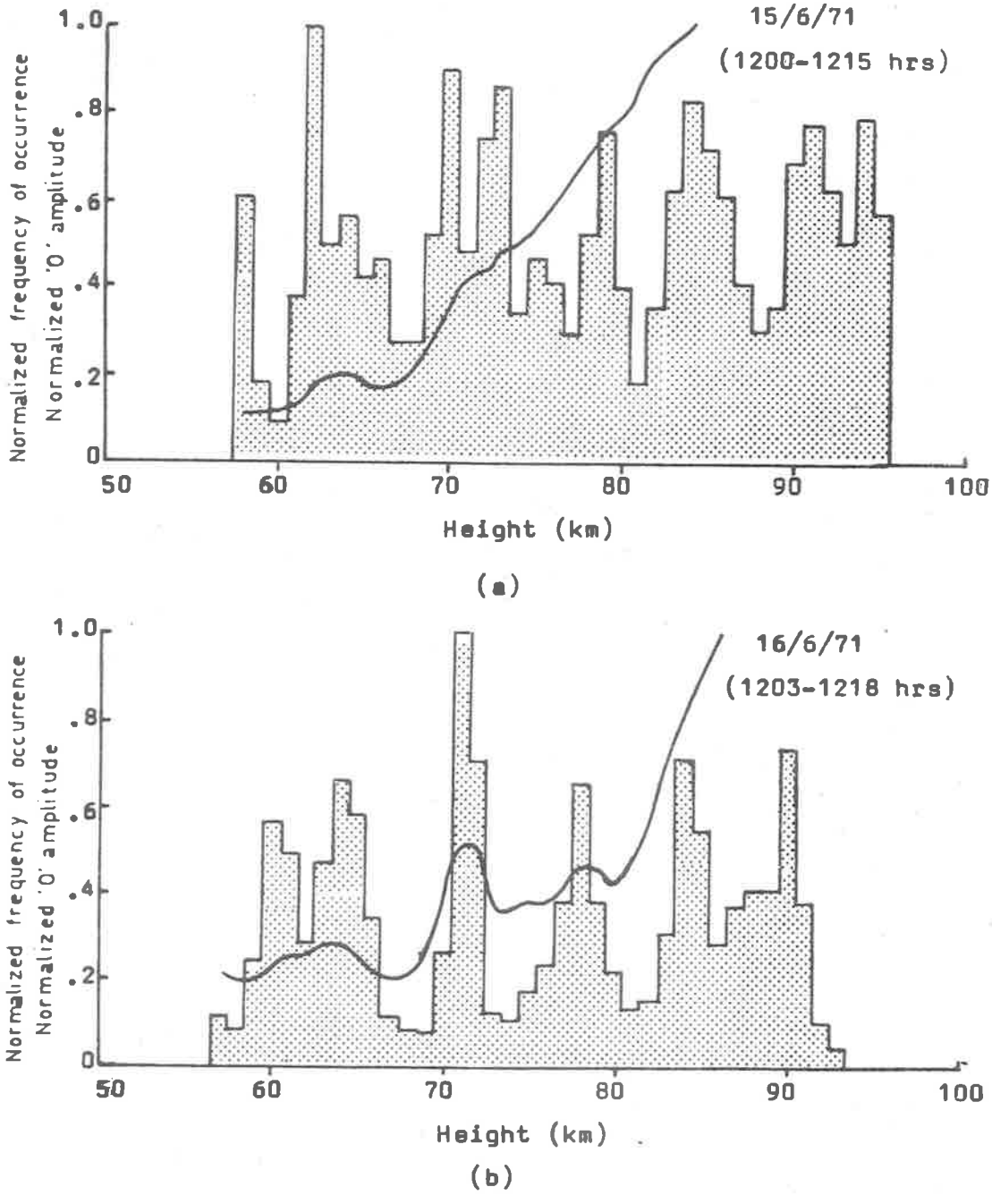


Figure 6.4 The mean $A_o$ profile superimposed on the histogram showing the relative frequencies of heights of occurrence of partial reflections, for two separate recording periods.

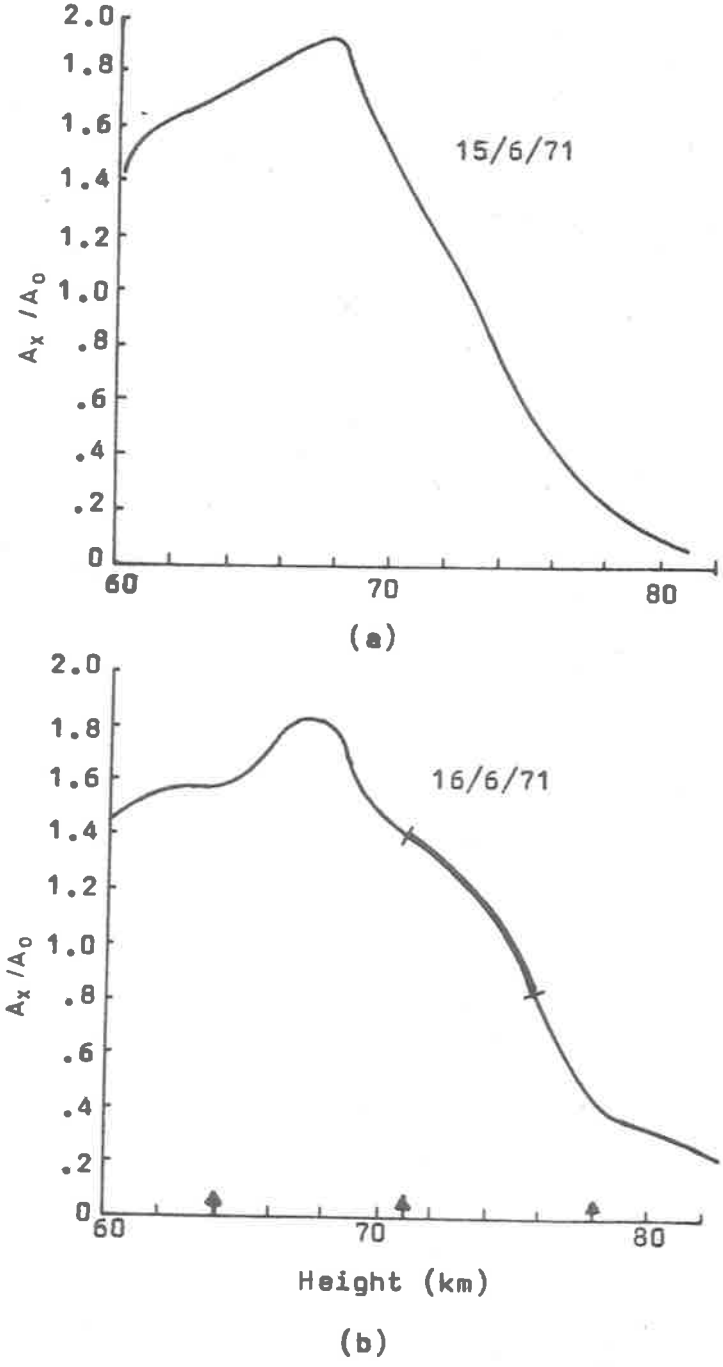


Figure 6.5 $A_x/A_o$ curves derived from the same data as the statistics shown in Figure 6.4.

transmitter pulsewidth, the $A_x/A_o$ ratios and hence the N(h) profiles at heights adjacent to preferred reflection heights will be affected by contributions arising from the preferred heights. In this regard, an interesting feature of Figure 6.5b is the levelling out or "bump" in the slope of the $A_x/A_o$ curve near 72 km, close to a strongly preferred reflection height. Our attention is directed to this feature (shown by the heavy portion of the curve in the figure) because it lies within the height range where reliable electron densities are thought to be usually obtained from the DAE. While this "bump" in the $A_x/A_o$ curve might be regarded as arising from the influence of the preferred reflection height at 71 km on neighbouring heights, due to a finite transmitter pulsewidth, and an effect in this sense could be expected, the possibility of it arising from a physical feature of the electron density profile should not be precluded without some examination. For example, an electron density profile which had a steep decrease in electron density at 71 km and then a relatively smooth increase with increasing height would produce the same features pointed out in Figure 6.5b. The steep dip in electron density could result in a preferred reflection height and the decreased electron densities above this would slow down the rapid increase of differential absorption with increasing height, so producing a levelling out or "bump" in the $A_x/A_o$ curve as recognised in Figure 6.5b at about 72 km.

The problem has therefore been to resolve whether, and to what extent, a feature of the true electron density profile has been

important in producing the "bump" of interest in the $A_x/A_o$ curve. This "bump" corresponds to a dip in electron density (as equation 5.6 will verify) if accepted in the calculation of the electron density profile. The solution to this problem in all records where such uncertainties have arisen has been approached in the following manner:

(1) A detailed N(h) profile has been calculated using a 2 km steplength and the $A_x/A_o$ curve with the "bump" feature included.

(2) Where preferred heights occurred on either side of a "bump" in the $A_x/A_o$ profile, the mean electron density between such adjacent preferred heights has been calculated. For example, in Figure 6.4b this would be between 71 and 78 km. This mean value of electron density has been checked for consistency with the corresponding quantity obtained from the detailed profile calculated as in (1) and:-

(a) if there was good consistency, the detailed profile was accepted.

(b) If there was inconsistency, the detail in the profile of (1) was discarded in favour of what is expected to be an accurate mean value obtained from between the preferred heights.

The final electron density profiles produced in the above manner from the $A_x/A_o$ curves of Figure 6.5 are shown in Figure 6.6. It is interesting to note that the "bump" in the $A_x/A_o$ curve for 16/6/71

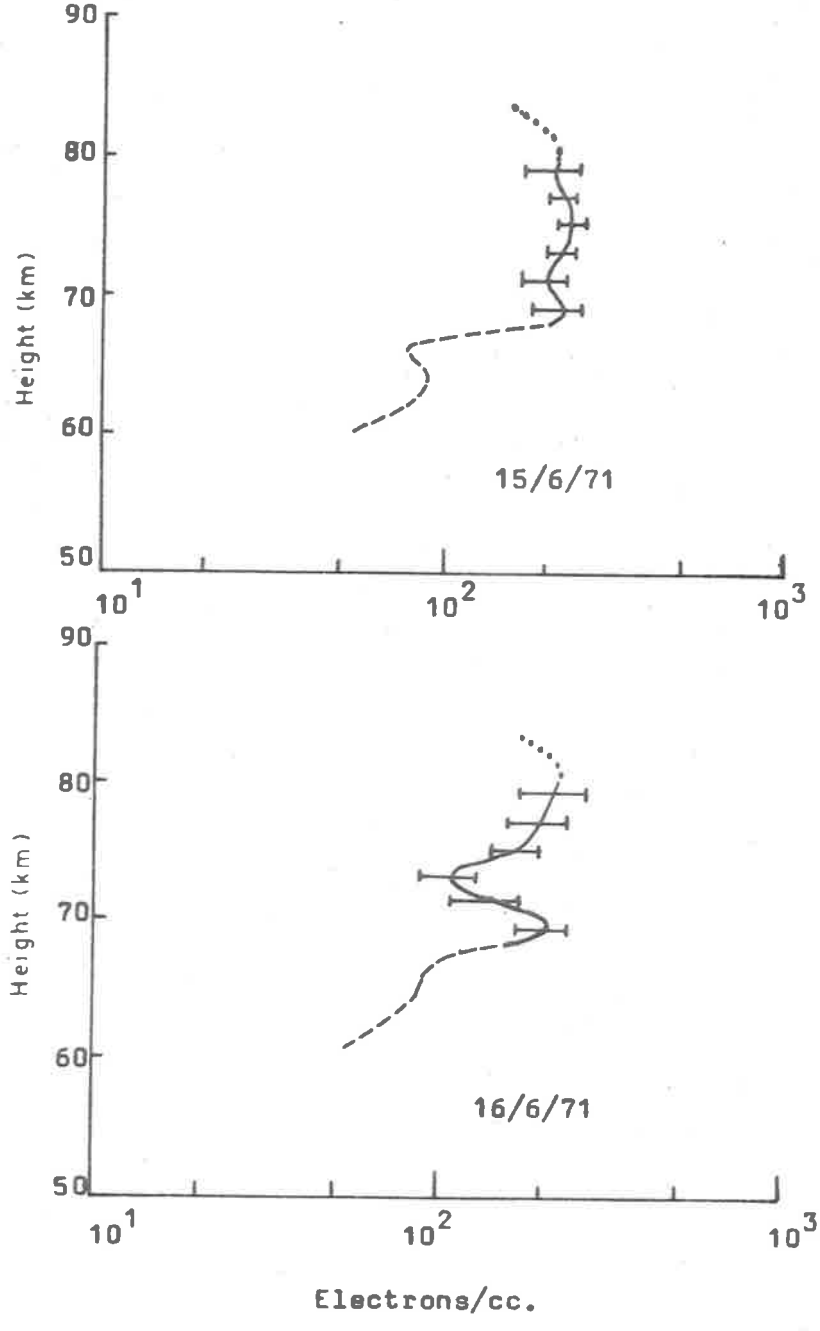


Figure 6.6 Electron density profiles corresponding to the $A_x/A_o$ curves of Figure 6.5.

has been interpreted as being due predominantly to the nature of the electron density profile which exhibits a corresponding dip in electron density. Good consistency between the mean electron density determined between the preferred heights and the corresponding quantity calculated from the detailed N(h) profile have been interpreted as justifying the dip in electron density. Furthermore, it is seen that in the present case, the separation of the preferred heights of interest (i.e. at 71 and 78 km) is sufficient to ensure that some intermediate heights are expected to be virtually unaffected due to transmitter pulsewidth effects, as a 20 μsec wide shaped pulse, allowing contributions from 1.5 km either side of a given range to appear at that range, was employed in the experiment. Consistency of electron densities determined at these unaffected heights with the adjacent detailed N(h) profile showing a dip was taken as further justification for the acceptance of a dip in electron density at about 72 km on this occasion. In other cases, where checks such as those described above appeared advisable, because a preferred height occurred near a dip in electron density, it was found that the dip was often only partially due to a preferred height effect and this tended to accentuate the dip slightly. The smallness of this effect was considered to be due to the narrow transmitter pulsewidths employed.

The dashed lower portions of the N(h) profiles of Figure 6.6 have been derived on the assumption (Belrose and Burke, 1964) that N(h) is proportional to the '0' mode amplitude $A_o(h)$ at these heights. The dotted upper portions of the curves are considered to be unreliable

and 80 km represents what is considered to be the upper limit to which reliable estimates of electron density can be made with the present system.

In general the assignment of realistic error limits to any electron density determination is difficult if all factors are to be taken into account. In the evaluation of electron density profiles only uncertainties due to $A_x/A_o$ fluctuations and height determinations have been calculated using formulae derived in Appendices 1 and 2. Figure 6.7 shows the percentage uncertainties in the electron density profiles of Figure 6.6 due to such considerations. Calculations for three different steplengths are shown. The uncertainties shown are fairly representative of those generally obtained although towards summer, slightly better accuracy is often obtained. Some features evident in Figure 6.6 are:-

(1) Accuracy rapidly deteriorates below the $A_x/A_o$ turnover height (68 km in this case) and above about 80 km. Above 80 km it is considered that the low signal to noise ratio for 'X' amplitudes is probably the main cause. The significance of effects due to off vertical reflections and volume scattering processes, although confined to angles within $\pm 5^o$ of vertical by the large receiving array, are not entirely certain and have not been conclusively rejected as contributing to the unreliability of electron densities above about 80 km. Below the turnover height, high sensitivity to small changes in slope of the $A_x/A_o$

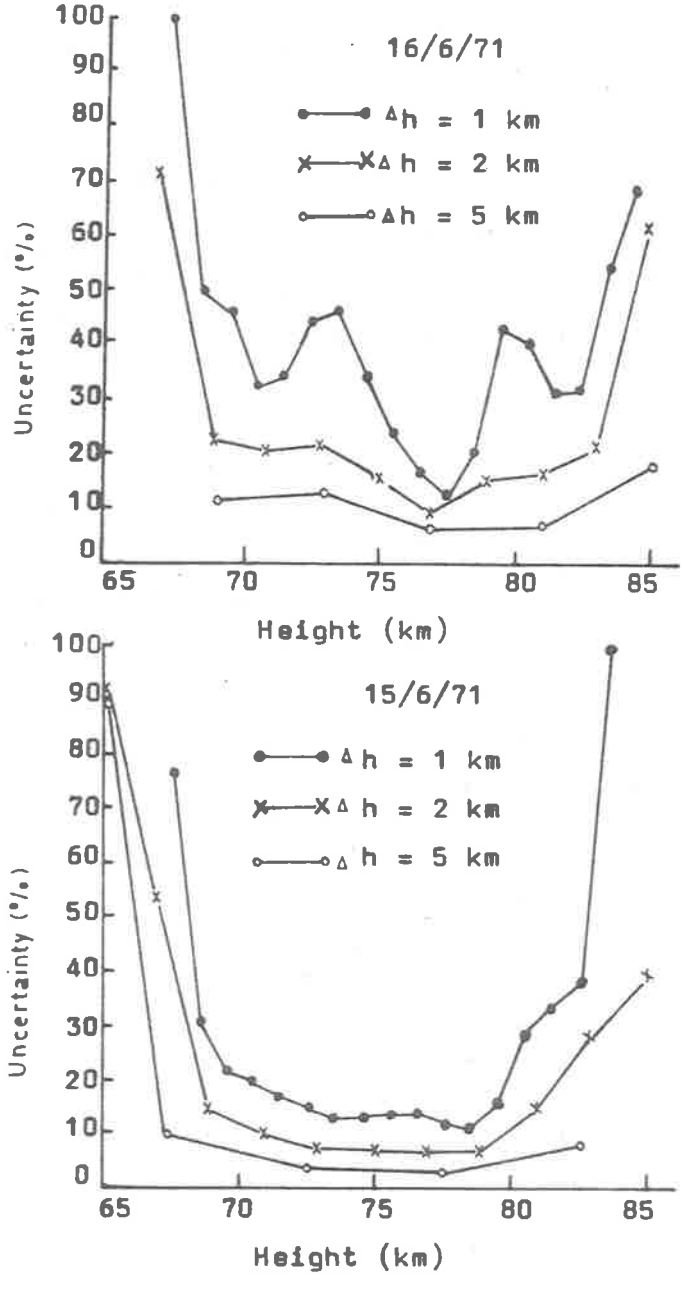


Figure 6.7 Uncertainties in electron density profiles as a result of the spread in measured $A_x/A_o$ and height values.

curves causes the largest contribution to uncertainties in electron densities.

(2) Less uncertainty in average electron density values can be achieved at the expense of height resolution by using larger steplengths.

(3) The shortest steplength gives variable accuracy depending on whether preferred reflection heights occur or not; electron density values near the preferred heights are more accurate (due to the larger number of observations).

(4) The electron density profiles which have been evaluated using a 2 km steplength, the basic steplength generally used in this work, will have uncertainties typically between 10% and 20% in the height range 68 - 80 km, as a consequence of the statistical uncertainties in height determinations and the spread of measured $A_x/A_o$ values.

6.4.2 Noon electron density profiles

Observations of differential absorption near noon were carried out on several days near the middle of each month throughout 1971. The recorded data was reduced to electron density profiles on the assumption of a collision frequency profile and in the manner described in the previous section. Separate collision frequency profiles were used for each month. Electron density profiles used for the purposes of obtaining a mean noon electron density profile have been taken from between about 1030 and 1330 hrs local time. Figure 6.8 shows the mean monthly electron density profiles obtained in this way. Each profile

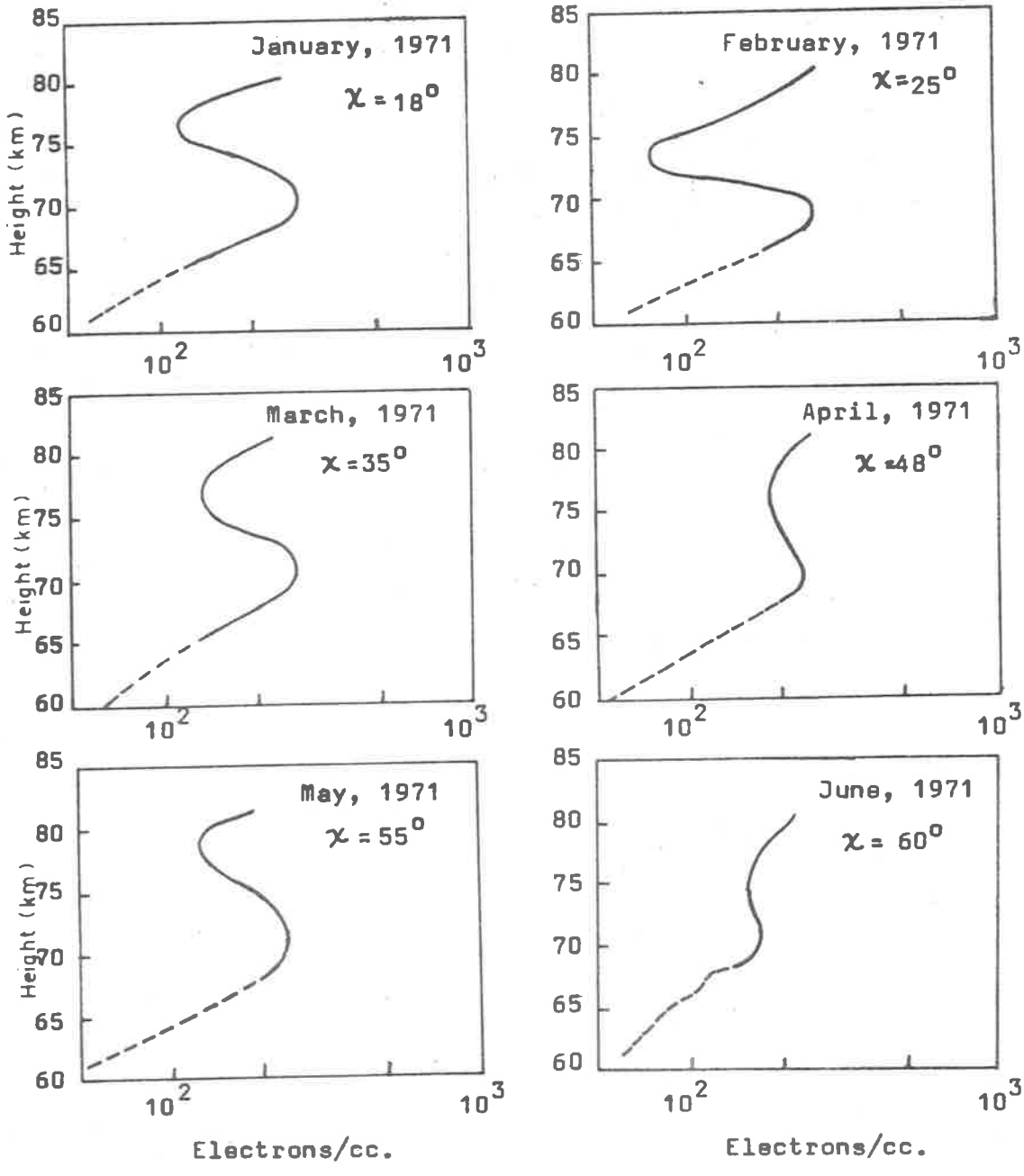


Figure 6.8 Mean monthly profiles of electron density measured near local noon.

...../Jul-Dec

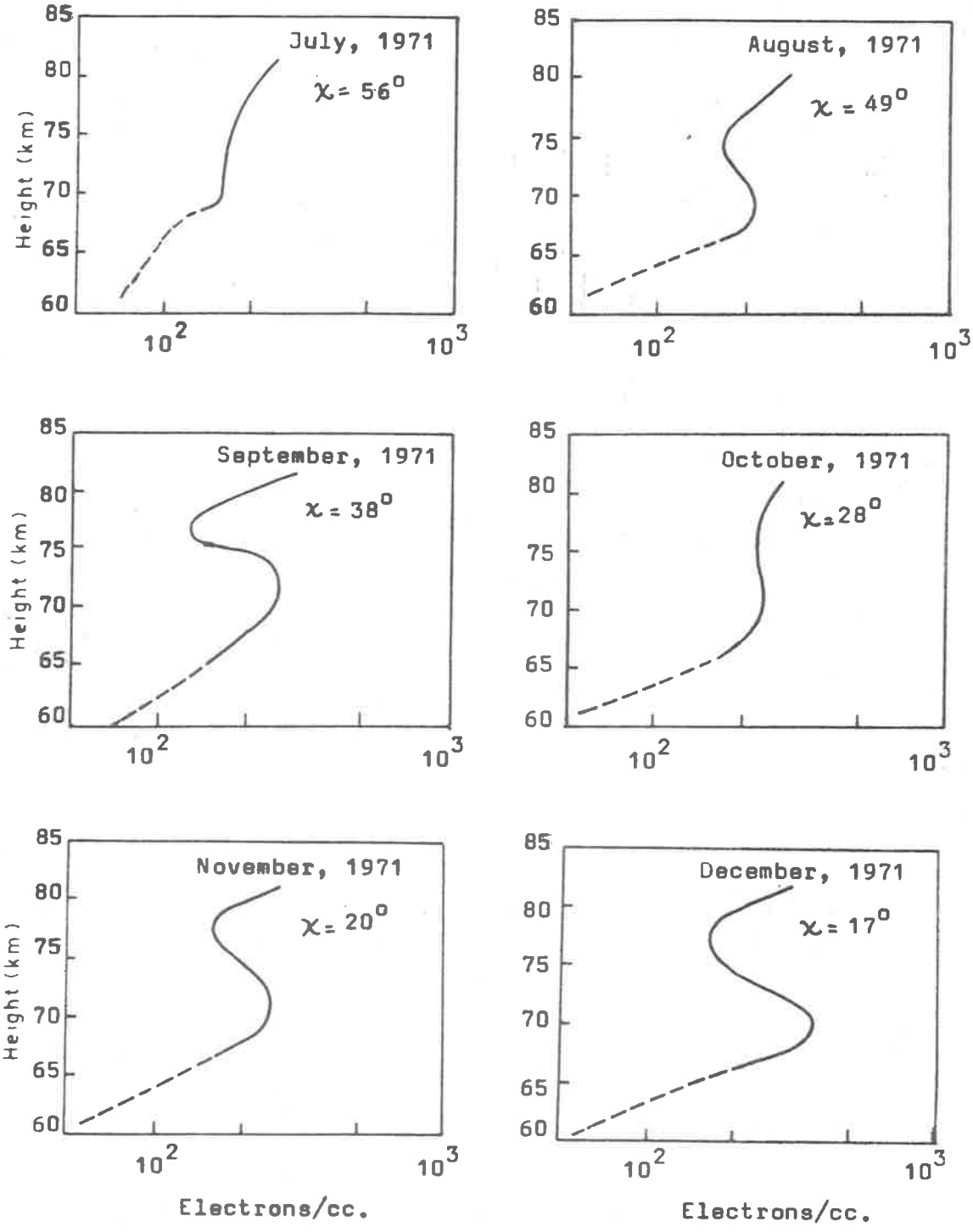


Figure 6.8 Mean monthly profiles of electron density measured near local noon.

has the mean solar zenith angle $\chi$ which it represents marked next to it. In Figures 6.9a,b,c and d seasonal profiles are given, being derived from averages over 3 month periods. For convenience of comparison, these have all been reproduced on one diagram in Figure 6.10. On the basis of Figures 6.8, 6.9 and 6.10, the following observaticns can be made:-

(1) A peak in electron density at about 70 km followed by a dip above this is evident in all seasons. The effect is least pronounced in winter, and most pronounced in summer.

(2) Figure 6.10 shows that the peak in electron density is clearly under solar influence.

(3) Above about 75 km the average winter electron densities exhibit values greater than those expected due to seasonal variations of solar zenith angle at noon.

An indication of the type of day to day variability of noon electron density profiles that has been encountered is given by the examples shown in Figure 6.11. Here it is seen that electron density profiles can vary fairly widely in form from day to day in winter, while in summer the profiles are much more consistent from one day to the next.

### 6.4.3 Night time electron densities

Observing conditions at night were generally fairly poor due to increased noise and interference levels. Nevertheless, on some nights, echoes from two or three heights in the lower ionosphere could

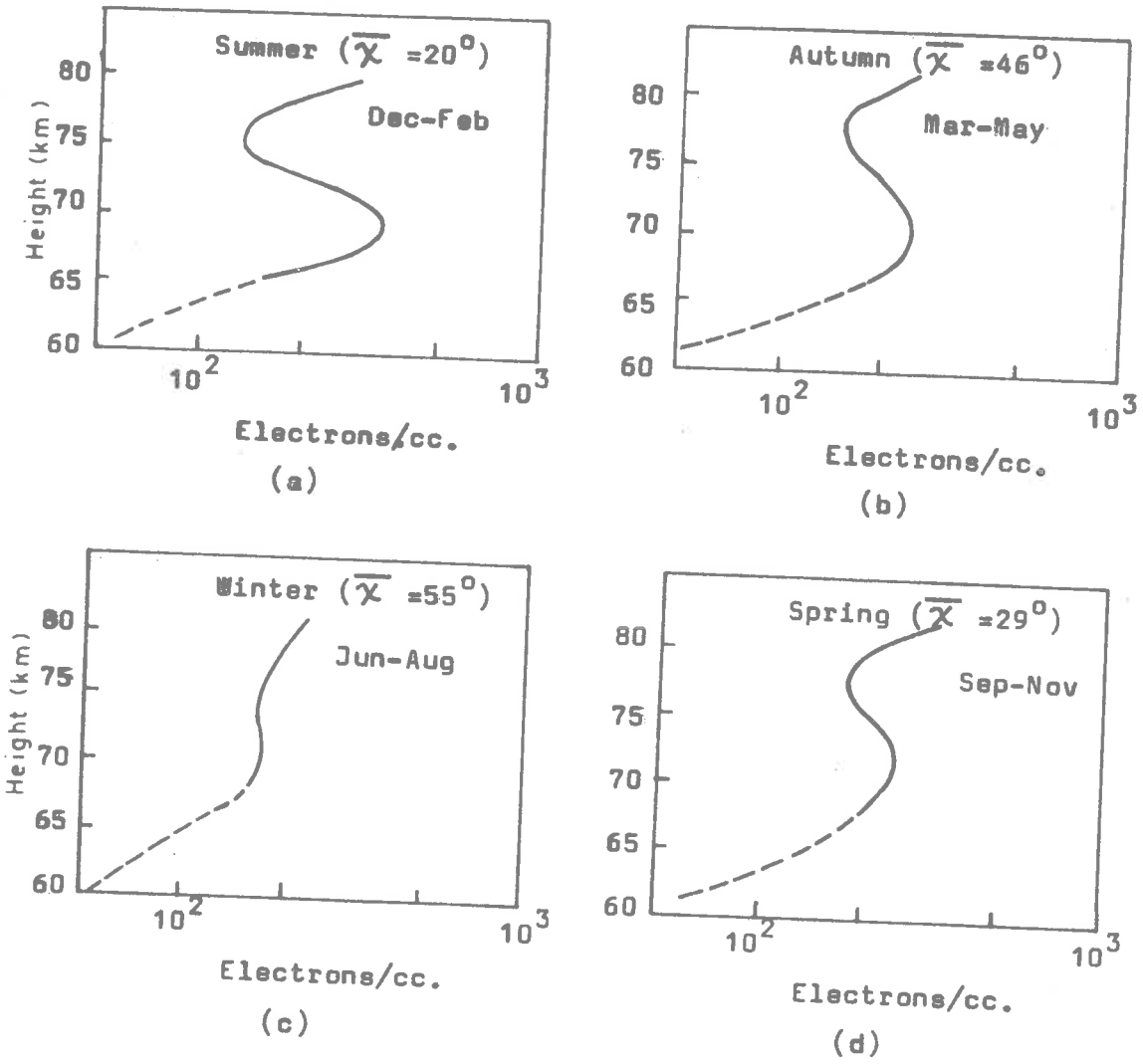


Figure 6.9 Average seasonal profiles of D-region electron density.

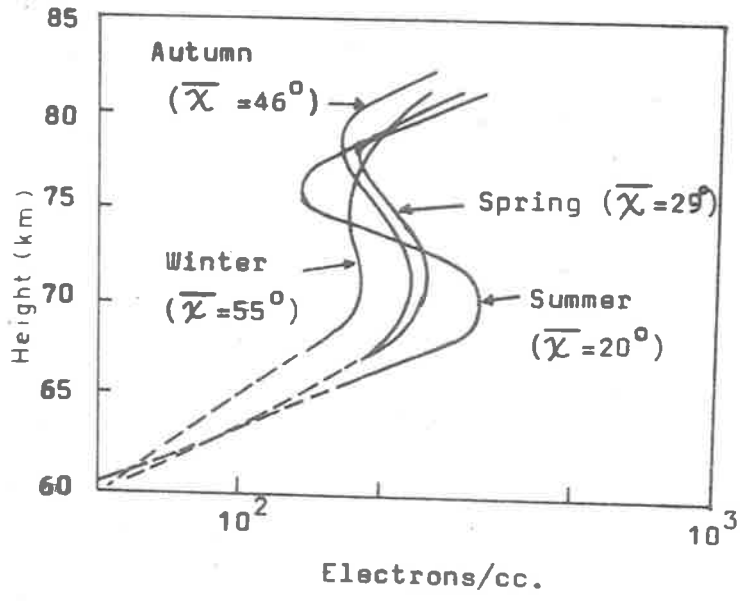


Figure 6.10 Average seasonal profiles of D-region electron density.

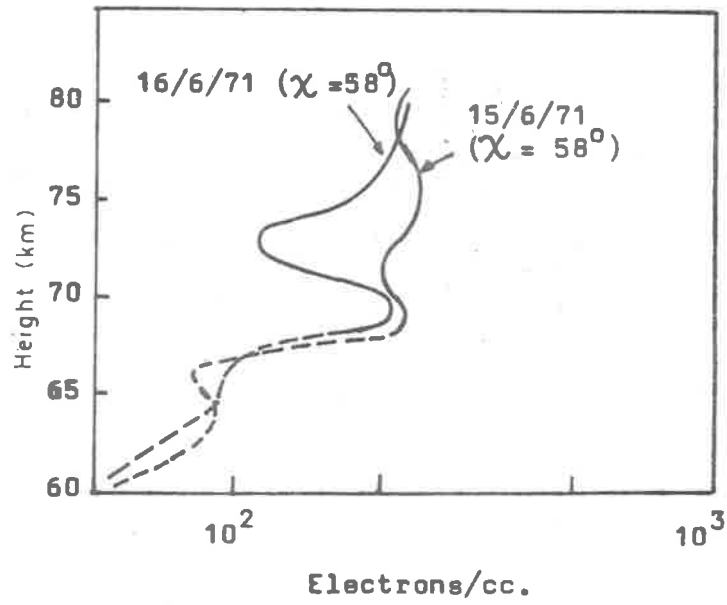


(a)

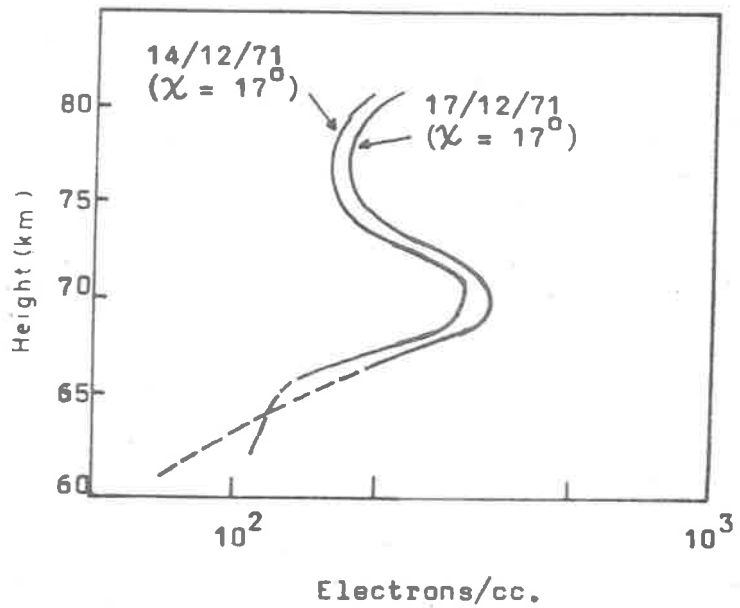


(b)

Figure 6.11 Comparison of the day to day variability of D-region electron density profiles in summer and winter.

be obtained. Generally no echoes were observed below 85 km, and most echoes were from between about 90 and 96 km. As a consequence, usually only one value of electron density was obtainable from a given record so that no estimation of electron density variations with height has been possible. A few results that have been obtained are shown in Table 6.2. There seems to be some disagreement between values obtained on 2/8/71 and 16/8/71 for similar local times but due to the lack of further results it is difficult to draw any significant conclusions. The results for the night of 16/8/71 to 17/8/71 suggest that at about 93 km a minimum of electron density occurred around local midnight or in the very early hours of the morning and that by 0400 hours electron density had increased substantially and increased further as dawn approached. The apparent large increase from 0200 to 0400 hours cannot be easily accounted for at present.

TABLE 6.2

| Date | Local Time (hours) | Height Interval (km) | Electrons/cc. |
|---|---|---|---|
| 2/8/71 | 1700 ($\chi=85^{\circ}$) | 69 - 76 | 55 |
| | 1915 | 91 - 96 | 55 |
| | 2020 | 90 - 96 | 50 |
| 16/8/71 | 2000 | 91 - 95 | 186 |
| | 2200 | 92 - 98 | 185 |
| 17/8/71 | 0200 | 90 - 96 | 22 |
| | 0400 | 90 - 06 | 315 |
| | 0600 ($\chi=100^{\circ}$) | 90 - 96 | 437 |

## 6.5 Summary and discussion

The conclusions which may be drawn from the results of the differential absorption measurements described in this chapter can be summarized as follows:-

(1) Under sunspot maximum conditions solar influences seem to dominate ionization production in the lower D-region in contrast to solar minimum conditions, where galactic cosmic rays are believed to be the principal ionizing flux. This might reasonably be expected when consideration is taken of the fact that production rates due to the latter source are expected at solar maximum to fall to half their value at solar minimum (Webber, 1962), with solar fluxes increasing substantially towards solar maximum.

(2) A peak in electron density at about 70 km followed by a dip at about 75 km is evident in most N(h) profiles, except in some individual winter profiles.

(3) Anomalously high values of winter electron densities in the upper D-region are evident after allowing for the seasonal variation of noon solar zenith angle.

The fact that observed electron densities, even at sunspot minimum, often show greater variation below 70 km than is predicted by the simple theory of ionization production by galactic cosmic rays has been noticed by Thrane (1966) and Thrane et al. (1968) and they have postulated that a primary ionizing source with "some secondary zenith-angle-dependent mechanism" may be active. Smith et al. (1965) have

also observed a solar influence on electron densities below 70 km.

Although many electron density profiles have been published in the literature over the years, only a few are useful for comparison purposes. Geographic differences and the difficulty of putting realistic uncertainty limits on measured profiles contribute to this situation. Furthermore, most published profiles have been obtained near sunspot minimum conditions and in the Northern hemisphere. Only profiles for mid-latitudes will be considered here. Gregory and Manson (1967) have published noon electron densities measured at 35°S for the period 25 - 30 May 1965, over which period the mean sunspot number was about 8. Since their profiles were obtained towards the end of May they are best compared with the mean of the May and June profiles of the present work. The average noon profile of Gregory and Manson shows a fairly steady increase from about 100 electrons/cc at 70 km to about 200 electrons/cc near 80 km. The present results would indicate that electron densities are a factor of 2 higher at 70 km reducing to about the same values near 80 km. The increased electron density in the present results is probably attributable to the increased solar activity during the present observations, for which the mean sunspot number $R_z$ was 54. Deeks (1966) using LF techniques has drawn a comparison between two mean noon electron density profiles obtained at a northern mid-latitude (Slough) for solar minimum and maximum conditions. The two profiles are quite similar throughout the D-region, differing by only about 20% at most. Above about 75 km the comparison is very similar to the comparisons drawn

between the present results and those of Gregory and Manson (1967) but below this, electron densities were found to be smaller at sunspot maximum, in contrast to the comparison drawn above. Deeks considered that the decreased electron densities below 75 km at sunspot maximum were explicable by the expected decrease of galactic cosmic ray flux at solar maximum. Such an explanation would require that ionization production in the lower ionosphere is due predominantly to galactic cosmic radiation throughout the solar cycle. Bain and May (1967) have suggested however that some of Deek's (1966) profiles should be lowered by about 6 km, in which case, electron densities at all heights above about 65 km would be greater at sunspot maximum than minimum.

The results of Gregory and Manson (1969) for Christchurch, N.Z. ($43^{o}$S), represent a period of five years' observations (1963 - 1967). The mean summer profile presented in this chapter is in reasonable agreement with the summer profile of these workers, with their profile having an indication of a peak at about 70 km, similar to the present results, followed by a slight dip above this. This dip is much more pronounced in the summer profile presented here. The present profiles also show a pronounced dip in electron density near 75 km for the equinox profiles while the corresponding profiles of Gregory and Manson show a dip nearer to 70 km. At this height the present electron densities are about a factor of 2 higher, probably being attributable again to the difference in solar activity. Upwards of 75 km, the electron densities are in closer agreement. The

present winter profile is in good agreement with that of Gregory and Manson (1969) although the latter profile shows evidence of an increase of electron density below about 65 km which is not evident in the present average winter profiles. It is thought, however, that at these low heights, uncertainties in the DAE method are large enough to make useful comparisons very difficult.

Titheridge (1962a), from measurements of the difference in absorption for two different medium frequency radio waves reflected from the D-region, has obtained a noon summer profile for sunspot maximum conditions at 52°N. Considering the fact that he assumed collision frequency values almost double those assumed in the present work, which would tend to enhance his electron densities compared with the present results, reasonable agreement with the present results is obtained. His summer profile shows a peak in electron density just above 65 km and a shallow dip above this and centred on about 75 km. A series of electron density observations has been made by Thrane et al. (1968) at Crete (35°N) for the Autumn of 1965. These workers concentrated mainly on diurnal variations and showed that electron densities displayed a smooth zenith angle dependence throughout the D-region and that electron densities showed a fairly smooth exponential increase with increasing height.

Belrose et al. (1967), Gregory and Manson (1969) and many other workers have noted the increased variability of electron densities in winter which has also been found in the present investigation. Variability has been found to be a maximum in June. The measurements of

the angular spread of partial reflections described in chapter 4 also showed maximum variability in June above about 75 km. It is believed that both of these situations are the result of a generally decreased stability of the mesosphere during winter.

A feature of the comparisons made so far is the more pronounced peak of electron density at about 70 km and the dip above this, observed in the present work. Smith et al. (1965) at Armidale, Australia ($30^{\circ}$S) have published daytime profiles, obtained from pulse wave interaction experiments, which clearly show a similar feature, with a summer profile showing a peak at about 74 km ($\chi = 15.5^{\circ}$) and a winter profile showing a less pronounced peak at about 72 km. In both cases, a dip in electron density just below 80 km is evident, being most pronounced in summer as in the present results. The profiles of Smith et al. show higher electron densities at the peaks near 74 km than at the peaks in the present results although the results of the former workers represent isolated measurements so that no conclusive comparisons can be drawn.

Some other interesting results obtained for solar maximum conditions are those of Landmark and Lied (1961) who have given electron density profiles measured at Kjeller ($60^{\circ}$N) and although latitudinal differences make quantitative comparisons difficult, it is interesting to note that their profiles show a peak in electron density in the lower D-region followed by a pronounced dip above this height. These features, like those shown in Figure 6.9a here, become less pronounced in winter although the features in the profiles of Landmark

and Lied are shifted down by about 5 km with respect to those observed here. Some of the most extensive ground based studies of D-region electron densities which have been carried out (Belrose and Burke, 1964; Belrose et al., 1966) show that in Canada, electron densities generally increase fairly smoothly with increasing height, although some later profiles (Belrose, 1970) show a marked dip near 75 km as is observed in the present results. These latter profiles, however, tend to show larger electron densities than the present ones, particularly near 80 km.

After an examination of all possible sources of error in the present system, it was concluded that in view of the experimental system used and the critical methods of analysis applied, the profiles presented in this chapter, subject to the assumptions of the theory described in the last chapter, are good estimates of the electron density profile over Adelaide ($35^{\circ}$S). A useful addition to the system will be the use of an additional probing frequency of 6 MHz which will be expected to increase the reliability of electron density estimates near 80 km, which are possibly under-estimated using the present frequency of 1.98 MHz, and extend observations up to about 90 km. The need for at least two operating frequencies to adequately cover the whole D-region height range has been expressed by Belrose (1970) whose results suggest that using probing frequencies lower than about 3 MHz may result in electron densities being under-estimated in the upper D-region.

It is apparent that when inter-comparisons of all available D-region electron density profiles are made, that a considerable spread in the degree of agreement between various workers is evident and it is uncertain to what extent these reflect differences in experimental techniques or true geographic and temporal variability of the D-region. If all results are to be accepted at face value, considerable spatial and temporal variability of the D-region is implied, so that continued observations on a wider geographic scale are desirable to gain a better understanding of these variations.

# CHAPTER 7

# INVESTIGATIONS OF D-REGION ELECTRON DENSITIES USING A MAGNETIC TAPE RECORDING SYSTEM

## 7.1 Introduction

The Differential Absorption Experiment (DAE) is probably the most useful method available for the determination of D-region electron densities. However, carried out in the form described in the preceding chapters, where photographic recording of data was used, the method suffers from some drawbacks. The chief of these is the very tedious and time consuming process of scaling the data and coverting it into computer compatible format. In addition, the data recording medium (35 mm film) is not re-usable. Consequently, due to factors such as these, extensive running of the experiment in this form becomes expensive and largely impracticable.

In this chapter, a magnetic tape system which was developed for the recording of differential absorption data in the latter stages of the DAE project is discussed. Such a system overcomes the principal limitations stated above, although not without some concessions to the photographic method of recording. Some sample N(h) profiles are discussed and comparisons with the photographic technique are made.

## 7.2 Description of techniques and analysis

### 7.2.1 The recording techniques

The detailed features of the equipment have been described in §2.4.3; however it is appropriate at this stage to briefly summarize the recording procedures, as they have some bearing on the determination of a suitable method of analysis. The block diagram of Figure 2.5 summarizes the magnetic tape system.

A transmitter PRF of 50 Hz was employed and a range scanning gate selected signals from successive height increments in a selected range of interest. The scanning gate progressed one height increment with each transmitter pulse, feeding the gated receiver output to a digitizer/tape logging system. The tape recording system divided the data into 10 second sequences with end of record pulses and these pulses were used to trigger the alternation of the receiver and transmitter polarizations between 'O' and 'X' mode. All synchronization was derived from the internal clock of the digitizer/tape unit.

A recorded digitized level obtained from the gated receiver output corresponded to the peak amplitude occurring within the width of the scanning gate. Generally the gatewidth was 2 km and the range 50 - 90 km was scanned. The recording sequence is possibly best described in terms of an A-scan trace of received signal amplitude as a function of height (or delay time). Figure 7.1 illustrates the way in which a hypothetical A-scan would be sequentially sampled and digitized. Levels $\ell_1$, $\ell_2$ and $\ell_3$ would be digitized to give recorded values corresponding to the first three height increments sampled.

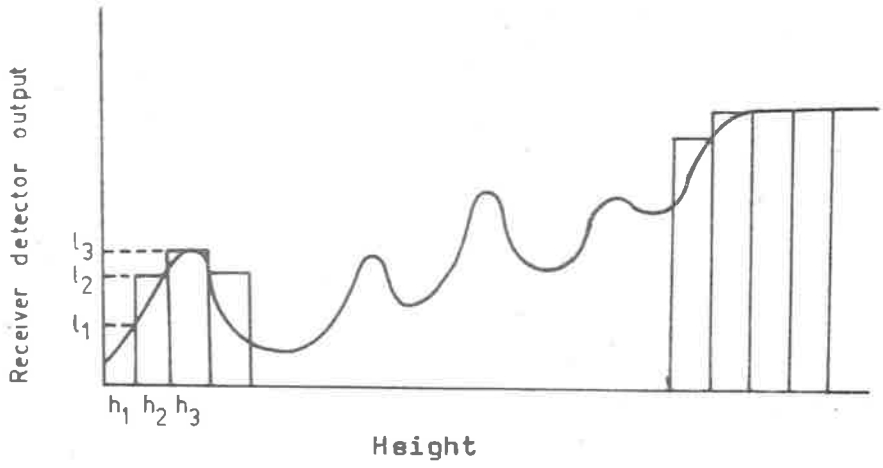


Figure 7.1 Graphic illustration of the digitizing sequence for the magnetic tape DAE system.

The tape logging system had a fixed sampling rate of 500 Hz compared with a transmitter PRF of 50 Hz and consequently 90% of recorded data was redundant. Computer processing was used to condense the data and transfer it to a data bank where each tape had the capacity for 120 hours of condensed recorded data.

In addition to the tape recording of DAE data a simultaneous photographic recording of an intensity modulated display representing signal strength as a function of height (height/time film) was taken. This record was used as a visual aid to determining the nature of records obtained on tape, as a magnetic tape system alone has no record which can be easily evaluated visually. The film record was found very useful for selecting records suitable for analysis and rejecting those in which either the noise level was high, or system faults were evident. Alternate 'O' and 'X' record blocks on film (e.g. see Figure 7.2) were easily identified with the corresponding tape records as the digitizer clock display was flashed onto the photographic record at one minute intervals. Any faulty data which might have been recorded was subsequently removed in the analysis of the tape records. The difficulty of performing the same task without such an aid is quite apparent.

### 7.2.2 Analysis of tape records

The magnetic tape recording techniques which have been described differ considerably from the photographic recording method discussed in the previous chapter and consequently the procedures of analysis were reconsidered. Since 'O' and 'X' data was not recorded

simultaneously, but in 10 second alternating periods, the short term temporal resolution of the magnetic tape system was inferior to that of the photographic method. It was felt that no attempt should be made to obtain an N(h) profile with less than 5 minutes of averaged data, and in the main at least 10 or 15 minutes of data was averaged.

The "peak-scaling" method used in the photographic method is inherently unsuited to the analysis of the tape data purely due to the sampling and recording technique, so that an "envelope-scaling" procedure was employed. Mean height profiles of 'O' and 'X' amplitudes were constructed at 2 km intervals corresponding to the range scanned by the scanning gate. The effects of a finite sampling gate-width and transmitter pulsewidth were considered to justify smoothing the mean $A_x$ and $A_o$ curves with a three-point filter in exactly the same manner used in the analysis of photographic records described in the previous chapter. A fixed smoothing process as described there was used in all computations for the sake of consistency of data reduction and in order to make comparisons between various profiles as reliable as possible. The $A_x/A_o$ curve was then formed as the ratio of the smoothed mean $A_x$ and $A_o$ curves, and was used to determine the electron density profile using equation 5.6.

## 7.3 Examples of results

### 7.3.1 The height/time records

Figure 7.2 shows a series of consecutive film records taken on 18/11/71 simultaneously with tape records of partial reflection amplitudes for reduction to electron density profiles. White traces in

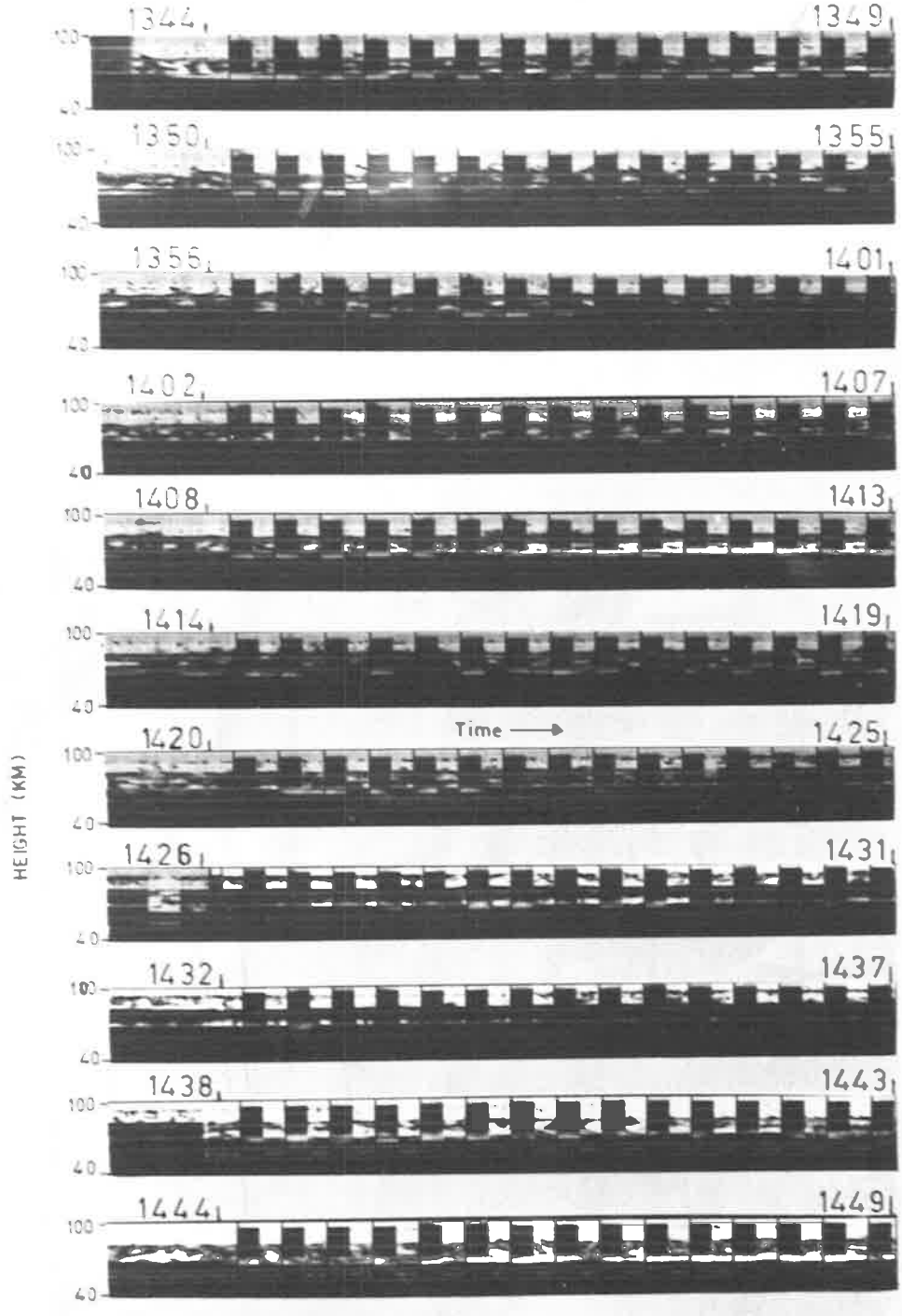


Figure 7.2 Height/time records taken simultaneously with magnetic tape records of differential absorption.

the figure correspond to high signal strength. The records extend over a period of more than an hour, time marks being labelled at the beginning and end of each 5 minute recording sequence. Each separate strip in Figure 7.2 corresponds to such a 5 minute sequence. White horizontal range marker lines are spaced at 10 km intervals, the lowest corresponding to 40 km and the highest to 100 km. The frames within each 5 minute sequence alternate at 10 second intervals between 'O' and 'X' polarized transmission and reception. The two polarizations are easily distinguished by the stronger E-region (100 km approx.) signal on 'O' mode. The 5 minute recording sequences are separated by 1 minute gaps where data was not recorded on tape and the polarization remained on 'O' mode. These sections are seen at the beginning of each 5 minute sequence. These 1 minute intervals allowed adjustments to equipment to be made and such adjustments were restricted to these periods. An examination of the records shown in Figure 7.2 enables several interesting features to be identified:

(1) Echoes consistently keep appearing at heights of approximately 66, 71, 75 and 86 km over the length of the record.

(2) The 'X' signal is stronger than the 'O' signal at 66 km but at 71 km the 'O' signal is much stronger. This feature is most clearly seen in the sequence beginning at 1438 hours. The $A_x/A_o$ "turnover height" is probably near 66 km and certainly below 71 km.

(3) Turbulent echo structure is seen above about 85 km. This is particularly evident in the 1 minute blocks preceding each 5 minute sequence. Fading periods are of the order of seconds in contrast to the lower echoes which have much longer periods.

7.3.2 Electron density profiles and their temporal variations

Electron densities have been computed from measured $A_x/A_o$ curves using the techniques described in §7.2 and the equations given in chapter 5. A series of electron density profiles compiled from records taken on 28/10/71 is shown in Figure 7.3. The profiles have been computed from consecutive 10 minute averages of the $A_x/A_o$ curve so that each electron density profile represents the average over an 11 minute period (a 1 minute gap occurs between 5 minute data records on tape). Error bars shown on the profiles incorporate both fluctuations in measured amplitudes as well as the errors in height and amplitude measurements inherently due to the nature of the system. A more detailed description of errors is given in §7.4.5 and Appendices 1 and 2. In this case, a combination of factors is thought to account for unreliable results above about 77 km and these portions of the profiles have been dotted in. Small ratios are expected above this height and the accuracy with which the height profile can be measured is limited by the resolution of the digitizer for the small 'X' amplitudes.

The profiles of Figure 7.3 extend over the period 1258 - 1433 hours local time and serve to show the type of results that can be obtained using a magnetic tape system to investigate temporal

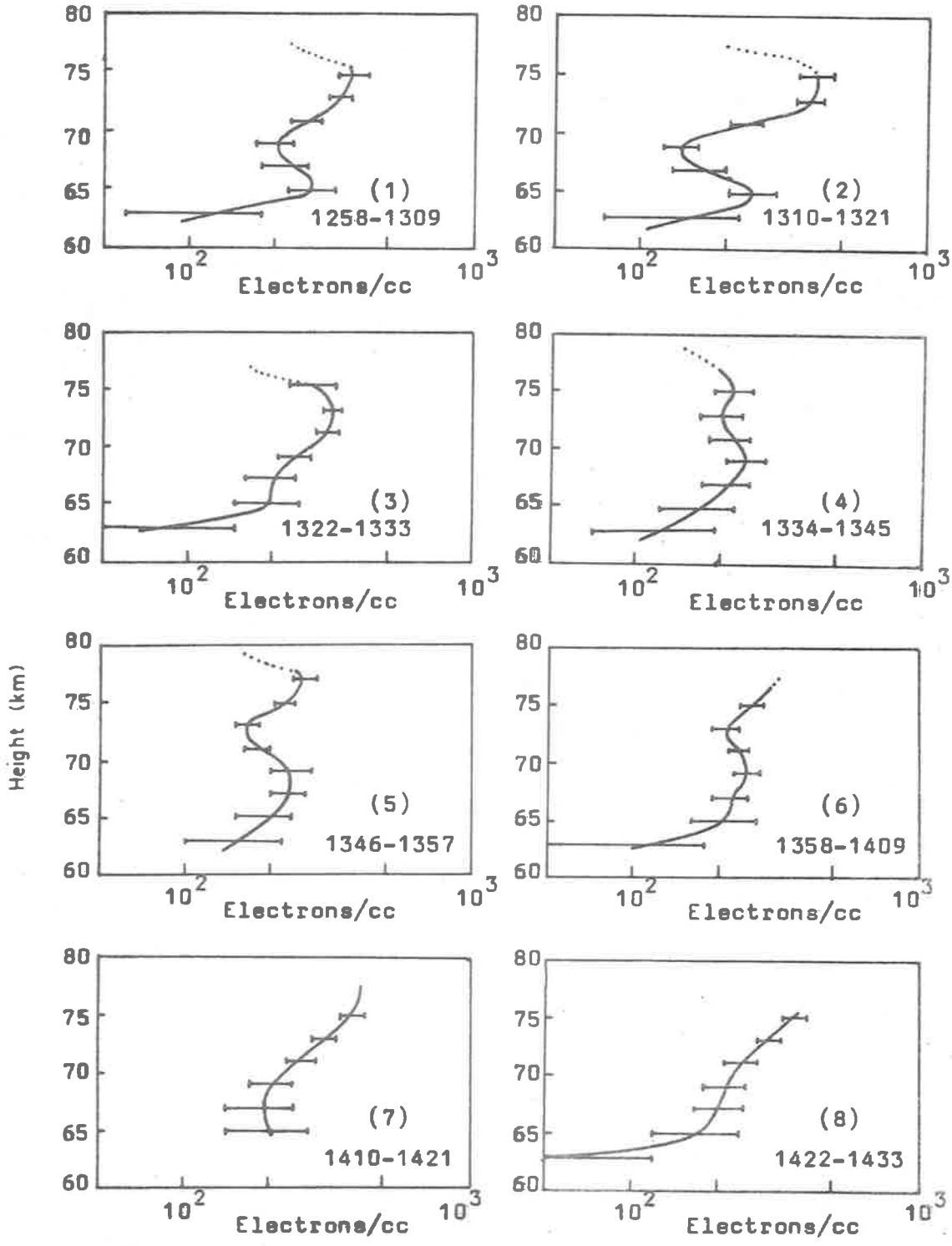


Figure 7.3 Electron density profiles for 28/10/71, derived from the magnetic tape system.

variations of D-region electron density profiles. Over the course of about 1½ hours Figure 7.3 shows that the electron density profile apparently changed considerably in form. However, the error bars shown do not incorporate uncertainties related to assumptions made regarding D-region scattering models in the derivation of a theory of differential absorption. To what extent variations in scattering processes contribute to the apparent electron density variations shown in Figure 7.3 is not entirely certain. An examination of associated height/time records suggests that qualitatively, the reflection mechanism does not appear to vary over the recording period so that the variations shown in Figure 7.3 have been interpreted as electron density variations. A dip in electron density just below 70 km is evident in the first two profiles with peaks at 65 km and possibly 75 km. A systematic decrease in electron density at 75 km accompanied by a filling in of the dip just below 70 km occurs in the following two profiles. The next two profiles show the build up of a broad peak of electron density at about 70 km. Finally, the last two profiles show the transition to a fairly smooth monotonically increasing profile. The sequence of profiles (2) - (6) could be interpreted as being consistent with a model invoking the downward transport of ionization, ionizable neutral constituents or heat energy from about the 75 km region to just below 70 km. Vertical velocities of a few metres/second would be implied. Velocities of this magnitude have been observed on phase path records taken during angular spread and scattering model experiments (see chapter 4) although in general phase records

have not been systematically studied from this point of view. Such velocity measurements, however, actually refer to the motion of the ionospheric reflection point rather than the motion of ionization.

Finally, Figure 7.4 shows two average profiles representative of the whole recording period covered by the individual profiles of Figure 7.3. The solid curve is derived from 'O' and 'X' profiles averaged over the whole recording period while the dashed curve is the average of the individual 10 minute N(h) profiles shown in Figure 7.3. The good agreement between the two profiles is taken as some verification of the reliability of the individual 10 minute profiles of Figure 7.3 and the temporal variations that have been described.

## 7.4 Comparisons of the magnetic tape and photographic DAE recording systems

### 7.4.1 Observations of temporal variations

In the photographic recording of DAE data, as described in chapters 2 and 6, 'O' and 'X' reflected signal strengths are recorded quasi-simultaneously at 1 second intervals. Under certain conditions discussed in chapter 8, the method allows the possibility of deducing short term (of the order of some tens of seconds) variations of mean electron density between stable reflecting heights. The magnetic tape system, on the other hand, which records 'O' and 'X' signals in alternating 10 second periods, is believed to be limited to resolving variations with time scales only greater than about 5 minutes. This is largely due to the fact that 'O' and 'X' amplitudes are not measured simultaneously and that a finite sampling gatewidth dictates averaging

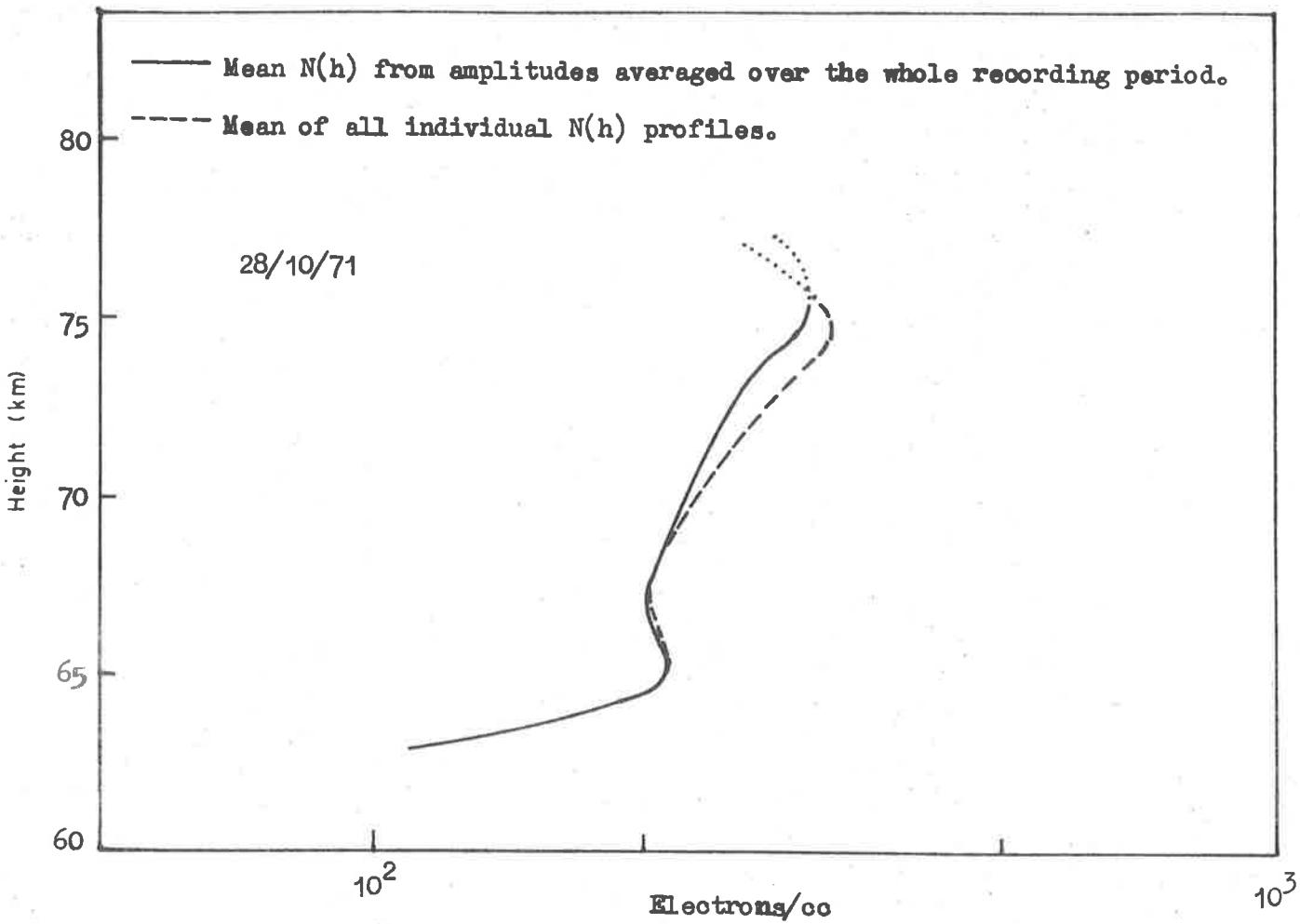


Figure 7.4 Comparison of two methods of formulating an average electron density profile N(h) for the whole recording period illustrated by the profiles of Figure 7.3.

over several minutes to obtain reliable electron densities. These aspects are discussed quantitatively in §7.4.4. The inherent necessity for envelope scaling in the tape system also effectively precludes the type of identification and analysis of special situations which can be carried out on peak scaled records, as is discussed in chapter 8.

While the tape system is unsuitable for studying short term temporal variations in N(h) the suitability for studying larger scale variations more than compensates for this, for, as will be pointed out in chapter 8, the number of occasions on which the photographi DAE data can be applied to giving short term fluctuations is relatively small. Studies of variations of N(h) over a few tens of minutes can be very useful in studying the dynamics of the D-region and the tape system then becomes far more suitable than the photographic method due to the large decrease in labour of data reduction.

7.4.2 Reflection statistics

Where peak scaling of DAE data is used, as in the photographic DAE system, it becomes possible, as is outlined in chapter 8, to deduce the statistics of the heights of occurrence and relative strengths of scaled D-region echoes. Due to the inherent nature of th data sampling method, the magnetic tape system is at a disadvantage in this respect, for, apart from the difficulty of formulating a "peak-scaling" process, the resolving of closely spaced discrete echoes becomes impossible due to the finite width of the scanning gate. It is possible, however, that a sophisticated technique used in conjunction

with simultaneously recorded height/time records (e.g. Figure 7.2) could be developed for studying height distributions of echoes. No such analysis has yet been attempted with the tape recorded data.

The usefulness of echo statistics in interpreting electron density profiles has been discussed in the previous chapter. Preferred reflection heights were used to gauge the reliability of features of the N(h) profile and it is apparent that such a technique is virtually impracticable for a tape system. This represents a disadvantage again over the photographic system as uncertainties in features of the electron density profiles cannot be easily resolved.

7.4.3 Errors inherently associated with the recording systems

In Appendix 1 the errors in electron density which arise as a result of uncertainties in reflected signal amplitudes and height determinations are derived. It is interesting to consider the application of the error formulae to the two DAE systems. It can be shown (Appendix 1) that the relative error in the determination of an electron density N, subject to the assumptions outlined in the Appendix and as a result of uncertainties or errors in amplitude and height determinations, is given by

$$\frac{\sigma_N}{N} = \left\{\frac{A}{N^2} + B\right\}^{\frac{1}{2}}, \qquad 7.1$$

where we have written

$$A = \frac{\left(\frac{\sigma_{A_2}}{A_2}\right)^2 + \left(\frac{\sigma_{A_1}}{A_1}\right)^2}{\{2.\ (k_x - k_o)\cdot(h_2 - h_1)\}^2}, \qquad 7.2$$

$$B = \frac{\sigma_{h_2}^2 + \sigma_{h_1}^2}{(h_2 - h_1)^2} \quad , \qquad 7.3$$

$A_1 = A_x/A_o$ at height $h_1$ ,

$A_2 = A_x/A_o$ at height $h_2$ ,

$k_x - k_o$ = mean differential absorption factor between heights $h_1$ and $h_2$ .

We shall firstly consider the quantity B which represents the component of error due to height uncertainties. Since the terms A and B are each greater than or equal to zero, equation 7.1 shows that a lower bound to the relative error is given by

$$\frac{\sigma_N}{N} \geqslant B^{\frac{1}{2}} \quad ,$$

$$\text{i.e.} \qquad \frac{\sigma_N}{N} \geqslant \frac{(\sigma_{h_2}^2 + \sigma_{h_1}^2)^{\frac{1}{2}}}{|h_2 - h_1|} \quad . \qquad 7.4$$

The terms which are required to be estimated in equation 7.4 are the $\sigma_h$ terms.

Where peak scaling is used, as in the photographic recording of DAE data, an artificial gating effect (analogous to the gating used in the magnetic tape sampling system method) is introduced when an average $A_x/A_o$ curve is compiled from the discrete measured values. It was described in §6.3.1 how the average $A_x/A_o$ ratio as a function of height was compiled at 1 km intervals, where each average was formed from those discrete amplitude values which lay within ½ km of the range under consideration. The 'true' range of each scaled echo pair which was used to form the average ratio was known, and so the

average range and its standard deviation were also able to be computed for the defined 1 km height increments, so that they were directly available for use in equation 7.4 to evaluate uncertainties in N.

In the case of the magnetic tape system the effects of a finite gatewidth cannot be treated in the above manner since no signal structure within the width of the sampling gate is known. Instead, assuming that an echo peak is equally likely to occur anywhere within a given gate, it can be shown (Appendix 2) that the relative error in an electron density calculation due to the assigning of the average $A_x/A_o$ value to the centre of the gate is given by

$$\frac{\sigma_N}{N} \simeq \frac{1}{\ell(6n)^{\frac{1}{2}}} \qquad 7.5$$

for large n, where n is the number of gated $A_x/A_o$ values averaged over and $\ell$ is the steplength (in units of the gatewidth) used for the electron density determinations. Equation 7.5 shows that the relative error decreases as n is increased (i.e. as the averaging interval is increased) and also decreases as $\ell$ is increased. The increase in accuracy as a result of increasing steplength is achieved at the expense of resolution in the final N(h) profile. In reducing magnetic tape data averaging has generally been carried out over at least 5 minute intervals so that the term represented by equation 7.5 is approximately 4%, this being quite acceptable in view of other more significant errors, such as those due to uncertainties in the appropriate theory of reduction and due to amplitude variations.

Due to the high resolution of the film reading equipment, the measurement of amplitudes from photographic records of DAE A-scans was able to be performed very accurately and was limited mainly only by the care with which measurements were made. Since the magnetic tape system required the digitizing of analog signals into one of a series of levels, the possible error in any one digitized reading was plus or minus 1 level. In the system used, data was digitized into one of 64 levels so that the minimum amplitude error expected for any one reading was one in sixty four for a saturating amplitude. Using equations 7.1 and 7.2, the component of uncertainty in an electron density determination, which arose as a result of an uncertainty of 1 level in each digitized amplitude was calculated for all profiles. This quantity depends on the steplength and the reflection coefficient ratios at the heights under consideration as well as the averaging time interval used and in practical situations was found to be of the order of a few percent except for a marked increase above about 77 km as 'X' amplitudes became close to zero. The use of longer averaging intervals helps to minimize such errors and in fact total error estimates for the two types of recording systems have been found to be fairly comparable when averaging is carried out over 10 or 15 minutes. The physical variations of the measured reflected signal strengths have then formed the main contribution to the calculated uncertainty in electron density determinations.

### 7.4.4 Comparison of electron density profiles

The two systems for measuring differential absorption which have been compared in the previous sections differ widely in their modes of equipment arrangement so that simultaneous records using the two systems could not be obtained. Nevertheless, a fairly direct comparison between N(h) profiles was obtained on 18/11/71 and the comparison is shown in Figure 7.5. The solid curve shows the electron density profile obtained from film records between 1210 - 1225 hours local time, while the dashed curve shows the mean electron density profile obtained from the tape DAE system between 1344 - 1444 hours local time. The two profiles show good agreement considering the uncertainty limits of about 20% associated with each profile and the difference in the times at which they were measured.

## 7.5 Conclusions

Although detailed D-region studies using a magnetic tape system have not been undertaken in this project, the development of the system in the latter stages of the project has been considered to be well worthwhile. The considerable saving in labour of reduction and the simplicity of the recording procedures have made it a system suitable for synoptic applications. Although short term temporal variations and considerations of special situations (e.g. where strongly preferred reflection levels exist) such as those described in the next chapter are virtually impracticable, the greater usefulness for observations of longer scale time variations is evident. In such studies the main

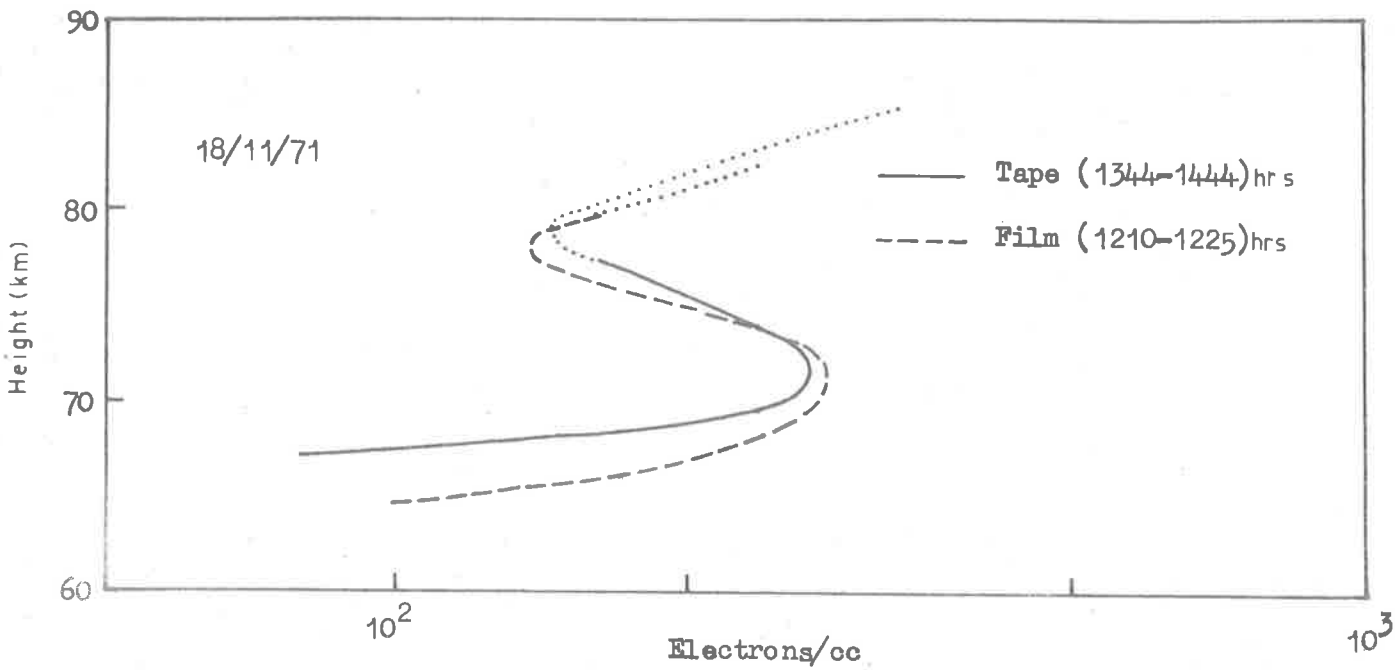


Figure 7.5 A comparison of electron density profiles measured on the same day using two different recording systems.

contribution to estimated uncertainties in the computed N(h) profile, provided averaging is carried out over more than about 10 minutes, has been found to arise as a consequence of actual signal variations, and not to come from the system parameters, the latter contributions decreasing with increasing averaging interval. Due to the digitizer resolution becoming important at low 'X' amplitudes, the maximum height to which reliable studies have been possible in the present preliminary investigations has been found to be about 3 km lower than in the photographic system. An increase in the number of levels in the digitizer would probably help to eliminate this.

# CHAPTER 8

## STATISTICS OF THE STRENGTHS AND HEIGHTS OF OCCURRENCE OF PARTIAL REFLECTIONS

### 8.1 Introduction

The study of the D-region of the ionosphere often involves ground based observations of the weak partial reflections of radio waves which can be detected from this region, and the distribution of height from which such reflections occur partly determines the detail in which height variations of the various properties of interest derived from such observations can be described.

Naismith and Bramley (1951), from measurements of the equivalent height of reflection of 2MHz radio waves over oblique incidence propagation paths, produced some early evidence indicating that reflections were not equally likely from all heights, but that preferred levels of reflection occurred in the D-region. At about the same time Bracewel et al. (1951), from LF/VLF oblique incidence propagation studies, made brief reference to an appearance of preferred levels of reflection during the day, while Helliwell et al. (1951) from night time LF propagation studies at vertical incidence concluded that there appear to be partially reflecting strata at discrete heights in the lower night time ionosphere. Other workers (e.g. Dieminger, 1952; Gardner and Pawsey, 1953) also made reference in the following years to the apparent occurrence of preferred heights of reflection, but the first

comprehensive survey appears to have been made by Gregory (1956) using pulsed vertical incidence sounding. Again conclusions were drawn that partially reflecting levels existed at preferred heights in the D-region. Ellyett and Watts (1959) in a review of the available experimental evidence concluded that such a situation did not exist consistently on a large geographic scale. On the other hand Titheridge (1962b) in a later review considered that considerable consistent evidence existed to support the hypothesis of a series of preferred or horizontally stratified reflecting levels in the D-region, and he surmised that insufficient consideration of the various different experimental techniques when making comparisons led Ellyett and Watts to a differing conclusion.

The relative paucity of statistics in general, and especially in the southern hemisphere, prompted the present study of heights of occurrence of echoes, which were inherently obtainable from the DAE data manually digitized from photographic records. The experiment was carried out principally for the deduction of D-region electron densities as described in chapter 6. In the following sections the procedures of compilation of the statistics and examples of results for individual records are discussed. Following this the seasonal variations of the results are discussed, followed by an interpretation of some specially selected records in terms of apparent temporal variations of electron density between strongly preferred reflection heights.

## 8.2 Compilation of the statistics

The bulk of DAE results discussed in this thesis were deduced from photographic records of A-scan displays of received signal strength as a function of height. Each photographic frame contained a record of two A-scan traces, one being for 'X', and the other (inverted) for 'O' mode transmission (e.g. see Figure 6.1). In all such records the peak scaling method of data reduction was used and the heights at which peaks in both 'O' and 'X' amplitudes occurred were digitized and recorded, along with the individually scaled 'O' and 'X' peak amplitudes. In a subsequent computer analysis the mean scaled amplitudes of partial reflections were computed as a function of height as well as the numbers of scaled echoes falling in 1 km height increments predefined throughout the D-region. For the purposes of displaying the results, the histogram showing the frequency of heights of occurrence and the mean 'O' amplitude profile were separately normalized and then both plotted on the one graph by a computer line printer.

The monthly averages given in this chapter correspond to conditions near noon. Since each monthly average is compiled from only 15 minute samples for days near the middle of each month, they do not carry the degree of statistical certainty of true representation of average monthly conditions as do the more comprehensive studies of some other workers (e.g. Gregory, 1956, 1961). Nevertheless the results have displayed some interesting features and have the advantage of superior height resolution compared with many other methods.

## 8.3 Examples of individual records

Before going on to discuss the quantitative results it is worth presenting some interesting photographic records which give a qualitative indication of the fairly high degree of stability in both amplitude and height of reflection that is present on some occasions. Some photographic records were taken where, instead of recording successive pairs ('O' and 'X') of A-scans on separate frames, the film was kept stationary, allowing successive A-scans to be superimposed on the one frame. The period of time for which such a superposition was carried out was varied for a series of separate frames to allow some qualitative assessment of short term temporal variations. In the examples shown in Figure 8.1 the stable echo appearing at about 55 km is to be disregarded as it is of non-ionospheric origin. The sequence of frames, taken on 8/10/71 at about mid-day, shows evidence of partial reflections from about 69 and 78 km which are very stable in both amplitude and range.

Another experiemental technique which is useful for displaying the characteristics of partial reflections is one in which received signal strength is used to modulate the intensity of a vertical trace serving as a height axis on a cathode ray oscilloscope display. A film slowly moving at right angles to the trace acts as a time base and records the temporal variations of the recorded signals. Two examples of such records taken on 11/2/71 and 12/2/71 are shown in Figure 8.2. Here signal strength is proportional to the brightness (or whiteness) of the trace and in segment (b) a fairly stable stratified echo is

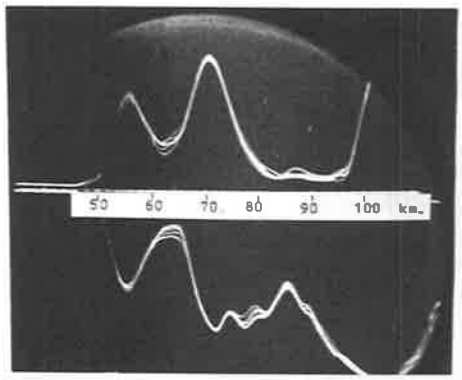


5 scans

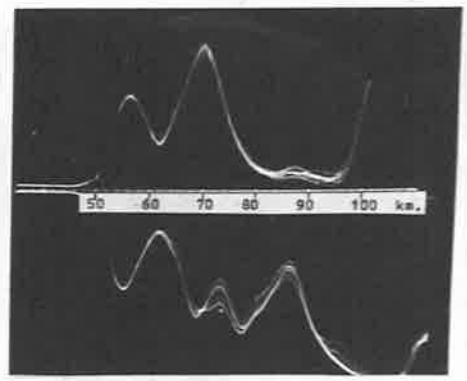


10 scans

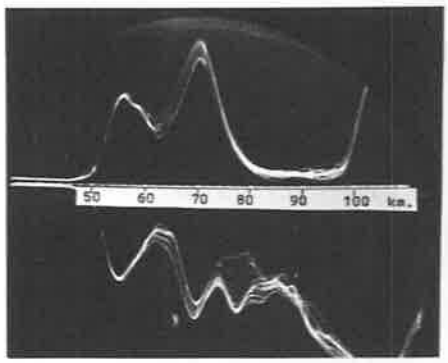


20 scans

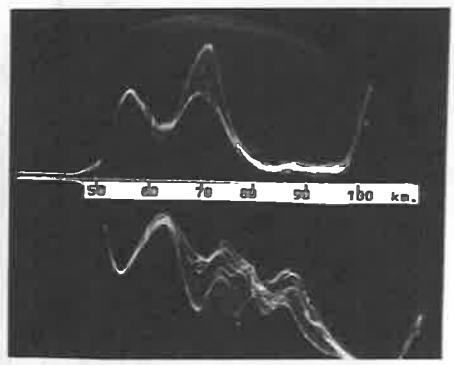


30 scans

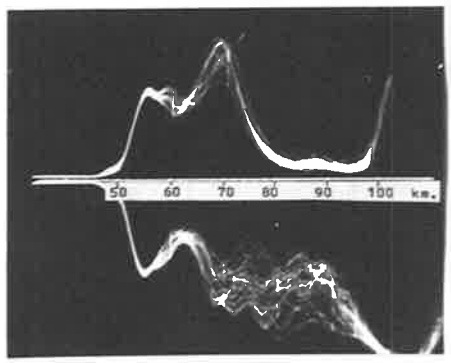


60 scans

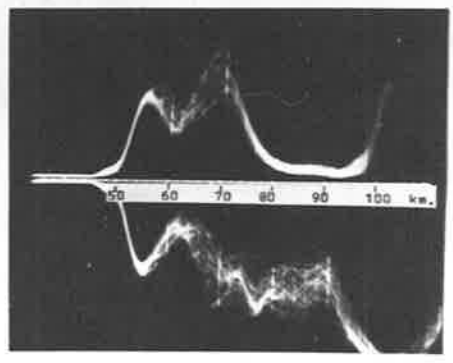


120 scans

Figure 81 Examples of superposed A-scans.

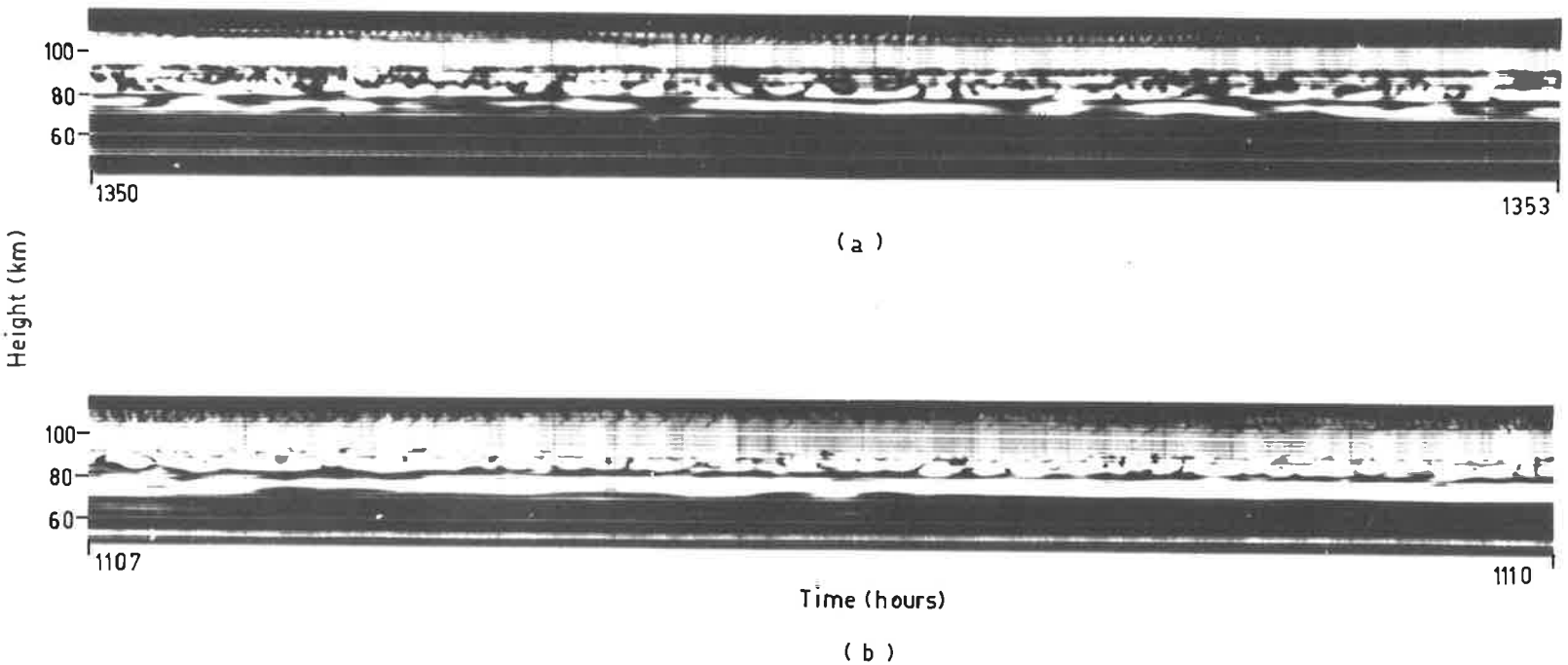


Figure 8.2 Segments of height/time records taken on (a) 11/2/71 and, (b) 12/2/71.

evident at about 75 km, while at about 85 km an echo is seen which is much less stable in amplitude, but which nevertheless is fairly stable in range. Segment (a) taken at a lower receiver gain, again displays these features but with the structure of the echoes near the 85 km level more clearly defined. The examples of Figure 8.2 also illustrate the distinction often found between the amplitude fading speeds above and below 85 km which was discussed in §4.5.2. Figure 8.3, which depicts similar records but taken in conjunction with a DAE tape recording, shows successive 5 minute sequences, each sequence alternating between 'O' and 'X' polarization at 10 second intervals. A stable echo group at about 70 km is evident throughout the records. A comparison of the height resolution of such a recording with that obtained on a conventional A-scan display is evident on inspection of the histogram of heights of occurrence shown at the bottom of Figure 8.3. The histogram was compiled from photographically recorded A-scans over a 15 minute period immediately after the tape run.

While pictorial representations such as those in Figures 8.1, 8.2 and 8.3 serve well to give some qualitative impressions of the characteristics of partial reflections, the statistics compiled in the manner described in the previous section offer further quantitative information. One could not hope to discuss all of the individual results obtained and so, alternatively, some of the results commonly obtained and their various features will be discussed here, while the monthly averages will be discussed in the next section.

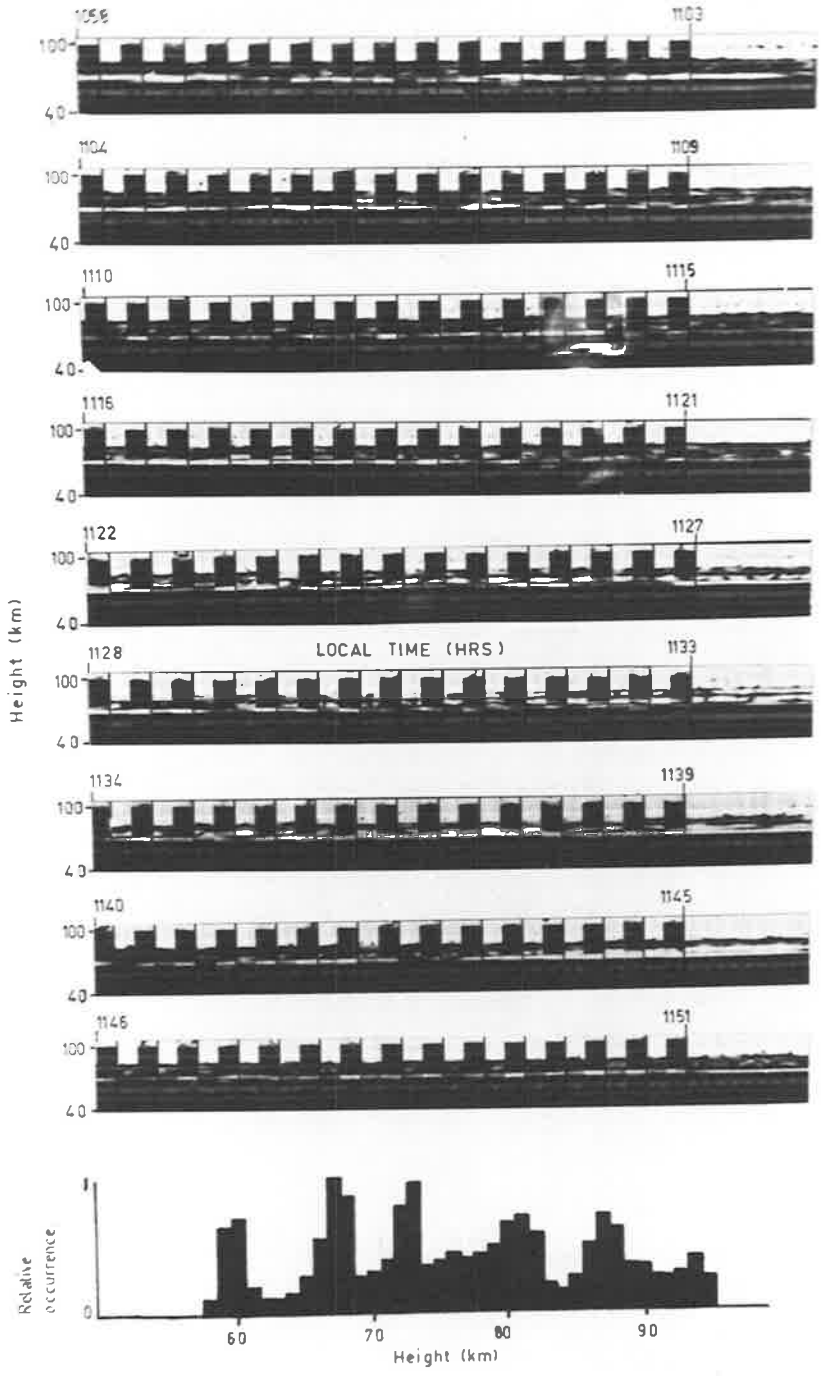


Figure 8.3 Height/time records of strengths of partial reflections. The histogram shows the relative frequency of occurrence of heights of reflection as deduced from A-scan records.

Several examples of histograms of the heights of occurrence of partial reflections superimposed on the normalized ordinary mode amplitude profiles to which they correspond are given in Figure 8.4. The examples shown should be interpreted with caution above about 90 km as in some of the records echoes were not consistently scaled much above this height. Figure 8.4a shows a record in which the degree of stratification is relatively low except for a fairly prominent peak in the histogram of heights of occurrence at 67 km. Records (b) and (c) taken about an hour apart on another day show quite marked preferred heights which are quite consistent between records. The same consistency throughout a day's observations is fairly often observed. A notable feature of many of the examples shown in Figure 8.4 has been the high coincidence of peaks in amplitude with preferred heights of occurrence. If, as is normally assumed, reflections are presumed to originate at sharp gradients in electron density, this would imply that the strongest irregularities exist preferentially at discrete levels in the lower ionosphere. On the other hand the results of Figure 8.4f show only a small correlation between the mean amplitude and the preferred heights of occurrence. Such situations occur usually only in winter.

On some occasions preferred heights of reflection tend to occur at a series of heights with a fairly regular spacing of about 5 km and the examples of Figures 8.4b,e,f,g and j display some results showing this phenomenon. This tendency appears to show no seasonal dependence

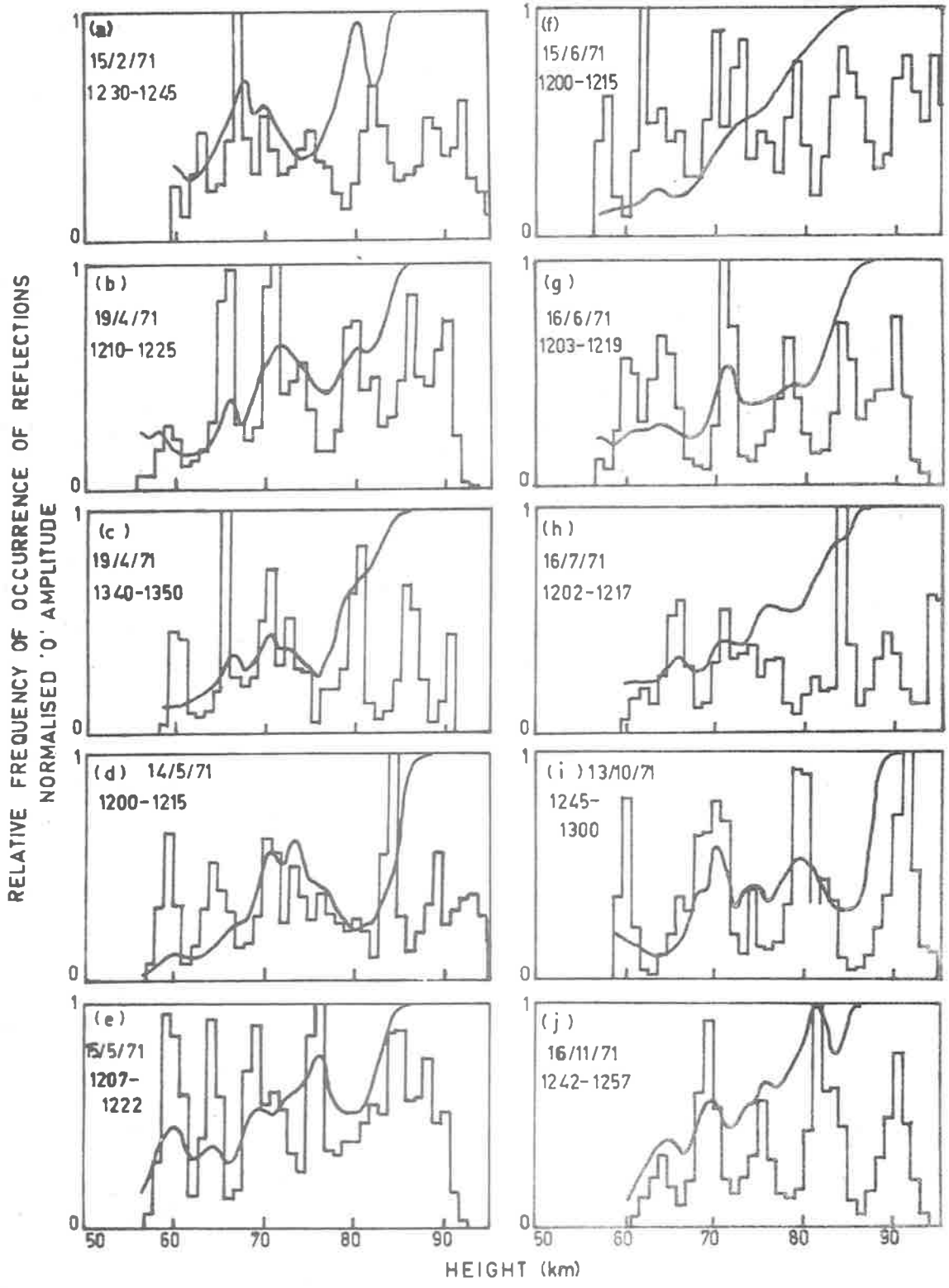


Figure 8.4 Examples of statistics derived from photographic DAE records. The histograms show the relative occurrence of heights of reflection and the solid curves depict the mean $A_0$ curve for the same recording period.

## 8.4 Seasonal variations of the heights of occurrence of partial reflections

The statistics for all individual recording periods, examples of which have been shown in Figure 8.4, were used in forming a monthly mean histogram of the relative frequencies of heights of occurrence of partial reflections. Originally the DAE was carried out principally for the purpose of determining electron density profiles. Since the normal method becomes unreliable in the upper D-region many records were not scaled above 90 km and, as a consequence, the statistics presented in this chapter, which arose as a subsequent by-product of the DAE data, lack consistent data above 90 km, and the histograms have been terminated at this level. At the lower end of the height range a persistent ground echo at a range of about 55 km effectively placed a lower height limit of about 57 km on the resolvability of ionospheric echoes.

The mean monthly histograms are shown in Figure 8.5. It can be seen that echoes tend to occur from the lowest heights in the D-region mainly during winter. Although they were present, no echoes were recorded below 60 km in the July recordings due to instrumental problems. In most months a preferred echo height appears at about 84 km and represents the most stable feature of the results. From October to December (1971), however, this feature was not evident or else had possibly shifted down by 3 or 4 km. Another group of echoes at a preferred range of 63 - 65 km is consistently present from April to July while several other preferred height groups appear to persist from one

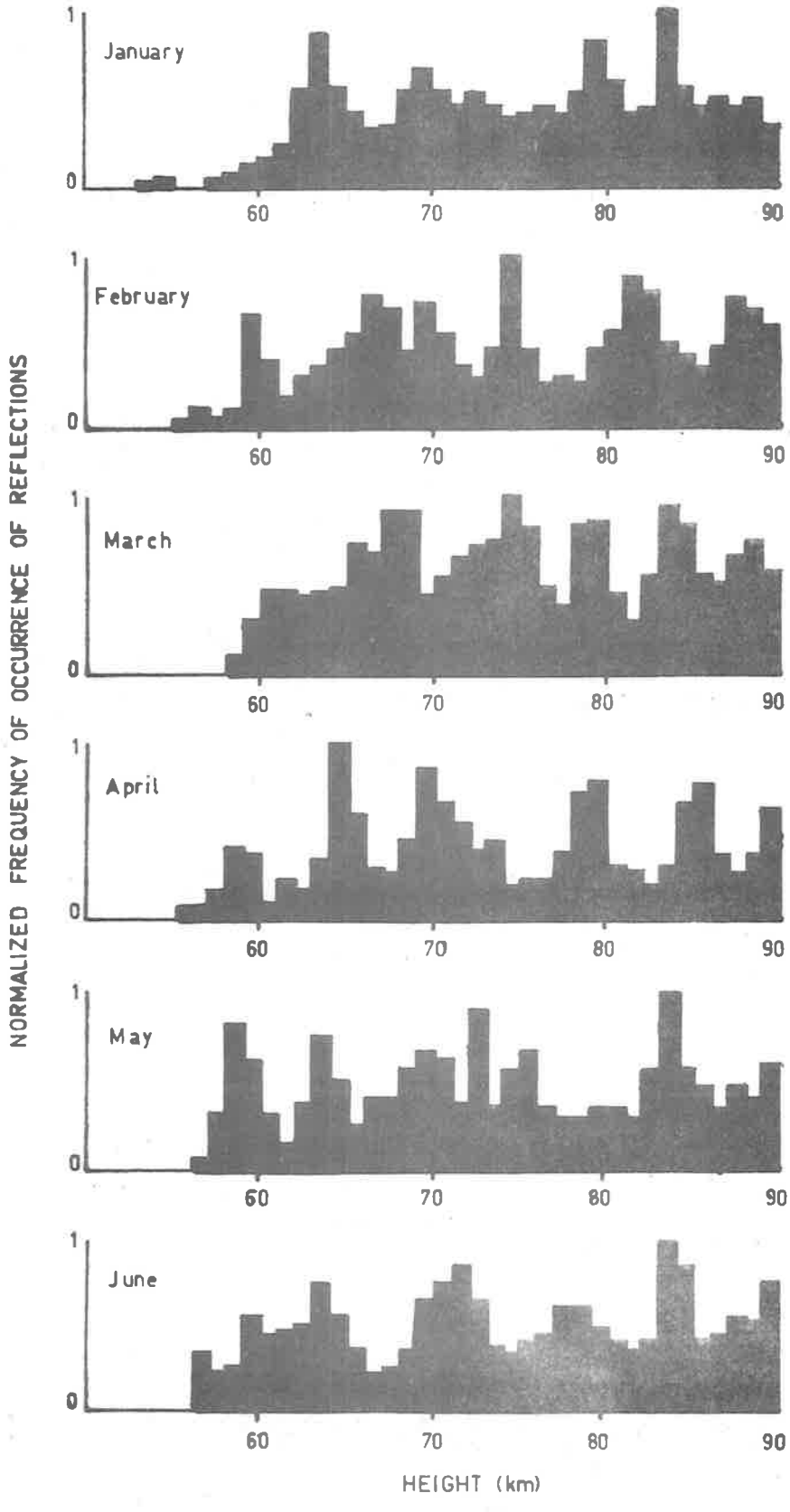


**Figure 8.5** Monthly mean histograms of the relative frequency of occurrence of heights of partial reflections....

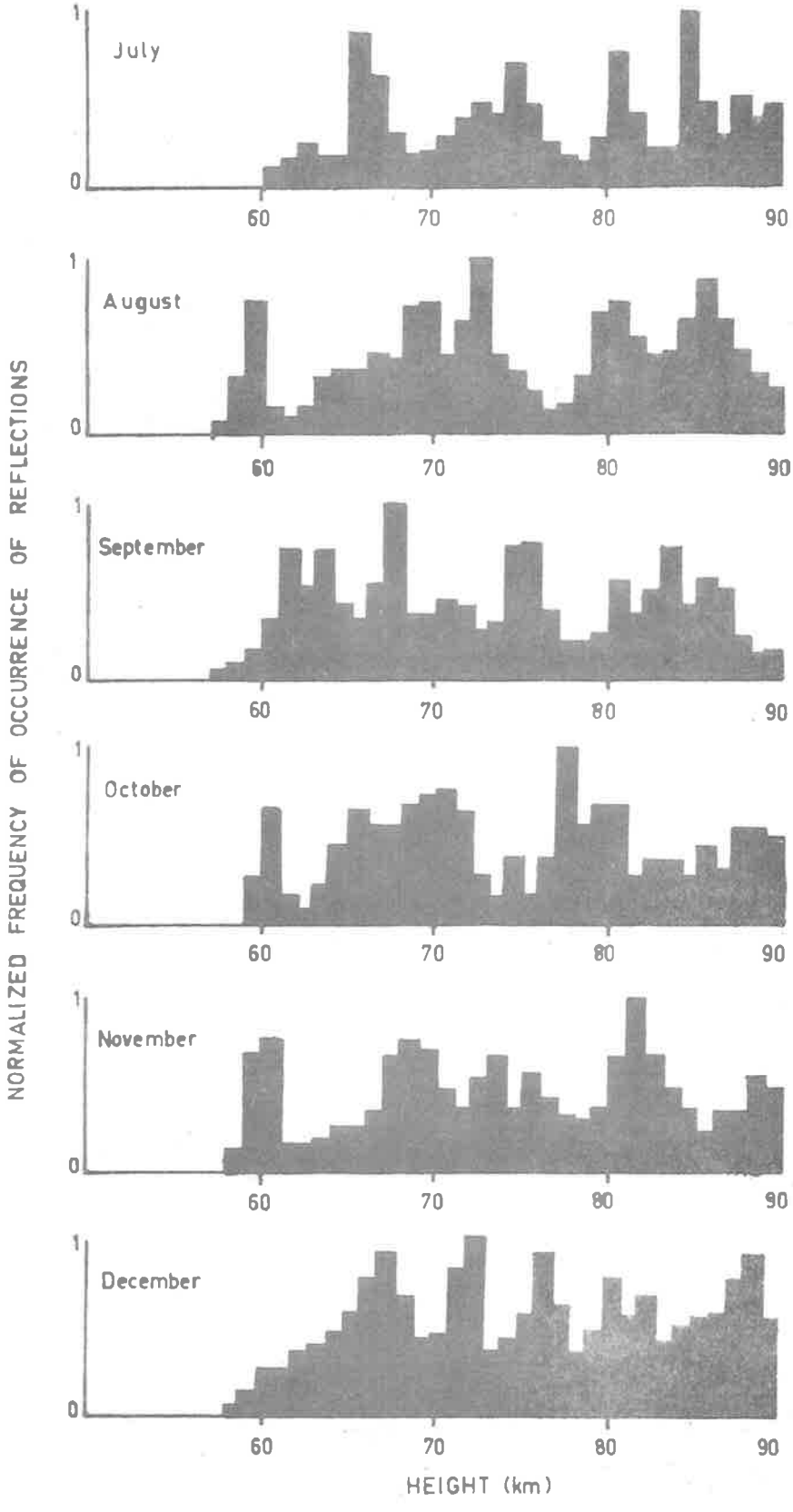


Figure 8.5 Monthly mean histograms of the relative frequency of occurrence of heights of partial reflections.

month to the next. The 74 km group in February and March, the 78 km group in March and April, an 80 km group in July and August and a 60 km group in October and November are examples.

## 8.5 Discussion and comparisons with other results

An accurate comparison with the results of other workers is difficult due to differences in experimental technique and this is manifested in the difficulty of adjusting all height measurements to equivalent values. Some workers have given results in terms of heights of lower boundaries and a knowledge of the thickness of reflecting region becomes necessary in order to effect comparisons with results which measure the height of the centre of the reflecting region, as in the present study. Furthermore, the determination of thicknesses of these regions is complicated by the uncertainty introduced by off-vertical contributions to echoes, especially in the upper D-region. Nevertheless some useful general comparisons with other available evidence can be made.

The tendency, which has been found in the present results, for the lowest echoes from the D-region to occur in winter has been widely noticed by many workers studying the D-region (e.g. Gregory, 1956, 1961; Titheridge, 1962b) and appears to be a well established phenomenon. Gregory and Vincent (private communication) in a recent reappraisal of data from 1956 - 57 (Gregory, 1961) as well as further data from 1963 - 64 (sunspot minimum) have placed the lower boundary of the most stable preferred height feature they have observed (at 44°

at 83 km. Within the limits of the uncertainties discussed above there is good agreement in the present results in that the most stable feature has been a preferred height at about 84 km. Many other workers have recognised a strongly preferred reflection level at about 85 km (e.g. Bracewell et al., 1951; Pineo, 1956; Titheridge, 1962b; Holt et al., 1961) and Ellyett and Watts (1959) in a review of evidence for the stratification of the D-region concluded that although there was generally little consistency between the series of preferred heights observed at different locations, an 85 km level was consistently observed by many workers.

Other results of Gregory and Vincent (private communication) show that at sunspot maximum principal preferred heights exist at about 74 and 65 km, being least pronounced in summer. The present results which show a preferred group at about 65 km in winter months and a preferred group at about 74 km in February, March, May, July and September can probably be identified with the two similar preferred height groups found by Gregory and Vincent, although the latter results show a smoother seasonal variation.

Although the tendency is not as marked in the monthly averages of Figure 8.5, quite a strong tendency for a series of preferred reflection heights at intervals of roughly 5 km has been present for indivdiual records (see Figure 8.4). Similar tendencies to favour multiples of about 5 km have been noticed by Watts and Brown (1954) in h'(f) experiments and are evident in some of the results of Gregory (1956, 1961), although the principal preferred heights in the

latter results show a spacing of about 10 km. Titheridge (1962b), from MF observations, noted that a series of preferred heights at spacings of about 5 km was prominent in winter and he suggested that there is evidence that such a phenomenon occurs on a fairly large geographic scale. Seddon (1960) from in situ rocket studies of electron densities has shown that striking stratification is evident and that sharp ledges of electron density occur at about 5 km intervals above about 90 km. Below this measurements were thought to be rather unreliable but there was a suggestion of a similar tendency. The tendency found in the present results for the peaks in received amplitude to occur at roughly equal height spacings of about 5 km suggests that a similar phenomenon may exist in the D-region, but the ledges in electron density are probably not as accentuated. The same coincidence of peaks in $A_o$ amplitude with preferred heights of reflection which has been found in the present study has also been found to occur in Canada when stratification is present (Belrose et al., 1966; Belrose, 1970). The degree of stratification generally observed by these workers appears to be less than that encountered in the Southern hemisphere. The results of Figure 8.3 strongly suggest that preferred heights tend to occur at the heights of steepest gradients in electron density (which are identified with maxima in received signal strength) Gregory and Vincent (private communication) have also suggested that such a situation occurs.

The puzzling problem of what mechanism is responsible for the preferred heights has not been conclusively resolved, although many suggestions have been put forward. Gregory (1958) has suggested that either an accumulation of meteoric dust at the mesopause or a temperature minimum may be associated with the stable 85 km preferred height. In a later study (Gregory, 1961) wind shears, turbulence and large vertical gradients of ionization were considered. Seddon and Jackson (1958) have noted an average separation of about 6.5 km for wind shear levels and this shows some consistency with the often observed spacings of preferred heights of about 5 to 6 km.

## 8.6 The apparent temporal variation of mean electron density between highly preferred reflection heights

It has been shown in §8.3 that some of the differential absorption results show several strongly preferred reflection levels co-existing throughout a recording period. It was decided to explore the possibility of making determinations of electron density between such heights for each frame of the film records, so producing a series of electron density values at fixed heights at one second intervals. Since echoes at a pair of preferred heights are necessary to be simultaneously present in order to calculate such electron densities a fairly stringent requirement is placed on the stability of the D-region in order to provide a reasonably continuous series of values of electron densities. A few recordings of such a nature were obtained. It is not claimed that the results discussed here necessarily represent the general situation, but rather that which occurred when

several especially stable reflecting layers were present at suitable height spacings.

8.6.1 Compilation of the sequence of values of electron density

The digitized DAE data was firstly analysed to compile the statistics of the heights of occurrence of partial reflections as described in §8.4. Those records which displayed more than one strongly preferred height were reprocessed using another computer program to derive temporal variations of the electron densities. The format of the data was such that it was possible to search through data from each frame of the original film record for the presence of echoes from the formerly determined preferred heights (within ± ½ km). When echoes from a pair of preferred heights were present an electron density determination between these heights was attempted. If an electron density was undefined or negative according to equation 5.6 it was discarded. For the purposes of displaying the results a computer plotter was used to produce a point representing the mean of the electron densities so calculated over a 15 second period, and an error bar corresponding to the standard deviation of this mean was also plotted. In addition to this output other statistics were also compiled. Averages and standard deviations over all individual electron density determinations were made and these could be compared with an alternative result obtained by firstly averaging the amplitudes over the entire record and then determining the electron density from this average. In addition, probability distributions of the electron densities were compiled and a value for the preferred height was

calculated to a better accuracy than the estimate based on the initial analysis of the heights of occurrence.

8.6.2 Results and discussion

In Table 8.1 some of the statistics are given for the records which have been used to study apparent temporal variations of electron density. A comparison of the two methods of obtaining a mean electron density between a given pair of preferred heights over the length of a recording period shows that in all cases the mean electron densities differ by very little. It is evident though that in all cases the standard deviation of a single reading as a percentage of the mean is greater where all amplitude readings have been averaged to get $\overline{N}$ than where individual estimates of N have been averaged. In some cases this difference amounts to a factor of more than two. Probably the reason for this is that undefined or negative values of N are discarded in one process whereas the amplitudes from which this result was derived were retained in obtaining an average $A_x/A_o$ value over the record in the alternative process. The rejection criterion in the first process is apparently advantageous and rejects those reflections which are incompatible with the normal DAE theory. The results suggest that an accurate alternative way to the normal amplitude averaging methods of producing electron density profiles might be to compile individual estimates of N for each successive echo pair recorded on individual A-scan records, discarding all negative and undefined values of N and then reducing all estimates from the entire record to an average electron density profile. Such a method might require less

| Date | Local time (hrs) | Preferred Height (km) | Simultaneous occurrence of echoes (%) | Av. over densities | | Av. over amplitudes | |
|---|---|---|---|---|---|---|---|
| | | | | $\overline{N}$ | s.d. (%) | $\overline{N}$ | s.d. (%) |
| 15/5/71 | 1208-1223 | 64.1 | 66 | 181 | 32 | 187 | 41 |
| | | 68.9 | 76 | 278 | 15 | 275 | 24 |
| | | 75.6 | | | | | |
| 15/6/71 | 1200-1215 | 72.8 | 56 | 246 | 14 | 245 | 33 |
| | | 78.9 | | | | | |
| 14/8/71 | 1213-1228 | 67.1 | 65 | 193 | 18 | 184 | 84 |
| | | 73.0 | | | | | |
| 13/9/71 | 1205-1218 | 66.8 | 46 | 211 | 18 | 228 | 34 |
| | | 70.9 | | | | | |
| 18/11/71 | 1210-1225 | 67.1 | 64 | 298 | 17 | 291 | 31 |
| | | 72.8 | | | | | |
| 17/12/71 | 1327-1345 | 66.0 | 63 | 415 | 21 | 415 | 29 |
| | | 71.8 | | | | | |

TABLE 8.1 Statistics derived from records showing several strongly preferred heights of partial reflection in the D-region.

temporal averaging of data because "poor data" is automatically removed rather than being rendered insiginificant by averaging over large amounts of data.

The apparent temporal variations which were derived from the records summarized by Table 8.1 are shown in Figure 8.6. The time axis is calibrated to zero time at the beginning of the recording period. An inspection of the various examples shows that a range of temporal structure scales is present. Most records display a fine structure component with a period between about ½ - 1½ minutes, but some records show evidence of much longer time scale variations and these have been drawn in with a dashed line. The examples of Figures 8.6a,b,c,f,g,h suggest that fairly strong components with periods in the range 3 - 10 minutes are present. The examples of Figures 8.6d,e on the other hand show only relatively fine scale structure in the temporal variations and many other similar examples of this kind were obtained.

Preferred height separations of about 5 km have been selec ted, as this figure represents a suitable spacing for the probing system used; for although a small separation is desirable to attain good height resolution of the electron density variations, a lower limit on the separation is necessary in order to avoid uncertainties introduced by the effects of overlapping contributions of signal from both height as a result of a finite transmitter pulsewidth. It is difficult to assess to what degree the examples of Figure 8.6 actually represent tr temporal variations in the mean electron density between two heights.

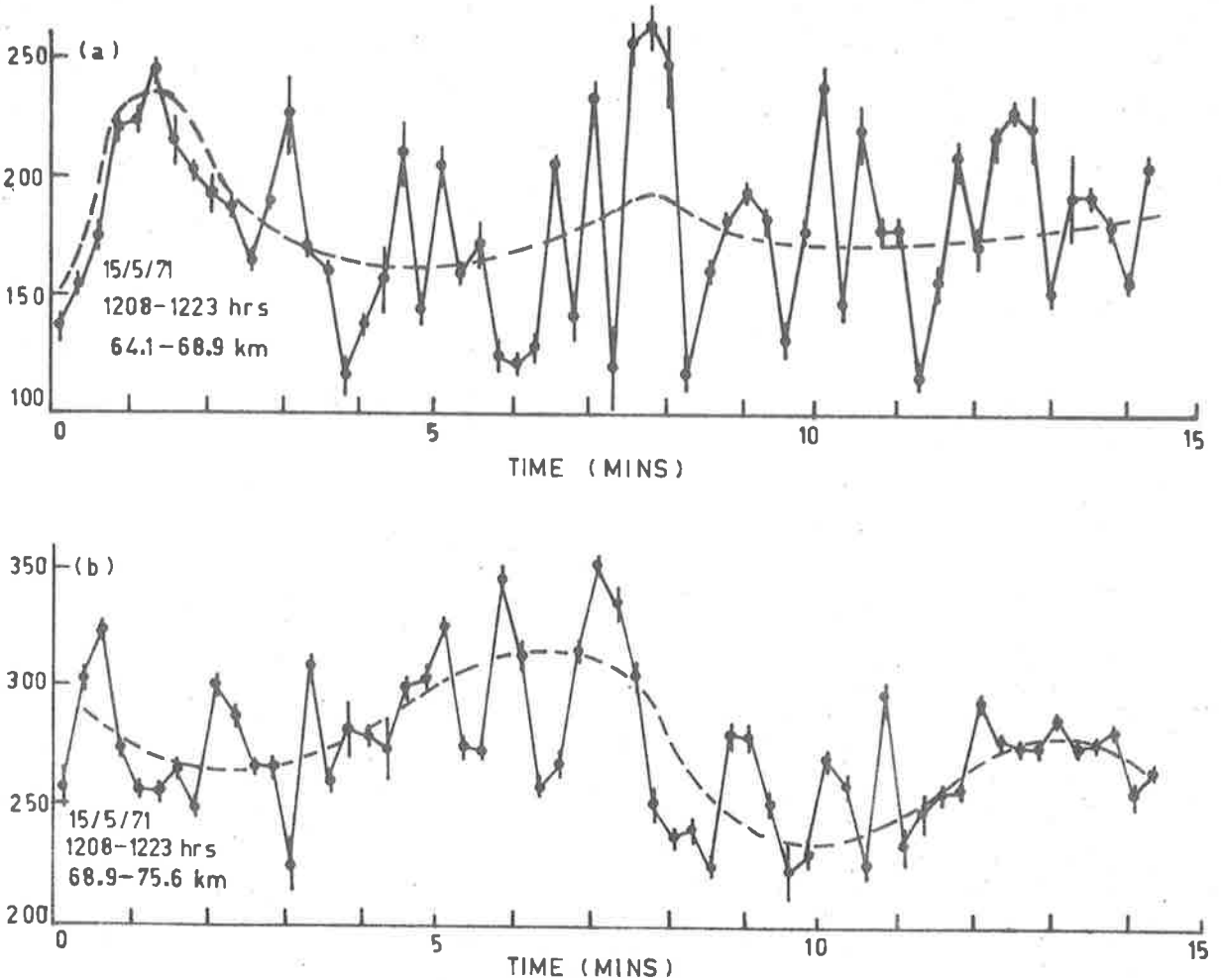


Figure 8.6a,b Apparent temporal variations of electron density between preferred heights of reflection.

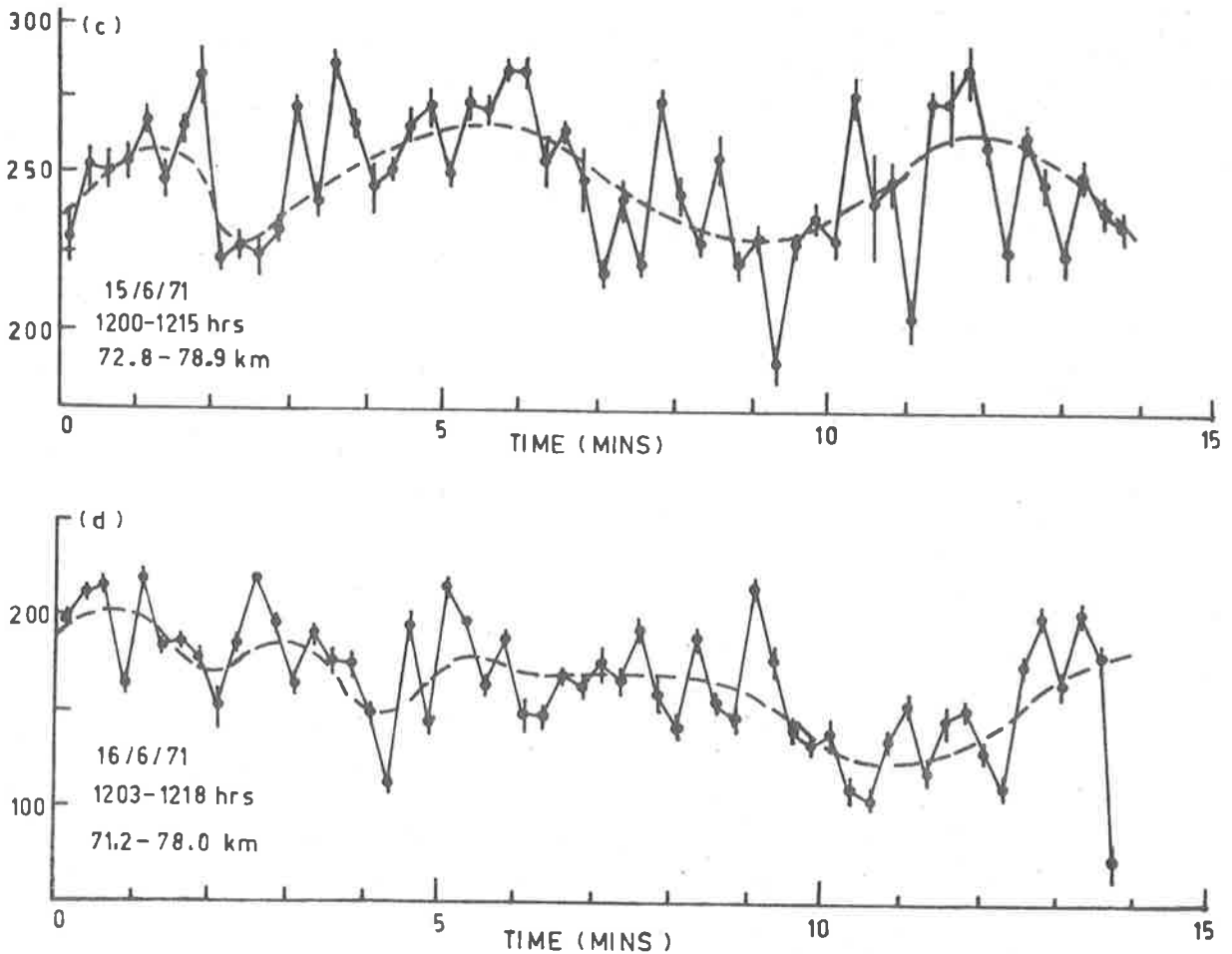


Figure 8.6c,d Apparent temporal variations of electron density between preferred heights of reflection.

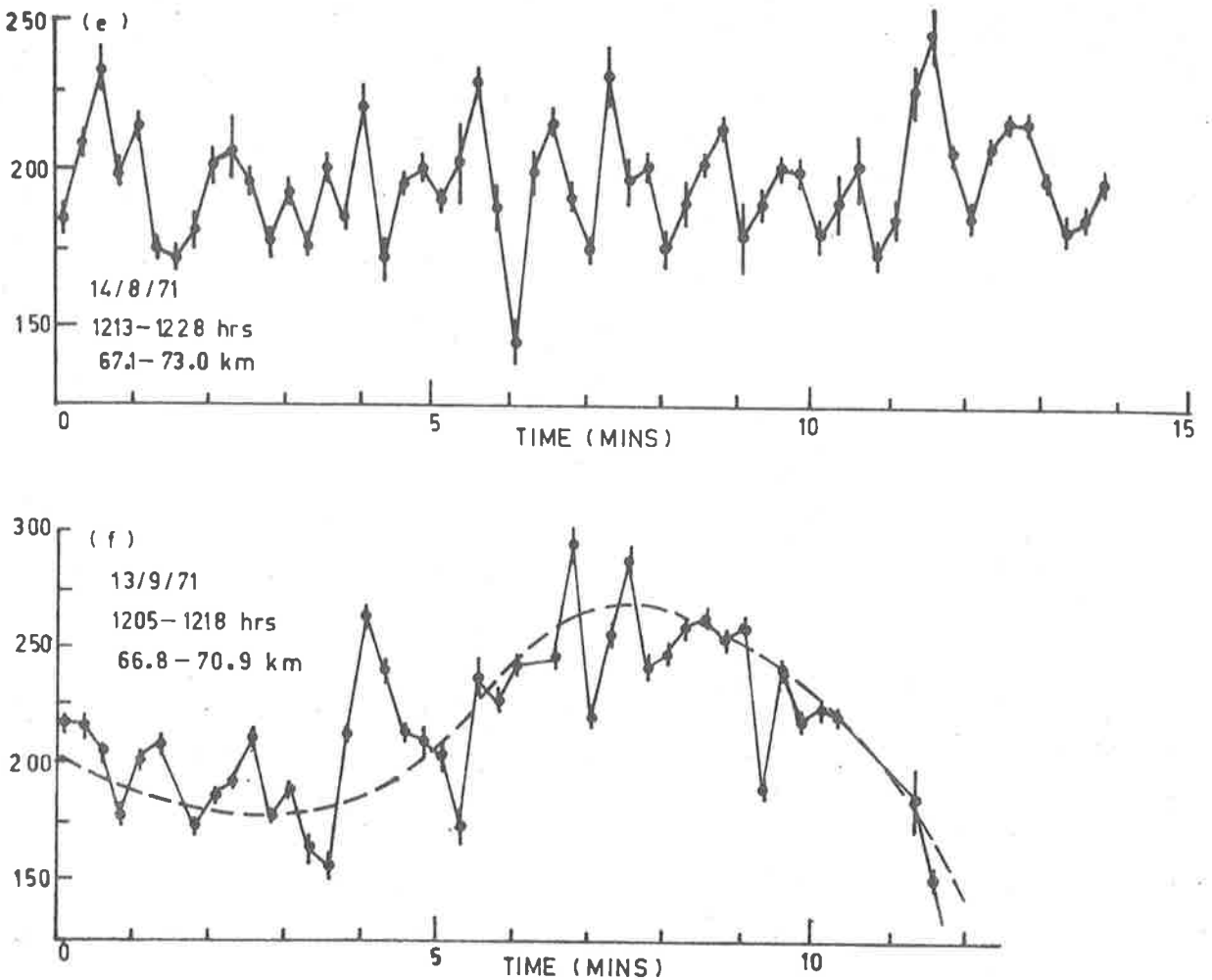


Figure 8.6e,f Apparent temporal variations of electron density between preferred heights of reflection.

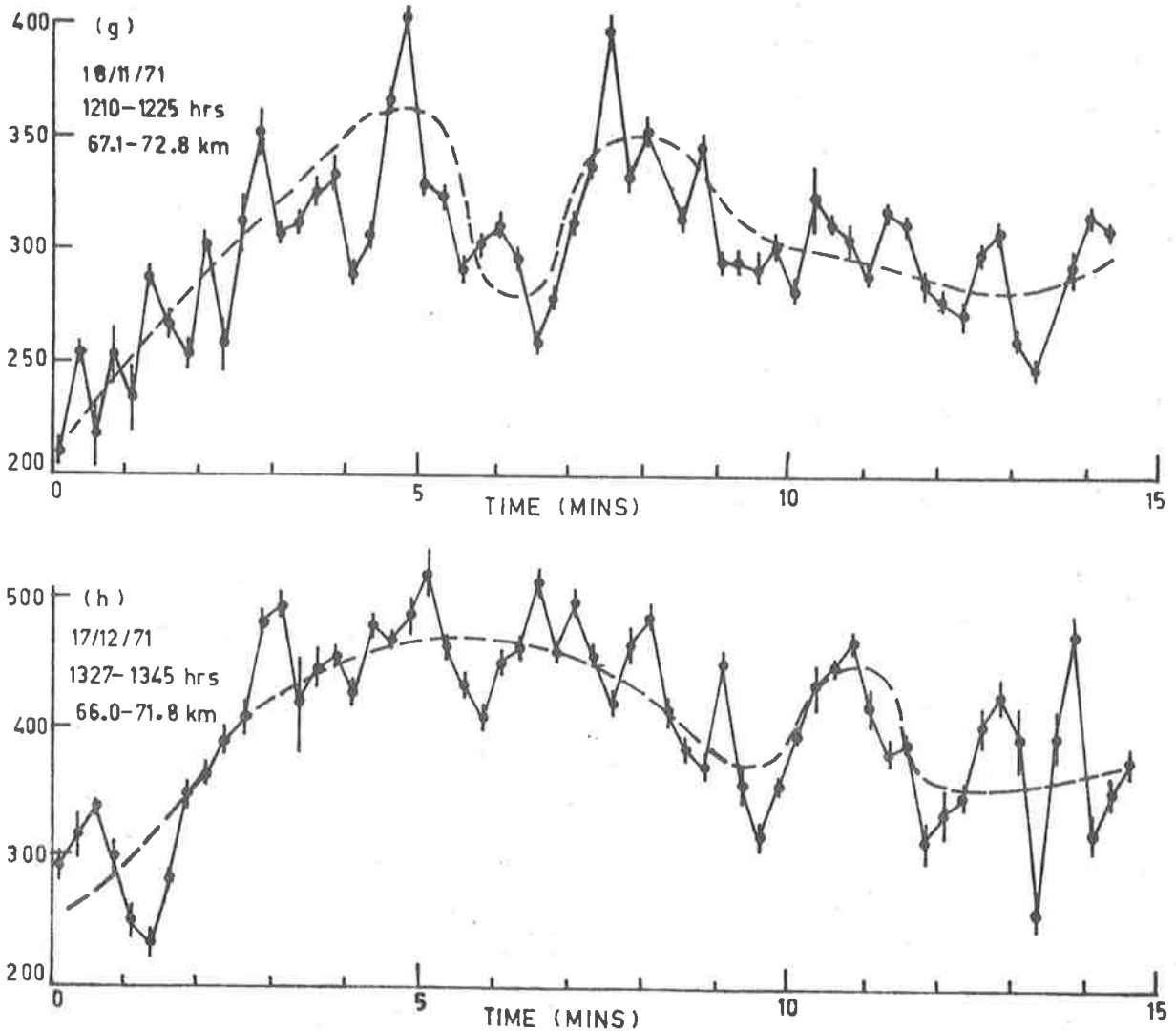


Figure 8.6g,h Apparent temporal variations of electron density between preferred heights of reflection.

For the present results the reflection mechanism was assumed to be constant in all calculations so that all variations were effectively considered to be due to absorption changes associated with electron density variations. The error associated with such an assumption is uncertain but could possibly account for the small scale structure present in the results.

If changes in ionization production rates are considered to be responsible for electron density variations estimates of the associated time constants can be made if effective electron loss coefficients are known. Estimates of these coefficients vary considerably with a resultant uncertainty in the time constants expected. The results of Mitra (1968) would prescribe relevant time constants of at least several minutes. On the other hand, recent theoretical estimate (Reid, 1970) would predict time constants as small as about 20 or 30 seconds, in which case the present observations could be accounted fo by variations of ionization production.

If the ionosphere is considered to be in a continual state of drift motion, an alternative mechanism for the observed variations could be spatial variations of electron density. For such a model the time scale of observed variations would be determined by the drift velocity and the spatial scale of irregularities. It is difficult to assess which of the two mechanisms proposed for producing the observe temporal variations of electron density is more likely. In any case it is considered that variations with time scales greater than about 1 min. are likely to be most significant. If the second model discussed

above is assumed, an estimate of the spatial scale of ionization irregularities can be obtained from the present results. Assuming a drift velocity of the order of 50 m/sec, gives a conversion factor between observed temporal scales and corresponding spatial scales of about 3 km/min. The example in Figure 8.6b showing a component with a period of about 7½ minutes might be interpreted as being due to an irregularity of about 22 km horizontal extent drifting overhead. A similar scale is evident in Figure 8.6c while 8.6f shows a scale of about 15 km. The examples of Figures 8.6g,h show evidence of more than one component and each suggests that scales of about 8 and 40 km are present.

# CHAPTER 9

# CONCLUSIONS

The main conclusions of the work will be described under three headings:

9.1 The nature of D-region partial reflections.

9.2 Studies of D-region electron densities.

9.3 Suggestions for future work.

## 9.1 The nature of D-region partial reflections

### 9.1.1 Strengths and heights of occurrence

In a study of the strengths and heights of occurrence of partial reflections, as observed in the Differential Absorption Experiment, it was found that reflections from the lowest D-region heights were observed in winter. On many occasions, regardless of season, reflections were not equally likely from all heights in the D-region and quite strongly preferred heights of reflection were found to exist. Some of these preferred heights could consistently be identified for days or even months, the most stable feature being a strongly preferred height of reflection at about 84 km which was evident almost throughout a year's observations. Another curious feature of these results was the tendency, on many occasions, for a series of preferred heights to occur at equal spacings of about 5 km. A high correlation was generally observed between peaks in received signal amplitude and preferred heights of reflection, implying that at these preferred heights the

strongest irregularities in electron density occur. The reason for a regular spacing of such levels is not clear.

9.1.2 The angular spread of partial reflections

A study of the angular spread of partial reflections revealed that other than a sudden increase of the spread in June for reflections from above about 75 km, only a small systematic seasonal variation of the height profile of angular spread was present. The day to day variability of the measured angular spread was found to have a marked maximum in winter months. The graph of Figure 4.3b depicted the angular spread averaged over a year's observations as a function of height of partial reflection and it was found that a slow increase from 2 or 3 degrees occurs with increasing height until a sharp increase in angular spread occurs above about 85 km. There was some evidence to suggest that a maximum angular spread occurred for reflections from about 90 km and that above this the angular spread decreased with increasing height. Other studies showed that at night reflections were not observed below about 85 km and that the measured angular spread was often significantly smaller than the smallest values ever observed for similar reflection heights during the day. It was concluded that coherent contributions are occasionally obtained for reflections from above 85 km at night in contrast to the day time when coherent contributions are rarely observed from this height region.

9.1.3 Studies of scattering models and other evidence

Using an extension of the system employed for determining the angular spread of ionospheric reflections, an investigation of the nature of the angular spectrum of partial reflections in terms of scattering models was carried out. The observation, on many occasions of low correlation between signals on spaced receiving aerials necessitated the generalization of the theory of interpretation due to Bramley (1951) which assumed high correlation. The necessity for this generalization of equations was experimentally verified with one interesting exception. It was initially recognized that the same relation,

$$\theta_o = \frac{\lambda \overline{|\phi|}}{2\pi d} ,$$

relating the mean absolute phase difference between signals received on a spaced pair of aerials $\overline{|\phi|}$ and $\theta_o$, the angular spread, was valid for two quite different scattering models and it was intuitively suggested that the same relation might be valid in general. A generalization of Bramley's (1951) theory leading to this equation showed that, although the relation between $\theta_o$ and $\overline{|\phi|}$ differed in form when generalized, very little difference in resultant estimates of $\theta_o$ ensued in practice, tending to support the validity of the high degree of generality of the original equation above.

As a prelude to quantitative studies of D-region scattering models a qualitative assessment of the randomness of the complex wave field, observed at a point on the ground, was carried out by plotting phasor diagrams of the time variation of the complex field

vector of the received partially reflected signal. It was demonstrated that in general there appeared to be an increase of randomness of received signal with increasing height of reflection with a rapid transition in this sense above about 85 km. Quantitative studies confirmed these observations and lent strong support to the notion of two quite distinct reflecting height regimes within the D-region with a boundary at about 85 km. Table 4.4 summarized the distinctions between the two regions with regard to the nature of the scattering mechanisms and it was concluded that in the lower height region reflections on about 50% of occasions have some coherent or specular component whereas in the upper height region reflections were found to be almost invariably described by a spectrum of randomly phased components. It was found that many of the results for the lower D-region were not strictly compatible with either of the two scattering models investigated; where one assumed a spectrum of randomly phased components and the other assumed the addition of a steady specular component to such a spectrum. It was concluded that in many of the cases there was evidence for the existence of a "specular" component varying in amplitude and direction of arrival, or even the possibility of several (but less than 5) such components with amplitudes varying in time. An analysis of partial reflection fading periods, summarized by Figures 4.9 and 4.10, yielded results consistent with many of the characteristics of partial reflections already discussed in this section. For reflections from above about 80 km fading was observed to be consistently more rapid than for reflections from below this height and showed less variability. The

lower reflections showed a wide range of periods which were considered to be consistent with the variability of the scattering mechanisms in this height range. Night time fading periods for heights above 85 km were much longer than most daytime results for the same heights, these longer fading periods being associated with smaller values of angular spread than those usually observed during the day.

Finally, we can summarize the collaborative evidence supporting the notion of two distinct height regimes within the daytime D-region as follows:

(1) A sharp increase in the angular spread of partial reflections from heights above 85 km occurs.

(2) Studies of scattering models show that the scattering from above 85 km shows far less coherence than for the lower D-region.

(3) Slower fading is observed for the lower D-region than for the higher regions indicating greater stability and coherence of partial reflections from the lower D-region.

It is seen that all of these observations appear to be consistent with each other and it is suggested that the strongly preferred height of reflection observed at about 84 km almost throughout a year's observations may also be related to the same feature, consistently marking a physical boundary between the two regions. It is noted that 85 km also marks a strong gradient of ionization often thought of as the lower boundary of the E-region.

## 9.2 Studies of D-region electron densities

Two systems were developed for recording differential absorption data for reduction to electron density profiles. Using a photographic DAE method a series of electron density profile determinations for the D-region were carried out over a period of a year (January - December 1971) representing conditions near the maximum of solar activity. A pronounced seasonal variation of the mean noon $A_x/A_o$ "turnover height" was interpreted as indicating a strong solar influence on the production of ionization below 70 km in contrast to the ionizing sources expected in this height region at solar minimum, when galactic cosmic rays are believed to constitute the principal source of ionizing flux. Except for some winter N(h) profiles which showed a fairly smoothly increasing electron density with increasing height, most profiles exhibited a peak in electron density at about 70 km with a dip at about 75 km. The mean seasonal profiles shown in Figure 6.10 established that this peak in electron density was under solar control but that electron densities in the upper D-region showed anomalously high winter concentrations assuming solar radiations were the principal ionizing flux. A few night time measurements of D-region electron densities near 90 km showed a minimum concentration in the very early hours of the morning with a progressive increase of ionization towards dawn.

The photographic DAE method described also allowed statistics of the strengths and heights of occurrence of partial reflections to be computed and some rather special cases, where strongly preferred heights of reflection were evident throughout a recording period, were used to

determine the temporal variation of mean electron density between such heights. Many of the results showed apparent scales in electron density of between ½ and 1½ minutes, the significance of which are doubtful. Other features of the results suggested fairly strong components in the temporal variation of electron density with periods in the range 3 to 10 minutes and it was considered that such structure is significant. If the observed variations are assumed to be due to ionization irregularities drifting overhead, assuming an ionospheric drift velocity of about 50 m/sec suggests spatial scales in electron density ranging from about 10 to 30 km.

A second system using magnetic tape recording for the DAE was described, and in a comparison of the two systems it was concluded that both yielded comparable results, and that provided averaging was carried out over more than about 10 minutes of data uncertainties in the computed N(h) profiles resulting from uncertainties due to the recording system were rendered less significant than other factors. The greater value of the tape system for synoptic studies of electron densities was emphasized.

## 9.3 Suggestions for future work

The system which was used for studying the nature of scattering models was also capable of yielding simultaneous values of drift velocity. Although little use was made of the latter facility it is felt that some interesting results could emerge if a search for a relationship between the drift velocity and the angular spread (or

other parameters descriptive of the scattering model) was carried out; for these quantities are all related to the dynamics of the D-region. It is possible, for example, that the "roughness" of the ionosphere at any given height, as described by $\theta_o$ say, could be related to the magnitude of the drift velocity. The system could be significantly improved by recording amplitude and phase data on magnetic tape, allowing more rapid reduction of recorded data. A similar system would also be suitable for recording amplitude and phase information for interpretation using the generalized auto-correlation techniques outlined in chapter 3, and this would prove to be a useful extension of the experimental work on scattering models described in chapter 4.

In the studies of scattering models it was recognized that variable absorption effects below the height of reflection could "mask" the true nature of the angular spectrum of diffractively reflected waves and it is thought that some useful theoretical work could be carried out in this regard. The height dependence of such an effect and an extension to the case of oblique incidence propagation would be very useful, having particular application in the translation of the results obtained at vertical incidence to the problems of HF radio wave communications on oblique incidence propagation paths.

With regard to the production of D-region ionization it is suggested that investigations of the solar dependence of the $A_x/A_o$ "turnover height" over the next few years would be useful for determining the role, as a function of sunspot activity, of solar ionizing fluxes in the production of ionization in the D-region below 70 km.

Uncertainties in the relative roles of collision frequency and electron density irregularities, as described by the parameter $\alpha = (\Delta\nu/\nu)/(\Delta N/N)$, in partial reflection mechanisms suggest that exper ments for determining $\alpha$, particularly in the lower D-region, would be extremely useful as an adjunct to the DAE to enable more accurate evaluations of the N(h) profile. Unfortunately no suitable technique is available for determining $\alpha$ over the whole D-region height range. Differential phase experiments are expected to yield some information in the lower D-region, when differential absorption is negligible, and such a technique might be a useful first step in these studies.

The polarization discriminator described in chapter 2 is capable of simultaneously monitoring both the 'O' and 'X' components of received signals and it is thought that using this facility a study of polarization inter-mode coupling or the magneto-ionic splitting of linearly polarized transmitted waves would be worthwhile. The effects of off-vertical reflections would need consideration, for any off-vertical contribution, as a result of purely geometric considerations, will appear to be elliptically polarized on horizontal receiving aerials. The implications of such a study to the DAE would also prove useful.

As described in chapter 2, the Buckland Park system was designed for operation at two frequencies, 2 and 6 MHz, although operation at 6 MHz has only recently become possible on a limited scale. It is considered that studies at the higher frequency would provide useful comparisons with results obtained at 2 MHz for the angular spread and

the nature of scattering models. At 2 MHz the upper limit to which the DAE has been found reliable has been about 80 km due principally to the high absorption of 'X' polarized waves at this frequency in the D-region, and to a possibly lesser extent the effect of off-vertical reflections and volume scatter effects. At 6 MHz the differential absorption is not as large, and combined with the receiving array response of beam width ± 1½° a DAE system operating at this frequency would undoubtedly usefully supplement the 2 MHz system and extend reliable estimates of N(h) up to at least 90 km.

Finally, it is recommended that comprehensive night time studies of electron densities, the nature of lower ionospheric scattering, and the heights of occurrence of reflections should be undertaken, for very little is known about the properties of the lower ionosphere at night.

## APPENDIX 1

### FORMULAE FOR ERRORS IN ELECTRON DENSITY EVALUATIONS

On the assumptions outlined in chapter 5, the electron density N at a level midway between two heights $h_1$ and $h_2$ is given by the expression

$$N = \frac{[\log_e(R_x/R_o)_{h_2} - \log_e(R_x/R_o)_{h_1}] - [\log_e(A_x/A_o)_{h_2} - \log_e(A_x/A_o)_{h_1}]}{2(k_x - k_o)(h_2 - h_1)} \qquad (1)$$

where the various symbols have already been explained in chapter 5.

Putting

$$(R_x/R_o)_{h_2} = R_2 ,$$

$$(R_x/R_o)_{h_1} = R_1 ,$$

$$(A_x/A_o)_{h_2} = A_2 ,$$

$$(A_x/A_o)_{h_1} = A_1 ,$$

$$K = (k_x - k_o) ,$$

and $$h = h_2 - h_1 ,$$

equation (1) becomes

$$N = \frac{\log_e (R_2/R_1) - \log_e (A_2/A_1)}{2 K h} .$$

Replacing $R_2/R_1$ by R, and $A_2/A_1$ by A, we have

$$N = \frac{\log_e (R) - \log_e (A)}{2 K h} . \qquad (2)$$

It is required to evaluate the uncertainty in N due to the standard deviations in the measurements of A and h. Using the well-known relationship for standard deviations we obtain

$$\sigma_N^2 = \left(\frac{\partial N}{\partial A}\right)^2 \sigma_A^2 + \left(\frac{\partial N}{\partial h}\right)^2 \sigma_h^2 \quad . \tag{3}$$

Now from equation (2)

$$\frac{\partial N}{\partial A} = -\frac{1}{A} \cdot \frac{1}{2\,K\,h} \quad ,$$

and since $A = A_2/A_1$ ,

$$\frac{\sigma_A}{A} = \left(\left(\frac{\sigma_{A_2}}{A_2}\right)^2 + \left(\frac{\sigma_{A_1}}{A_1}\right)^2\right)^{\frac{1}{2}} .$$

Thus

$$\left(\frac{\partial N}{\partial A}\,\sigma_A\right)^2 = \frac{\left(\left(\frac{\sigma_{A_2}}{A_2}\right)^2 + \left(\frac{\sigma_{A_1}}{A_1}\right)^2\right)}{(2\,K\,h)^2}$$

$$= N^2\left[\left(\frac{\sigma_{A_2}}{A_2}\right)^2 + \left(\frac{\sigma_{A_1}}{A_1}\right)^2\right] \Big/ \left(\log_e \left(\frac{R_2 A_1}{R_1 A_2}\right)\right)^2 \tag{4}$$

which is the first term in equation (3) and arises due to uncertainties in the measured amplitude ratios at the two heights $h_1$ and $h_2$. From equation (2) we find

$$\frac{\partial N}{\partial h} = -\frac{\log_e (R) + \log_e (A)}{2\,K\,h^2} \quad .$$

Thus

$$\left(\frac{\partial N}{\partial h}\,\sigma_h\right)^2 = \left(\frac{\log_e (A) - \log_e (R)}{2\,K\,h^2}\right)^2 \sigma_h^2 ,$$

and since $h = h_2 - h_1$ , then

$$\sigma_h^2 = \left(\sigma_{h_2}^2 + \sigma_{h_1}^2\right) ,$$

so that

$$\left(\frac{\partial N}{\partial h}\,\sigma_h\right)^2 = \left(\frac{\log_e (A) - \log_e (R)}{2 K h^2}\right)^2 \left(\sigma_{h_2}^2 + \sigma_{h_1}^2\right)$$

$$= \left(\frac{N}{h}\right)^2 \cdot \left(\sigma_{h_1}^2 + \sigma_{h_2}^2\right)$$

$$= \frac{N^2 \cdot \left(\sigma_{h_2}^2 + \sigma_{h_1}^2\right)}{h^2} .$$

Equation (3) now becomes

$$\sigma_N^2 = N^2 \frac{\left[\left(\frac{\sigma_{A_2}}{A_2}\right)^2 + \left(\frac{\sigma_{A_1}}{A_1}\right)^2\right]}{\left(\log_e \left(\frac{R_2 A_1}{R_1 A_2}\right)\right)^2} + \frac{N^2\left(\sigma_{h_2}^2 + \sigma_{h_1}^2\right)}{h^2} . \qquad (5)$$

Recalling that $A_2 = \left(\frac{A_x}{A_o}\right)_{h_2}$ and $A_1 = \left(\frac{A_x}{A_o}\right)_{h_1}$, it can be seen that the standard deviations $\sigma_{A_2}$ and $\sigma_{A_1}$ depend on the manner in which the mean $A_x/A_o$ curves are evaluated. If they are formed by averaging a series of discrete measurements of $A_x/A_o$ (i.e. $\overline{A} = \left(\overline{A_x/A_o}\right)$), the standard deviation is given by the well-known relation for the standard deviation of the mean of n samples, viz

$$\sigma_{\overline{A}} = \left[\frac{\sum_1^n (A_i - m)^2}{n(n-1)}\right]^{\frac{1}{2}}$$

$$= \left[\frac{n \sum_1^n A_i^2 - \left(\sum_1^n A_i\right)^2}{n^2(n-1)}\right]^{\frac{1}{2}} \qquad (6)$$

where

$$m = \frac{\sum_{1}^{n} A_i}{n}$$

and the $A_i$ form the set of measured amplitude ratios at the height under consideration.

On the other hand, N in equation (1) may also be calculated from the ratio of the average 'X' amplitude to the average 'O' amplitude. Then $\overline{A} = (\overline{A_x}/\overline{A_o})$ at a given height. The $\sigma_A$ terms in equation (5) are then evaluated from

$$\left(\frac{\sigma_A}{\overline{A}}\right)^2 = \left(\frac{\sigma_{A_x}}{\overline{A_x}}\right)^2 + \left(\frac{\sigma_{A_o}}{\overline{A_o}}\right)^2 . \qquad (7)$$

Either of the above methods for evaluating the amplitude ratio profile are used by various workers, so that depending on the method used either equation (6) or equation (7) should be used in conjunction with equation (5) to determine the error in any single determination of N between two levels $h_1$ and $h_2$ .

# APPENDIX 2

## ERRORS ASSOCIATED WITH A FINITE GATE-WIDTH

The magnetic tape system for recording DAE data involves digitizing the peak signal level within a gated height range. This recorded value, for the purposes of analysis, is regarded as being representative of the amplitude at the centre of the gate. An estimate of the possible error in this assumption and its resultant effect on the accuracy of electron density calculations is pursued in the following analysis.

In practice, when electron densities are being calculated, the average signal amplitude for a given height is formed from many gated samples centred on that height. Consider a gate of width W, and that n observations of the peak amplitude within the gate have been made. Next we assume that the peak amplitude from any one gate sample is equally likely to have occurred at any height within the gate. We may reformulate this assumption by saying that the n samples correspond to a set of heights evenly distributed across the gate and that the mean true height corresponding to the mean gated signal is therefore at the centre of the gate. We now consider n evenly spaced points within a given gate of width W. The spacing of such a set of points is $\frac{W}{n-1}$. For odd n we may calculate the standard deviation from the centre of the gate in the normal way, observing that one point will lie at the mid-point and that all points are distant from the centre by a multiple

of the points spacing. Furthermore, the grid of points is symmetrical about the centre of the gate, so that a summation for only half the gate-width, but with each term doubled to account for the other half of the gate, is needed. The standard deviation of the mean then becomes

$$\sigma_h = \left[ \frac{\sum_{j=1}^{\frac{n-1}{2}} 2 \cdot \left(\frac{j\,W}{n-1}\right)^2}{n \cdot (n-1)} \right]^{\frac{1}{2}} \qquad (1)$$

$$= \left[ \frac{2W^2 \sum_{j=1}^{\frac{n-1}{2}} j^2}{(n-1)^3 \cdot n} \right]^{\frac{1}{2}} .$$

Recalling that the algebraic sum of the series

$$\sum_{i=1}^{k} i^2 = \frac{k(k+1)(2k+1)}{6} ,$$

we get

$$\sigma_h = \left[ \frac{W^2(n+1)}{12(n-1)^2} \right]^{\frac{1}{2}} . \qquad (2)$$

Now from equation (5) of Appendix 1 we find the relative error in electron density:

$$\frac{\sigma_N}{N} \geqslant \left[ \frac{\sigma_{h_2}^{\,2} + \sigma_{h_1}^{\,2}}{(h_2 - h_1)^2} \right]^{\frac{1}{2}} , \qquad (3)$$

where we may set $\sigma_{h_2} = \sigma_{h_1} = \sigma_h$ from equation (2). The 'steplength' $(h_2 - h_1)$ in the reduction analysis is assumed to be a multiple of the gate-width, say $h_2 - h_1 = \ell W$. Substituting these values into

equation (3) the following relation is obtained:

$$\frac{\sigma_N}{N} \geqslant \frac{(n+1)^{\frac{1}{2}}}{\ell(n-1)\sqrt{6}} \quad .$$

For large n we have $n + 1 \simeq n - 1 \simeq n$ and thus

$$\frac{\sigma_N}{N} \geqslant \frac{1}{\ell\sqrt{6n}} \quad . \qquad (4)$$

For even values of n, the expression for the standard deviation of the mean height becomes

$$\sigma_h = \left[\frac{2W^2}{4(n-1)^2} \frac{\sum_{j=1}^{n/2} (2j-1)^2}{n(n-1)}\right]^{\frac{1}{2}} \quad .$$

For large n equation (5) of Appendix 1 then gives the relative error in electron density as

$$\frac{\sigma_N}{N} \geqslant \frac{1}{\ell\sqrt{6n}} \quad . \qquad (5)$$

The result is seen to be identical to that obtained for odd n as might be reasonably expected. It can be seen that large values of n decrease the error in electron density. For very large n this is achieved at the expense of temporal resolution of electron density changes. Similarly, errors reduce with increased steplength $\ell$ but at the expense of height resolution in the electron density profiles, so that a compromise in the choice of n and $\ell$ is required.

## BIBLIOGRAPHY

Aikin, A. C., Kane, J. A., and Troim, J., (1964) J. geophys. Res. 64, 4621.

Ananthakrishnan, S., and Ramanathan, K., (1962) Nature, Lond., 223, 488.

Appleton, E. V., (1927) Union Int. Radioteleg. Sci. Pap. Gen. Assembly Wasington 1, Pt. I.

Appleton, E. V., (1930) Proc. Roy. Soc., A126, 542.

Appleton, E. V., (1935) Rep. Progr. Phys. (Physical Society), 2, 129.

Appleton, E. V., (1937) Proc. Roy. Soc., A162, 451.

Appleton, E. V., and Piddington, J. H., (1938) Proc. Roy. Soc., A164, 467.

Appleton, E. V., and Piggott, W. R., (1954) J. Atmosph. Terr. Phys. 5, 141.

Appleton, E. V., and Ratcliffe, J. A., (1930) Proc. Roy. Soc. A128, 155.

Austin, G. L., and Manson, A. H., (1969) Rad. Sci. 4, 35.

Awe, O., (1961) J. Atmosph. Terr. Phys. 21, 142.

Bailey, D. K., Bateman, R., and Kirby, R. C., (1955) Proc. I.R.E., 43, 1181.

Bain, W. C., and May, B. R., (1967) Proc. I.E.E., 114, 1593.

Barth, C. A., (1966) Annls. Geophys., 22, 198.

Belrose, J. S., (1970) J. Atmosph. Terr. Phys. 32, 567.

Belrose, J. S., Bode, L. R., and Hewitt, L. W., (1966) "Electron density profiles in Ionosphere and Exosphere"., North-Holland Pub. Co., Amsterdam, P48.

Belrose, J. S., Bourne, I. A., and Hewitt, L. W., (1967) Proc. of Conf. on Ground-Based Radio Wave Propagation Studies of the Lower Ionosphere. P125-151. Defence Research Board (Ottawa).

Belrose, J. S., and Burke, M. J., (1964) J. geophys. Res., 69, 2799.

Berning, W. W., (1951) J. Met., 8, 175.

Best, J. E., and Ratcliffe, J. A., (1938) Proc. Phys. Soc., 50, 233.

Best, J. E., Ratcliffe, J. A., and Wilkes, M. V., (1936) Proc. Roy. Soc., A156, 614.

Beynon, W. J. G., and Rangaswamy, S., (1969) J. Atmosph. Terr. Phys., 31, 891.

Booker, H. G., (1935) Proc. Roy. Soc., A, 150, 267.

Booker, H. G., Ratcliffe, J. A., and Shinn, D. H., (1950) Phil. Trans. Roy. Soc., London, Ser. A242, 579.

Bossolosca, M., and Elena, A., (1963) Compt. Rend. 256, 4491.

Bourne, I. A., Heilbronn, D. J., Lehmann, P., and Perera, P., (1972) Proc. Conf. on the Ionosphere, Sydney (June 1972).

Bowhill, S. A., (1969) J. Atmosph. Terr. Phys., 31, 731.

Bowhill, S. A., (1969) Annals of the IQSY, 5, 83.

Bracewell, R. N., Budden, K. G., Ratcliffe, J. A., Straker, T. W., and Weekes, K., (1951) Proc. I.E.E., 98, 221.

Bramley, E. N., (1951) Proc. I.E.E., 98, 18.

Bramley, E. N., (1955) Proc. I.E.E., B102, 533 (paper 1713 R).

Briggs, B. H., Elford, W. G., Felgate, D. G., Golley, M. G., Rossiter, D. E., and Smith, J. W., (1969) Nature, Lond. 223, 1321.

Budden, K. G., (1961) "Radio waves in the Ionosphere" (Cambridge Univ. Press).

Budden, K. G., Ratcliffe, J. A., and Wilkes, M. V., (1939) Proc. Roy. Soc., A171, 188.

Charney, J. G., and Drazin, P. G., (1961) J. geophys. Res., 66, 83.

Christie, A. D., (1970) J. Atmosph. Terr. Phys., 32, 35.

Colwell, R. C., and Friend, A. W., (1936) Nature, 137, 782.

Colwell, R. C., Friend, A. W., Hall, N. I., and Hill, L. R., (1936) Nature, 138, 245.

Deeks, D. G., (1966) Proc. R. Soc. A291, 413.

Deland, R. J., and Friedman, R. M., (1972) J. Atmosph. Terr. Phys., 34, 295.

Dieminger, W., (1952) J. Atmosph. Terr. Phys., 2, 340.

Dieminger, W., Rose, G., Schwentek, H., and Weddel, H. V., (1967) Space Research VII, 228, North-Holland, Amsterdam.

Edwards, P. J., Burtt, G. J., and Knox, F., (1969) Nature, Lond., 222, 1053.

Elford, W. G., (1959) Planet. Space. Sci., 1, 94.

Ellyett, C. D., (1947) Terr. Magnetism & Atmos. Elec., 52, 1.

Ellyett, C. D., and Watts, J. M., (1959) J. Res. NBS, 63D, 117.

Farmer, F. T., and Ratcliffe, J. A., (1935) Proc. Roy. Soc. A151, 370.

Fejer, J. A., (1955) J. Atmosph. Terr. Phys., 7, 322.

Findlay, J. W., (1951) J. Atmosph. Terr. Phys., 1, 353.

Fiocco, G., and Smullin, L. D., (1963) Nature, 199, 4900.

Flood, W. A., (1968) J. geophys. Res., 73, 5585.

Flood, W. A., (1969) J. geophys. Res., 74, 5183.

Fraser, G. J., (1965) J. Atmos. Sci., 22, 217.

Fraser, G. J., (1968) J. Atmosph. Terr. Phys., 30, 707.

Fraser, G. J., and Vincent, R. A., (1970) J. Atmosph. Terr. Phys., 32, 1591.

Friedman, H., (1960) "Physics of the Upper Atmosphere", Ed. J. A. Ratcliffe, Academic Press, Lond., P133.

Friend, A. W., and Colwell, R. C., (1937) Proc. Inst. Radio Engrs., 25, 1531.

Friend, A. W., and Colwell, R. C., (1939) Proc. Inst. Radio Engrs., 27, 626.

Fürth, R., and MacDonald, D. K. C., (1947) Proc. Phys. Soc., 59, 388.

Gardner, F. F., and Pawsey, J. L., (1953) J. Atmosph. Terr. Phys., 3, 321.

Goldstein, H., (1958) "Propagation of Short Radio Waves", Ed. D. Kerr, McGraw-Hill, N.Y., P580.

Golley, M. G., and Rossiter, D. E., (1970) J. Atmosph. Terr. Phys., 32, 1215.

Green, A. L., (1932) Radio Res. Board, Aust., Report No. 2, 37.

Gregory, J. B., (1956) Aust. J. Phys., 9, 324.

Gregory, J. B., (1958) Nature, Lond. 181, 753.

Gregory, J. B., (1965) J. Atmos. Sci., 22, 18.

Gregory, J. B., and Manson, A. H., (1967) J. geophys. Res., 72, 1073.

Gregory, J. B., and Manson, A. H., (1969) J. Atmosph. Terr. Phys., 31, 703.

Gregory, J. B., and Vincent, R. A., (1970) J. geophys. Res., 75, 6387.

Groves, G. V., (1970) Air Force Surveys in Geophysics, No. 218, AFCRL, Bedford, Massachusetts.

Helliwell, R. A., Mallincrodt, A. J., and Kruse, F. W., (1951) J. geophys. Res., 56, 53.

Hines, C. O., (1960) Can. J. Phys., 42, 1424.

Hollingworth, J., (1926) Journal I.E.E., 64, 579.

Holt, O., (1969) J. geophys. Res., 74, 5179.

Holt, O., Landmark, B., and Lied, F., (1961) J. Atmosph. Terr. Phys., 23, 318.

Jackson, J. E., (1954) J. geophys. Res., 59, 377.

Kane, J. A., (1959) J. geophys. Res., 64, 133.

Knoebel, H. W., and Skaperdas, D. O., (1966) Rev. Sci. Instru., 37, 1395.

Landmark, B., and Lied, F., (1961) J. Atmosph. Terr. Phys., 23, 92.

Lauter, F. A., and Nitzsche, P., (1967) J. Atmosph. Terr. Phys., 29, 533.

Lauter, E. A., and Schäning, B., (1970) J. Atmosph. Terr. Phys., 32, 1619.

MacDonald, D. K. C., (1949) Proc. Cambridge Phil. Soc., 45, 368.

McNicol, R. E., and Thomas, J. A., (1960) Aust. J. Phys., 13, 120.

Manson, A. H., (1966) J. geophys. Res., 71, 3783.

Manson, A. H., (1968) J. Atmosph. Terr. Phys., 30, 627.

Manson, A. H., and Merry, M. W. J., (1970) J. Atmosph. Terr. Phys., 32, 1169.

Mechtly, E. A., Bowhill, S. A., Smith, L. G., and Knoebel, H. W., (1967) J. geophys. Res., 72, 5239.

Mechtly, E. A., and Smith, L. G., (1970) Rad. Sci., 5, 1407.

Meira, L. G., (1971) J. geophys. Res., 76, 202.

Mitra, A. P., (1968) J. Atmosph. Terr. Phys., 30, 1065.

Mitra, S. K., and Bhar, J. N., (1936) Science and Culture, 1, 782.

Mitra, S. K., and Syam, P., (1935) Nature, 135, 953.

Mitra, S. N., (1949) Proc. I.E.E., 96 (Part III), 441.

Naismith, R., and Bramley, E. N., (1951) Wireless Engr., 28, 271.

Narcisi, R. S., and Bailey, A. D., (1965) J. geophys. Res., 70, 3687.

Nicolet, M., (1945) Mém. Inst. r. mét. Belg., 19, 83.

Nicolet, M., and Aikin, A. C., (1960) J. geophys. Res., 65, 1469.

Nordberg, W., Katchen, L., Theon, J., and Smith, W. S., (1965) J. Atmosph. Terr. Phys., 22, 69.

Nordberg, W., and Smith, W., (1963) Proc. Int. Symp. on Stratospheric and Mesospheric Circulation (ed. Scherhag, R., and Warnethe, G.,), Berlin.

Ogawa, T., and Tohmatsu, T., (1966) Rep. Ionosph. Space Res., Japan, 20, 395.

Pearce, J. B., (1969) J. geophys. Res., 74, 853.

Peavey, R. C., (1946) Terr. Mag., 51, 125.

Phelps, A. V., and Pack, J. L., (1959) Phys. Rev. Letters, 3, 340.

Piddington, J. H., (1939) Proc. Inst. Radio Engrs., 27, 753.

Piggott, W. R., and Thrane, E. V., (1966a) J. Atmosph. Terr. Phys., 28, 311.

Piggott, W. R., and Thrane, E. V., (1966b) J. Atmosph. Terr. Phys., 28, 467.

Pineo, V. C., (1956) J. geophys. Res., 61, 165.

Rakshit, H., and Bhar, J. N., (1936) Nature, 138, 283.

Ramanamurtry, Y. V., Mitra, A. P., and Jain, V. C., (1970) J. Atmosph. Terr. Phys., 32, 1721.

Ratcliffe, J. A., (1956) Rep. Progr. Phys., 19, 188, (Phys. Soc., Lond.).

Ratcliffe, J. A., (1959) "Magneto-ionic Theory", (Cambridge Univ. Press).

Reid, G. G., (1970) J. geophys. Res., 75, 2551.

Rice, S. O., (1945) Bell Syst. Tech. J., 24, 46.

Rofe, B., (1966) Dept. of Supply, Australia. Weapons Research Establishment, Tech. Note PAD 115.

Roper, R. G., (1966) J. geophys. Res., 71, 5746.

Rossiter, D. E., (1970) "Studies of the Lower Ionosphere using a large antenna array", Ph.D. thesis, University of Adelaide, S.A.

Rowe, J. N., Ferraro, A. J., Lee, H. S., and Mitra, A. P., (1969) J. Atmosph. Terr. Phys., 31, 1077.

Schwentek, H., (1963) J. Atmosph. Terr. Phys., 25, 733.

Schwentek, H., (1966) Ann. de Geophys., 22, No. 2, 276.

Schwentek, H., (1971) J. Atmosph. Terr. Phys., 33, 1839.

Seddon, J. C., (1953) J. geophys. Res., 58, 323.

Seddon, J. C., (1958) J. geophys. Res., 63, 209.

Seddon, J. C., (1960) Trans. Amer. Geophys. Un. 41, 113.

Seddon, J. C., and Jackson, J. E., (1958) Annals I.G.Y., 12, 591.

Sen, H. K., and Wyller, A. A., (1960) J. geophys. Res., 65, 3931.

Shapley, A. H., and Beynon, W. J. G., (1965) Nature, Lond., 206, 1242.

Shrestha, K. L., (1971) J. Atmosph. Terr. Phys., 33, 213.

Sillitoe, S., (1934) Canadian J. Res., 11, 163.

Sinno, K., and Higashimura, M., (1969) J. Atmosph. Terr. Phys., 31, 1353.

Smith, N., and Kirby, S. S., (1937) Phys. Rev., 51, 890.

Smith, R. A., Bourne, I. A., Loch, R. G., Setty, C. S. G. K., Coyne, T. N. R., Barratt, P. H., and Prasad, B. S. N., (1965) Air Force Cambridge Res. Lab. Rep. No. AFCRL 65.

Stroebel, D. F., Hunten, D. M., and McElroy, M. B., (1970) J. geophys. Res., 75, 4307.

Svennesson, J., Reder, F., and Crouchley, J., (1972) J. Atmosph. Terr. Phys., 34, 49.

Syam, P., (1936) Indian J. Phys., 10, 13.

Taubenheim, J., (1971) J. Atmosph. Terr. Phys., 33, 1481.

Thomas, L., (1962) J. Atmosph. Terr. Phys., 23, 301.

Thomas, L., (1968) J. Atmosph. Terr. Phys., 30, 1211.

Thomas, L., (1971) J. Atmosph. Terr. Phys., 33, 157.

Thrane, E. V., (1966) NDRE Report No. 54.

Thrane, E. V., Haug, A., Bjelland, B., Anastassiades, M., and Tsagakis, E., (1968) J. Atmosph. Terr. Phys., 30, 135.

Titheridge, J. E., (1962a) J. Atmosph. Terr. Phys., 24, 269.

Titheridge, J. E., (1962b) J. Atmosph. Terr. Phys., 24, 283.

Tulinov, V. F., (1967) Space Research VII, 386. North-Holland, Amsterdam.

Vallance-Jones, A., and Gattinger, R. L., (1963) Planet. Space Sci., 11, 961.

Vincent, R. A., (1967) "Lower Ionospheric Irregularities". Ph.D. thesis, University of Canterbury, N.Z.

Vincent, R. A., (1972) Private communication.

von Biel, H. A., (1971) J. geophys. Res., 76, 8365.

Watson-Watt, R. A., (1945) Nature, 156, 319.

Watson-Watt, R. A., Bainbridge-Bell, L. H., Wilkins, A. F., and Bowen, E. G., (1936) Nature, 137, 866.

Watson-Watt, R. A., Wilkins, A. F., and Bowen, E. G., (1937) Proc. Roy. Soc., A161, 181.

Watts, J. M., and Brown, J. N., (1954) J. geophys. Res., 59, 71.

Webber, W., (1962) J. geophys. Res., 67, 5091.

Weeks, L. H., and Smith, L. G., (1968) Planet. Space. Sci., 16, 1189.

Whale, H. A., and Gardiner,C. W., (1966) Rad. Sci., 1, 557.

White, F. W. G., and Brown, L. W., (1936) Proc. Roy. Soc., A153, 639.

Witt, G., Hemenway, C. L., and Soberman, R. K., (1964) Space Res., 4, 197.

Yabsley, D. E., (1945) Aust. C.S.I.R.O., Division of Radiophys., R.P. 264/1. P15.

Zimmerman, S. P., and Narcisi, R. S., (1970) J. Atmosph. Terr. Phys., 32, 1305.